ISSN: 2958-8995. 2958-8987
Doi: 10.59799/APPP6605
No: 6 Val:1/ June / 2024

Journal of Natural and Applied Sciences URAL

A Quarterly Multidisciplinary Scientific Journal Issued by European Academy for Development and Research / Brussels and Center of Research and Human Resources Development Ramah- Jordan

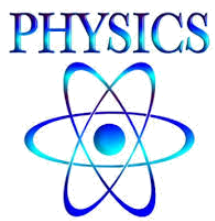

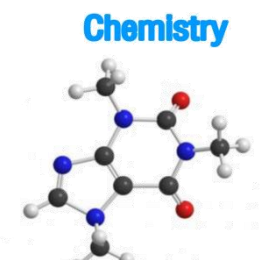

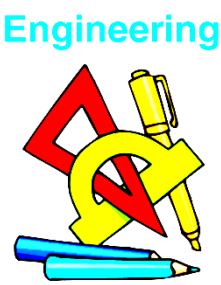

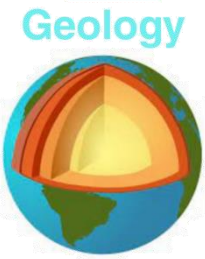

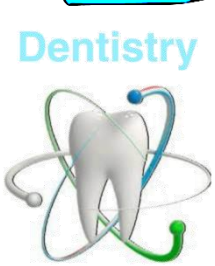

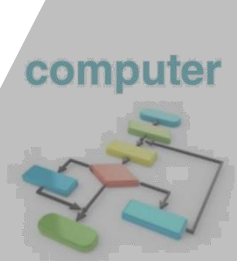

Editorial Team			
Prof. Dr. Ghassan Ezzulddin Arif	**Tikrit University\ College of Education for Pure Science's\ Department of Mathematics.**	**Iraq**	**Editor-in-Chief of the Journal**
Assist. Prof. Baraa Mohammed Ibrahim Al-Hilali	**University of Samarra\ College of Education\ Biology Department**	**Iraq**	**Managing Editor of the Journal**
Asst. inst. Alyaa Hussein Ashour	**University of Mashreq/ College of Medical Sciences Technologies Department of Medical Physics**	**Iraq**	**Editorial Secretary of the Journal**

Prof. Dr. Younis A. Rasheed	**Al-Iraqia University, College of Medicine**	**Iraq**
Assist. Prof. Dr. Hadeer Akram Al-Ani	**Dept. of Public Health Sciences UC Davis School of Medicine**	**USA**
Assist. Prof. Dr. Jawdat Akeel Mohammad Alebraheem	**College of Science Al-Zulfi Majmaah University, Al-Majmaah**	**KSA**
Assist. Prof. Dr. Almbrok Hussin Alsonosi OMAR	**Sebha University**	**Libya**
Assist. Prof. Dr. Saad Sabbar Dahham	**University of Technology and Applied Sciences**	**Sultanate oman**
Assist. Prof. Dr. Marrwa Abdullah Salih	**Tikrit University\ College of Education for Pure Science's\ Department of Mathematics.**	**Iraq**
Mr. Ans Ibrahim Mahameed	**Tikrit University\ College of Education for Pure Science's\ Department of Mathematics.**	**Iraq**

Advisory and Scientific Board			
Prof. Dr. Ahamed Saied Othman	**Tikrit University**	**Iraq**	**Head**
Prof. Dr. Salih Hamza Abbas	**University of Basrah**	**Iraq**	**Member**
Prof. Dr. Leith A. Majed	**University of Diyala**	**Iraq**	**Member**
Assist. Prof. Dr Ali Fareed Jameel	**Institute of Strategic Industrial Decision Modeling (ISIDM), School of Quantitative Sciences (SQS), University Utara (UUM), 06010**	**Malaysia**	**Member**

	Sintok		
Assist. Prof. Mustafa Abdullah Theyab	**University of Samarra**	**Iraq**	**Member**
Dr. Modhi Lafta Mutar	**The Open Educational College, Iraqi Ministry of Education, Thi-Qar**	**Iraq**	**Member**
Dr. Asaad Shakir Hameed	**Quality Assurance and Academic Performance Unit, Mazaya University College, Thi-Qar, Iraq**.	**Iraq**	**Member**
Ahmad Mahdi Salih Alaubaydi	**Assist. Lect.; PhD Student in the University of Sciences USM, Malaysia**	**Malaysia**	**Member**
Assist. Prof. Dr. Qutaiba Hommadi Mahmood Al.Samarrraie	**University of Samarra/College of Applied Sciences/ Department of Biotechnology**	**Iraq**	**Member**
Ph.D. Ali Mahmood Khalaf	**Gujarat University**	**India**	**Member**
Dr. Amel D. Hussein	**Wasit University**	**Iraq**	**Member**

Focus & Scope:

Journal of Natural and Applied Sciences URAL

Journal welcomes high quality contributions investigating topics in the fields of Biology, physics, computer science, Engineering, chemistry, Geology, Agriculture, Medicine, Mathematics, Pharmacy, Veterinary, Nursing, Dentistry, and Environment.

Publication specializations in the journal	
Biology	**Chemistry**
Physics	**Geology**
Computer	**Agriculture**
Engineering	**Mathematics**
Medicine	**Pharmacy**
Veterinary	**Dentistry Veternity,**

Environment	**Nursing**

Phone: +962799424774

On converse theorems of trigonometric approximation in weighted spaces

[1]**Enas Atalla Turky** [2]**Alaa Adnan Auad**

Department of Mathematics, College of Education for Pure Science,
University of Anbar

On converse theorems of trigonometric approximation in weighted spaces

[1]Enas Atalla Turky [2]Alaa Adnan Auad

Department of Mathematics, College of Education for Pure Science, University of Anbar

Email: ena22u2007@uoanbar.edu.iq alaa.adnan.auad@uoanbar.edu.iq

Abstract:

Many researchers in the field of functional analysis have proved the direct theorems for approximating functions in several known spaces. As for us in this work, we will prove inverse theorems for approximating unbounded functions using trigonometric polynomial in weighted spaces via modulus of smoothness functions.

Keywords: Maximal operator, Weighted spaces, weighted fractional moduli of smoothness, converse theorem

1.Introduction: There is an increasing interest in the spaces of functions with, bounded properties in Lebesgue spaces, whose is variable exponent , and there weighted spaces are based on homogeneous spaces .We also need the extinction theorems to determine these limits in these spaces for the various factors of harmonic analysis ,the trigonometric application has inverse estimates that determine the membership of a function in some of the smoothness classes(like Lipschitz class) , and it is known in terms of the approximation rate

$$\varphi_s\left(g,\frac{1}{m}\right) \le \frac{d_1}{m^s}\{\sum_{n=0}^{m}(n+1)^{s-1}\,\mathcal{E}_n\,(g)_t\} \ldots\ldots\ldots \quad (1.1)$$

The trigonometric approximation applies to Lebesgue spaces

$\mathcal{L}^t(\mathcal{F}),1 \le p < \infty, or\ \mathcal{B}(\mathcal{F})$, (the continuous function on $\mathcal{F}$) for $t = \infty$, $(t = \infty, p < \infty)$ since $\mathcal{F} := [0, 2\pi), g \in \mathcal{L}^t(\mathcal{F}), 1 \le p < \infty$,

$s, m \in N := \{1, 2, 3, \ldots\}$, $\mathcal{F}_f\, g(\circ) := g(\circ + f)$ *by translation operator*,
$\varphi_s(g, Q)_{p,\mu} := \sup\left\{\left\|(\mathcal{F}_f)^s\, g\right\|_{p,\mu} : 0 < f \leq Q\right\}$
the s th moduli of smoothness of the function g , I is identity operator , $\mathcal{F}_m$ .There is a class of trigonometric polynomials whose degree is no more than m,

$$\mathcal{E}_m(g)_{p,\mu} := \inf\{\| g - \mathcal{F} \|_{p,\mu} : \mathcal{F} \in \mathcal{F}_m\}$$

where d_1 a constant and it just depends on s , t .After that , various applications of (1 .1) and generalizations were reached . In 1958 Timan proved this development (1 .1)also applies to

If $1 < p < \infty, g \in \mathcal{L}^t(\mathcal{F}), m, s \in N, p = \min\{2, t\}$ *then*

$$\varphi_s\left(g, \frac{1}{m}\right) \leq \frac{d_2}{m^s}\left\{\sum_{n=1}^{m} n^{s\,p-1}\, \mathcal{E}_{n-1}^{p}(g)_{p,\mu}\right\}^{\frac{1}{p}} \qquad (1.2)$$

where d_2 a constant and it just depends on s , t

We noticed that the value $min\{2, t\}$ in (1.2) it is the optimal value , we notice that there are similar problems within the spaces of weighted functions , for example,Lebesgue spaces $L_{p,\mu}(X)$, weighted variable exponent spaces .Now we need different parameters for smoothness ,note the definition below

Let $\varphi \in B_t, 1 < t < \infty, g \in L_{p,\mu}(X), s, m \in N$

Also let

$$\delta_f\, g(y) := \frac{1}{2f}\int_{y-f}^{y+f} g(x)dx \;\; for\; f \in R \; and \; y \in \mathcal{F}.$$

We now need to determine the modulus

$$\mathcal{J}_s(g, Q)_{p,\mu} := \sup_{0 \leq f_j \leq Q}\left\|\prod_{j=1}^{s}\left(I - \delta_{f_j}\right) g\right\|_{p,\mu}, Q \geq 0$$

Now

$$\jmath_s\left(g,\frac{1}{m}\right)_{p,\mu} \leq \frac{d_3}{m^{2s}}\left\{\mathcal{E}_0(g)_{p,\mu}+\sum_{n=1}^{m} n^{2s-1}\ \mathcal{E}_n\ (g)_{p,\mu}\right\} \ldots\ldots\ldots\ldots (1.3)$$

$where\ d_3$ a constant and it just depends on s , t

Now $1 < p < \infty$, $\varphi \in B_t$, $g \in L_{p,\mu}(X)$, s , $m \in N$, $where\ d_4\ is$ a positive constant and it just depends on s , t such that

$$\jmath_s\left(g,\frac{1}{m}\right)_{p,\mu} \leq \frac{d_4}{m^{2s}}\left\{\sum_{n=1}^{m} n^{2p\,s-1}\ \mathcal{E}_{n-1}^{p}\ (g)_{p,\mu}\right\}^{\frac{1}{p}} \ldots\ldots\ldots\ldots..(1.4)$$

$\forall\, s \in \mathbb{R}^+$, now we will use the weighted fractional smoothness coefficients (1.4) ,the variable exponent is weighted with respect to $L_{p,\mu}(X)$ is (1.4) with $s \in \mathbb{R}^+$. In our work , we now prove the right side of (1.4) $2s$ and replace it with s. Variable exponent $L_{p,\mu}(X)$. For the first time , the un weighted fractional coefficients of smoothness were evaluated in spaces by Taberski and Butzer in 1977. Now we will use some definitions . Suppose T be a class of Lebesgue fraction that are measurable

Then
$t : \mathcal{F} \longrightarrow (1,\infty) such\ that\ 1 < t_* := essinfp_{\ y\in\mathcal{F}}(y) \leq t^* := essinfp_{\ y\in\mathcal{F}}(y) < \infty$

.

We will write the definition of the conjugate exponent of $t(y)$ as

$$\acute{t}(y) := t(y)/t(y) - 1$$

The class $\mathcal{L}_{2\pi}^{t(\cdot)}$ we define it of 2π periodic measurable functions $g : \mathcal{F} \longrightarrow \mathbb{C}$ then

$$\int_{\mathcal{F}} |g(y)|^{t(y)}\ dy < \infty$$

$\mathbb{C}$ is the complex plane and $t \in T$.

The $\mathcal{L}_{2\pi}^{t(.)}$ it is a class of a Banach space with the norm

$$\|g\|_{p,\mu} := \inf\left\{b > 0 : \int_{\mathcal{F}} \left|\frac{g(y)}{b}\right|^{t(y)} dy \leq 1\right\}.$$

The functions $\varphi : \mathcal{F} \longrightarrow [0, \infty]$ is called a weight if it is proven to be measurable almost everywhere positive , the functions of Lebesgue measurable $g : \mathcal{F} \to \mathbb{C}$ hold $\varphi\, g \in \mathcal{L}_{2\pi}^{t(.)}$, $\mathcal{L}_{\varphi}^{t(.)}$

and we called weighted Lebesgue spaces with variable exponent and is Banach space with norm

$$\|g\|_{p,\mu} := \|\varphi\, g\|_{p,\mu}$$

And 2π periodic weight φ then we can denote by $\mathcal{L}_{\varphi}^{t}$ the weighted Lebesgue spaces 2π periodic measurable functions $g : \mathcal{F} \to \mathbb{C}$ then

$$g\,\varphi^{\frac{1}{t}} \in \mathcal{L}^{t}(\mathcal{F}) \text{the set } \|g\|_{p,\mu} := \left\|g\,\varphi^{\frac{1}{t}}\right\|_{p,\mu} \text{for } g \in \mathcal{L}_{\varphi}^{t}$$

We take $t \in T$, the following condition [1] is fulfilled by the weight class

$$\|\varphi^{t(x)}\|_{p,\mu} := \sup_{r \in \mathcal{R}} \frac{1}{\|R\|_{p,\mu}^{TR}} \|\varphi^{t(x)}\|_{p,\mu} \left\|\frac{1}{\varphi^{t(x)}}\right\|_{p,\mu} < \infty$$

We will use $B_{t(.)}$ *to refer to it. Since*

$$T_R := \left(\frac{1}{\|R\|_{p,\mu}} \int_R \frac{1}{t(y)}\, dy\right)^{-1} \text{also } \mathcal{R} \text{ is the class of all intervals in } \mathcal{F}$$

There is a condition and there is a positive constant d_5 , so it is said to $T(y)$ it satisfies local log-Holder continuity

$$\|T(y_1) - T(y_2)\|_{p,\mu} \leq \frac{d_5}{\log\left(\frac{e+1}{\|y_1 + y_2\|_{p,\mu}}\right)} \forall\, y_1, y_2 \in \mathcal{F} \ldots\ldots\ldots\ldots\ldots (1.5)$$

The class $t \in T$ satisfying (1.5), now we will refer to it as T^{log}

Suppose $g \in \mathcal{L}_{\varphi}^{t(.)}$ and

$$\mathcal{H}_f\, g(y) := \frac{1}{f} \int_{y-f/2}^{y+f/2} g(x)\, dx, \quad y \in \mathcal{F}$$

The Hardy Littlewood maximum operator $\mathcal{U}$ is bounded by $\mathcal{L}_{\varphi}^{t(.)}$ if and only if $\varphi \in B_{t(.)}$ it has been proven in condition [1] and $t \in T^{log}$ Steklov's mean operator , if $t \in T^{log}$ and $\varphi \in B_{t(.)}, then\ B_f$ is bounded in $\mathcal{L}_{\varphi}^{t(.)}$. After using numbers and facts $y, f \in \mathcal{F}, 0 \leq s$, we will determine through binomial expansion that

$$\mathcal{S}_f^s\, g(y) = (\mathcal{H}_f - J)^s\, g(y)$$

$$= \sum_{c=0}^{\infty} (-1)^c \binom{s}{c} \frac{1}{f^c} \int_{-f/2}^{f/2} \ldots \int_{-f/2}^{f/2} g(y + h_1 + h_c)\, dh_1 \ldots dh_c,$$

Where

$$g \in \mathcal{L}_{\varphi}^{t(.)}, \qquad \binom{s}{c} := \frac{s(s-1)\ldots(s-f+1)}{c!} \; for\; c > 0,$$

$$\binom{s}{1} := s \; and \; \binom{s}{0} := 1, \qquad \sum_{c=0}^{\infty} \left|\binom{s}{c}\right| < \infty$$

If $t \in T^{log}, \varphi \in B_{t(.)}\; and\; g \in \mathcal{L}_{\varphi}^{t(.)}, there\ is\ a$positive constant d_6

Just depends on $s\; and\; t$ then

$$\left\|\mathcal{S}_f^s\, g\right\|_{p,\mu} \leq d_6\ \|g\|_{p,\mu,} < \infty \ldots\ldots\ldots\ldots (1.6)$$

For $0 \leq s$ we can now determine the fractional moduli of smoothness below s for

$t \in T^{log}, \varphi \in B_{t(.)}$ and $g \in \mathcal{L}_{\varphi}^{t(.)}$

$$\jmath_s(g, Q)_{p,\mu} := \sup_{0<f_j, x \leq Q} \left\| \prod_{j=1}^{[s]} \left(J - \mathcal{H}_{f_j}\right) \mathcal{S}_x^{s-[s]} g \right\|_{p,\mu}, Q \geq 0,$$

Where

$$\jmath_0(g, Q)_{p,\mu} := \|g\|_{p,\mu}; \prod_{j=1}^{0} \left(J - \mathcal{H}_{f_j}\right) \mathcal{S}_x^s g := \mathcal{S}_x^s g$$

Such that $0 < s < 1$ and $[s]$ *it is the integer part of the real number* s

We have that $t \in T^{log}, \varphi \in B_{t(.)}$ and $g \in \mathcal{L}_{\varphi}^{t(.)}$ by (1.6)

*there is a*positive constant d_7 Just depends on s and t then

$\jmath_s(g, Q)_{p,\mu} \leq d_7 \|g\|_{p,\mu}$.

If $t \in T^{log}, \varphi \in B_{t(.)}$, then $\varphi^{t(y)} \in \mathcal{L}^1(\mathcal{F})$. The set of trigonometric polynomials in $\mathcal{L}_{\varphi}^{t(.)}$. On another side $t \in T^{log}$ and $\varphi \in B_{t(.)}$,

then $\mathcal{L}_{\varphi}^{t(.)} \subset \mathcal{L}^1(\mathcal{F})$. For given $g \in \mathcal{L}^1(\mathcal{F})$,

suppose $g(y) \sim \frac{b_0(g)}{2} + \sum_{c=1}^{\infty} (b_c(g) \cos c\, y + r_c(g) \sin c\, y)$

$$= \sum_{c=-\infty}^{\infty} d_c(g)\, e^{j\, c\, y} \ldots\ldots\ldots\ldots\ldots (1.7)$$

The Fourier series of g with $d_c(g) = \left(\frac{1}{2}\right)(b_c(g) - j\, r_c(g))$, now we set

$\mathcal{L}_0^1(\mathcal{F}) := \{g \in \mathcal{L}^1(\mathcal{F}) : d_0(g) = 0$ *for the* series in $(1.7)\}$.

Suppose $\beta \in \mathbb{R}^{+}$.We specify fractional derivative of a function $g \in \mathcal{L}_0^1(\mathcal{F})$ as

$$g^{(\beta)}(y) := \sum_{c=-\infty}^{\infty} d_c(g)\,((j\,c)_{p,\mu})^{\beta}\; e^{j\,c\,y}$$

Provided that the right side is where $((j\,c)_{p,\mu})^{\beta} := \|c\|_{p,\mu}\, e^{(1/2)\pi\, j\, \beta\, signk}$ as principal value . Now we talk about the function $g \in \mathcal{L}_{\varphi}^{t(.)}$ it has a fractional derivative of rank $\beta \in \mathbb{R}^{+}$ if $there\ is\ a$ function $i \in \mathcal{L}_{\varphi}^{t(.)}$ so that it satisfy Fourier coefficients $d_c(\mathrm{i}) = d_c(\mathrm{g})\,((j\,c)_{p,\mu})^{\beta}$ we will write in this case $g^{(\beta)} = \mathrm{i}$.

Suppose $K_{t(.),\varphi}^{\beta}$, $\mathrm{t} \in \mathrm{T}$, $\beta > 0$ be the class of functions $g \in \mathcal{L}_{\varphi}^{t(.)}$ in which

$$g^{(\beta)} \in \mathcal{L}_{\varphi}^{t(.)}.\ K_{t(.),\varphi}^{\beta}$$

Becomes a Banach space with the norm

$$\|g\|_{p,\mu} := \|g\|_{p,\mu} + \left\|g^{(\beta)}\right\|_{p,\mu}.$$

The set $\mathcal{E}_m(g)_{p,\mu} := \inf\left\{\|g - \mathcal{F}\|_{p,\mu} : \mathcal{F} \in \mathcal{M}\right\} for\ g \in \mathcal{L}_{\varphi}^{t(.)}$.

In 2014 H¨ast¨o and L. Diening, Muckenhoupt weights in variable exponent spaces [1] , studied variable exponent spaces was the hope that many classical results from Lebesgue space theory could be generalized to this setting, but not to general Musielak–Orlicz spaces , in 2003 , Kokilashvili and S.G. Samko, Singular integrals weighted Lebesgue spaces with variable exponent [2] , The mapping properties of Cauchy singular integrals defined on the Lyapunov curve and on curves of bounded rotation are also investigated, in 2007 , Kokilashvili and Yildirir, On the approximation in weighted Lebesgue [3] , the approximation problems for periodic functions are investigated in weighted Lebesgue spaces with the Muckenhoupt weights. For this case we obtain inverse type inequality for the derivatives of 2π periodic function in terms of generalized modulus of continuity. The introduction of such structural characteristic of functions was caused by the failure of continuity of shift operator in weighted spaces. In unweighted Lebesgue spaces the inequalities for classical modulus of continuity

and the best approximations of derivatives , in 2007, Kokilashvili and Yildirir, On the approximation in weighted Lebesgue spaces [4] , we deal with the estimation of the best approximation and generalized modulus of continuity of derivatives of periodic functions in weighted reflexive Lebesgue spaces, in 2008 , Akgun and Israfilov, Approximation and moduli of fractional orders in Smirnov [5] , we investigate the approximation problems in the Smirnov-Orlicz spaces in terms of the fractional modulus of smoothness. We prove the direct and inverse theorems in these spaces and obtain a constructive descriptions of the Lipschitz classes of functions defined by the fractional order modulus of smoothness, in particular , in 2009 , A refined inverse inequality of approximation in weighted variable exponent Lebesgue spaces [6] , improved converse theorems of trigonometric approximation in variable exponent Lebesgue spaces with some Mucken-houpt weights , 1n 2009 , Operators of Harmonis Analysis in weighted spaces with non-standard growth [7] , e develop a certain variant of Rubio de Francia's extrapolation theorem. This extrapolation theorem is applied to obtain the boundedness in such spaces of various operators of harmonic analysis, such as maximal and singular operators, potential operators, Fourier multipliers, dominants of partial sums of trigonometric Fourier series and others, in weighted Lebesgue spaces with variable exponent. There are also given their vectorvalued analogues.,in 2010 , Sharp Jackson and converse theorems of trigonometric approximation in weighted Lebesgue spaces [8] , prove that improved Jackson type direct theorem of trigonometric polynomial approximation in Lebesgue spaces with Muckenhoupt weights with respect to fractional order moduli of smoothness holds. In addition, we obtain sharp converse and Marchaud inequalities of trigonometric approximation of functions and its fractional derivatives in these weighted Lebesgue spaces

2.Auxilary lemma In this section, we will present lemma that is needed in our main results

Lemma 2.1 If $\varphi^{-t_0} \in B_{\left(\frac{t(.)}{t_0}\right)^{\cdot}}$ and $t \in T^{log}$ for some $t_0 \in (1, t_*)$

$then\ \varphi \in B_{t(.)}$.

Proof :-Using the Extrapolation theorem 3.2 of [7] we get that Hardy Littlewood maximum operator $\mathcal{U}$ is bounded in $\mathcal{L}_{\varphi}^{t(.)}$ this means [1] that $\varphi \in B_{t(.)}$.

3.Main results In this part, the theorems we need are presented in order to reach important results that we need later

Theorem 3.1 If $\varphi^{-t_0} \in B_{\left(\frac{t(.)}{t_0}\right)^{\cdot}}$ and $t \in T^{log}$ for some

$$T_0 \in (1, t_*), m \in \mathbb{N}, s \in \mathbb{R}^+, i := \min\{2, t_*\} \text{ and}$$

$$g \in \mathcal{L}_{\varphi}^{t(.)}, \text{there is a positive constant } d_8 \text{ it just depends } t \text{ and } s \text{ as in}$$

$$\jmath_s \left(g, \frac{1}{m}\right)_{p,\mu} \leq \frac{d_8}{m^s} \left\{ \sum_{n=1}^{m} n^{i\,s-1} \, \mathcal{E}_{n-1}^{i} \, (g)_{p,\mu} \right\}^{\frac{1}{i}}$$

Then y^i *is convex for* $i = \min\{2, t_*\}$ *we do have*

$$\left(n\, n^{s-1} \, \mathcal{E}_n \, (g)_{p,\mu}\right)^i - \left((n-1)\, n^{s-1} \, \mathcal{E}_n \, (g)_{p,\mu}\right)^i$$

$$\leq \left(\sum_{\omega=1}^{n} \omega^{s-1} \, \mathcal{E}_{\omega} \, (g)_{p,\mu} \right)^i - \left(\sum_{\omega=1}^{n-1} \omega^{s-1} \, \mathcal{E}_{\omega} \, (g)_{p,\mu} \right)^i .$$

Now we will add the last inequalities $n = 1, 2, 3, \ldots$ to get

$$\sum_{n=1}^{m} \left\{ \left(n\, n^{s-1} \, \mathcal{E}_n \, (g)_{p,\mu}\right)^i - \left((n-1)\, n^{s-1} \, \mathcal{E}_n \, (g)_{p,\mu}\right)^i \right\}$$

$$\leq \sum_{n=1}^{m} \left\{ \left(\sum_{\omega=1}^{n} \omega^{s-1} \, \mathcal{E}_{\omega} \, (g)_{p,\mu} \right)^i - \left(\sum_{\omega=1}^{n-1} \omega^{s-1} \, \mathcal{E}_{\omega} \, (g)_{p,\mu} \right)^i \right\}$$

Also

$$\left\{\sum_{n=1}^{m} n^{i\,s-1}\ \mathcal{E}_{n-1}^{i}\,(g)_{p,\mu}\right\}^{\frac{1}{i}} \leq\ 2\sum_{n=1}^{m} n^{s-1}\ \mathcal{E}_{n-1}^{i}\,(g)_{p,\mu}\ .$$

The last inequality indicates that the theorem 3.1 it is an improvement of the converse theorem , the theory 3.1 of inequality has given highly accurate results

If

$$\mathcal{E}\,(g)_{p,\mu} = \mathcal{Y}\left(\frac{1}{m^{s}}\right)\ ,\ n\ \in\ \mathbb{N}$$

Then

$$\mathcal{J}_{s}\left(g,\frac{1}{m}\right)_{p,\mu} = \mathcal{Y}\left(\frac{1}{m^{s}}\left\|\log\frac{1}{m}\right\|_{p,\mu}\right)$$

By theorem 3.1 we get

$$\mathcal{J}_{s}\left(g,\frac{1}{m}\right)_{p,\mu} = \mathcal{Y}\left(\frac{1}{m^{s}}\left\|\log\frac{1}{m}\right\|_{p,\mu}\right)^{\frac{1}{i}}\ .$$

Proof:- In the beginning , using Lemma 2.1 by condition of theorem 3.1 the condition $\varphi\ \in B_{t(.)}$ satisfy . We notice that on the other hand , it is known as

$\mathcal{S}_{x,f_1,f_2,\ldots\ldots f_{[s]}}^{s}\ g := \prod_{j=1}^{[s]}\left(J-\mathcal{S}_{,f_j}\right)(J-\mathcal{S}_{x})^{s-[s]}\ g$ has Fourier series

$$\mathcal{S}_{x,f_1,f_2,\ldots\ldots f_{[s]}}^{s}\ g\,(.) \sim \sum_{n=-\infty}^{\infty}\left(1-\frac{\sin n\,x}{nx}\right)^{s-[s]}\left(1-\frac{\sin n\ f_1}{n\ f_1}\right)\ldots\left(1-\frac{\sin n\ f_{[s]}}{n\ f_{[s]}}\right)d_n\ e^{j\,n}$$

Also

$$\mathcal{S}_{x,f_1,f_2,\ldots\ldots f_{[s]}}^{s}\ g\,(.) = \mathcal{S}_{x,f_1,f_2,\ldots\ldots f_{[s]}}^{s}\left(g\,(.)-W_{2^{u-1}}(.\,,g)\right) + \mathcal{S}_{x,f_1,f_2,\ldots\ldots f_{[s]}}^{s}\,W_{2^{u-1}}(.\,,g)\,.$$

By $\mathcal{E}_{\mathrm{m}}(\mathrm{g})_{p,\mu} \downarrow 0$ we have

$$\left\| \mathcal{S}^{s}_{\mathrm{x},f_1,f_2,\ldots,f_{[s]}} \left(\mathrm{g}(.) - \mathrm{W}_{2^{\mathrm{u}-1}}(.,\mathrm{g}) \right) \right\|_{p,\mu} \leq \mathrm{d}_{14}(\mathrm{s},\mathrm{t}) \left\| \mathrm{g}(.) - \mathrm{W}_{2^{\mathrm{u}-1}}(.,\mathrm{g}) \right\|_{p,\mu}$$

$$\leq \mathrm{d}_{15}(\mathrm{s},\mathrm{t})\, \mathcal{E}_{2^{\mathrm{u}-1}}(\mathrm{g})_{p,\mu}$$

$$\leq \frac{\mathrm{d}_{16}(\mathrm{s},\mathrm{t})}{\mathrm{m}^{\mathrm{s}}} \left\{ \sum_{\mathrm{n}=1}^{\mathrm{m}} \mathrm{n}^{i\,\mathrm{s}-1}\, \mathcal{E}^{i}_{\mathrm{n}-1}\ (\mathrm{g})_{p,\mu} \right\}^{\frac{1}{i}}.$$

on the other hand through 3.2 we conclude

$$\left\| \mathcal{S}^{s}_{\mathrm{x},f_1,f_2,\ldots,f_{[s]}}\ \mathrm{W}_{2^{\mathrm{u}-1}}(.,\mathrm{g}) \right\|_{p,\mu} \leq \mathrm{d}_{17}(\mathrm{s},\mathrm{t}) \left\| \sum_{\omega=1}^{\mathrm{u}} |Q_{\omega}|^2 \right\|_{p,\mu}$$

Where

$$Q_{\omega} := \sum_{|n|=2^{\omega-1}}^{2^{\omega-1}} \left(1 - \frac{\sin n\,x}{nx}\right)^{s-[s]} \left(1 - \frac{\sin n\ f_1}{n\ f_1}\right) \ldots \left(1 - \frac{\sin n\ f_{[s]}}{n\ f_{[s]}}\right) d_n\, e^{j\,n\,y}$$

By [6]

$$\left\| \sum_{\omega=1}^{\mathrm{u}} |Q_{\omega}|^2 \right\|_{p,\mu} \leq \left\{ \sum_{\omega=1}^{u} \|Q_{\omega}\|^{i_1}_{p,\mu} \right\}^{\frac{1}{i_1}}.$$

The estimate $\|Q_{\omega}\|_{p,\mu}$ then

$$\|Q_{\omega}\|_{p,\mu} = \left\| \sum_{|n|=2^{\omega-1}}^{2^{\omega-1}} \left[|n|^{s} \sum_{|n|=2^{\omega-1}}^{2^{\omega-1}} \left(1 - \frac{\sin n\,x}{nx}\right)^{s-[s]} \left(1 - \frac{\sin n\ f_1}{n\ f_1}\right) \ldots \left(1 - \frac{\sin n\ f_{[s]}}{n\ f_{[s]}}\right) \right] \cdot \left[\frac{1}{|n|^{s}}\ d_n\, e^{j\,n\,y} \right] \right\|_{p,\mu}$$

Using Abel's transformation we conclude

$$\|Q_\omega\|_{p,\mu} \le \sum_{|n|=2^{\omega-1}}^{2^{\omega-2}} \left| n^s \left(1-\frac{\sin n\,x}{nx}\right)^{s-[s]} \left(1-\frac{\sin n\ f_1}{n\ f_1}\right)\dots\left(1-\frac{\sin n\ f_{[s]}}{n\ f_{[s]}}\right) - (n+1)^s \left(1-\frac{\sin(n+1)\,x}{(n+1)x}\right)^{s-[s]} \left(1-\frac{\sin(n+1)\ f_1}{(n+1)\ f_1}\right)\dots\left(1-\frac{\sin(n+1)\ f_{[s]}}{(n+1)\ f_{[s]}}\right)\right| \cdot \left\| \sum_{|\ell|=2^{\omega-1}}^{n} \frac{1}{|\ell|^s} \left| d_\ell\, e^{j\,\ell\,y} \right| \right\|_{p,\mu}$$

$$+ \left|(2^\omega-1)^s \left(1-\frac{\sin(2^\omega-1)x}{(2^\omega-1)x}\right)^{s-[s]} \left(1-\frac{\sin(2^\omega-1)f_1}{(2^\omega-1)f_1}\right)\dots\left(1-\frac{\sin(2^\omega-1)\,f_{[s]}}{(2^\omega-1)\,f_{[s]}}\right)\right| \left\| \sum_{|\ell|=2^{\omega-1}}^{2^\omega-1} \frac{1}{|\ell|^s} \left| d_\ell\, e^{j\,\ell\,y} \right| \right\|_{p,\mu}$$

With us

$$\left\| \sum_{|\ell|=2^{\omega-1}}^{2^\omega-1} \frac{1}{|\ell|^s} \left| d_\ell\, e^{j\,\ell\,y} \right| \right\|_{p,\mu} \le \frac{d_{18}(s,t)}{|2^{\omega-1}|^s} \left\| \sum_{|\ell|=2^{\omega-1}}^{2^\omega-1} \left| d_\ell\, e^{j\,\ell\,y} \right| \right\|_{p,\mu}$$

$$= \frac{d_{18}(s,t)}{|2^{\omega-1}|^s} \left\| \sum_{|\ell|=2^{\omega-1}}^{2^\omega-1} e^{-j\arg(d_\ell\, e^{j\,\ell\,y})} \left| d_\ell\, e^{j\,\ell\,y} \right| \right\|_{p,\mu}$$

$$= \frac{d_{18}(s,t)}{|2^{\omega-1}|^s} \left\| \sum_{|\ell|=2^{\omega-1}}^{2^\omega-1} \left| d_\ell\, e^{j\,\ell\,y} \right| \right\|_{p,\mu} \le \frac{d_{19}(s,t)}{2^{\omega s}}\, \mathcal{E}_{2^{\omega-1}-1}(g)_{p,\mu}$$

And also

$$\left\| \sum_{|\ell|=2^{\omega-1}}^{2^{\omega}-1} \frac{1}{|\ell|^{s}} \left| d_{\ell}\, e^{j\,\ell\, y} \right| \right\|_{p,\mu} \leq \frac{d_{19}(s,t)}{2^{\omega s}}\, \mathcal{E}_{2^{\omega-1}-1}(g)_{p,\mu}$$

And because $y^{s}(1-\frac{\sin y}{y})^{s}$ not decreasing also $\left(1-\frac{\sin y}{y}\right) \leq y$ for $y>0$

we get

$$\| Q_{\omega} \|_{p,\mu} \leq \frac{d_{20}(s,t)\, 2^{-\omega s}}{x^{s-[s]}\, f_1 \dots f_{[s]}} \left[\sum_{|n|=2^{\omega-1}}^{2^{\omega}-2} \left| (nx)^{s-[s]} \left(1-\frac{\sin n x}{nx}\right)(n f_1) \cdot \left(1 - \frac{\sin n f_1}{n f_1}\right) \dots (n f_{[s]}) \left(1-\frac{\sin n f_{[s]}}{n f_{[s]}}\right) \right.\right.$$
$$- ((n+1)x)^{s-[s]} \left(1-\frac{\sin(n+1)x}{(n+1)x}\right)^{s-[s]} \cdot ((n+1)f_1) \left(1 - \frac{\sin(n+1) f_1}{(n+1) f_1}\right) \dots (n+1) f_{[s]} \left(1-\frac{\sin(n+1) f_{[s]}}{(n+1) f_{[s]}}\right) \left.\left| \right]\right. .$$

.

$$\mathcal{E}_{2^{\omega-1}-1}(g)_{p,\mu} +$$
$$d_{20}(s,t)\, 2^{-\omega s} \left| ((2^{\omega}-1)x)^{s-[s]} \left(1-\frac{\sin(2^{\omega}-1)x}{(2^{\omega}-1)x}\right)^{s-[s]} \cdot (2^{\omega}-1) f_1 \left(1 - \frac{\sin(2^{\omega}-1) f_1}{(2^{\omega}-1) f_1}\right) \dots (2^{\omega}-1) f_{[s]} \left(1-\frac{\sin(2^{\omega}-1) f_{[s]}}{(2^{\omega}-1) f_{[s]}}\right) \right| .$$

$$\mathcal{E}_{2^{\omega-1}-1}(g)_{p,\mu}$$
$$\leq d_{21}(s,t) \left(1-\frac{\sin(2^{\omega}-1)x}{(2^{\omega}-1)x}\right)^{s-[s]} \left(1-\frac{\sin(2^{\omega}-1) f_1}{(2^{\omega}-1) f_1}\right) \dots \left(1 - \frac{\sin(2^{\omega}-1) f_{[s]}}{(2^{\omega}-1) f_{[s]}}\right) \mathcal{E}_{2^{\omega-1}-1}(g)_{p,\mu}$$
$$\leq d_{22}(s,t) \cdot 2^{\omega s}\, x^{s-[s]}\, f_1 \dots f_{[s]}\, \mathcal{E}_{2^{\omega-1}-1}(g)_{p,\mu}$$

So

$$\| Q_{\omega} \|_{p,\mu} \leq d_{22}(s,t) \cdot 2^{\omega s} x^{s-[s]} f_1 \dots f_{[s]} \mathcal{E}_{2^{\omega-1}-1}(g)_{p,\mu} .$$

And therefore

$$\left\| \mathcal{S}^{s}_{x,f_1,f_2,\dots,f_{[s]}} W_{2^{u-1}}(.,g) \right\|_{p,\mu}$$

$$\leq d_{23}(s,t)\, x^{(s-[s])} f_1, f_2, \dots, f_{[s]} \left\{ \sum_{\omega=1}^{u} 2^{2\omega s i} \mathcal{E}^{i}_{2^{\omega-1}-1}(g)_{p,\mu} \right\}^{\frac{1}{i}}$$

$$\leq d_{24}(s,t)\, x^{(s-[s])} f_1, f_2, \dots, f_{[s]} \left\{ 2^{i_1 s} \mathcal{E}^{i}_{0}(g)_{p,\mu} \right\}^{\frac{1}{i}}$$

$$+ d_{25}(s,t)\, x^{(s-[s])} f_1, f_2, \dots, f_{[s]} \left\{ \sum_{\omega=1}^{u} \sum_{n=2^{\omega-2}}^{2^{\omega-1}-1} n^{i s-1} \mathcal{E}^{i}_{n-1}(g)_{p,\mu} \right\}^{\frac{1}{i}}$$

$$\leq d_{26}(s,t)\, x^{(s-[s])} f_1, f_2, \dots, f_{[s]} \left\{ \sum_{n=1}^{2^{u-1}-1} n^{i s-1} \mathcal{E}^{i}_{n-1}(g)_{p,\mu} \right\}^{\frac{1}{i}} .$$

The recent inequality means

$$\jmath_s\left(g, \frac{1}{m}\right)_{p,\mu} \leq \frac{d_{27}(s,t)}{m^{s}} \left\{ \sum_{n=1}^{m} n^{i s-1} \mathcal{E}^{i}_{n-1}(g)_{p,\mu} \right\}^{\frac{1}{i}}$$

Theorem 3.2 Under theoretical conditions **Theorem 3.1 , there are** d_{12} , $d_{13} > 0$

just depend on s *and* t such that

$$\mathrm{d}_{12}\left\|\left(\sum_{\omega=n}^{\infty}|\triangle_{\omega}|^{2}\right)^{\frac{1}{2}}\right\|_{p,\mu}\leq\left\|\sum_{|\omega|=2^{n-1}}^{\infty}d_{n}\,e^{j\,n\,y}\right\|_{p,\mu}$$

$$\leq \mathrm{d}_{13}\left\|\left(\sum_{\omega=n}^{\infty}|\triangle_{\omega}|^{2}\right)^{\frac{1}{2}}\right\|_{p,\mu} \qquad (2.1)$$

where

$$\triangle_{\omega}:=\triangle_{\omega}\,(y,g):=\sum_{|n|=2^{\omega-1}}^{2^{\omega}-1}d_{n}\,e^{j\,n\,y}\,.$$

The proof of this theorem same theorem proof in [7] Littlewood – Paley

Theorem 3.3 Under theoretical conditions **Theorem 3.1**

$$\sum_{c=1}^{\infty}c^{i\,\beta-1}\;\mathcal{E}_{c}^{i}\,(g)_{p,\mu}<\infty \qquad (1,8)$$

$\mathcal{E}_{m}\,(g^{(\beta)})_{p,\mu}\leq d_{10}\left(m^{\beta}\;\mathcal{E}_{m}\,(g)_{p,\mu}+\left\{\sum_{n=m+1}^{\infty}n^{\beta\,i-1}\;\mathcal{E}_{c}^{i}\,(g)_{p,\mu}\right\}^{\frac{1}{i}}\right)$ sat isfy corollary

Proof :- Suppose $\mathcal{F}_{m}$ be a polynomial of class $\mathcal{M}_{m}$ such that

$\mathcal{E}_{m}\,(g)_{p,\mu}=\|g-\mathcal{F}_{m}\|_{p,\mu}\;\;then$

$\mathcal{A}_{0}\,(y):=\mathcal{F}_{1}\,(y)-\;\mathcal{F}_{0}\,(y)\,;\,\mathcal{A}_{n}\,(y):=\mathcal{F}_{2^{n}}\,(y)\;-\;\mathcal{F}_{2^{n-1}}\,(y)\,,$

$n=1\,,2\,,3\,,\ldots.$

Now

$$\mathcal{F}_{2^{M}}\,(y)=\;\mathcal{F}_{0}\,(y)+\sum_{n=0}^{M}\mathcal{A}_{n}\,(y)\,,\;\;M=0\,,1\,,2\,,\ldots.$$

$\forall\varepsilon\;>0\;,\exists\,\mathcal{D}\;\in\;\mathbb{N}\;\;by\;\;(2.1)such\;that$

$$\sum_{n=2^{\mathcal{D}}}^{\infty} n^{i\beta-1}\ \mathcal{E}_n^i(g)_{p,\mu} < \varepsilon \qquad (2.2)$$

By fractional Bernstein's

$$\left\|\mathcal{F}_m^{(\beta)}\right\|_{p,\mu} \le d_{28}(\beta,t)\, m^{\beta}\, \|\mathcal{F}_m\|_{p,\mu}\ , \qquad \beta \in \mathbb{R}^+$$

But we have

$$\left\|\mathcal{A}_n^{(\beta)}\right\|_{p,\mu} \le d_{29}(\beta,t)\, 2^{n\beta}\, \|\mathcal{A}_n\|_{p,\mu} \le d_{30}(\beta,t)\, 2^{n\beta}\, \mathcal{E}_{2^{n-1}}(g)_{p,\mu}\ , n \in \mathbb{N}.$$

It is easy for us to see this from the other side

$$2^{n\beta}\, \mathcal{E}_{2^{n-1}}(g)_{p,\mu} \le d_{31}(\beta,t) \left\{ \sum_{\omega=2^{n-2}+1}^{2^{n-1}} \omega^{i\beta-1}\, \mathcal{E}_{\omega}^i(g)_{p,\mu} \right\},$$

$$n = 2,3,4,\ldots.$$

With respect to positive integers $C < M$

$$\mathcal{F}_{2^M}^{(\beta)}(y) - \mathcal{F}_{2^C}^{(\beta)}(y) = \sum_{n=C+1}^{M} H_n^{(\beta)}(y)\ , \qquad y \in \mathcal{F}$$

And later , if it is large enough, we get from (2 . 2)

$$\left\|\mathcal{F}_{2^M}^{(\beta)}(y) - \mathcal{F}_{2^C}^{(\beta)}(y)\right\|_{p,\mu} \le \sum_{n=C+1}^{M} \left\|\mathcal{A}_n^{(\beta)}(y)\right\|_{p,\mu}$$

$$\le d_{31}(\beta,t) \sum_{n=C+1}^{M} 2^{n\beta}\, \mathcal{E}_{2^{n-1}}(g)_{p,\mu}$$

$$\le d_{32}(\beta,t) \sum_{n=C+1}^{M} \left\{ \sum_{\omega=2^{n-2}}^{2^{n-1}} \omega^{i\beta-1}\, \mathcal{E}_{\omega}^i(g)_{p,\mu} \right\}^{\frac{1}{i}}$$

$$\leq d_{33}(\beta,t)\left\{\sum_{\omega=2^{C-2}+1}^{2^{M-1}}\omega^{i\beta-1}\,\mathcal{E}_{\omega}^{i}\,(g)_{p,\mu}\right\}^{\frac{1}{i}}\leq d_{33}(\beta,t)\,\varepsilon^{\frac{1}{i}}.$$

$\left\{\mathcal{F}_{2^M}^{(\beta)}\right\}$ *is Cauchy sequence in* $\mathcal{L}_{\varphi}^{t(.)}$ *then there is b* $\sigma\in\mathcal{L}_{\varphi}^{t(.)}$ *hold*

$$\left\|\mathcal{F}_{2^M}^{(\beta)}-\sigma\right\|_{p,\mu}\to 0,\qquad as\ M\to\infty$$

from the other side we get

$$\left\|\mathcal{F}_{2^M}^{(\beta)}-g^{(\beta)}\right\|_{p,\mu}\to 0,\qquad as\ M\to\infty.$$

$g^{(\beta)}=\sigma$ *b.a.* $\quad then\ g\in K_{t(.),\varphi}^{\beta}$.

Now

$$\mathcal{E}_m(g^{(\beta)})_{p,\mu}\leq\left\|g^{(\beta)}-W_m\,g^{(\beta)}\right\|_{p,\mu}$$

$$\leq\left\|W_{2^{u+2}}\,g^{(\beta)}-W_m\,g^{(\beta)}\right\|_{p,\mu}+\left\|\sum_{c=u+2}^{\infty}\left[W_{2^{c+2}}\,g^{(\beta)}-W_{2^c}\,g^{(\beta)}\right]\right\|_{p,\mu}\qquad(2.3)$$

We use the fractional Bernstein's inequality we get for $2^u<m<2^{u+1}$

$$\left\|W_{2^{u+2}}\,g^{(\beta)}-W_m\,g^{(\beta)}\right\|_{p,\mu}\leq d_{35}(\beta,t)2^{(u+2)}\,\mathcal{E}_m\,(g)_{p,\mu}\quad(2.4)$$

$$\leq d_{36}(\beta,t)\,m^{\beta}\,\mathcal{E}_m\,(g)_{p,\mu}.$$

By (2.1) we get

$$\left\|\sum_{c=u+2}^{\infty}\left[W_{2^{c+2}}\,g^{(\beta)}-W_{2^c}\,g^{(\beta)}\right]\right\|_{p,\mu}$$

$$\leq d_{37}(\beta,t)\left\|\sum_{c=u+2}^{\infty}\left|\sum_{|n|=2^c+1}^{2^{c+1}}((jn)_{p,\mu})^{\beta}\;d_n\;e^{jny}\right|^2\right\|_{p,\mu`}$$

And

$$\left\| \sum_{c=u+2}^{\infty} \left[W_{2^{c+2}} g^{(\beta)} - W_{2^c} g^{(\beta)} \right] \right\|_{p,\mu}$$

$$\leq d_{38}(\beta, t) \left(\sum_{c=u+2}^{\infty} \left\| \sum_{|n|=2^c+1}^{2^{c+1}} ((jn)_{p,\mu})^{\beta} d_n e^{jny} \right\|_{p,\mu}^{\frac{1}{i}} \right).$$

We put

$$\|Q_n^*\|_{p,\mu} := \sum_{|n|=2^c+1}^{2^{c+1}} ((jn)_{p,\mu})^{\beta} d_n e^{jny} = \sum_{n=2^c+1}^{2^{c+1}} n^{\beta} 2 Re(d_n e^{j(ny+\beta\pi/2)})$$

And we have

$$\|Q_n^*\|_{p,\mu} := \left\| \sum_{n=2^c+1}^{2^{c+1}} n^{\beta} H_n(y) \right\|_{p,\mu}$$

Such that $H_n(y = 2 Re(d_n e^{j(ny+\beta\pi/2)})$.Using Abel's transformation we get

$$\|Q_n^*\|_{p,\mu} \leq \sum_{n=2^c+1}^{2^{c+1}-1} |n^{\beta} - (n+1)^{\beta}| \left\| \sum_{\ell=2^c+1}^{n} H_{\ell}(y) \right\|_{p,\mu}$$

$$+ |(2^{c+1})^{\beta}| \left\| \sum_{\ell=2^c+1}^{2^{c+1}-1} H_{\ell}(y) \right\|_{p,\mu}$$

$2^c + 1 \leq n \leq 2^{c+1} \quad (c \in \mathbb{N})$ *we have*

$$\left\| \sum_{\ell=\ 2^c+1}^{n} H_\ell\,(y) \right\|_{p\,,\mu} \leq d_{39}\,(\beta\,,t)\ \mathcal{E}_{2^c}\ (g)_{p\,,\mu}$$

Since

$$(\mathrm{n}+1)^{\beta} - \mathrm{n}^{\beta} \leq \begin{cases} \beta\ (\mathrm{n}+1)^{\beta-1} & ,\beta \geq 1\,, \\ \beta\,\mathrm{n}^{\beta-1} & ,0 \leq \beta < 1\,, \end{cases}$$

Then

$$\|Q_n^*\|_{p\,,\mu} \leq d_{40}\,(\beta\,,t)\,2^{c\,\beta}\ \mathcal{E}_{\ 2^{c-1}}\ (g)_{p\,,\mu}\,.$$

Also

$$\left\| \sum_{c\ =\ u+2}^{\infty} \left[W_{2^{c}+1}\ g^{(\beta)} - W_{2^c}\ g^{(\beta)} \right] \right\|_{p\,,\mu}$$

$$\leq\ d_{41}\,(\beta\,,t) \left\{ \sum_{c=\ u+2}^{\infty} 2^{c\,\beta\,i}\ \ \mathcal{E}^{i}_{2^n-1}\ (g)_{p\,,\mu} \right\}^{\frac{1}{i}}$$

$$\leq\ d_{42}\,(\beta\,,t)\ \left\{ \sum_{c=\ u+2}^{\infty} n^{i\,\beta-1}\ \ \mathcal{E}^{i}_{n}\ (g)_{p\,,\mu} \right\}^{\frac{1}{i}}$$

Corollary 3.4 If

$s\,,\ell\ \in\ \mathbb{R}^{+}\,,\ s < \ell\ and$

$0 < \mathrm{x} \leq \frac{1}{2}$, then *there is* a positive constant d_9 depending only on $s\,,\ell\ and\ t$

Such that

$$\jmath_s\,(g\,,x)_{t\,(.)\,,\varphi} \leq \mathrm{d}_9\,x^s \left\{ \int_x^1 \left[\frac{\jmath_\ell\,(g\,,\ h)_{t\,(.)\,,\varphi}}{h^s} \right]^i \ \frac{dh}{h} \right\}^{\frac{1}{i}}$$

Corollary 3.5 Under theoretical conditions **Theorem 3.1,** then *there is* a positive constant d_{11} depending only on s , β *and* t

Such that

$$\jmath_s \left(g^{(\beta)} , \frac{1}{m} \right)_{p,\mu} \leq \mathrm{d}_{11} \left(\frac{1}{m^s} \left(\sum_{n=1}^{m} n^{i(s+\beta)-1} \ \mathcal{E}_c^i (g)_{p,\mu} \right)^{\frac{1}{i}} + \left(\sum_{n=m+1}^{m} n^{\beta i - 1} \ \mathcal{E}_c^i (g)_{p,\mu} \right)^{\frac{1}{i}} \right)$$

For $m \in \mathbb{N}$ *and* $\beta , s \in \mathbb{R}^+$

References

[1] P. H¨ast¨o and L. Diening, Muckenhoupt weights in variable exponent spaces, Preprint, Albert Ludwings Universit¨at Freiburg, Mathematische Fakult¨at,(2014) http://www.helsinki.fi/˜ pharjule/varsob/publications.shtml.

[2] V. Kokilashvili and S.G. Samko, Singular integrals weighted Lebesgue spaces with variable exponent, Georgian M. J. 10 (2003), No:1, 145-156.

[3] V. Kokilashvili and Y.E. Yildirir, On the approximation in weighted Lebesgue spaces, Proc. A. Razmadze Math. Inst. 143 (2007), 103-113.

[4] V. Kokilashvili and Y.E. Yildirir, On the approximation in weighted Lebesgue spaces, Proc. A. Razmadze Math. Inst. 143 (2007), 103-113.

[5] R. Akgun and D.M. Israfilov, Approximation and moduli of fractional orders in Smirnov- Orlicz classes, Glas. Mat. Ser. III 43(63) (2008), no. 1, 121-136.

[6] --, A refined inverse inequality of approximation in weighted variable exponent Lebesgue spaces, Proc. A. Razmadze Math. Inst. 151 (2009), 134-138

[7] --, Operators of Harmonis Analysis in weighted spaces with non-standard growth, J. Math. Anal. Appl. 352 (2009), 15-34.

[8] --, Sharp Jackson and converse theorems of trigonometric approximation in weighted Lebesgue spaces, Proc. A. Razmadze Math. Inst. 152 (2010), 1-18.

Reliability Single Stress-Strength Model Estimation Using Exponential T-X (Fréchet)Family Distributions

Doaa khairi hamad [1] and Feras Sh. M. Batah [2]

[1,2] Anbar University, Education Collage for Pure Science, Mathematical Department, Iraq

Reliability Single Stress-Strength Model Estimation Using Exponential T-X (Fréchet)Family Distributions

Doaa khairi hamad [1] and Feras Sh. M. Batah [2]

[1,2] Anbar University, Education Collage for Pure Science, Mathematical Department, Iraq
https://orcid.org/0000-0003-1254-3080
dua21u2004@uoanbar.edu.iq
ferashaker2001@uoanbar.edu.iq

Abstract. The reliability of the single and parameter estimate $R_{single} = p[t < u]$ arrangement in the stress-strength model, which has strength (t) according to a stress (u), provided our inspiration for writing this paper. They follow the Exp. T – X Fréchet distribution m(σ,α,β). Numerous estimate methods are reviewed and proposed in this paper. To compare these methods, three metrics Bias, MSE, and MAPE were employed. This paper's conclusions are derived from an analysis of real data collected by Monte Carlo simulation.

Keywords: Exp. T – X distribution, Fréchet distribution, Reliability, Estimation methods, Stress – strength model.

1. INTRODUCTION

In practical domains such as risk management, economic, financial, and actuarial sciences, statistical distributions are widely used in data modeling. However, the presumptive probability model of the phenomenon under study ultimately determines how well the techniques work. Insurance losses in applied areas are typically positive, right-skewed, unimodal, and have substantial tails (see [9]). Actuaries typically search for distributions with a high tail in order to accurately assess the level of business risk involved. The distributions with greater right tail probabilities than exponential ones are known as heavy-tailed distributions [8][9]. Numerous scientific and engineering applications make use of the stress-strength (S.S) example.[14] The Fréchet distribution undergoes transformed through Fréchet distribution with three-parameter used data modeling applications from the fields of engineering and medicine. Here, we present the exponential T-X (ETX) Fréchet family[6], a family of distributions. When modeling heavy-tailed data, the suggested model is incredibly adaptable. Following are some of the statistical properties of (ETX) Fréchet distribution, including the probability density (pdf), cumulative distribution (cdf), reliability (R),the hazard (H), the first raw moment (m_1) functions, respectively, as : (see figure 1and 2) [11][12]

$$m(x,\sigma,\alpha,\beta) = \frac{\sigma(\sigma-1)\alpha\beta^{\alpha}x^{\alpha-1}e^{-(x\beta)^{\alpha}}}{(\sigma-1+e^{-(x\beta)^{\alpha}})^2} \qquad x>0 \qquad (1)$$

$$M(x,\sigma,\alpha,\beta) = 1-\left(\frac{\sigma e^{-(x\beta)^{\alpha}}}{\sigma-1+e^{-(x\beta)^{\alpha}}}\right) \qquad x\geq 0 \qquad (2)$$

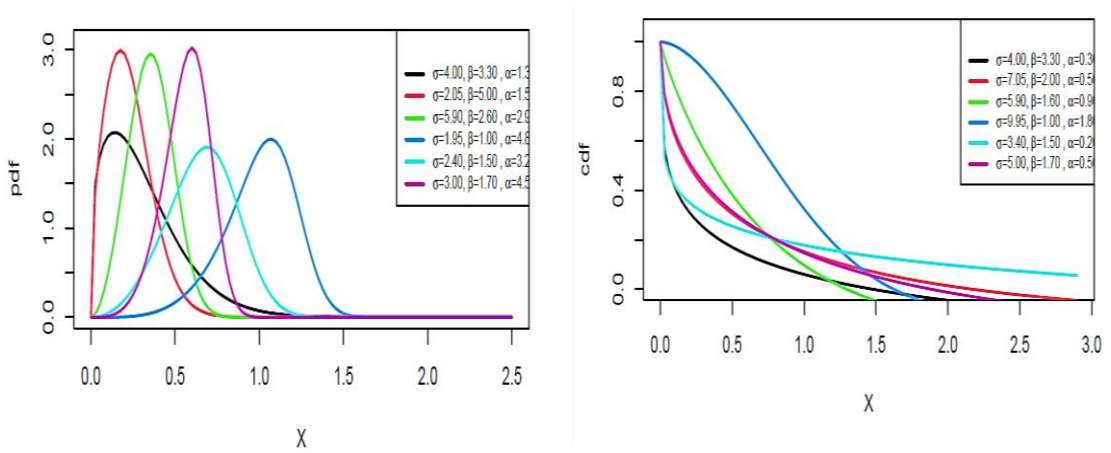

Figure 1: pdf and cdf functions for a ETX (Fréchet) distribution and different value of parameters.

$$R(x) = \frac{\sigma e^{-(x\beta)^{\alpha}}}{\sigma - 1 + e^{-(x\beta)^{\alpha}}} \qquad (3)$$

$$H(x) = \frac{(\sigma - 1)\alpha\beta^{\alpha}x^{\alpha-1}}{\sigma - 1 + e^{-(x\beta)^{\alpha}}} \qquad (4)$$

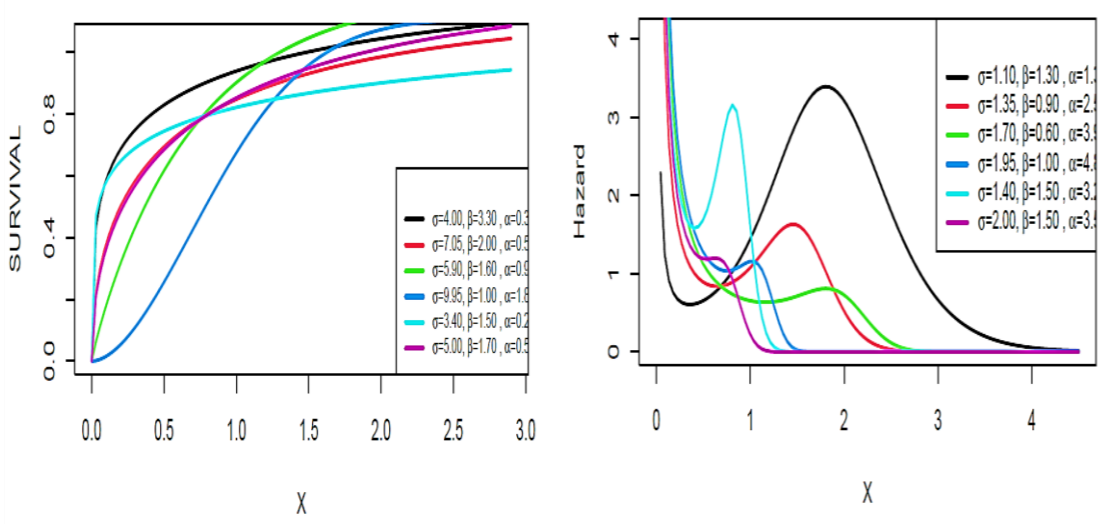

Figure 2: Reliability and hazard functions for a ETX (Fréchet) distribution and different value of parameters.

$$m_1 = \frac{\sigma((\log(4 - 4\sigma) + \log\sigma) + \log(2\sigma - 1))}{\alpha\beta}. \qquad (5)$$

Where σ, α are shape parameters, and β is scale parameter. The paper aims to find a single stress strength model for T-X family statistical distribution. We derived from the family of the exponential distribution and the baseline Fréchet distribution. In addition to conduct simulations for different values of parameters and with different sample sizes. The paper consists of four sections. The second section consisted of finding the stress and strength

model for the ETX (Fréchet) distribution. The third section contained estimating the distribution parameters using eight different methods. The fourth section consisted of a Monte Carlo simulation of the distribution. The fourth and the final section contained the most important conclusions that we reached during the paper.

2. The Proposed model (a single reliability model).

Let u be the stress and t be the strength independent random variables. We used the ETX (Fréchet) distribution to derive the stress strength for single reliability as:

$$R_{single} = p[t < u] = \int_0^{\infty} \int_0^{t} m(u)\, m(t)\, dudt \qquad (6)$$

$$= \int_0^{\infty} \int_0^{t} \frac{\sigma(\sigma-1)\alpha_1\beta^{\alpha_1}u^{\alpha_1-1}e^{-(\beta u)^{\alpha_1}}\sigma(\sigma-1)\alpha_2\beta^{\alpha_2}t^{\alpha_2-1}e^{-(\beta t)^{\alpha_2}}}{(\sigma-1+e^{-(\beta u)^{\alpha_1}})^2(\sigma-1+e^{-(\beta t)^{\alpha_2}})^2} dudt$$

$$R_{single} = \frac{\sum_{j=0}^{\infty}\sum_{z=1}^{\infty}\frac{z}{\sigma^z}\binom{z-1}{j}(-1)^j(\sigma-1)\alpha\beta^{\alpha}}{\alpha_1(i+1)\beta^{\alpha_1}}$$

$$- \frac{\sum_{j=0}^{\infty}\sum_{z=1}^{\infty}\frac{z}{\sigma^z}\binom{z-1}{j}(-1)^j(\sigma-1)\alpha\beta^{\alpha}\sum_{z=0}^{\infty}\sum_{j=0}^{\infty}\sum_{0}^{\infty}\binom{z}{j}\frac{(-1)^{z+j+k}}{\sigma^z}}{(i+1)\alpha_1\beta^{\frac{1}{\alpha_1}+1}}$$

$$\cdot\sum_{n=0}^{\infty}\frac{(-1)^n}{n!}\Gamma\left(\frac{\alpha_2}{\alpha_1}n+1\right). \text{ for } \quad z = 1, 2, \ldots. \qquad (7)$$

3. Methods of estimation.

In this section, we derived eight estimation methods such as (Maximum likelihood, Exact estimators of moment, Percentile, Approximate least squares, Weighted least squares, and three shrinkage) methods as follows:

3.1.Maximum likelihood Estimator (mle) [3][4] .

The process of estimation in this way can be defined as making parameter values of a function where have a great values as possible. It is characterized by efficiency, adequacy, stability and consistency, in addition to its lack of bias. if $t_1, t_2, \ldots t_n$ are random variables (stress) have probability density function of a distribution ETX (Fréchet). The following formula is the likelihood function, denoted by $L(\theta, t)$ as follows

$$L(\theta, t) = \prod_{i=1}^{n} \frac{\sigma(\sigma-1)\alpha\beta^{\alpha}t_i^{\alpha-1}e^{-(\beta t_i)^{\alpha}}}{(\sigma-1+e^{-(\beta t_i)^{\alpha}})^2}. \qquad (8)$$

Where θ are the distribution parameters(σ,α,β), then take the nutural logarthim to the equation (8) as

$$L = nlog(\sigma) + nlog(\sigma-1) - nlog(\alpha) - nalog(\beta) + (\alpha-1)\sum_{i=1}^{n} logt_i - \sum_{i=1}^{n}(\beta t_i)^{\alpha}$$
$$- 2\sum_{i=1}^{n} log\left(\sigma - 1 + e^{-(\beta t_i)^{\alpha}}\right). \qquad (9)$$

To find the (β, σ, and α) estimators by taking the partial derivative of equation (9) with respect to (β, σ, and α) respectively as follows:

$$\frac{\partial L}{\partial \beta} = \frac{n\alpha}{\beta} - \sum_{i=1}^{n} \alpha t_i^{\alpha}\beta^{\alpha-1} + 2\sum_{i=1}^{n}\frac{\alpha e^{-(\beta t_i)^{\alpha}}t_i^{\alpha}\beta^{\alpha-1}}{\sigma-1+e^{-(\beta t_i)^{\alpha}}}, \qquad (10)$$

with respect to σ

$$\frac{\partial L}{\partial \sigma} = \frac{n}{\sigma} + \frac{n}{\sigma - 1} - 2\sum_{i=1}^{n} \frac{1}{\sigma - 1 + e^{-(\beta t_i)^{\alpha}}} \qquad (11)$$

and with respect to α

$$\frac{\partial L}{\partial \alpha} = \frac{n}{\alpha} - n\log(\beta) + \sum_{i=1}^{n} \log t_i - \sum_{i=1}^{n} (\beta t_i)^{\alpha} \log(\beta t_i) + 2\sum_{i=1}^{n} \frac{e^{-(\beta t_i)^{\alpha}} \log(\beta t_i)\,(\beta t_i)^{\alpha}}{\sigma - 1 + e^{-(\beta t_i)^{\alpha}}}. \qquad (12)$$

Similirty , when $u_1, u_2, \ldots, u_m$ be a random sample from the strength u which is distributed as ETX(Fréchet), when σ, β is known and shape parameter α unknown. The method for the mle strength is presented by

$$\frac{\partial L}{\partial \beta} = \frac{n\alpha}{\beta} - \sum_{i=1}^{n} \alpha u_i^{\alpha} \beta^{\alpha - 1} + 2\sum_{i=1}^{n} \frac{\alpha e^{-(\beta u_i)^{\alpha}} t_i^{\alpha} \beta^{\alpha - 1}}{\sigma - 1 + e^{-(\beta u_i)^{\alpha}}},$$

$$\frac{\partial L}{\partial \sigma} = \frac{n}{\sigma} + \frac{n}{\sigma - 1} - 2\sum_{i=1}^{n} \frac{1}{\sigma - 1 + e^{-(\beta u_i)^{\alpha}}},$$

$$\frac{\partial L}{\partial \alpha} = \frac{n}{\alpha} - n\log(\beta) + \sum_{i=1}^{n} \log u_i - \sum_{i=1}^{n} (\beta u_i)^{\alpha} \log(\beta u_i) + 2\sum_{i=1}^{n} \frac{e^{-(\beta u_i)^{\alpha}} \log(\beta u_i)\,(\beta u_i)^{\alpha}}{\sigma - 1 + e^{-(\beta u_i)^{\alpha}}},$$

There is no exact formula to estimate the parameters of EXT(Fréchet) distribution. However, we can estimate them by nonlinear numerical analysis methods.

3.2. The Precise Estimators of Moments Method (PEMM) . [1] [15]

We suggest the expected value $E(r)$, the variance $var(r)$ and coefficient of variation $cv(r)$ for a ETX (Fréchet) distribution's as follows:

$$E(r) = \frac{\varphi\Gamma\left(\frac{1}{\alpha} + 1\right)}{\alpha(i+1)^{\frac{1}{\alpha}+1}\beta^{1+\alpha}}, \qquad \text{for } \alpha, \beta > 0 \qquad (13)$$

$$var(r) = \frac{\varphi\Gamma\left(\frac{2}{\alpha} + 1\right)}{\alpha(i+1)^{\frac{2}{\alpha}+1}\beta^{2+\alpha}} - \left(\frac{\varphi\Gamma\left(\frac{1}{\alpha} + 1\right)}{\alpha(i+1)^{\frac{1}{\alpha}+1}\beta^{1+\alpha}}\right)^2 \qquad (14)$$

$$cv(r) = \frac{\sqrt{var}}{\mu_1} = \frac{\sqrt{\frac{\varphi\Gamma\left(\frac{2}{\alpha} + 1\right)}{\alpha(i+1)^{\frac{2}{\alpha}+1}\beta^{2+\alpha}} - \left(\frac{\varphi\Gamma\left(\frac{1}{\alpha} + 1\right)}{\alpha(i+1)^{\frac{1}{\alpha}+1}\beta^{1+\alpha}}\right)^2}}{\frac{\varphi\Gamma\left(\frac{1}{\alpha} + 1\right)}{\alpha(i+1)^{\frac{1}{\alpha}+1}\beta^{1+\alpha}}}. \qquad (15)$$

Then the PEMM is given below:

$$\alpha_{1PEMM} = \frac{\sqrt{\frac{\varphi\Gamma\left(\frac{2}{\alpha_{01}}+1\right)}{\alpha_{01}(i+1)^{\frac{2}{\alpha_{01}}+1}\beta^{2+\alpha_{01}}} - \left(\frac{\varphi\Gamma\left(\frac{1}{\alpha_{01}}+1\right)}{\alpha_{01}(i+1)^{\frac{1}{\alpha_{01}}+1}\beta^{1+\alpha_{01}}}\right)^2}}{\frac{\varphi\Gamma\left(\frac{1}{\alpha_{01}}+1\right)}{\alpha_{01}(i+1)^{\frac{1}{\alpha_{01}}+1}\beta^{1+\alpha_{01}}}} \quad (16)$$

$$\alpha_{2PEMM} = \frac{\sqrt{\frac{\varphi\Gamma\left(\frac{2}{\alpha_{02}}+1\right)}{\alpha_{02}(i+1)^{\frac{2}{\alpha_{02}}+1}\beta^{2+\alpha_{02}}} - \left(\frac{\varphi\Gamma\left(\frac{1}{\alpha_{02}}+1\right)}{\alpha_{02}(i+1)^{\frac{1}{\alpha_{02}}+1}\beta^{1+\alpha_{02}}}\right)^2}}{\frac{\varphi\Gamma\left(\frac{1}{\alpha_{02}}+1\right)}{\alpha_{02}(i+1)^{\frac{1}{\alpha_{02}}+1}\beta^{1+\alpha_{02}}}} \quad (17)$$

3.3.The Percentile Estimator. (prec) [16]

Using the graphical approximation to the best linear unbiased estimators, Kao (1959) first investigated this strategy, by a straight line between the theoretical points derived from the distribution function and the sample percentile points, one may obtain the estimators. When dealing with a ETX (Fréchet) distribution, one might apply the same. idea to get the estimators of and based on percentiles due to the distribution function's structure.[10]

$var_1 = \sum_{i=1}^{n}(M(t_i) - q_i)^2$ and $var_2 = \sum_{j=1}^{m}\left(M(u_j) - q_j\right)^2$,where $q_i = \frac{i}{n+i}, q_j = \frac{j}{m+j}$ then,

$$\hat{\alpha}_{1\text{Pres}} = \sum_{i=1}^{n} \frac{\ln[-\ln[\sigma - \sigma(1-q_i) + (1-q_i)] - \ln(1-q_i+\sigma)]}{2\ln\beta t_i} \quad (18)$$

$$\hat{\alpha}_{2\text{Pres}} = \sum_{i=1}^{n} \frac{\ln[-\ln[\sigma - \sigma(1-q_i) + (1-q_i)] - \ln(1-q_i+\sigma)]}{2\ln\beta u_i} \quad (19)$$

3.4.The Approximate Least Squares Estimator (alst)

Approximated least squares technique estimators can be made by reducing the sum of square error between the value and its expected value. Among the most efficient and well-liked techniques, the LS approach is widely used to fit models and solve mathematical and engineering problems, particularly in linear and non-linear situations. [7].

$$Q_1(\theta, t) = \sum_{i=1}^{n}(M(t_i) - \frac{i}{n+1})^2 \ , \qquad \forall \text{ i} = 1,2,\ldots,\text{n}$$

$$\frac{\partial Q_1}{\partial \sigma} = \sum_{i=1}^{n}(1 - \frac{\sigma e^{-(t\beta)^{\alpha}}}{(\sigma - 1 + e^{-(t\beta)^{\alpha}})} - \frac{i}{n+1})\frac{e^{-(t\beta)^{\alpha}}\left(1 - e^{-(t\beta)^{\alpha}}\right)}{(\sigma - 1 + e^{-(t\beta)^{\alpha}})^2}). \quad (20)$$

$$\frac{\partial Q_1}{\partial \beta} = \sum_{i=1}^{n}\left(1 - \frac{\sigma e^{-(t\beta)^{\alpha}}}{(\sigma - 1 + e^{-(t\beta)^{\alpha}})} - \frac{i}{n+1}\right) * \left(\frac{\left(\alpha\sigma t e^{-(t\beta)^{\alpha}}\right)(t\beta)^{\alpha-1}(\sigma-1)}{(\sigma - 1 + e^{-(t\beta)^{\alpha}})^2}\right). \quad (21)$$

$$\frac{\partial Q_1}{\partial \alpha} = \sum_{i=1}^{n}\left(1 - \frac{\sigma e^{-(t\beta)^{\alpha}}}{(\sigma - 1 + e^{-(t\beta)^{\alpha}})} - \frac{i}{n+1}\right) \frac{\left(1 - e^{-(t\beta)^{\alpha}}\right)(\sigma - 1)((t\beta)^{\alpha}(\ln t\beta)e^{-(x\beta)^{\alpha}}}{(\sigma - 1 + e^{-(t\beta)^{\alpha}})^2}). \quad (22)$$

when $u_1, u_2, \ldots, u_m$ be a random sample from the strength u which is distributed as ETX(Fréchet), when σ, β is known and shape parameter α is unknown . The alst method for the strength u is presented by

$$Q_2(\theta, u) = \sum_{j=1}^{m}\left(M(u_i) - \frac{j}{n+1}\right)^2, \qquad \forall j = 1,2,\ldots,m$$

$$\frac{\partial Q_2}{\partial \sigma} = \sum_{j=1}^{m}\left(1 - \frac{\sigma e^{-(u\beta)^{\alpha}}}{(\sigma - 1 + e^{-(u\beta)^{\alpha}})} - \frac{j}{n+1}\right) \frac{e^{-(u\beta)^{\alpha}}\left(1 - e^{-(u\beta)^{\alpha}}\right)}{(\sigma - 1 + e^{-(u\beta)^{\alpha}})^2}). \quad (23)$$

$$\frac{\partial Q_2}{\partial \beta} = \sum_{i=1}^{m}\left(1 - \frac{\sigma e^{-(u\beta)^{\alpha}}}{(\sigma - 1 + e^{-(u\beta)^{\alpha}})} - \frac{j}{n+1}\right) * \left(\frac{(\alpha\sigma u)(u\beta)^{\alpha-1}(\sigma-1)}{(\sigma - 1 + e^{-(u\beta)^{\alpha}})^2}\right). \quad (24)$$

$$\frac{\partial Q_2}{\partial \alpha} = \sum_{j=1}^{m}\left(1 - \frac{\sigma e^{-(u\beta)^{\alpha}}}{(\sigma - 1 + e^{-(u\beta)^{\alpha}})} - \frac{j}{n+1}\right) * \left(\frac{\left(1 - e^{-(u\beta)^{\alpha}}\right)(\sigma - 1)((u\beta)^{\alpha}(\ln u\beta)e^{-(u\beta)^{\alpha}}}{(\sigma - 1 + e^{-(u\beta)^{\alpha}})^2}\right). \quad (25)$$

3.5. The weighted least squares estimator (wls).

The weighted least squares estimator of ETX (Fréchet) distribution These can be acquired by reducing as follows:

$$W_1(\theta, t) = \sum_{i=1}^{n} \frac{(n+1)^2(n+2)}{i(n-i+1)}\left(M(t_i) - \frac{i}{n+1}\right)^2. \quad (26)$$

$$\frac{\partial W_1}{\partial \sigma} = \sum_{i=1}^{n}\left(1 - \frac{\sigma e^{-(t\beta)^{\alpha}}}{(\sigma - 1 + e^{-(t\beta)^{\alpha}})} - \frac{i}{n+1}\right).\frac{(n+1)^2(n+2)}{i(n-i+1)}.\left(\frac{e^{-(t\beta)^{\alpha}}\left(1 - e^{-(t\beta)^{\alpha}}\right)}{(\sigma - 1 + e^{-(t\beta)^{\alpha}})^2}\right), \quad (27)$$

$$\frac{\partial W_1}{\partial \beta} = \sum_{i=1}^{n}\left(1 - \frac{\sigma e^{-(t\beta)^{\alpha}}}{(\sigma - 1 + e^{-(t\beta)^{\alpha}})} - \frac{i}{n+1}\right).\frac{(n+1)^2(n+2)}{i(n-i+1)}\left(\frac{\left(\alpha\sigma t e^{-(t\beta)^{\alpha}}\right)(t\beta)^{\alpha-1}(\sigma-1)}{(\sigma - 1 + e^{-(t\beta)^{\alpha}})^2}\right). \quad (28)$$

$$\frac{\partial W_1}{\partial \alpha} = \sum_{i=1}^{n}\left(1 - \frac{\sigma e^{-(t\beta)^{\alpha}}}{(\sigma - 1 + e^{-(t\beta)^{\alpha}})} - \frac{i}{n+1}\right).\frac{(n+1)^2(n+2)}{i(n-i+1)}\left(\frac{\left(1 - e^{-(t\beta)^{\alpha}}\right)(\sigma-1)((t\beta)^{\alpha}(\ln t\beta)e^{-(t\beta)^{\alpha}}}{(\sigma - 1 + e^{-(t\beta)^{\alpha}})^2}\right). \quad (29)$$

In the same way, the wls method for the strength is presented by

$$W_2(\theta, u) = \sum_{j=1}^{m} \frac{(m+1)^2(m+2)}{j(m-j+1)}\left(M(u_j) - \frac{j}{m+1}\right)^2. \quad (30)$$

$$\frac{\partial W_2}{\partial \sigma} = \sum_{j=1}^{m}\left(1 - \frac{\sigma e^{-(u\beta)^{\alpha}}}{(\sigma - 1 + e^{-(u\beta)^{\alpha}})} - \frac{j}{m+1}\right).\frac{(m+1)^2(m+2)}{j(m-i+1)}.\left(\frac{e^{-(u\beta)^{\alpha}}\left(1 - e^{-(u\beta)^{\alpha}}\right)}{(\sigma - 1 + e^{-(u\beta)^{\alpha}})^2}\right) \quad (31)$$

$$\frac{\partial W_2}{\partial \beta} = \sum_{j=1}^{m}\left(1 - \frac{\sigma e^{-(u\beta)^{\alpha}}}{(\sigma - 1 + e^{-(u\beta)^{\alpha}})} - \frac{j}{m+1}\right)\left(\frac{(m+1)^2(m+2)}{j(m-j+1)}\right).\left(\frac{\left(\alpha\sigma u e^{-(u\beta)^{\alpha}}\right)(u\beta)^{\alpha-1}(\sigma-1)}{(\sigma - 1 + e^{-(u\beta)^{\alpha}})^2}\right). \quad (32)$$

$$\frac{\partial W_2}{\partial \alpha} = \sum_{j=1}^{m}\left(1 - \frac{\sigma e^{-(u\beta)^{\alpha}}}{(\sigma - 1 + e^{-(u\beta)^{\alpha}})} - \frac{j}{m+1}\right).\frac{(m+1)^2(m+2)}{j(m-j+1)} * \left(\frac{\left(1 - e^{-(u\beta)^{\alpha}}\right)(\sigma-1)((u\beta)^{\alpha}(\ln u\beta)e^{-(u\beta)^{\alpha}}}{(\sigma - 1 + e^{-(u\beta)^{\alpha}})^2}\right). \quad (33)$$

3.6. The Method for Estimating Shrinkage (shr) [5] [17]

The shrinkage estimation method can be conceptualized as a Bayesian approach that depends on prior information. Thompson in (1968) has suggested the problem of shrink an unbiased estimator and he presented the primary reasons for using earlier estimates [4]. The parameter was used as an initial value α_0, where $[\alpha_0 = \alpha_0 \pm \epsilon]$, $\epsilon = 0.001$, in the shrinkage estimation approach. The normal estimator ($\hat{\alpha}_{MLE}$) was then applied to them using a shrinkage weight factor $\Omega(\alpha)$, $0 < \Omega(\alpha) \leq 1$, which may be expressed as:

$$\widehat{\alpha_{1_{sh}}} = \psi(\hat{\alpha})\hat{\alpha}_{MLE} + \left(1 - \psi(\hat{\alpha})\right)\hat{\alpha}_0 . \quad (34)$$

3.6.1. The Weight-Based Shrinkage Function (shr1).[13]

We shall examine the weight reduction function. The function form in this subsection is represented by $\Omega(\hat{\alpha}) = \left[\frac{\tan n}{n}\right]$, where $\hat{\alpha}$ represents the sample size and n represents the number of participants. The value of $\Omega(\hat{\alpha})$ is between 0 and 1. Using the given expressions $\Omega(\hat{\alpha}_1) = \left[\frac{\tan n}{n}\right]$ and $\Omega(\hat{\alpha}_2) = \left[\frac{\tan m}{m}\right]$, where n and m represent number of particioants (the sample sizes of u and t) respectively, the shrinkage estimator utilizes the $\hat{\alpha}_1$ and $\hat{\alpha}_2$ shrinkage weight functions described in equation (34).

$$\widehat{\alpha_{1_{shr1}}} = \left|\frac{\tan n}{n}\right| \hat{\alpha}_{1_{MLE}} + \left(1 - \left|\frac{\tan n}{n}\right|\right)\hat{\alpha}_{1_0} \quad (35)$$

$$\widehat{\alpha_{2_{shr1}}} = \left|\frac{\tan m}{m}\right| \hat{\alpha}_{2_{MLE}} + \left(1 - \left|\frac{\tan m}{m}\right|\right)\hat{\alpha}_{2_0} \quad (36)$$

Now, from equations (35), and (36) were used to get the single stress strength relaibility formula as follows

$$\hat{R}_{Shr1} = 1 - \sum_{f=0}^{\infty} \frac{(-1)^f}{f!}\Gamma\left(\frac{\widehat{\alpha_{1_{shr1}}}}{\widehat{\alpha_{2_{shr1}}}}f + 1\right) \quad (37)$$

3.6.2 The Constant Shrinkage Estimate(shr2).[13].

In the scenario, there is a constant shrinkage factor, we can suppose that $\Omega(\hat{\alpha}) = \left|\frac{\tan n}{n}\right| = 0.001$, and has a value between 0 and 1 where , n refer to the sample size.

In order to obtain the constant shrinkage estimators, we substitute $\hat{\alpha}_1$ and $\hat{\alpha}_2$ into equation (34) by taking the forms below as $\Omega(\hat{\alpha}_1) = \left|\frac{\tan n}{n}\right|$, and $\Omega(\hat{\alpha}_2) = \left|\frac{\tan m}{m}\right|$, $0 \leq \Omega(\hat{\alpha}_i) \leq 1$. as shown:

$$\widehat{\alpha_{1_{shr1}}} = \Omega(\hat{\alpha}_1)\hat{\alpha}_{1_{MLE}} + \left(1 - \Omega(\hat{\alpha}_1)\right)\hat{\alpha}_{1_0} \quad (38)$$

and

$$\widehat{\alpha_{2_{shr1}}} = \Omega(\hat{\alpha}_2)\hat{\alpha}_{2_{MLE}} + \left(1 - \Omega(\hat{\alpha}_2)\right)\hat{\alpha}_{2_0} \quad (39).$$

Here, we substuted by $\widehat{\alpha_{1_{shr1}}} = 0.001\hat{\alpha}_{1_{MLE}} + 0.999\hat{\alpha}_{1_0}$ and $\widehat{\alpha_{2_{shr1}}} = 0.001\hat{\alpha}_{2_{MLE}} + 0.999\hat{\alpha}_{2_0}$. Therefore, from equations (38), and (39) to get the single relability as follows:

$$\hat{R}_{Shr2} = 1 - \sum_{f=0}^{\infty} \frac{(-1)^f}{f!} \Gamma\left(\frac{\widehat{\alpha_{1_{shr2}}}}{\widehat{\alpha_{2_{shr2}}}} f + 1\right) \qquad (40)$$

3.6.3 The Shrinkage function (shr3).[4]

In this part, the shrinkage weight factor is determined by the sizes g and h. Specifically, we define $\Omega(\hat{\alpha}_1)$ as e^{-g} and $\Omega(\hat{\alpha}_2)$ as e^{-g}, where $\Omega(\hat{\alpha})$ is a function that satisfies $0 \leq \Omega(\hat{\alpha}) < 1$. Hence, the shrinkage estimator employs the shrinkage function of $\hat{\alpha}_1$ and $\hat{\alpha}_2$, as defined in equation (34) below:

$$\widehat{\alpha_{1_{shr3}}} = e^{-g}\hat{\alpha}_{1_{MLE}} + (1 - e^{-g})\hat{\alpha}_{1_0} \qquad (41)$$

and

$$\widehat{\alpha_{2_{shr3}}} = e^{-h}\hat{\alpha}_{2_{MLE}} + (1 - e^{-h})\hat{\alpha}_{2_0} \qquad (42)$$

Now, in which equations (41), and (42) were used to get

$$\hat{R}_{Shr3} = 1 - \sum_{f=0}^{\infty} \frac{(-1)^f}{f!} \Gamma\left(\frac{\widehat{\alpha_{1_{shr3}}}}{\widehat{\alpha_{2_{shr3}}}} f + 1\right) \qquad (43)$$

4. The simulation.

The Monte Carlo simulation was employed to validate the effectiveness of the proposed estimate approach for assessing the reliability of a single component system. [2] The eight proposed estimate methods are implemented using various sample sizes (25, 50, 75, 100). The statistical results for each sample are determined using bias, mean absolute percentage error, and mean squared error criteria, with 1000 repeats. Hence, the subsequent procedures elucidate the Monte Carlo simulations for each model.

Step 1: To determine the performance, begin by initializing and generating random samples that adhere to a continuous uniform distribution within the range of 0 to 1. The distribution U is a uniform distribution with a range from 0 to 1.

Step 2: Convert the given uniform random sample into a random sample of the power Fréchet distribution by utilising the cumulative distribution function.

Step 3: Calculate the estimated parameters of the 8 method mentioned as in section 2.

Step 4: The estimated reliability of stress-strength models using various estimating methods, such as $\hat{R}_{MLE}, \hat{R}_{Pres}, \hat{R}_{alst}, \hat{R}_{wls}, \hat{R}_{Shr1}, \hat{R}_{Shr2}, \hat{R}_{Shr3},$, and $\hat{R}_{PEMM}$, have been calculated in section 2. The reliability of estimation is explained by the findings in Tables 1, 3, and 5. On the other hand, the results in Tables 2, 4, and 6 demonstrate the comparison between these approaches when biassed MSE and MAPE criteria are utilised. Nevertheless, all estimators rely on the values of the sample size.

Table 1 : $R = 0.9973695, \sigma = 0.2 ; \beta = 0.7 ; \alpha_1 = 2; \alpha_2 = 1$

n ,m	$\bar{R}_{MLE}$	$\bar{R}_{Prec}$	$\bar{R}_{alst}$	$\bar{R}_{wls}$	$\bar{R}_{Slr1}$	$\bar{R}_{Slr2}$	$\bar{R}_{Slr3}$	$\bar{R}_{PEMM^*}$
25,25	0.9954028	0.9884392	0.9886431	0.9884258	0.9883402	0.9883279	0.9883297	0.9898492
25,50	0.9955645	0.98843528	0.9887909	0.9884218	0.9883475	0.9883318	0.9883297	0.9903102
25,75	0.9955544	0.98833736	0.9890803	0.9883400	0.9883400	0.9883255	0.9883297	0.9902962
25,100	0.9954077	0.9883614	0.9891485	0.9883478	0.9883959	0.9883392	0.9883297	0.9902216
50,25	0.9942659	0.9884850	0.9884850	0.9884718	0.9883313	0.9883298	0.9883297	0.9887191
50,50	0.9923691	0.9882344	0.9886239	0.9882205	0.9883323	0.9883302	0.9883297	0.9885987
50,75	0.9951661	0.9883673	0.9886011	0.9883537	0.9883414	0.9883284	0.9883297	0.9893366
50,100	0.9926940	0.9881839	0.9887758	0.9881699	0.9883417	0.9883300	0.9883297	0.9889866
75,25	-5.447361	0.9883762	0.9880236	0.9883627	0.9882569	0.9883163	0.9883297	0.9881923
75,50	0.9950735	0.9883237	0.9883594	0.9883100	0.9883782	0.9883350	0.9883297	0.9885378
75,75	0.9902873	0.9883806	0.9883417	0.9883671	0.9883321	0.9883302	0.9883297	0.9886158
75,100	0.9901972	0.9883844	0.9883743	0.9883709	0.9883329	0.9883303	0.9883297	0.9887106
100,25	0.9851628	0.9883954	0.9878708	0.9883819	0.9883151	0.9883270	0.9883297	0.9876542
100,50	0.9872024	0.9883604	0.9882654	0.9883468	0.9883129	0.9883265	0.9883297	0.9881602
100,75	0.9886783	0.9883304	0.9883209	0.9883168	0.9883249	0.9883288	0.9883297	0.9883116
100,100	0.9899873	0.9883544	0.9884088	0.9883408	0.9883308	0.9883299	0.9883297	0.9885465

Table2 : $R = 0.997369 , \sigma = 0.2 ; \beta = 0.7 ; \alpha_1 = 2; \alpha_2 = 1$

n ,m	Criteria	$\bar{R}_{MLE}$	$\bar{R}_{Pres}$	$\bar{R}_{alst}$	$\bar{R}_{wls}$	$\bar{R}_{Slr1}$	$\bar{R}_{Slr2}$	$\bar{R}_{Slr3}$	$\bar{R}_{PEMM^*}$	Finest
25,25	Baise	2.0318909	2.0318859	2.0320898	2.0318725	2.0317870	2.0317747	2.0317765	2.0332959	$\bar{R}^*_{Slr2}$
	MSES	4.1569083	4.1285606	4.1293891	4.1285062	4.1281584	4.1281085	4.1281157	4.1342924	$\bar{R}^*_{Slr2}$
	Map	1.9539565	1.9472828	1.9474782	1.9472700	1.9471880	1.9471762	1.9471779	1.9486341	$\bar{R}^*_{Slr2}$
25,50	Baise	2.0390113	2.0318820	2.0322377	2.0322377	2.0318686	2.0317785	2.0317765	2.0337569	$\bar{R}^*_{Slr3}$
	MSES	4.1575677	4.1285445	4.1299901	4.1299901	4.1284900	4.1281240	4.1281157	4.1361675	$\bar{R}^*_{Slr3}$
	Map	1.9541115	1.9472790	1.9476199	1.9476199	1.9472662	1.9471799	1.9471779	1.9490759	$\bar{R}^*_{Slr3}$

25,75	Baise	2.0390011	2.0317841	2.0325271	2.0317704	2.0317868	2.0317722	2.0317765	2.0337430	R^{*}_{wls}
	MSES	4.1575269	4.1281466	4.1311665	4.1280912	4.1281577	4.1280985	4.1281157	4.1361107	R^{*}_{wls}
	Map	1.9541017	1.9471852	1.9478973	1.9471721	1.9471878	1.9471739	1.9471779	1.9490625	R^{*}_{wls}
25,100	Baise	2.0388544	2.0318081	2.0325952	2.0317946	2.0318426	2.0317860	2.0317765	2.0336684	R^{*}_{Shr3}
	MSES	4.1569291	4.1282445	4.1314435	4.1281893	4.1283847	4.1281545	4.1281157	4.1358072	R^{*}_{Shr3}
	Map	1.9539612	1.9472083	1.9479626	1.9471953	1.9472414	1.9471871	1.9471779	1.9489910	R^{*}_{Shr3}
50,25	Baise	2.0377126	2.0319318	2.0314562	2.0319185	2.0317780	2.0317766	2.0317765	2.0321658	R_{aLst}
	MSES	4.1522741	4.1287470	1.9468710	4.1286929	4.1281222	4.1281162	4.1281157	4.1296981	R^{*}_{Shr3}
	Map	1.9528669	1.9473268	1.9468710	1.9473140	1.9471794	1.9471780	1.9471779	1.9475511	R^{*}_{Shr3}
50,50	Baise	2.0358158	2.0316812	2.0320706	2.0316673	2.0317791	2.0317769	2.0317765	2.0320454	R^{*}_{wls}
	MSES	4.1445482	4.1277285	4.1293112	4.1276721	4.1281263	4.1281175	4.1281157	1.9474357	R^{*}_{Shr3}
	Map	1.9510491	1.9470866	1.9474598	1.9470733	1.9471804	1.9471783	1.9471779	1.9474357	R^{*}_{Shr3}
50,75	Baise	2.0386128	2.0318140	2.0320478	2.0318005	2.0317881	2.0317751	2.0317765	2.0327833	R^{*}_{Shr2}
	MSES	4.1559454	4.1282685	4.1292185	4.1282133	4.1281630	4.1281102	4.1281157	4.1322083	R^{*}_{Shr2}
	Map	1.9537296	1.9472139	1.9474380	1.9472009	1.9471891	1.9471766	1.9471779	1.9481429	R^{*}_{Shr2}
50,100	Baise	2.0361408	2.0316307	2.0322226	2.0316167	2.0317884	2.0317768	2.0317765	2.0324333	R^{*}_{wls}
	MSES	4.1458760	4.1275233	4.1299287	4.1274664	4.1281643	4.1281170	4.1281157	4.1307856	R^{*}_{wls}
	Map	1.9513605	1.9470382	1.9476054	1.9470248	1.9471894	1.9471782	1.9471779	1.9478074	R^{*}_{wls}
75,25	Baise	0.0440391	2.0318230	2.0314703	2.0318094	2.0317037	2.0317630	2.0317765	2.0316391	R^{*}_{aLst}
	MSES	2.0984883	4.1283048	4.1268719	4.1282497	4.1278199	4.1280612	4.1281157	4.1275575	R_{MLE}
	Map	0.0717377	1.9472225	1.9468845	1.9472095	1.9471081	1.9471651	1.9471779	1.9470463	R_{MLE}
75,50	Baise	2.0385202	2.0317704	2.0318061	2.0317568	2.0318249	2.0317817	2.0317765	2.0319845	R^{*}_{wls}
	MSES	4.1555687	4.1280913	4.1282363	4.1280358	4.1283126	4.1281372	4.1281157	4.1289614	R^{*}_{wls}
	Map	1.9536409	1.9471722	1.9472063	1.9471591	1.9472244	1.9471830	1.9471779	1.9473773	R^{*}_{wls}
75,75	Baise	2.0337340	2.0318274	2.0317885	2.0318138	2.0317789	2.0317769	2.0317765	2.0320625	R^{*}_{Shr3}
	MSES	4.1360749	4.1283226	4.1281645	4.1282676	4.1281256	4.1281176	4.1281157	4.1292782	R^{*}_{Shr3}
	Map	1.9490540	1.9472267	1.9471894	1.9472137	1.9471803	1.9471784	1.9471779	1.9474521	R^{*}_{Shr3}
75,1	Baise	2.0336439	2.0318312	2.0318211	2.0318177	2.0317796	2.0317770	2.0317765	2.0321574	R^{*}_{Shr3}

00	MSES	4.1357079	4.1283381	4.1282971	4.1282832	4.1281287	4.1281181	4.1281157	4.1296638	$\hat{R}_{Shr3}$
	Map	1.9489676	1.9472304	1.9472207	1.9472174	1.9471810	1.9471785	1.9471779	1.9475430	$\hat{R}_{Shr3}$
100, 25	Baise	2.0286095	2.0318422	2.0313175	2.0318287	2.0317619	2.0317738	2.0317765	2.0311009	$\hat{R}_{MLE}$
	MSE	4.1152671	4.1283827	4.1262511	4.1283279	4.1280565	4.1281047	4.1281157	4.1253713	$\hat{R}_{MLE}$
	Mape	1.9441429	1.9472409	1.9467381	1.9472279	1.9471640	1.9471753	1.9471779	1.9465305	$\hat{R}_{MLE}$
100, 50	Baise	2.0306491	2.0318072	2.0317122	2.0317936	2.0317596	2.0317733	2.0317765	2.0316070	$\hat{R}_{MLE}$
	MSE	4.1235373	4.1282405	4.1278545	4.1281853	4.1280473	4.1281028	4.1281157	4.1274272	$\hat{R}_{MLE}$
	Map	1.9460975	1.9472074	1.9471163	1.9471943	1.9471618	1.9471749	1.9471779	1.9470155	$\hat{R}_{MLE}$
100, 75	Baise	2.0321250	2.0317772	2.0317677	2.0317635	2.0317716	2.0317755	2.0317765	2.0317583	$\hat{R}_{PEMM}$
	MSES	4.1295325	4.1281186	4.1280801	4.1280631	4.1280961	4.1281120	4.1281157	4.1280420	$\hat{R}_{PEMM}$
	Map	1.9475120	1.9471786	1.9471695	1.9471655	1.9471733	1.9471770	1.9471779	1.9471605	$\hat{R}_{PEMM}$
100, 100	Baise	2.0334341	2.0318011	2.0318556	2.0317875	2.0317775	2.0317767	2.0317765	2.0319933	$\hat{R}_{Shr3}$
	MSES	4.1348543	4.1282160	4.1284372	4.1281607	4.1281199	4.1281165	4.1281157	4.1289968	$\hat{R}_{Shr3}$
	Map	1.9487665	1.9472016	1.9472537	1.9471885	1.9471789	1.9471781	1.9471779	1.9473857	$\hat{R}_{Shr3}$

Table 3: $R = 4.6092809\ , \sigma = 4\ ; \beta = 2\ ; \alpha_1 = 2;\ \alpha_2 = 3$

n ,m	$\hat{R}_{max}$	$\hat{R}_{Prec}$	$\hat{R}_{alst}$	$\hat{R}_{wlse}$	$\hat{R}_{Shr1}$	$\hat{R}_{Shr2}$	$\hat{R}_{Shr3}$	$\hat{R}_{Em}$
25,25	0.6355840	0.9608324	0.9608149	0.9608321	0.9608350	0.9608332	0.9608338	0.9605842
25,50	0.9134389	0.9608309	0.9608147	0.9608314	0.9607615	0.9608343	0.9608338	0.9602425
25,75	0.9125204	0.9608359	0.9607999	0.9608361	0.9606346	0.9608335	0.9608338	0.9604520
25,100	0.9178498	0.9608334	0.9607775	0.9608339	0.9608106	0.9608337	0.9608338	0.9603778
50,25	0.9159595	0.9608279	0.9608187	0.9608270	0.9608374	0.9608348	0.9608338	0.9608113
50,50	0.9273577	0.9608356	0.9608369	0.9608351	0.9608319	0.9608333	0.9608338	0.9608116
50,75	0.9246708	0.9608369	0.9608362	0.9608368	0.9608328	0.9608344	0.9608338	0.9608165
50,100	0.9170091	0.9608374	0.9608330	0.9608373	0.9596853	0.9608346	0.9608338	0.9607846
75,25	0.9455679	0.9608241	0.9607747	0.9608231	0.9608366	0.9608344	0.9608338	0.9607029
75,50	0.9608354	0.9608345	0.9608349	0.9608006	0.9608006	0.9608343	0.9608338	0.9608208
75,75	0.9211503	0.9608356	0.9608365	0.9608352	0.9608363	0.9608336	0.9608338	0.9608311
75,100	0.9189571	0.9608357	0.9608363	0.9608353	0.9608341	0.9608335	0.9608338	0.9608315

100,25	0.9096935	0.9608241	0.9607970	0.9608230	0.9608205	0.9608358	0.9608338	0.9606625
100,50	0.9553279	0.9608324	0.9608313	0.9608317	0.9608336	0.9608338	0.9608338	0.9608213
100,75	0.9209811	0.9608330	0.9608322	0.9608324	0.9608369	0.9608348	0.9608338	0.9608351
100,100	0.9273271	0.9608325	0.9608331	0.9608318	0.9608353	0.9608340	0.9608338	0.9608222

Table 4: $R = 4.6092809 , \sigma = 4 ; \beta = 2 ; \alpha_1 = 2; \alpha_2 = 3$

n ,m	Criteria	$\bar{R}_{MLE}$	$\bar{R}_{Prec}$	$\bar{R}_{alst}$	$\bar{R}_{wls}$	$\bar{R}_{Shr1}$	$\bar{R}_{Shr2}$	$\bar{R}_{Shr3}$	$\bar{R}_{PEMM}$	Finest
25,25	Baise	3.7236968-	3.3984489-	3.3984659	3.3984487-	-3.3984458	-3.3984476	-3.3984470	-3.3986966	$\bar{R}_{MLE}$
	MSES	98.643629	11.549452	11.549570	11.549453	11.549434	11.549446	11.549442	11.551139	$\bar{R}_{PEMM}$
	Map	0.8541998	0.7795892	0.7795932	0.7795892	0.7795886	0.7795890	0.7795889	0.7796461	$\bar{R}_{Shr1}$
25,50	Baise	3.4458419-	3.3984499-	3.3984661-	3.3984494-	3.3985193-	3.3984465-	3.3984470-	3.3990383-	$\bar{R}_{MLE}$
	MSES	12.533945	11.549462	11.549572	11.549458	11.549933	11.549439	11.549442	11.553615	$\bar{R}_{Shr2}$
	Map	0.7993959	0.7795895	0.7795932	0.7795894	0.7796054	0.7795888	0.7795889	0.7797245	$\bar{R}_{Shr2}$
25,75	Baise	-3.4467604	-3.3984449	-3.3984809	3.3984447-	-3.3986462	-3.3984474	-3.3984470	-3.3988288	$\bar{R}_{MLE}$
	MSES	11.903523	11.549427	11.549672	11.549426	11.550796	11.549444	11.549442	11.552037	$\bar{R}_{Shr1}$
	Map	0.790671	0.7795884	0.7795966	0.7795883	0.7796346	0.7795889	0.7795889	0.7796764	$\bar{R}_{wls}$
25,100	Baise	-3.4414310	-3.3984474	-3.3985033	-3.3984469	-3.3984702	-3.3984471	-3.3984470	-3.3989030	$\bar{R}_{MLE}$
	MSES	11.8434812	11.5494452	11.5498250	11.5494417	11.549600	11.5494431	11.5494424	11.5525422	$\bar{R}_{wls}$
	Map	0.7894492	0.7795890	0.7796018	0.7795888	0.7795942	0.7795889	0.7795889	0.7796935	$\bar{R}_{wls}$
50,25	Baise	-3.4433213	-3.3984529	-3.3984621	-3.3984538	-3.3984434	-3.3984460	-3.3984470	-3.3984695	$\bar{R}_{MLE}$
	MSES	11.8566433	11.5494826	11.5495450	11.5494887	11.549417	11.5494354	11.5494424	11.5495955	$\bar{R}_{Shr1}$
	Map	0.78988288	0.77959027	0.77959237	0.77959047	0.7795880	0.77958867	0.77958891	0.77959408	$\bar{R}_{Shr1}$
50,50	Baise	-3.4319231	3.3984452-	-3.3984439	3.3984457-	-3.3984489	-3.3984475	-3.3984470	3.3984692	$\bar{R}_{MLE}$
	MSES	11.7796620	11.5494303	11.5494210	11.5494333	11.5494552	11.5494456	11.5494424	11.5495932	$\bar{R}_{alst}$
	Map	0.7872681	0.7795885	0.7795881	0.7795886	0.7795893	0.7795890	0.7795889	0.7795940	$\bar{R}_{alst}$
50,75	Baise	-3.4346100	3.3984439-	3.3984446-	3.3984440-	3.3984480-	3.3984464-	3.3984470-	3.3984643-	$\bar{R}_{MLE}$
	MSES	11.7966173	11.5494213	11.5494260	11.5494216	11.5494491	11.549438	11.5494424	11.5495599	$\bar{R}_{Pres}$

	Map	0.7878845	0.7795882	0.7795883	0.7795882	0.7795891	0.7795887	0.7795889	0.779592	$\ddot{R}_{Pres}$
50,100	Baise	3.4422717-	3.3984434-	3.3984478-	3.3984435-	3.3995955-	3.3984462-	3.3984470-	3.3984962-	$\ddot{R}_{MLE}$
	MSES	11.8492474	11.5494176	11.5494479	11.5494182	11.5572552	11.5494368	11.5494424	11.5497767	$\ddot{R}_{Pres}$
	Map	0.7896421	0.7795880	0.7795891	0.7795880	0.7798523	0.7795887	0.7795889	0.7796001	$\ddot{R}_{Pres}$
75,25	Baise	11.5495079	11.5498440	11.5495149	11.5494231	11.5494379	11.5494424	11.5503319	11.5503319	$\ddot{R}_{wls}$
	MSES	0.7795911	0.7796024	0.7795913	0.7795882	0.7795887	0.7795889	0.7796189	0.7796189	$\ddot{R}_{wls}$
	Map	3.4405100-	3.3984454-	3.3984468-	3.3984475-	3.3986033-	3.3984446-	3.3984470-	3.3984526-	$\ddot{R}_{MLE}$
75,50	Baise	11.8371533	11.5494316	11.5494413	11.5494455	11.5505047	11.5494258	11.5494424	11.5494802	$\ddot{R}_{Slr2}$
	MSES	0.7892379	0.7795885	0.7795888	0.7795890	0.7796247	0.7795883	0.7795889	0.7795901	$\ddot{R}_{Slr2}$
	Map	3.4381305-	3.3984452-	3.3984443-	3.3984456-	3.3984445-	3.3984472-	3.3984470-	3.3984497-	$\ddot{R}_{MLE}$
75,75	Baise	11.8207942	11.5494301	11.5494237	11.5494330	11.5494256	11.5494440	11.5494424	11.5494608	$\ddot{R}_{aLst}$
	MSES	0.7886921	0.7795885	0.7795882	0.7795885	0.7795883	0.7795889	0.7795889	0.7795895	$\ddot{R}_{aLst}$
	Map	-3.4403237	-3.3984451	-3.3984445	-3.3984455	-3.3984467	-3.3984473	-3.3984470	-3.3984493	$\ddot{R}_{MLE}$
75,100	Baise	11.8358614	11.5494295	11.5494250	11.5494323	11.5494406	11.5494441	11.5494424	11.5494580	$\ddot{R}_{aLst}$
	MSES	0.7891952	0.7795884	0.7795883	0.7795885	0.7795888	0.7795889	0.7795889	0.7795894	$\ddot{R}_{aLst}$
	Map	-3.4134258	3.3984621-	-3.3984977	-3.3984634	-3.3984638	-3.3984490	-3.3984470	-3.3985290	$\ddot{R}_{MLE}$
100,25	Bais	11.6517511	11.5495448	11.5497866	11.5495537	11.5495567	11.5494559	11.5494424	11.5499997	$\ddot{R}_{Slr3}$
	MSE	0.7830249	0.7795923	0.7796005	0.7795926	0.7795927	0.7795893	0.7795889	0.7796077	$\ddot{R}_{Slr3}$
	Mape	-3.4039529	3.3984484-	-3.3984495	-3.3984491	-3.3984472	-3.3984470	-3.39844706688121	-3.3984595	$\ddot{R}_{MLE}$
100,50	Baise	11.5882587	11.5494519	11.5494596	11.5494565	11.5494436	11.5494426	11.5494424	11.5495277	$\ddot{R}_{Slr3}$
	MSE	0.7808519	0.7795892	0.7795894	0.7795893	0.7795889	0.7795889	0.7795889	0.7795917	$\ddot{R}_{Slr3}$
	Map	-3.4382997	-3.3984478	-3.3984486	-3.3984484	-3.3984439	-3.3984460	-3.3984470	-3.3984457	$\ddot{R}_{MLE}$
100,75	Bais	11.8220771	11.5494474	11.5494533	11.5494519	11.5494214	11.5494352	11.5494424	11.5494336	$\ddot{R}_{Slr1}$

	MSES	0.7887309	0.7795890	0.7795892	0.7795892	0.7795882	0.7795886	0.7795889	0.7795886	$\bar{R}_{Shr1}$
	Map	-3.4319537	-3.3984483	-3.3984477	-3.3984490	-3.3984455	-3.3984468	-3.3984470	-3.3984586	$\bar{R}_{MLE}$
100,100	Baise	11.7784328	11.5494513	11.5494468	11.5494559	11.5494319	11.5494410	11.5494424	11.5495212	$\bar{R}_{Shr2}$
	MSES	0.7872751	0.7795892	0.7795890	0.7795893	0.7795885	0.7795888	0.7795889	0.7795915	$\bar{R}_{Shr1}$
	Map	11.5495079	11.5498440	11.5495149	11.5494231	11.5494379	11.5494424	11.5503319	11.5503319	$\bar{R}_{wls}$

5. The Conclusions

In this work, simulation were conducted for different values of parameters , and in Tables (1-4) for random data, two cases were set for the values of α_1 and α_2 when $\alpha_1$is greater than α_2 and vice versa, we conclude the following:

1- The MSE value decreases with increasing sample size (n, m) for all the factors mentioned below.

2- When the value of α decreases, the estimated stability value decreases.

3- When $\alpha_1 > \alpha_2$, the (Sh3) method is the best.

4- When $\alpha_1 < \alpha_2$, the estimation methods alternate with each other depending on the sample

Size.but the best methods are (Sh3, MLE, LSE, WLS), respectively.

References.

[1] Abid , S. The fréchet stress-strength model "International Journal of Applied MathematicalResearch, International Journal of Applied Mathematical Research, 3(3): 207-213,2014.

[2] Bader, M. and Priest, A. Statistical Aspects of Fibre and Bundle Strength in Hybrid Composites, Progress in Science and Engineering of Composites, ICCM-IV, Tokyo, 1129-1136, 1982.

[3] Abdalrazaq, A.S. and Batah, F.S.M. (2022). Maximum Likelihood Estimates and a survival function for fuzzy data for the Weibull-Pareto parameters. *Journal of Physics: Conference Series*, 2322(1), 012022.

[4] Batah, F. and Abdulrazaq, A. On Estimation of Hazard, Survival and Density Functions for Weibull Pareto Distribution by Ranking Algorithm. In 5th International Conference on Engineering Technology and its Applications (IICETA), IEEE, 97 – 101. (2022).

[5] Batah, F.S.M. (2023). Some methods of estimating the hazard function of exponentiated Q-exponential distribution. AIP Conference Proceedings, 2820, 040008

[6] Batah, F.S.M and Jalal, M.S. A general class of some inverted distributions. Bayesian Estimation for the Stress Strength Reliability Exponentiated q-Exponential Distribution based on Singly Type II Censoring Data. Pakistan Journal of Statistics, 38(4), 399 – 429, (2022).

[7] Batah, F.S.M. and Abdulrazaq, A.S. On Estimation of Hazard, Survival and Density Functions for Weibull Pareto Distribution by Ranking Algorithm. In 5 th International Conference on Engineering Technology and its Applications (IICETA), IEEE, 97 – 101. (2022).

[8] Jalal, M.S. and Batah, F.Sh.M. Reliability of Stress-Strength and Its Estimation of Exponentiated Q-Exponential Distribution. Iraqi Journal of Science, 64(3): 1299-1306. (2023).

[9] Bhat, A.A.& Ahmad, S. P., "A New Generalization of Rayleigh Distribution: Properties and Applications", Pakistan Journal of Statistics, 36(3):.225 – 250, (2020).

[10] Dey, S., Dey, T. & Kundu, D., "Two-parameter Rayleigh distribution: Different methods of estimation", American Journal of Mathematical and Management Sciences, 33, 55 – 74, (2014).

[11] Haddad, E., & Batah, F., On Estimating Reliability of a Stress – Strength Model in Case of Rayleigh Pareto Distribution". Iraqi Journal of Science, 62(12): 4847 – 4858, (2021).

[12] Hamad, D. and Batah, F. An investigation into the Exponential T-X Family Distributions to Simulation study AICCONF 24, May 25–26, 2024, İstanbul, Turkiye, ACM ISBN 979-8-4007-1692-8/24/05. https://doi.org/10.1145/3660853.3660897.
[13] Hassan, A. & Basheikh,H., Estimation of Reliability in Multicomponent Stress – strength Model Following Exponentiated Pareto Distribution , The Egyptian Statistical Journal, Institute Of Statistical Studies & Research, Cairo University, vol.56(2): 82 – 95, (2012).
[14] Jasim, .A.J. and Batah, F.S.M. (2023). On the Estimation of Stress-Strength Model Reliability Parameter of Power Rayleigh Distribution. Iraqi Journal of Science, 2023, 64(2), 809-822.
[15] Kalaf , B. A., Batah, F. Sh. M and Salman, A. N., (2024). Employing Meta-Heuristic Algorithm for Estimating the Survival Function of Inverse Kumaraswamy Distribution. Pakistan Journal of Statistics, 40(2):151 – 162. (2024).
[16] Kao , J., "computer methods for estimating Weibull parameters in reliability studies, transaction of IRE- Reliability and Quality control, 13, 15 – 22, (1958).
[17] Salman .A & Hamad .A, estimating the shape parameter for power function distribution through shrinkage technique, *International Journal of science and research* , 78(96): 1316 – 1319, (2015).

Disinfectant-Induced Surface Changes in Injectable Denture Base Polymer

Ali Saad Ahmed [1]

1* Department of Prosthodontics, College of dentistry, Tikrit University, Tikrit, Iraq

ali.s.ahmed@tu.edu.iq

Ahmed Ammer Ibraheem [2]

2* Department of Oral and Maxillofacial Surgery, College of dentistry, Tikrit University, Tikrit, Iraq

ahmedameribraheem@tu.edu.iq

Rusul Saad Ahmed [3]

3* Department of Pedodontics, College of dentistry, Tikrit University, Tikrit, Iraq

Rusul.s.ahmed23@tu.edu.iq

Saif Saad Kamil [4]

4* Department of Conservative Dentistry, College of dentistry, Tikrit University, Tikrit, Iraq

Saif1990@tu.edu.iq

Disinfectant-Induced Surface Changes in Injectable Denture Base Polymer

Ali Saad Ahmed [1]

1* Department of Prosthodontics, College of dentistry, Tikrit University, Tikrit, Iraq

ali.s.ahmed@tu.edu.iq

Ahmed Ammer Ibraheem [2]

ahmedameribraheem@tu.edu.iq

2* Department of Oral and Maxillofacial Surgery, College of dentistry, Tikrit University, Tikrit, Iraq

Rusul Saad Ahmed [3]

3* Department of Pedodontics, College of dentistry, Tikrit University, Tikrit, Iraq

Rusul.s.ahmed23@tu.edu.iq

Saif Saad Kamil [4]

4* Department of Conservative Dentistry, College of dentistry, Tikrit University, Tikrit, Iraq

Saif1990@tu.edu.iq

Abstract

Introduction:

A variety of challenges confront dentists, including the requirement for optimal materials to successfully provide dental care to their patients. To create functional prosthetics with pleasing aesthetics, these materials need to be biologically compatible, cost-effective, easy to manipulate using controlled technological processes, and readily usable. Within the realm of removable prosthodontics, a multitude of tools and versatile materials are utilized, but they present difficulties in terms of sterilization and cleaning. Prostheses, impressions, and stone casts are examples of such items that increase the likelihood of cross-contamination occurrence among dental clinics and laboratories.

Materials and methods: Polycarbonate and polyamide specimens were immersed in Sodium Hypochlorite (NaOCl) and chlorhexidine solutions at concentrations (0.5% and 2% respectively). In total, 60 specimens were prepared and divided into 3 groups, a control group, 2% chlorhexidine group, and 0.5% NaOCl group. 30 specimens for each of the materials. 10 specimens for each test (Hardness and roughness). The specimens were immersed in the disinfection solutions for five minutes, three times a day, for 12 days. One way ANOVA was utilized for each material followed by independent t test to compare between polycarbonate and polyamide.

Results: The results revealed a significant decrease in hardness of both polycarbonate and polyamide after immersion, while surface roughness was increased.

Conclusions: It was concluded that the immersion of polycarbonate and polyamide in 0.5% sodium hypochlorite and 2% Chlorhexidine solutions can alter surface properties of the injectable denture base materials.

1. Introduction

Numerous materials are employed in the construction of dentures, and each of these materials has an impact on the dimensions of the denture base during fabrication, as well as

various factors relevant to clinical utilization. These elements include stability, support, retention, adaptability, resistance to impact, texture of the surface, and additional aspects. Denture base materials are categorized into various categories and groups depending on their manufacturing method, chemical structure, and processing techniques.

Some thermoplastic polymers like PMMA can be processed by different processing technique such as compression molded and injected molded technique. However, the compression molding of PMMA is the most widely used technique to produce acrylic denture base but change in dimension and shrinkage of the denture base throughout the polymerization, and the presence of residual monomer are the main limitations of this technique. Regarding the fact that the qualities of the denture can be altered not only by the material type used to produce the denture, but also affected by the processing techniques selected, new processing technique were developed to overcome the limitation in conventional compression molded technique such as injected molded technique to improve dentures' efficiency and properties **[1].**

Since its introduction in 1937, polymethyl methacrylate has remained the most widely favored material for denture fabrication. In recent years, thermoplastic materials crafted through injection molding techniques had become popular for denture base fabrication due to their favorable qualities, which include having a higher degree of flexibility than heat-polymerizing base resins and the ability to help retain dentures by making use of the undercuts present in the design of the denture base around abutment teeth. **[2]**

In the 1950s, polyamide emerged as a suggested material for denture base construction **[3]**. Polyamide is a crystalline polymer, whereas PMMA is amorphous. The crystalline nature of polyamide contributes to its resistance to solvents, along with its notable attributes of elevated heat resistance and strong durability. However, this material is not without challenges. Issues such as water absorption, surface roughness, susceptibility to bacterial presence, warping, fading color, and challenges in achieving a polished finish have been reported **[4].**

Crafted from high-quality lightweight plastic, polycarbonate is an amorphous polymer that displays occasional crystalline regions **[5].** Its translucent nature is coupled with exceptional mechanical properties, including remarkable resistance to impacts and structural stability. However, polycarbonate does come with certain property-related drawbacks. These

include low tolerance to chemicals, restricted ability to withstand scratches, and a responsiveness to ultraviolet (UV) rays that initiates alterations in color. **[6].**

The ideal denture base material should be able to withstand masticatory forces, be easy to handle and disinfect, and be biocompatible with oral tissues **[7,8].** For individuals utilizing fixed and partial removable dentures, ensuring denture hygiene, and preserving the well-being of oral mucosa holds significant importance. **[9].** Disinfection involves the application of chemical agents to eliminate or eradicate potentially infectious organisms, and this category encompasses heat-based techniques as well. Various mechanical and chemical methods have been employed to cleanse and disinfect the surfaces of dentures, removing accumulated microorganisms. 0.5% Sodium hypochlorite (NaOCl), 2% chlorhexidine, and denture brushing are among the chemicals utilized for this purpose. Nevertheless, these measures have proven to have adverse effects on the structural integrity of the denture foundation. Sodium hypochlorite is an excellent disinfectant with excellent cleaning properties. The effectiveness of sodium hypochlorite in cleaning and disinfection operations is controlled by the amount of accessible chlorine and the pH of the disinfectant solution **[10].**

2% Chlorhexidine has become one of the best studied antimicrobial agents in recent years. It is the antiseptic of choice for dental biofilm control, and it is important in the prevention of dental caries, gingivitis, and stomatitis. It is also recommended for antisepsis of the hands **[11]**

2. Materials and methods

2.1 Materials used in the study

1. Polycarbonate (Extra rigid polymer M10 XR, Deflex, Argentina. (Figure 2-1B).
2. Polyamide injectable material (Sabilex, Argentina).
3. Isodent gypsum separating solution (Spofa Dental Czechoslovakian Europe).
4. Dental stone (Zermach, EXTRA HARD HIGH DENSITY DIESTONE, Spain).
5. Sodium hypochlorite 3% (PREVEST DENPRO, India).
6. Chlorhexidine 2% (CERKAMED Medical co., Poland).

2.2 Specimens grouping

60 specimens were prepared, 30 polyamide (PA) specimens and 30 polycarbonate (PC) specimens. 10 specimens were control kept in distilled water as control, 10 were immersed in NaOCl, and 10 immersed in Chx for each material.

NaOCl 3% was mitigated to 0.5% by the formula: Concentration before Vs Volume before = concentration after Vs Volume after.

2.3 Test specimens' preparation

The acrylic pattern measurements, designed using computer software (Auto CAD, 2015), was subsequently fabricated utilizing a laser cutting machine. A specialized cutting of clear acrylic sheets (Glass-look acrylic, Clairvauxles Lacsrance, France) was performed as bar shaped specimen with dimensions of (65mm x 10 mm x2.5 ± 0.1 mm) length, width, thickness respectively **[12],** used for surface roughness test and Vickers microhardness test **(Figure 1)**.

Figure 1: Plastic pattern cut using CNC.

2.4 Mold preparation for PC and PA

Separating medium was used to cover the pieces of the metallic dental flask, and then a stone mixture was made according to the manufacturer's recommendations, using 100 g/25ml (powder/water) to fill the lower half of the flask. Meanwhile, it was vigorously vibrated to remove air bubbles. The plastic patterns were then put, with care taken not to fully embed the plastic patterns in the dental stone in order to enable their removal after the flasking procedure is completed. Wax tubes (sprue) were affixed to the plastic pattern to facilitate the injection of material **(Figure 2).**

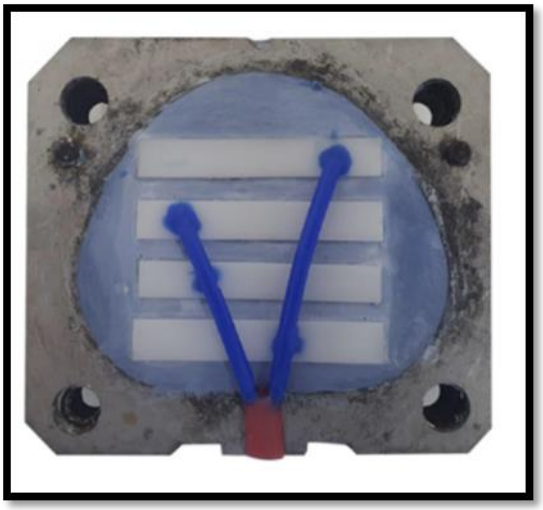

Figure 2: Wax sprue attached.

Both the stone surface and the plastic patterns were covered with separating medium and allowed to dry after the dental stone was fully set. Since assembling the flask's equivalent, the flask was filled by pouring another mix of stone and vibrating it again. The flask's upper lid was mounted, and the flask was tightly clamped until the stone was fully set. Then, the flask placed in boiled water bath for wax elimination.

2.5 Injecting, packing, and finishing of the test specimens.

Polycarbonate and polyamide capsules were placed in the automatic programmable device DEFLEX MAD (for polycarbonate), and Sabelix 2AD (for polyamide), respectively and injected into the flask according to manufacturer's instruction as following:

1. Polycarbonate was injected under pressure (5-7 Bar) and subjected to heat (305°C ± 10°C) for a duration of 15 minutes.
2. Injectable PA was introduced under pressure (5-7 Bar) and exposed to heat (240°C ± 10°C) for 15 minutes. Prior to the injection process, the pressure was verified in accordance with procedural requirements (5-7 bars). Preheating temperature and duration were also scrutinized based on manufacturer's instructions. The appropriate material cartridge for injection was chosen.

The injection process was executed using an automatic programmable device with the

following specifications: digital control, preset programs, user-defined programs, and a pressure gauge (manometer). Before commencing the injection, the pressure for injection was assessed to align with procedural requirements. Similarly, preheating temperature and duration were verified in accordance with the manufacturer's instructions. The appropriate injection material cartridge was selected. To facilitate the process, a Vaseline-based lubricant was applied to the closed end of the cartridge. Subsequently, the cartridge was placed into either of the two heating cylinders, directed towards the flask chamber (Figure 3A). Any excess lubricant on the heating cylinder's edge was removed using absorbent paper. The preheating process was initiated, and an audible signal indicated the end of the preheating duration as chosen.

Once the two halves of the flask were assembled and secured with screws, the flask was positioned within the injecting unit and fixed in place (Figure 3B). The opening of the flask was aligned directly with the cartridge and the heating cylinder. The injection process was initiated by pressing the start key on the control panel, activating the injection procedure.

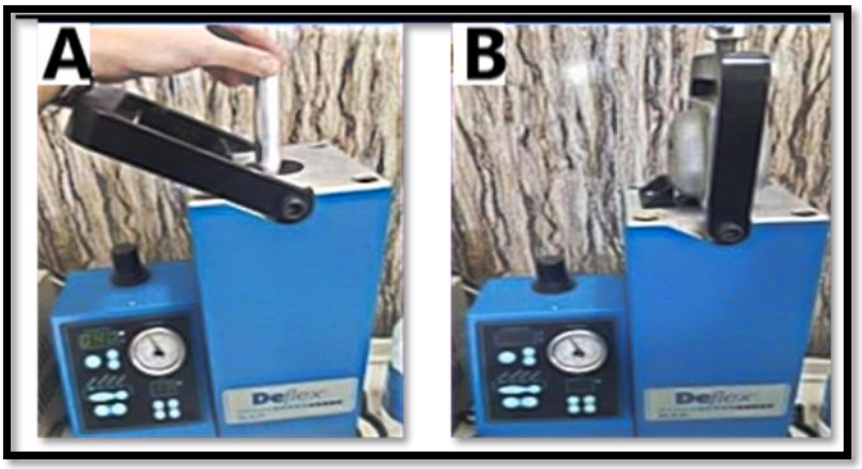

Figure 3: Injection of thermoplastic material; A: Cartilage placed in Automatic programmable device DEFLEX MAD; B: Flask attached to the device DEFLEX MAD.

The setting contraction was compensated for by automatically keeping the pressure constant for (1) minute. The cylinder was then moved about 3 to 4 mm away from the flask so that the cartridge could be separated. Subsequently, the flask was taken out, and the utilized cartridge was automatically released by pressing the evacuation button. To ensure the attainment of optimal material quality, the flask was subjected to gradual cooling over a period

of approximately 8 to 9 hours. Following the cooling process, the screws securing the flask were loosened, and the two halves of the flask were carefully separated. This allowed for the removal of the specimens from the molds (Figure 4).

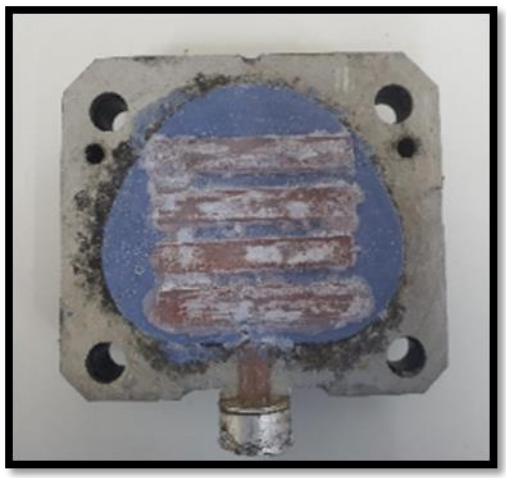

Figure 4: Specimens after de-flasking.

2.6 Finishing and polishing

After the process of removing the specimens from the molds (de-flasking), any excess material was carefully removed to achieve a clean finish. The specimens made from polycarbonate and Polyamide were separated, and the sprue was eliminated using a metal disk for cutting. Subsequently, each individual specimen underwent finishing using specialized plastic burs tailored for this purpose. The removal of excess material was performed with an acrylic bur. Following this, all specimens underwent a finishing process involving sandpaper with a grain size of 120. To prevent overheating, the specimens were periodically cooled by immersing them in a rubber bowl filled with distilled water. This cooling process involved a 15-second interval of finishing followed by a 15-second immersion in water.

The completed specimens of each test group were collected and housed within plastic containers. These containers were filled with distilled water and subsequently placed within an incubator set at 37°C for a period of 48 hours, adhering to the specifications outlined in the ADA 1999 standard [12]. The purpose of this incubation was to eliminate any residual byproducts from the specimens.

2.7 Disinfection procedure

Each specimen will be immersed in the disinfecting solutions for 5 minutes, 30 times a day for 12 days to simulate 1-year interval and after each immersion the specimen will be taken out and rinsed with running water and dried with absorbent paper and the procedure of immersion will be repeated simulating the patient denture cleaning **[9].**

2.8 Vickers hardness and surface roughness tests

The Vickers hardness test was performed with (laryee hvs-5Manufacturing Limited, Beijing, China), specimens were submitted to a 25-g load for 30 second. Three places were utilized on the specimen. One in the center and two on either end. The average of three readings was calculated (Figure 5).

Figure 5: Vickers hardness tester.

Surface roughness test was performed using a profilometer (Figure 6). This tester contains a diamond sensible needle (stylus) used to track the irregularities on the surface. Using a stylus, the surface of the specimen is engaged at three distinct points across its surface to obtain three readings from each specimen. The specimen is positioned on a stable and firm surface, and the stylus is allowed to make contact with the first point. Subsequently, the stylus is moved along the surface for a distance of 11 mm. The readings are automatically displayed

on a digital scale as they are generated. The average of the three readings is then calculated to determine the roughness value of the specimen.

Figure 6: Surface roughness testing Profilometer.

2.9 Statistical analysis

An ANOVA test was used to compare the mean values of the tested groups (one-way analysis of variance). Levene's test was used to assess the homogeneity of variance in each test. To see if there was a significant difference between the groups, Tukey's post-hoc test (multiple comparisons) was used.

3. Results and discussion

3.1 Surface hardness

Hardness refers to a material's capacity to withstand wear and abrasion from adjacent dental structures. It serves as an indicator of a material's resilience and its ability to resist damage. The concept of hardness is frequently employed to investigate various factors that impact the extent of resin conversion. Because of the simplicity of the process, it is possible to characterize the mechanical properties of a polymer. In addition to the availability of the specimen preparation and test procedure equipment **[13].** This experiment used a Vickers microhardness tester, which is appropriate for determining the hardness of denture bases. The Vickers microhardness tester eliminates the problem of elastic recovery due to its design. The application of a technology that directly measures the depth of the loaded indentation by a screen that displays the number of them **[14].**

Following immersion, a statistically significant reduction in surface hardness was observed in both the PC and PA groups when compared to the control groups **(Table 1).** This change can be attributed to the degradation induced by the concentrations of NaOCL and Chx.

Subsequent to immersion, the damage acquired by the material matrix intensifies the mechanism of water transport, thereby increasing water absorption **[15].** The presence of oxygen within carbonate groups (CO3) in PC and PA renders them vulnerable to water absorption. As water molecules accumulate around the polymer chains of PC and PA, the structure of the polymer becomes distorted and more open, leading to an increased free volume. This enhanced diffusion of water molecules into the polymers has a plasticizing effect, gradually relaxing the polymer chains, and consequently causing a decline in hardness **[16,17].**

Table 1: Descriptive statistics, one way ANOVA and Tuckey test of hardness for PC and PA.

Polycarbonate PC			**Post-hoc test**	**Polyamide PA**		
Groups PC	**Mean PC**	**ANOVA**	**P value**	**Groups PA**	**Mean PA**	**ANOVA**
Control (A)	**83.758**	**0.000 H. S**	**A and B 0.025 H. S**	**Control (A)**	**67.860**	**0.801 N.S**
Chx (B)	**82.051**		**A and C 0.000 H. S**	**Chx (B)**	**67.740**	
NaOCl (C)	**80.286**		**B and C 0.020 H. S**	**NaOCl (C)**	**67.660**	
Levene's test P-value: 0.192				**Levene's test P-value: 0.625**		

Independent t test was then conducted to evaluate the differences between the means of the groups (Pc and Pa). There were highly significant differences between all the groups in the study **(Table 2).**

Table 2: Independent T test of hardness test between PC and PA.

Material / Solution	**PC**		**PA**		**P–value**	**Sig.**
	Mean	**S.D.**	**Mean**	**S.D.**		

Distilled	**83.7580**	**1.10368**	**67.8600**	**0.73060**	**0.000**	**H.S.**
Chx	**82.0510**	**1.68362**	**67.7400**	**0.56608**	**0.000**	**H.S.**
NaOCl	**80.2860**	**1.23996**	**67.6600**	**0.71212**	**0.000**	**H.S.**

3.2 Surface roughness

The profilometer device was used in this study which was reported to be an excellent device for studying the surface roughness of restorative materials and giving measurements that can be evaluated and compared. Surface texture plays a crucial role as it can lead to the accumulation of bacteria on uneven denture surfaces, influencing oral well-being **[18].** The coarseness of denture surfaces is influenced by factors such as material properties, polishing methods, and the proficiency of the practitioner **[19].** All resin materials should aim for a smooth, scratch-free surface, because an increase in surface roughness can decrease denture esthetics, while a decrease in surface roughness can improve denture esthetics, Surface roughness helps to prevent bacterial build-up and plaque formation accumulation **[20].**

The results revealed an increase in surface roughness of both PC and PA after the immersion in disinfecting solutions **(Table 3).**

Table 3: Descriptive statistics, one way ANOVA and Tuckey test of roughness for PC and PA.

Polycarbonate			**Post-hoc test**	**Polyamide**		
Groups PC	**Mean PC**	**ANOVA**	**P value**	**Groups PA**	**Mean PA**	**ANOVA**
Control(A)	**3.393**	**0.000 H. S**	**A and B 0.024 H. S**	**Control(A)**	**1.794**	**0.297 N. S**
Chx (B)	**3.559**		**A and C 0.000 H. S**	**Chx (B)**	**1.982**	
NaOCl (C)	**3.794**		**B and C 0.002 H. S**	**NaOCl (C)**	**1.994**	
Levene's test P-value: 0.113				**Levene's test P-value: 0.201**		

The observed increase in surface hardness with the presence of sodium hypochlorite (NaOCl) and chlorhexidine (Chx) can be attributed to their induced increase in hydrophilicity and the presence of ester bonds in the material. Ester bonds are susceptible to degradation by water, particularly under alkaline conditions. This degradation process may involve the hydrolysis of a polyester chain into two sub-chains with carboxyl and hydroxyl terminations **[21].**

Increase the number of the molecular chain per unit cross section and increase in the junction number will cause increase in surface roughness **[21],** this agrees with Wang et al. in 2019 **[23].** An alternative explanation suggests that the observed increase could stem from the phenomenon where a polymer, upon exposure to a solution, undergoes hydrolytic breakdown. This breakdown is a consequence of the chemical interaction occurring between the solution and the organic matrix present within the interstitial spaces between the polymer chains **[24].**

Independent t test was conducted to reveal the differences between PC and PA groups in the immersion solutions, there were highly significant differences between all the groups **(Table 4).**

Table 2: Independent t test between PC and PA.

Material / Solution	PC		PA		P–value	Sig.
	Mean	S.D.	Mean	S.D.		
Distilled	3.392	0.1410	1.794	0.208592	0.000	H.S.
Chx	3.560	0.0939	1.982	0.372922	0.000	H.S.
NaOCl	3.794	0.1570	1.994	0.340424	0.000	H.S.

4. Conclusions

The study highlighted how sodium hypochlorite and chlorhexidine influenced surface hardness and roughness through hydrophilicity and ester bond interactions. This research contributes to our understanding of surface properties in dental materials and their implications for denture aesthetics and hygiene.

Conflict of interest

None

Funding

Self-funded study

References

1. A. Gharechahi, N. Asadzadeh, F. Shahabian, and M. Gharechahi, "Flexural strength of acrylic resin denture bases processed by two different methods," J Dent Res Dent Clin Dent Prospects, vol. 8, no. 3, pp. 148-152, 2014. [Online]. Available: https://doi.org/10.5681/joddd.2014.027

2. B. I. Hamanaka, Y. Takahashi, and H. Shimizu, "Mechanical properties of injection-molded thermoplastic denture base resins," Acta Odontol Scand, vol. 69, no. 2, pp. 75–79, 2010. [Online]. Available: https://doi.org/10.3109/00016357.2010.517557

3. M. Watanabe, "Degradation and formation of bisphenol A in polycarbonate used in dentistry," J Med Dent Sci, vol. 51, no. 1, pp. 1-6, 2004.

4. A. M. Milstone, C. L. Passaretti, and T. M. Perl, "Chlorhexidine: expanding the armamentarium for infection control and prevention," Clin Infect Dis, vol. 46, no. 2, pp. 274-281, 2008. [Online]. Available: https://doi.org/10.1086/524736

5. T. Kaneko, T. Tatara, and M. Hirose, "Response to Muggleton et al.," Acta Anaesthesiol Scand, vol. 64, no. 6, p. 866, 2020. [Online]. Available: https://doi.org/10.1111/aas.13590

6. G. Bozzano, M. Dente, and R. Del, "Poly(bisphenol A carbonate) recycling: High pressure hydrolysis can be a convenient way," Mater Recycling - Trends Perspect, 2012. [Online]. Available: https://doi.org/10.5772/32974

7. D. Winkler, "Fundamentals of color: Shade matching and communication in esthetic dentistry," Br Dent J, vol. 199, no. 1, p. 59, 2005. [Online]. Available: https://doi.org/10.1038/sj.bdj.4812563

8. F. Alla and G. Borgès Da Silva, "Pour une culture partagée de la promotion de la santé et des soins," Santé Publique, vol. 25, no. 1, p. 5, 2013. [Online]. Available: https://doi.org/10.3917/spub.131.0005

9. A. Peracini et al., "Effect of denture cleansers on physical properties of heat-polymerized acrylic resin," J Prosthodont Res, vol. 54, no. 2, pp. 78-83, 2010. [Online]. Available: https://doi.org/10.1016/j.jpor.2009.11.004

10. S. Fukuzaki, "Mechanisms of actions of sodium hypochlorite in cleaning and disinfection processes," Biocontrol Sci, vol. 11, no. 4, pp. 147-157, 2006. [Online]. Available: https://doi.org/10.4265/bio.11.147

11. R. Y. Rhee, L. J. Palmer, K. Okamoto, et al., "Differential Effects of Chlorhexidine Skin Cleansing Methods on Residual Chlorhexidine Skin Concentrations and Bacterial Recovery," Infect Control Hosp Epidemiol, vol. 39, no. 4, pp. 405-411, 2018. [Online]. Available: https://doi.org/10.1017/ice.2017.312

12. American National Standards Institute and American Dental Association, "Specification No. 14 for Dental Base Metal Casting Alloys," The Journal of the American Dental Association, vol. 105, no. 4, pp. 686–7, 1982. [Online]. Available: https://doi.org/10.14219/jada.archive.1982.0428

13. A. A. Khaledi, M. Bahrani, and S. Shirzadi, "Effect of Food Simulating Agents on the Hardness and Bond Strength of a Silicone Soft Liner to a Denture Base Acrylic Resin," Open Dent J, vol. 9, pp. 402-408, 2015. [Online]. Available: https://doi.org/10.2174/1874210601509010402

14. F. Unalan and I. Dikbas, "Effects of mica and glass on surface hardness of acrylic tooth material," Dent Mater J, vol. 26, no. 4, pp. 545-548, 2007. [Online]. Available: https://doi.org/10.4012/dmj.26.545

15. T. R. Crompton, "Physical testing of plastics," Smithers Rapra Technology, 2012. [Online]. Available: https://openlibrary.org/books/OL27629057M/Physical_Testing_of_Plastics

16. J. C. Oliveira et al., "Effect of storage in water and thermocycling on hardness and roughness of resin materials for temporary restorations," Mater Res, vol. 13, pp. 355-359, 2010.

17. V. K. Kutsch, J. Whitehouse, K. Schermerhorn, and R. Bowers, "The evolution and advancement of dental thermoplastics," Dentaltown Magazine, pp. 52-56, 2003.

18. J. S. Rahal, M. F. Mesquita, G. E. Henriques, and M. A. Nóbilo, "Surface roughness of acrylic resins submitted to mechanical and chemical polishing," J Oral Rehabil, vol. 31, no. 11, pp. 1075-1079, 2004. [Online]. Available: https://doi.org/10.1111/j.1365-2842.2004.01344.x

19. F. Pettini et al., "Roughness Analysis on Composite Materials (Microfilled, Nanofilled and Silorane) After Different Finishing and Polishing Procedures," Open Dent J, vol. 9, pp. 357-367, 2015. [Online]. Available: https://doi.org/10.2174/1874210601509010357

20. Z. W. Zhong, Z. F. Wang, and B. M. Zirajutheen, "Chemical mechanical polishing of polycarbonate and poly methyl methacrylate substrates," Microelectronic engineering, vol. 81, no. 1, pp. 117-124, 2005.

21. M. Horio, "Preface," Powder Technology, vol. 113, no. 3, pp. 227–229, 2000. [Online]. Available: https://doi.org/10.1016/s0032-5910(00)00316-8

22. X. Wang et al., "Microstructural analysis of Al alloys dispersed with TiB2 particulate for MMC applications," J Microsc, vol. 196, no. # (Pt 2), pp. 137-145, 1999. [Online]. Available: https://doi.org/10.1046/j.1365-2818.1999.00620.x

23. S. Kimoto et al., "Survival analysis of mandibular complete dentures with acrylic-based resilient liners," Gerodontology, vol. 30, no. 3, pp. 187-193, 2013. [Online]. Available: https://doi.org/10.1111/j.1741-2358.2012.00658.x

24. T. Kanno et al., "Novel denture-cleaning system based on hydroxyl radical disinfection," Int J Prosthodont, vol. 25, no. 4, pp. 376-380, 2012.

Building Mathematical Models to Estimate the Concentrations of Uranium and Radon Gas in Water

[1]Aliea Saad Mutlaq, [2]Ghassan Ezzulddin Arif

[1]Department of Mathematics, College of Education for women,Tikrit University,Iraq

[2]Department of Mathematics, College of Education for Pure Sciences, Tikrit University, Iraq.

[1]Aliea.saad23@st.tu.edu.iq
[2]ghasanarif@tu.edu.iq

Uranium and Radon Gas in Water

[1]Aliea Saad Mutlaq, [2]Ghassan Ezzulddin Arif

[1]Department of Mathematics, College of Education for women,Tikrit University,Iraq

[2]Department of Mathematics, College of Education for Pure Sciences, Tikrit University, Iraq.

[1]Aliea.saad23@st.tu.edu.iq

[2]ghasanarif@tu.edu.iq

Abstract

The goal of this research is to create accurate mathematical models using numerical approaches for estimating uranium and radon gases levels in water. For determining the quantities of uranium and radon gas in water, several mathematical approaches were used: Linear regression, linear least squares, and graph method The review of outcomes revealed a high degree of concordance for the experimental data. This study is essential because it helps with the development of accurate and effective methods for evaluating uranium as well as radon gas concentrations in water. These developments are critical to improving the tracking and control of any health risks linked with uranium radiation.

Keywords: Radon gas, Uranium, Experimental data, Mathematical approaches. linear regression

1. Introduction:

In this thesis, we create mathematical models to estimate the concentrations of uranium and radon gas in water using numerical analysis methods. We create mathematical models to obtain accurate results. Numerical analysis plays a major role in our research which is an important aspect in mathematics and other sciences.

We will use numerical analysis methods to achieve accurate estimates, ensuring that the estimated values closely approximate the true values with minimal error. It is worth noting that recent years have witnessed an increase in estimation studies. For example, Steven Balter et al. investigated techniques for fluoroscopic skin radiation dose estimation [1], and Haregeweyn N and Yohannes F examined non-agricultural pollution models on swamps in Ethiopia [2]. Also, Michael J. et al. Using second generation computer software to evaluate internal dose in nuclear medicine [3].

In 2001, Emily R. Unsworth and others in England conducted a study using ICP mass spectrometry to measure uranium concentrations in seawater and groundwater. Their findings showed amounts of 2.68 nanograms of uranium in seawater and 0.3 nanograms in groundwater [4]. In 2002, Håkonsson-Hayes et al evaluated the concentration of 238 units in well-irrigated tomato, pumpkin, lettuce and radish contents in the Nambe region using ICP-MS. The measured values were less than 1 µg-1, 150 µg-1, 500 µg-1, and 1200 µg-1, respectively [5]. In 2003, Reimann and others measured uranium activity concentrations in river water, sea water,

and tap water at 2.63%, 1.13%, and 1.37%, respectively. In a study by Koji Oshita et al using ICPMS in Japan, activation values in drinking water from East Africa were measured as 0.005-48 g/L, 598-45800 g/L, and 0.002-1.59 μg/L, respectively [6]. Moreover, in (2017), Arif et al. presented an estimate of the effects of uranium radiation on workers in selected chemical plants, relying on some numerical analysis methods, Neville and Spline [7].
Overall, our study underscores the importance of numerical methods to accurately estimate uranium concentration and radon gas in water, thus contributing to the understanding and monitoring of potential health risks associated with uranium exposure.

2 Research methodology:

To calculate the concentration of uranium and radon gas in water, the study relied on mathematical modeling based on graph theory and numerical methods such as the Least square method, and the Linear regression method. Consequently, mathematical models were created by relying on the methods of the three aforementioned methods. In this section, three methods are presented for creating mathematical models through which uranium estimate uranium concentration and radon gas in water are calculated.

2.1 Linear regression [8-9]

Linear regression is a statistical procedure for calculating the value of a dependent variable from an independent variable. Linear regression measures the association between two variables. It is a modeling technique where a dependent variable is predicted based on one or more independent variables. Linear regression analysis is the most widely used of all statistical techniques.

Linear regression equation

$$b = \frac{n\sum xiyi - \sum xiyi}{n\sum xi^2 - (\sum xi)^2} \qquad (2.1)$$

$$= \frac{10(296486.145) - (13411)(167.116)}{10(23802995) - (179854921)}$$

$$= \frac{723668.774}{58175029} = 0.0124395086$$

$$a = \frac{\sum yi \sum xi^2 - \sum xi \sum xiyi}{n\sum xi^2 - (\sum xi)^2}$$

$$= \frac{(167.116)(23802995) - (13411)(296486.145)}{10(23802995) - (79854921)}$$

$$= \frac{1685621.825}{58175029} = 0.0289750062$$

$$y = a + bx$$

$$y = 0.0289750062 + 0.012435086x \quad (2.2)$$

We got on Table (2.1) which represents the mathematical model so that we conclude the mathematical model (2.1)

Table 2.1. The calculated uranium concentration in the water using linear regression method.

No.	Grass name	X_i	$R_k Det.$	$R_k Exp.$	Xi^2	$\sum xif(xi)$	E	E^2
1	Dill	399	4.99	4.98	159201	1987.02	0.01	0.0001
2	Chamomile	525	6.55	6.55	275625	3438.75	0	0
3	Poot nut	969	12.08	12.13	938961	11753.97	0.05	0.0025
4	Slanderous	1125	14.02	14.051	1265625	15807.373	0.031	0.000961
5	Ginger	1153	1437	14.37	1329409	16568.61	0	0
6	Carway	1320	16.45	16.45	1742400	21714	0	0
7	Gray roses	1349	16.8	16.8	1819801	22663.2	0	0
8	Rose mary	1361	16.96	16.96	1852321	23082.56	0	0
9	Tablet	1954	24.34	24.27	3818116	47423.58	0.07	0.0049
10	Snack	3256	40.532	40.555	10601536	132047.08	0.02	0.0004
	∑	**13411**		**167.116**	**23802995**	**296486.145**		**0.031861**

Figure below shows the estimated and experimental values of uranium concentration effect on the water by using the linear regression method

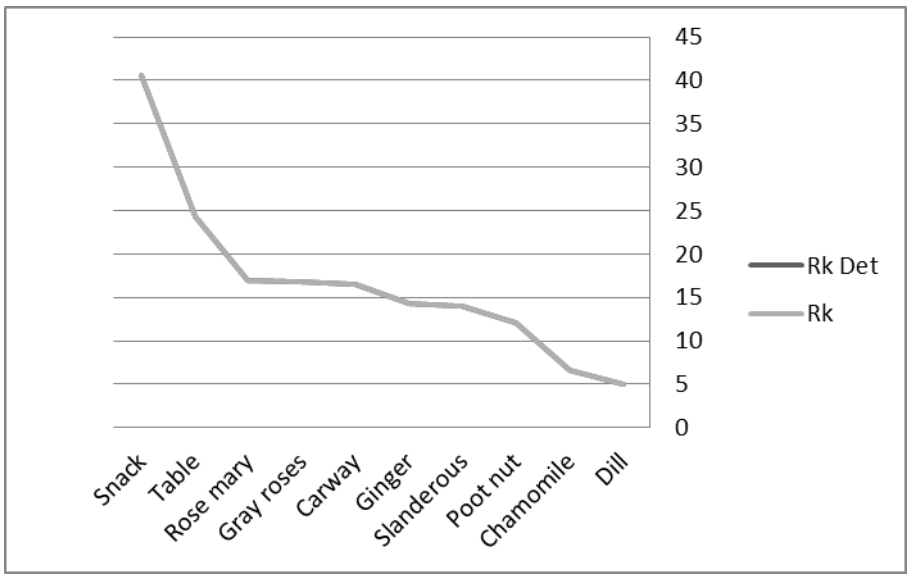

Fig. 2.1. The experimental and estimated values of the uranium Concentration in the water using the linear regression method.

2.2 Least square method [10-11]

The least squares approach is the technique of determining the best-fitted lines for any collection of data represented by a formula. This method includes decreasing the total of the total square of the remaining sections of the locations from a curve or line, and the overall pattern of results is determined statistically. The least square approach is used to fit curves during the analysis of regression.

Least square method can be stated as follows:
To establish the least squares method step by step, let's start from the beginning and go through each step:

Step 1: Begin with the given equations (2.3) and (2.4):

$$ma_o + a_I \sum_{i=1}^{m} N_i = \sum_{i=1}^{m} f(N_i) \qquad (2.3)$$

$$a_o \sum_{i=1}^{m} N_i + a_I \sum_{i=1}^{m} (N_i)^2 = \sum_{i=1}^{m} N_i f(N_i) \qquad (2.4)$$

Step 2: Solve equations (2.5) and (2.6):

$$Ioa_o + I3411a_I = 167.116 \qquad (2.5)$$

$$I3411a_o + 23802995a_I = 296486.145 \qquad (2.6)$$

Step 3: Multiply equation (2.5) by -1341.1:

$$-13411a_o - 17985492.1a_1 = -224119.2676 \qquad (2.7)$$

Step 4: Solve the resulting system of equations (2.6) and (2.7):

$$-13411a_o - 17985492.1a_1 = -224119.2676 \qquad (2.8)$$

$$13411a_o + 23802995a_I = 296486.145 \qquad (2.9)$$

Step 5: Solve for a_I by dividing equation (2.9) by 5817502.9: a_I= 0.012439508

Step 6: Substitute the value of a_I into equation (2.6) to solve for a_0:

$$13411a_0 + 23802995(0.012439508) = 296486.145$$

$$13411a_0 + 296097.5467 = 296486.145$$

$$13411a_0 = 296486.145 - 296097.5467$$

$$a_0 = 388.5983 / 13411 \approx 0.028976086$$

Step 7: Finally, substitute the values of a_0 and a_I into equation (2.5) to obtain the expression for R_k:

$$R_k = 0.028976086 + 0.012439508\,N \qquad (2.10)$$

We got on table (2.10) which represents the mathematical model so that we conclude the mathematical model (2.10).

Table 2.2 The calculated uranium concentration in the water using the last square method.

No.	**Grass name**	Ni	RkDet.	Rk Exp.	$\sum Nif(Ni)$	E	E^2
1	Dill	399	4,99	4,98	1987,02	0,01	0,0001
2	Chamomile	525	6,55	6,55	3438,75	0	0
3	Poot nut	969	12,08	12,13	11753,97	0,05	0,0025
4	Slanderous	1125	14,02	14,051	15,807,373	0,03	0,000961
5	Ginger	1153	1437	14,37	16568,61	0	0
6	Carway	1320	16,45	16,45	21714	0	0

7	Gray roses	1349	16,8	16,8	22663,2	0	0
8	Rose mary	1361	16,96	16,96	23082,56	0	0
9	Tablet	1954	24,34	24,27	47423,58	0,07	0,0049
10	Snack	3256	40,53	40,555	132047,08	0,02	0,0004
	∑	13411		167,116	296,486,145		0.009086

Below Figure shows the estimated and experimental values of uranium concentration effect on the water by using the last square method

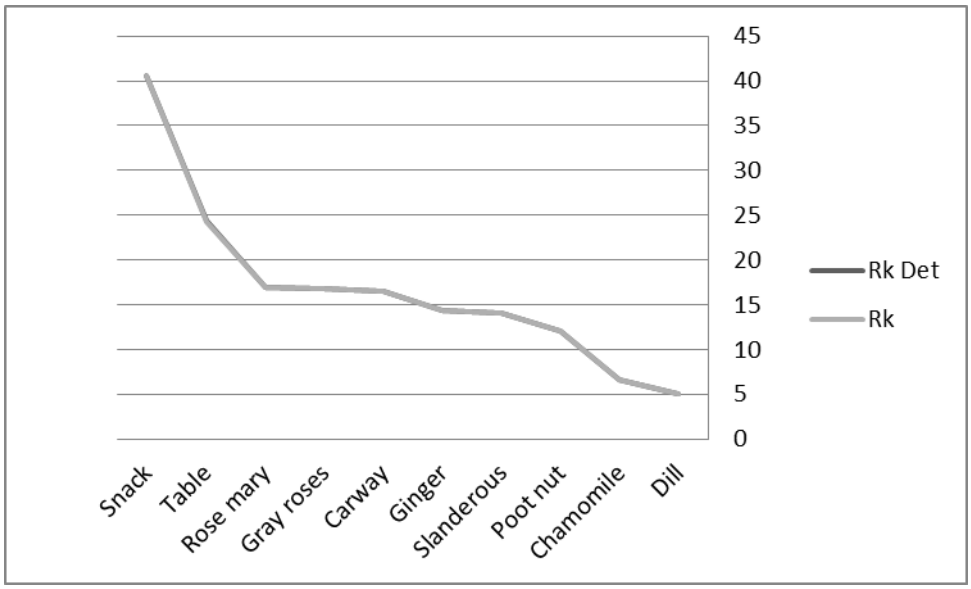

Fig 2. 2 The experimental and estimated values of the uranium Concentration in the water using the last square method.

2.3 Graph Theory [12-13]

Graph Theory is a branch of mathematics that studies the relationships and interactions between different objects, utilizing graphical representations to visualize these relationships. It is considered a fundamental field in pure mathematics, with applications extending to various domains such as computer science, networks, social relationships, recommendation systems, transportation, and many others**.** Graph Theory focuses on studying objects known as vertices or nodes and the links or edges that connect them. These nodes and edges are represented in graphical diagrams, where nodes are represented by points and edges are represented by lines or arcs connecting the nodes. Graph Theory provides mathematical tools and concepts to analyze and understand the structural properties and general characteristics of complex systems Graph Theory is a mathematical discipline that examines the connections and interactions among distinct entities using visual representations. It serves as a foundational area of pure

mathematics, finding applications in computer science, network analysis, social dynamics, recommendation systems, transportation, and more. Graph Theory centers on the examination of nodes (or vertices) and the edges (or links) that link them, represented visually as points and lines/arcs respectively. By employing mathematical tools and concepts, Graph Theory facilitates the analysis and comprehension of the structural properties and general characteristics of intricate systems depicted through graphical diagrams. Key concepts in Graph Theory encompass degree, path, cycle, connectivity, trees, shortest paths, and other theoretical constructs that aid in data analysis and understanding the relationships between objects**.**

The applications of Graph Theory are vast and diverse, encompassing social network analysis, data organization, computer network design, artificial intelligence applications, ecological system analysis, recommendation systems, operational planning, and numerous other domains**.**

A graph, which is a fundamental mathematical structure, comprises a collection of vertices (or nodes) and a series of edges (or arcs/links) that establish connections between pairs of vertices. The edges signify relationships or associations among the vertices. Graphs offer a means to model real-world scenarios and problems, enabling the examination of relationships and interactions between different entities**.**

The generation of interpolating polynomials can be carried out recursively, as illustrated in the subsequent examples.

Using the graph method to calculate of uranium and radon gases levels in water as follows:

$$N1 = 399 \qquad Rk1 = 4.98$$

$$N9 = 1954 \qquad Rk10 = 40.555$$

$$R_k = \frac{(N-N_1)Rk_{10}(N-N_9)Rk_1}{N9\_N1}$$

$$R_k = \frac{(N-399)(40.555)-(N-1954)4.98}{1954\_399}$$

$$= \frac{40.555N - 16181.445 - 4.98N + 9730.92}{1555}$$

$$= \frac{35.575N - 6450.525}{1555}$$

$$R_k = 0.0228778135N\_4.1482475884 \qquad (2.11)$$

Table 2.3. The calculated uranium concentration in the water using linear regression method. by using the graph method.

Grass name	N_i	$Det\ R_k$ Graph	$Exp\text{-}R_k$ Graph	E	E^2
Dill	399	4.98	4.98	0	0
Chamomile	525	7.86	6.55	1.31	1.71
Poot nut	969	18.02	12.13	5.89	34.69
Slanderous	1125	21.59	14.051	7.539	56.83
Ginger	1153	22.23	14.37	7.86	61.78
Carway	1320	26.05	16.45	9.6	92.16
Gray roses	1349	26.71	16.8	9.91	98.20
Rose mary	1361	62.98	16.96	10.02	100.4
Tablet	1954	40.55	24.27	16.28	265.03
Snack	3256	70.34	40.555	29.785	887.14
Σ					1597.94

A visual representation, known as Figure 2.3, illustrates the relationship between the observed and predicted values in determining uranium and radon gas levels in water using the graph method. This graphical depiction offers a straightforward means to compare the actual measured values with the values estimated by the mathematical model represented by the graph. By visually examining the graph, one can assess the degree of accuracy and agreement between the two datasets, thereby evaluating the reliability and consistency of the graph model in estimating uranium and radon gas levels in water.

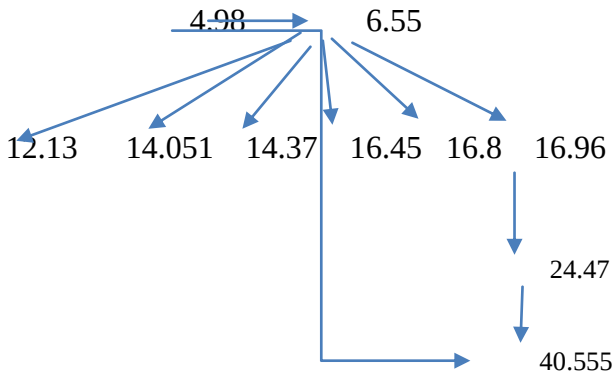

Fig. 2.3. shows the estimated and experimental values of uranium concentration effect on the water by using the graph method.

Conclusions

In this study, the linear regression method, the least squares method, and the histogram method were used to estimate the concentration levels of uranium and radon gases in water. The results obtained from these three methods were compared and analysed. The results indicated that the best method was the linear regression method, which showed the greatest effectiveness in estimating the concentrations of radon and uranium in water samples, as shown in Table 2.1, respectively. These results underscore the importance of choosing appropriate methods when developing models to estimate uranium and radon levels in water, as different methods may be more appropriate for different regions or sample types.

References

[1] Balter, Stephen, et al. "Techniques to estimate radiation dose to skin during fluoroscopically guided procedures α." *Skin Dose Measurements AAPM* (2002): 1-10.

[2] Haregeweyn, Nigussie, and Fekadu Yohannes. "Testing and evaluation of the agricultural non-point source pollution model (AGNPS) on Augucho catchment, western Hararghe, Ethiopia." *Agriculture, ecosystems & environment* 99.1-3 (2003): 201-212.

[3] Stabin, Michael G., Richard B. Sparks, and Eric Crowe. "OLINDA/EXM: the second-generation personal computer software for internal dose assessment in nuclear medicine." *Journal of nuclear medicine* 46.6 (2005): 1023-1027.

[4] Unsworth, Emily R., Jennifer M. Cook, and Steve J. Hill. "Determination of uranium and thorium in natural waters with a high matrix concentration using solid-phase extraction inductively coupled plasma mass spectrometry." *Analytica chimica acta* 442.1 (2001): 141-146.

[5] Hakonson-Hayes, Audrey C., P. R. Fresquez, and F. W. Whicker. "Assessing potential risks from exposure to natural uranium in well water." *Journal of environmental radioactivity* 59.1 (2002): 29-40.

[6] Reimann, Clemens, et al. "Drinking water quality in the Ethiopian section of the East African Rift Valley I—data and health aspects." *Science of the Total Environment* 311.1-3 (2003): 65-80.

[7] Arif, Ghassan Ezzulddin, et al. "Estimating the Amount of Uranium Radiation Effect on the Workers in Selected Chemical Factories by Using the Numerical Spline Method." *Diyala Journal for Pure Science* 13.4-part 1 (2017).

[8] M. H. Kutner, C. J. Nachtsheim, J. Neter, and W. Li, "Applied Linear Statistical Models," McGraw-Hill Education, 2004

[9] N. R. Draper and H. Smith, "Applied Regression Analysis," John Wiley & Sons, 2014.

[10] G. A. F. Seber and A. J. Lee, "Linear Regression Analysis," 2nd ed., John Wiley & Sons, 2012.

[11] Toledo, F. J., Blanes, J. M., & Galiano, V. (2018). Two-step linear least-squares method for photovoltaic single-diode model parameters extraction. *IEEE Transactions on Industrial Electronics*, *65*(8), 6301-6308.

[12] N. Biggs, E. K. Lloyd, and R. J. Wilson, "Graph Theory, 1736-1936," Oxford University Press, 1986.

[13] D. B. West, "Introduction to Graph Theory," vol. 2, Prentice Hall, Upper Saddle River, 2001.

بناء نماذج رياضياتية لتخمين تركيز اليورانيوم وغاز الرادون في الماء

1عاليه سعد مطلك ,٢غسان عزالدين عارف

١ قسم الرياضيات / كلية التربية للبنات / جامعة تكريت / العراق

٢ قسم الرياضيات / كلية التربية للعلوم الصرفة / جامعة تكريت / العراق

الخلاصه

الهدف من هذا البحث هو إنشاء نماذج رياضية دقيقة باستخدام الأساليب العددية لتقدير مستويات غازي اليورانيوم والرادون في الماء. لتحديد كميات اليورانيوم وغاز الرادون في الماء، تم استخدام عدة طرق رياضية: الانحدار الخطي، المربعات الصغرى الخطية، والرسم البياني. كشفت مراجعة النتائج عن وجود درجة عالية من التوافق للبيانات التجريبية. وتعد هذه الدراسة ضرورية لأنها تساعد في تطوير طرق دقيقة وفعالة لتقييم تركيزات اليورانيوم وغاز

الرادون في الماء. وتعتبر هذه التطورات حاسمة لتحسين تتبع ومراقبة أي مخاطر صحية مرتبطة بإشعاع اليورانيوم.

New Hybrid Explicit and Crank-Nicolson Method to Solve Wave Equation in Two Dimension

1st.: Amal Khalaf Kanon, 2nd.: Elaf Sabah AbdulWahid,

3the:Awni Muhammed Guftan,

Dept. of Math, College of Education for women, Tikrit University.

amal.khalaf23@st.tu.edu.iq

elafs.math@tu.edu.iq

Awny.muhammed@tu.edu.iq

New Hybrid Explicit and Crank-Nicolson Method to Solve Wave Equation in Two Dimension

1st.: Amal Khalaf Kanon, 2nd.: Elaf Sabah AbdulWahid,

3the:Awni Muhammed Guftan,

Dept. of Math, College of Education for women, Tikrit University.

amal.khalaf23@st.tu.edu.iq

elafs.math@tu.edu.iq

Awny.muhammed@tu.edu.iq

Abstract

In this paper, we introduce the new hybrid numerical method to solve the wave equation in 2-Dim, in this technique we use two steps in the first one we apply the Explicit method to find all the node points and the second step we apply the C-N method to find the mid-point between any two point which are find in the step1. The results are more accuracy than other results.

الخلاصة

في هذا البحث نقدم الطريقة العددية الهجينة الجديدة لحل المعادلة الموجية في البعدين، في هذه التقنية نستخدم خطوتين، في الأولى نطبق الطريقة الصريحة لإيجاد جميع النقاط العقدية وفي الخطوة الثانية نطبق الطريقة الهجينة للعثور على نقطة المنتصف بين أي نقطتين تم العثور عليهما في الطريقة الصريحة.

Key-words; Explicit method, C-N method, wave equation, Hybrid method.

1- introduction:

There are many of numerical methods, where these methods are used to solve many of problems which can't solve by the analytic methods, so we are used the numerical methods to solve many problems in elasticity problems, diffusion problems, waves equations, … ADI numerical method is one of the numerical which is used to solve the wave equations (one -dimension and two-dimension). In (1993), S.J. Farlow, introduce the general form of wave equation [ ]. In (2014), Haneen F. Shareef, was used ADI method to solve Bi-Harmonic Equation. [1]. Hanan A. Alukaily used the ADI numerical method to find numerical solution of Fractional partial differential equation [2]. In (2020) Bushra and Awni are used ADI method for solving Heat diffusion problems [3]. And in (2023), Awni and Mohammed H. Rahim are solved the Wave equation in two-dimensional by Implicit numerical method.

2- Theoretical part

In this section we introduce the main steps to apply the hybrid method:

1. Make the mesh's for the region solution by vertically (Rows) and horizontally (columns).
2. Applying the Explicit method in the formula:

2-1. The common formula of the correct calcution method.

$$(1-k)w_{i,j+1} = (4-2k)w_{i,j} - (1-k)w_{i,j-1} - w_{i-1,j} - w_{i+1,j} \quad (1)$$

To find all node points in the grid (mesh)-

3. Applying the C-N

2-2 The common formula of C-N.

$$w_{i,j+1} = w_{i,j} + \frac{1}{4}k\left(w_{i+1,j} - w_{i-1,j}\right) + \frac{1}{4}k\left(w_{i+1,j+1} - w_{i-1,j+1}\right) \quad (2)$$

To find all mid-points between every two points which are find there in the 2nd step.

3- Particular part:

In this part we applying the Algorithm hybrid method to solve the wave equation as shown in the following example:

We solve the first example by the normal method and the second example is solve by hybrid method

Example:

The following the tow dimension wave equation:

$$\frac{1}{6}w_{tt} = w_{xx} + w_{yy} \quad (3)$$

When

$t \in [0,1]$, $x \in [0,2]$

With the boundary conditions;

$$w(0,t) = w(1,t) = 1 \quad (4)$$

And initial conditions;

$$w(x,0) = F(x) = \cos x \,, \qquad w'(x,0) = g(x) \quad (5)$$

$$s.t \quad 0 < x < 2 \quad , h = 0.5 \quad , \Delta t = 0.5\, sec$$

Step1:

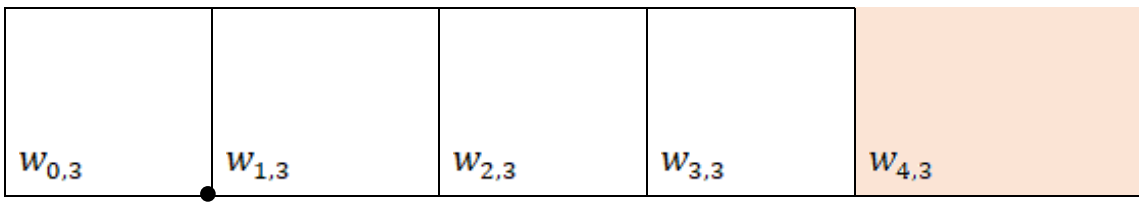

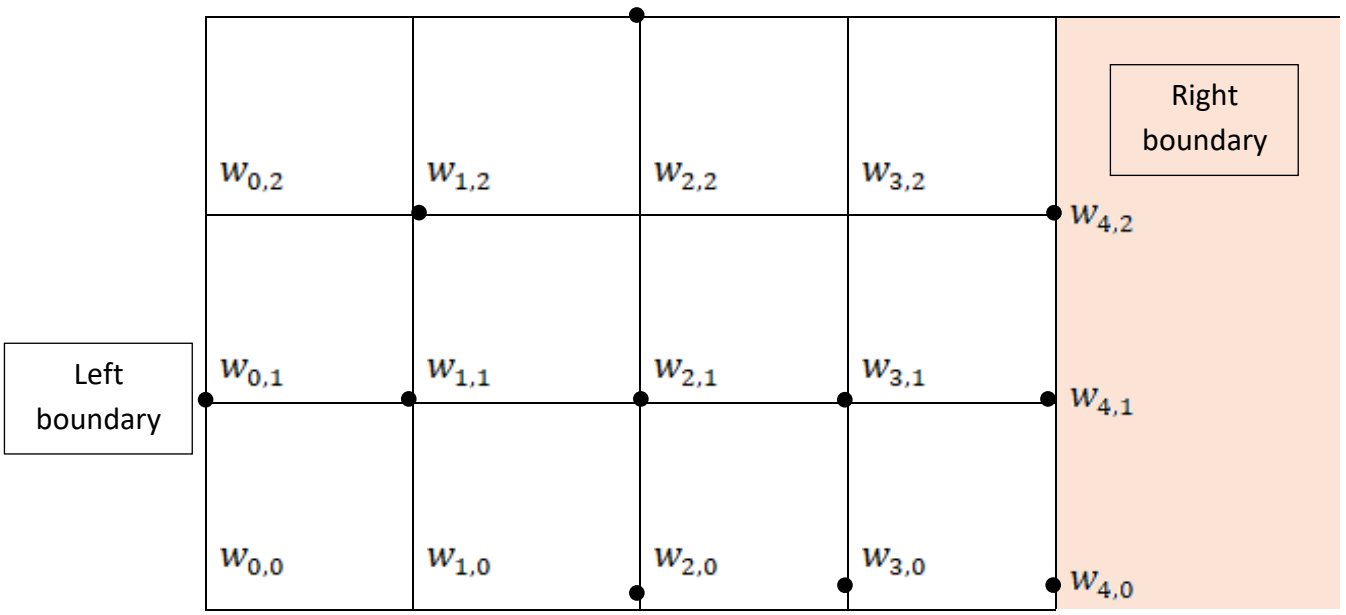

Fig (1-1): initial condition distribution of initial boundary condition mesh

Step2:

Applying the following formula;

$$(1-k)w_{i,j+1} = (4-2k)w_{i,j} - (1-k)w_{i,j-1} - w_{i-1,j} - w_{i+1,j} \quad (6)$$

$$\forall i = 1,2,3,\dots\dots n\,, \quad \forall j = 0,1,2,3,\dots\dots\dots m$$

And we have

$$w_{i,-1} = w_{i,1} - 2\,\Delta t\; g\; i \;\;, \quad \forall i = 1,2,3,\dots\dots\dots\dots n \qquad (7)$$

First find the value of (k)

$$k = \frac{h^2}{c^2(\Delta t)^2} = \frac{(0.5)^2}{16\,(0.5)^2} \Rightarrow k = 0.0625$$

$$w(x,0) = F(x) = \cos x$$

$$w_{(0,0)} = w_{0,0} = \cos 0 = 1$$

$$w_{(0.5,0)} = w_{1,0} = \cos(0.5) = 0.87758$$

$$w_{(1,0)} = w_{2,0} = \cos(1) = 0.5403$$

$$w_{(1.5,0)} = w_{3,0} = \cos(1.5) = 0.07073$$

$$w = w_{4,0} = 1$$

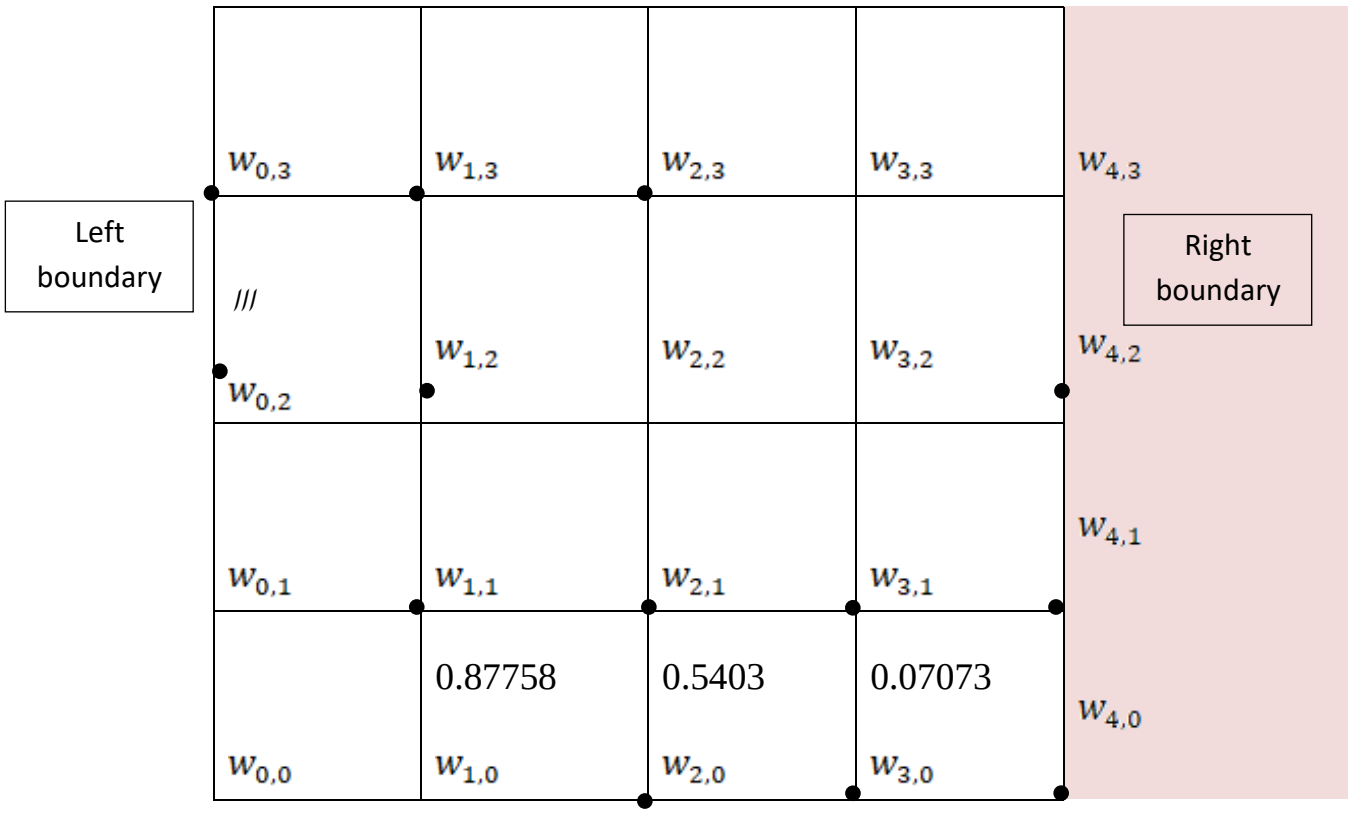

Fig(1-2): find the node points in level-1

Let j = 0 ، i = 1, 2, 3

$i = 1 \quad , j = 0$

$$(1-K)w_{1,1} = (4-2K)\, w_{1,0} - (1-K)w_{1,-1} - w_{0,0} - w_{2,0} \qquad (8)$$

And find the value of $W_{1,-1}$ by eq (7)

$$w_{1,-1} = w_{1,1} - 2\,\Delta t\; g\; i$$

$$w_{1,-1} = w_{1,1} - 2\,(0.5)(2)$$

$$w_{1,-1} = w_{1,1} - 2 \qquad (9)$$

$$(1-K)\,w_{1,1} = (4-2K)\,w_{1,0} - (1-K)\big(w_{1,1}-2\big) - w_{0,0} - w_{2,0} \quad (10)$$

$$2\,(1-K)w_{1,1} = (4-2K)w_{1,0} - w_{0,0} - w_{2,0} + 2(1-K) \quad (11)$$

Now, we substate the condition and the value of k in (11)

$$2\,(1-0.0625)w_{1,1} = \big(4-2(0.0625)\big)(\,0.87758) - 1 - 0.5403 + 2(\,1-0.0625)$$

$$1.875\,w_{1,1} = 3.73532$$

$$w_{1,1} = 1.99217$$

$$i = 2 \quad , \qquad j = 0$$

$$(1-K)w_{2,1} = (4-2K)w_{2,0} - (1-K)w_{2,-1} - w_{1,0} - w_{3,0} \quad (12)$$

And find the value of $w_{2,-1}$ by eq $w_{2,-1} = w_{2,1} - 2\,\Delta t\; g\; i$

$$w_{2,-1} = w_{2,1} - 2\,\Delta t\; g_2$$

$$w_{2,-1} = w_{2,1} - 2 \quad (13)$$

Substitute eq (12) in eq (11) to obtain;

$$(1-K)w_{2,1} = (4-2K)w_{2,0} - (1-K)\big(w_{2,1}-2\big) - w_{1,0} - w_{3,0} \quad (14)$$

Simplify and complete the process on eq (14)

$$2\,(1-K)w_{2,1} = (4-2K)w_{2,0} - w_{1,0} - w_{3,0} + 2(1-K) \quad (15)$$

$$2(1-0.0625)w_{2,1} = \big(4-2(0.0625)\big)(0.5403) - 0.87758 - 0.07073 + 2(1-0.0625)$$

$$1.875\,w_{2,1} = 3.02035$$

$$w_{2,1} = 1.61085$$

And soon we have:

$$w_{3,1} = 0.3246$$
$$w_{1,2} = 4.57182$$
$$w_{2,2} = 3.64852$$
$$w_{3,2} = -1.51443$$
$$w_{1,3} = 11.94626$$

$w_{2,3} = 10.20841$

$w_{3,3} = -11.542741$

Table (1-1): Exhibits the distribution of border and primary conditions and all nodal points on the rectangular network

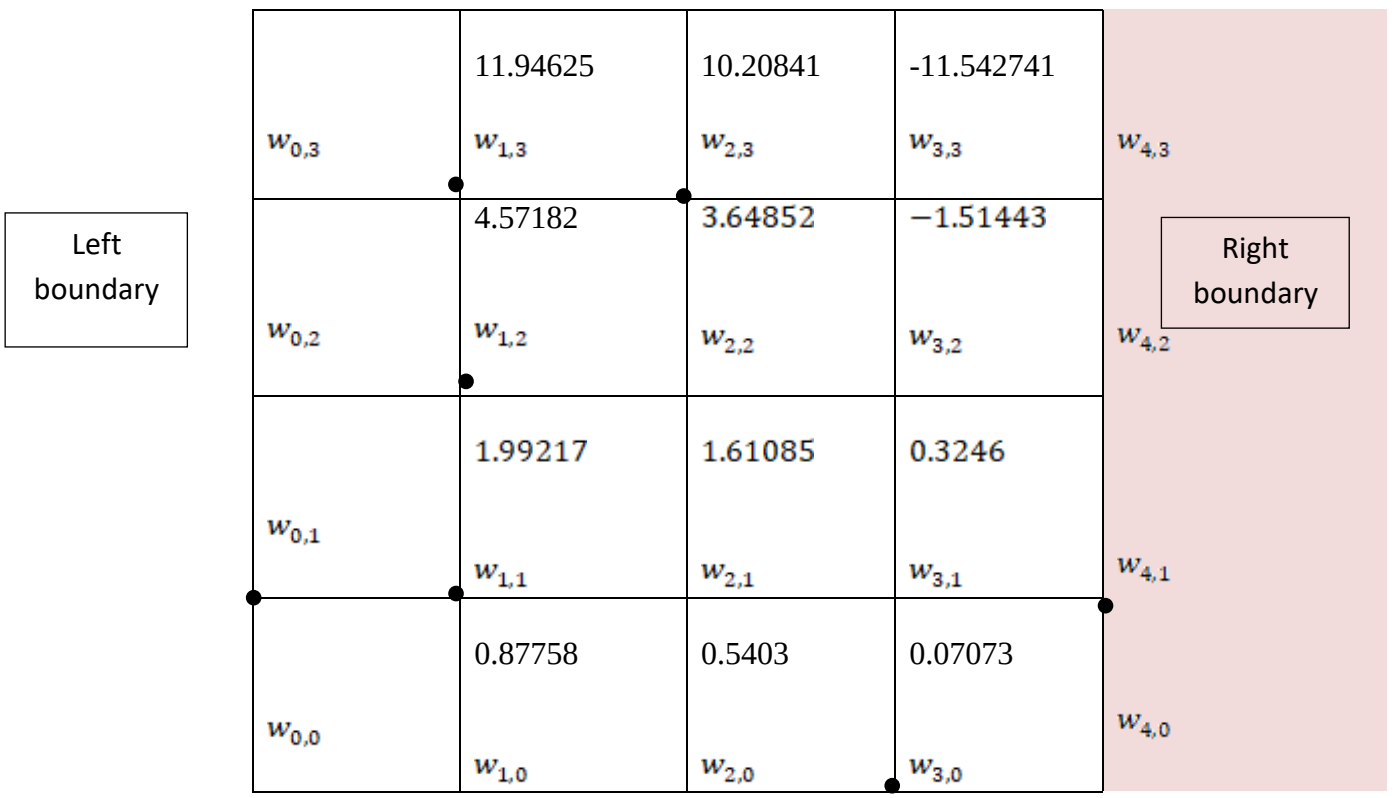

Application of hybrid method in this section we solve the previous section by the hybrid method, and we compare between the results of these examples:

$$\Delta x = h = \frac{0.5}{2} = 0.25$$

$$K = \frac{C\,\Delta t}{\Delta x} = \frac{16(0.5)}{0.25} = 32$$

$\cos(0) = w_{0,0} = 1$
$\cos(0.25) = w_{1,0} = 0.96891$
$\cos(0.5) = w_{2,0} = 0.87708$
$\cos(0.75) = w_{3,0} = 0.731689$
$\cos(1) = w_{4,0} = 0.54032$
$\cos(1.25) = w_{5,0} = 0.66687$
$\cos(1.5) = w_{6,0} = 0.07074$
$\cos(1.75) = w_{7,0} = -0.17825$
$\cos(2) = w_{8,0} = -0.41615$

Applying the Crank-Nicholson generic formula of wave equation.

$$w_{i,j+1} = w_{i,j} + \frac{1}{4}K\left(w_{i+1,j} - w_{i-1,j}\right) + \frac{1}{4}K\left(w_{i+1,j+1} - w_{i-1,j+1}\right)$$

And to compensate for $i = 1,3,5,7$ *and for* $j = 0,1$ وعن $K = 32$ *using the results of the method*

$$w_{1,1} = w_{1,0} + 8\left(w_{2,0} - w_{0,0}\right) + 8\left(w_{2,1} - w_{0,1}\right)$$
$$w_{1,1} = 0.96891 + 8(0.87708 - 1) + 8(1.61085 - 1)$$
$$w_{1,1} = 0.96891 + (-0.98336) + 4.8868$$
$$w_{1,1} = 4.87235$$

$$w_{3,1} = w_{3,0} + 8\left(w_{4,0} - w_{2,0}\right) + 8\left(w_{4,1} - w_{2,1}\right)$$
$$w_{3,1} = 0.73169 + 8(0.54030 - 0.87708) + 8\left((1.3707264) - (1.61085)\right)$$
$$w_{3,1} = 0.73169 + (-2.69424) + (-1.9209888)$$
$$w_{3,1} = -3.88354$$

And soon we have:

$$w_{5,1} = -6.970802$$

$$w_{7,1} = -9.277814$$

$$w_{1,2} = 30.94731$$

$$w_{3,2} = -10.0645568$$

$$w_{5,2} = -28.7347652$$

$$w_{7,2} = 3.7300286$$

$$w_{1,3} = 99.42726$$

$$w_{3,3} = -21.562998$$

$$w_{5,3} = -202.2258704$$

$$w_{7,3} = 54.3064286$$

Table (1-2): below shows a comparison between the results of the original explicit method and the hybrid method

Point	Explicit Method Results	Hybrid Method Results	Difference
$w_{1,1}$	1.99217	4.87235	-2.8818
$w_{3,1}$	0.3246	-3.88354	4.20814
$w_{1,2}$	4.28608	30.94731	-26.66123
$w_{3,2}$	-1.41902	-10.0645568	-11.4835768
$w_{1,3}$	11.94626	99.42726	-87.481
$w_{3,3}$	-11.542741	-21.562998	-33.105739

Fig(1-3): comparison between the results of the original explicit method and the hybrid method.

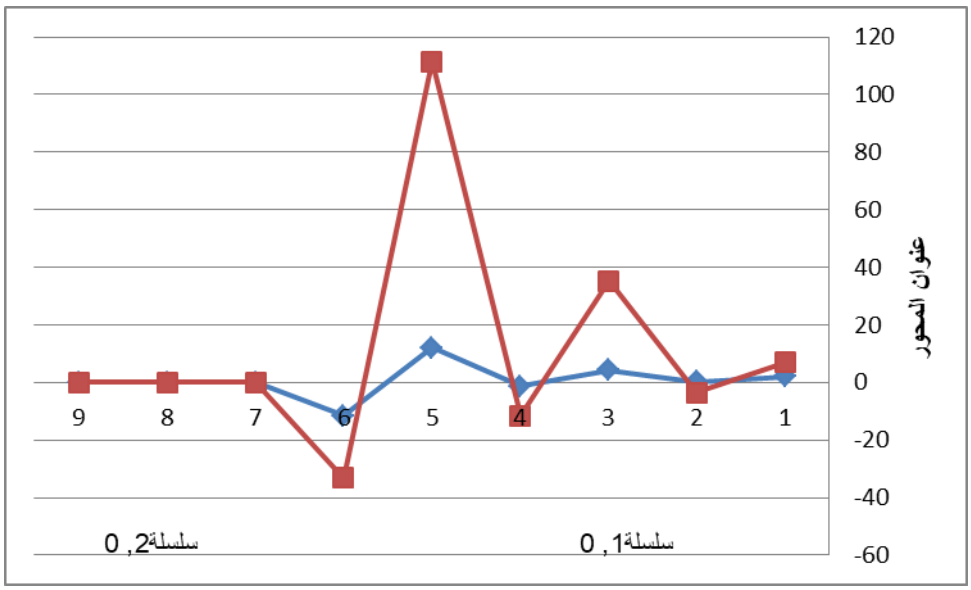

Conclusions:

1. The results which obtaining by hybrid method is faster than the results for the original method.
2. The results of hybrid method are more accuracy than other results.
3. The hybrid method saves time and reduces effort.

References:

[1] Haneen F. shannef, (2014). "ADI numerical method to solve Bi-Harmonic Equation" Msc thsis, Tikrit university, college of education for pure science.

[2] Hanan A Alukaily, (2015), "Using "ADI method to find numerical solution of fraction partial differential Equation" Msc. thsis, Tikrit university, college of education for pure science.

[3] Bushre sh. Mahmood, Awni M. Gaftan and Firas A. Fawzi, (2020), "Alternating Direction Implicit method for solving heat diffusion Equation" Ibn Al-Haitham Journal for pure and applied science, vol. 33(3).

[4] R. Chen. F. Liu, V. Anh, (2019). "A fractional altercating-direction implicit method for a multi-term times space fractional Bloch thorny equation in three-dimension, computers mathematics with applications.

[5] Bushras sh. Mahmood, Awni M. Gaftan and Firas A. Fawzi, (2020), "Alternating direction method for solving homogeneous heat equation". AL. Haitham Journal for pure and applied science, vol. 33(3) pp. 62-71.

[6] Awni M. Gaftan, "using boundary integral equation method to solve place strain problem of asymmetric elasticity Tikrit Journal for pure science vol.18 (3) pp. 196-198, (2013)

[7] Ashaju Abimbola samson Bright, (2015), "Alternating-Direction Implicit Finite-Difference method for transient 2D Heat Transfer in a Metal Bar using Finite differences method, "international Journal of scientific and Engineering Research.

[8]. S.J. Farlow, (1993), “Partial Differential Equation for Scientist and Engineers,” Courier Corporation.

[9]. Mohammed H. Rahim, Awni M. Gaftan, (2023), “ The Explicit Method for solving the two-Dimensional Wave Equation”, Journal of Natural and applied science, URAL, Vol.1(3),pp:103-118.

The appropriate method for dental adhesive application: A review

Mustafa H.Mohammad [1*], Samer A.Thyab (MSc) [1]

First author (correspondence author): ***Mustafa H. Mohammad (BDS.), Master candidate, Department of Conservative and Aesthetic Dentistry, Baghdad College of Dentistry, University of Baghdad, Baghdad, Iraq.

E-mail: altmemymostfa@gmail.com

https://orcid.org/0009-0004-8982-0087

second author: Samer Aun Thyab (B.D.S., MSc.conservative), Assistant professor in Conservative Dentistry/ Department of Conservative & aesthetic Dentistry, Baghdad College of Dentistry, Baghdad, Iraq

Tel.: 00964 7904897764

E-mail address: **samer.aun@codental.uobaghdad.edu.iq**

https://orcid.org/0000-0002-9452-4512

The appropriate method for dental adhesive application: A review

Mustafa H.Mohammad [1*], Samer A.Thyab (MSc) [1]

First author (correspondence author): *****Mustafa H. Mohammad (BDS.), Master candidate, Department of Conservative and Aesthetic Dentistry, Baghdad College of Dentistry, University of Baghdad, Baghdad, Iraq.

E-mail: altmemymostfa@gmail.com

https://orcid.org/0009-0004-8982-0087

second author: Samer Aun Thyab (B.D.S., MSc.conservative), Assistant professor in Conservative Dentistry/ Department of Conservative & aesthetic Dentistry, Baghdad College of Dentistry, Baghdad, Iraq

Tel.: 00964 7904897764
E-mail address: **samer.aun@codental.uobaghdad.edu.iq https://orcid.org/0000-0002-9452-4512**

Abstract

Different types of adhesives are used to bond composites for dentin. However, there was no specific manner for the application of adhesive that can enhance the bond strength between resin and dentin, so this review assesses the different techniques for the application of adhesive to the dentin surface; the review used three databases, PubMed, Web of science Embase, and Scielo to search the in vitro studies which can give the insight to the most appropriate bond enhancement technique. The various techniques of adhesive application, such as the application of the hydrophobic coating, the application of two layers of adhesive, and the application of adhesive by electrical current, active agitation, and sonic agitation, can improve the bond strength.

Keywords: dental adhesive, dentin bonding, adhesion

Introduction

Adhesion to dentin is more complex and more challenging than to enamel because of the dentin structure that requires special consideration to obtain reliable and high bond strength [1,2]. Adhesion of resin and dentin involves the formation of the hybrid layer, an interdiffusion

zone that forms the micromechanical retention between the resin and dentin. This hybrid layer is composed of hydroxyapatite, collagen fibrils, solvent, and monomer resin; this layer's durability depends on its component ability to resist the degradation process [3,4,5,6,7,8,9,10].

Self-etch (S.E.), etch & rinse, and universal adhesives are commonly used to bond to enamel and dentin; the bond strength of this adhesive can increase when the steps of the procedure are decreased the by reducing the error and sensitivity [4,7,11].

These adhesives consist of monomers containing hydrophilic and hydrophobic components, polymerization mediators, and solvents. This solvent dilutes the monomers and can help increase the spreading, wetness, and penetration of monomers to dentin structures during the bonding procedure. However, as these solvent percentages increase in the adhesive, the bond strength is negatively affected[12,13,14].

During the bonding procedure, the excess solvent should be removed; this can be achieved by allowing sufficient time for the solvent to evaporate before curing or employing dry air. Solvent evaporation depends on different factors such as the type of solvent and monomers, distance between teeth and air syringe, and air temperature [15,16,17,18].

Numerous techniques such as active agitation, sonic agitation, adding a hydrophobic coat, adding multiple layers of adhesive, using electric current, and increasing the application time can be used for adhesive application attempting to improve the bond strength between dentin and resin material. However, until now, there have been no standard ones that can recommended as the most appropriate method. [6.8.11.12.19.20] .

material and method

The electronic databases of Google Scholar, PubMed, and Science Direct were tried to search for papers about enhancement bond strength. The criteria of this review depend on the results of previous systemic reviews and meta-analyses [21].

A practical method to differentiate a commercial dentinal adhesive solution is by assessing its bonding strength[16,22,23]. The predominant procedures for measuring bond strength involve the application of tensile or shear stress; these tests can be applied to large areas of specimens.

Also, micro shear and micro tensile are created for small areas of spacemen, which produce more accurate results[17.18.19].

This study reviews different application techniques for bonding dental adhesive, such as adding a hydrophobic coat, active and sonic agitation, increasing the application time of adhesive, and adding multiple layers of bonding adhesive; that technique increased the bond strength.

The water-permeable nature of the monomers included in certain adhesives impairs the stability of dentinal bonding due to their hydrophilic properties; these phenomena occur because the monomer has a strong attraction to make the hydrogen ion bond to the hydrophilic part of the monomer that alters the formation of the polymer chain, so Many studies advise applying a hydrophobic coat of adhesive before curing. This approach aids in maintaining adhesive contact by preventing water absorption from the exterior oral cavity and water penetration by osmosis from the dentin substrate[20,24]. Adding a hydrophobic layer increases the bond strength, makes the adhesive layer thicker, increases sealing efficiency, increases the conversion rate, increases the mechanical properties, and reduces the degradation of the adhesive layer[24,25,26,27]. S.E. adhesives exhibit hydrophilic properties, hence requiring further protection. In addition, E&R adhesives, particularly those containing 2-hydroxyethyl methacrylate (HEMA), are hydrophilic. Therefore, applying an additional hydrophobic layer can decrease the amount of solvents and unreacted monomers retained within the hybrid layer[28]. Hence, to enhance the adhesive strength between the adhesive and dentin, it is preferable to apply an additional layer of hydrophobic coating,

The time between applying adhesive on the dentin surface and curing should be increased as it enhances the diffusion of the monomer into the dentin and increases the reaction between the minerals and monomers, increasing the bond strength[28,15]. This method enhances the concentration of collagen fibrils with resin, as it is preferable for the resin monomers to fill the gaps between the exposed collagen. Failure to do so may negatively impact the effectiveness and longevity of adhesive systems. In addition, increasing the duration of the adhesive application allowed for more solvated monomers to evaporate, which, in turn, facilitated the development of a stronger polymer on the dentinal surface and resulted in a higher bond strength between the resin and dentin[29,30].

Presently, the prevailing tendencies in bonding support the use of adhesive systems in a singular application. However, this approach does not allow for the creation of a thicker hybrid layer or adhesive layer that would enable micromechanical retention with the underlying composite resin. Prior studies have suggested that using multiple or triple adhesive layers can improve dentin's binding strength by facilitating monomers' entry into the hybrid layer (H.L.) and enhancing chemical interactions[28,31]. Therefore, it is vital to regard an additional layer application as an essential clinical procedure. Additionally, the 10-MDP monomer requires a specific time of 20 seconds for its chemical interaction to occur. Where is the reference for this statement? However, applying a second coat of this monomer without curing the first one allows the first layer to interact with hydroxyapatite crystals, resulting in effective additional bonding.

Additionally, it is essential to acknowledge that the increased strength of the dentin bond when applying the material twice is a result of multiple mechanisms functioning simultaneously; during the application of adhesive layers, the solvent contained within the adhesive evaporates; this causes an increase in the concentration of co-monomers that remain after each layer is applied. As a result, the quality of the H.L. (adhesive) improves; a prior study demonstrated that the dentin bond performance improved when several adhesive layers were applied without being cured[32].

This phenomenon cannot be attributed to the increase in the thickness of the adhesive layer but rather to the improved quality of the adhesive layer. The thickness of the adhesive film only grows when each coat is subjected to light curing. This ensures that the demineralized dentinal substrate will be adequately shielded, reducing the harmful consequences of oxygen inhibition by creating faulty bonds for self-etch (S.E.) and etch-and-rinse (E&R) adhesives. In summary, it is recommended that clinicians use multiple application layers, and they should evaluate the material and substrate contents of each adhesive[28,29].

The bond strength can be increased by applying an electric current to the dentin surface; this method enhances the chemical interaction between adhesive systems and tooth structures, resulting in increased infiltration of monomers into the demineralized dentinal substrate. This was achieved by modifying the surface charges and hydrogen bonding potential of the dentin substrate[33,34]. As a result, there is an improvement in the capacity of dentin to be wetted,

which causes the evaporation of solvents[32]. In addition, electrically assisted techniques improve the strength of the link between dentin and other materials and decrease the occurrence of nano leakage in the H.L. [35,36,37].

Nevertheless, the application of adhesive necessitates the use of a specific device that dispenses the adhesive solution through the utilization of an electrical potential difference between the adhesive system and the surfaces of the teeth[34].

Applying an electric current can improve the diffusion of resin monomers into etched dentin. This is because polar components like HEMA, polyalkanoic acid, biphenyl dimethacrylates copolymers, and dipentaerythritol penta-acrylate phosphate present in the adhesive formulation can interact with the electric field[33]. Previous research has indicated that electrical currents facilitate the mobility of a substrate that has been ionized[38,39]. However, it is still unclear whether the formation of appropriate dentin hybridization may be achieved by promoting the penetration of ionized substrates under various conditions and improving the elimination of water for self-etching adhesives[40,41]. Furthermore, applying an electric current can enhance the pace at which water is replaced by modifying the water dipoles. This modification promotes the exchange of water with the solvent during resin infiltration[20]. According to a claim, using electric currents ranging from 30 to 35 μA significantly enhanced the strength of bonds and the quality of bonding[42]. Using a current of 35 μA during bonding techniques has been shown to have no negative impact on cell viability, indicating that it can be considered safe. So, using electrical current is preferred for adhesive applications such as self-etch and ecth&rinse adhesive systems, which helps increase monomer penetration into dentin[34].

Applying adhesive with a bonding brush linked to an endo activator can increase the bond strength as it works at a speed of 10,000 CPM, which equals 3333 cycles in 20 seconds. This action produces an acoustic streaming force that increases the diffusion of monomers into dentin and increases the bond strength[43].

Another method to increase the bond strength is the application of adhesive with sonic energy that can enhance the bond between dentin and resin composite; a previous study confirms this improvement that applying the adhesive with a bonding brush linked to an endo activator can

increase the bond strength as it works at a speed of 10,000 CPM, which equals 3333 cycles in 20 seconds, This action produces an acoustic streaming force, and it increases the dynamic of adhesive solution that creates pressure and energy that enhances the diffusion of monomer to dentin, leading to a thicker hybrid layer with more extended resin tags[43].

Manual agitation is one of the recommendations for bonding application. Research indicated that active agitation of a two-step self-etch adhesive technique increased bond strength. The explanation for this phenomenon might be attributed to the complete dissolving of the smear layer into the adhesive[41]. while Miyazaki et al. discovered a dissimilar result while examining the identical adhesion approach[40]. Another research found that the effectiveness of S.E. adhesive systems was linked to the length of time the adhesive was agitated .[35]Overall, the stirring of the adhesive was able to enhance the movement of the particles and allow for improved diffusion of the monomers inside the dentinal tubule[41].

Ultrasonics is a branch of acoustics that focuses on using sound waves at frequencies higher than what humans can hear. It should be noted that the oscillating devices used in dentistry practice often operate at ultrasonic frequencies, specifically spanning from 20,000 to 40,000 Hz. Furthermore, a sound is classified as sonic when its frequency falls within 1000 to 6000 Hz[44]. Ultrasonic activation of adhesive was attempted to increase the bond strength by creating acoustic energy that increases monomer diffusion to the dentin. A systemic review found that ultrasonic agitation did not detect an improvement in dentin bond strength in all of the examined adhesives[45].

In summary, it is advisable to understand the chemistry of the adhesive being used and the previous application technique to assist in enhancing the bond strength.

conclusion

The bond strength between dentin and resin composite can be increased by using any of the application techniques: application of a hydrophobic resin layer, prolonged application period, a double-layer application, the use of an electric current to help the application, sonic agitation and actively applying the adhesive. It is advisable to understand the chemistry of the adhesive being used and the previous application technique to assist in enhancing the bond strength.

Reference

1. Van Meerbeek, B.; Peumans, M.; Poitevin, A.; Mine, A.; Van Ende, A.; Neves, A.; De Munck, J. Relationship between Bond-Strength Tests and Clinical Outcomes. Dent. Mater. 2010, 26, e100–e121.
2. AL-SHAMMA, Abdulla MW. Comparative evaluation of the effect of different universal adhesives and bonding techniques on the marginal gap of class I composite restoration (an S.E.M. study). 2016.
3. Perdigão, J. Current Perspectives on Dental Adhesion:(1) Dentin Adhesion–Not There Yet. Jpn. Dent. Sci. Rev. 2020, 56, 190–207. [CrossRef] [PubMed]
4. . Orilisi, G.; Monterubbianesi, R.; Notarstefano, V.; Tosco, V.; Vitiello, F.; Giuliani, G.; Putignano, A.; Orsini, G. New insights from Raman MicroSpectroscopy and Scanning Electron Microscopy on the microstructure and chemical composition of vestibular and lingual surfaces in permanent and deciduous human teeth. Spectrochim. Acta Part A Mol. Biomol. Spectrosc. 2021, 260, 119966. [CrossRef] [PubMed]
5. .Hardan, L.; Daood, U.; Bourgi, R.; Cuevas-Suárez, C.E.; Devoto, W.; Zarow, M.; Jakubowicz, N.; Zamarripa-Calderón, J.E.; Radwanski, M.; Orsini, G.; et al. Effect of Collagen Crosslinkers on Dentin Bond Strength of Adhesive Systems: A Systematic Review and Meta-Analysis. Cells 2022, 11, 2417. [CrossRef]
6. . Iliev, G.; Hardan, L.; Kassis, C.; Bourgi, R.; Cuevas-Suárez, C.E.; Lukomska-Szymanska, M.; Mancino, D.; Haikel, Y.; Kharouf, N. Shelf Life and Storage Conditions of Universal Adhesives: A Literature Review. Polymers 2021, 13, 2708. [CrossRef]
7. . Bourgi, R.; Hardan, L.; Rivera-Gonzaga, A.; Cuevas-Suárez, C.E. Effect of Warm-Air Stream for Solvent Evaporation on Bond Strength of Adhesive Systems: A Systematic Review and Meta-Analysis of in Vitro Studies. Int. J. Adhes. Adhes. 2021, 105, 102794. [CrossRef
8. .Hardan, L.; Devoto, W.; Bourgi, R.; Cuevas-Suárez, C.E.; Lukomska-Szymanska, M.; Fernández-Barrera, M.Á.; CornejoRíos, E.; Monteiro, P.; Zarow, M.; Jakubowicz, N.; et al. Immediate Dentin Sealing for Adhesive Cementation of Indirect Restorations: A Systematic Review and Meta-Analysis. Gels 2022, 8, 175. [CrossRef]

9. . Bourgi, R.; Daood, U.; Bijle, M.N.; Fawzy, A.; Ghaleb, M.; Hardan, L. Reinforced Universal Adhesive by Ribose Crosslinker: A Novel Strategy in Adhesive Dentistry. Polymers 2021, 13, 704. [CrossRef] 10. Hardan, L.; Bourgi, R.; Cuevas-Suárez, C.E.;Zarow, M.; Kharouf, N.; Mancino, D.; Villares, C.F.; Skaba, D.; Lukomska-Szymanska, M. The Bond Strength and Anti-bacterial Activity of the Universal Dentin Bonding System: A Systematic Review and MetaAnalysis. Microorganisms 2021, 9, 1230. [CrossRef] [PubMed]
10. Khalil RJ & Al-Shamma AM. Early and delayed effect of 2% chlorhexidine on the shear bond strength of composite restorative material to dentin using a total-etch adhesive. J Bagh College of Dent. 2015; 27, 24-31.
11. Yiu, C.K.; Pashley, E.L.; Hiraishi, N.; King, N.M.; Goracci, C.; Ferrari, M.; Carvalho, R.M.; Pashley, D.H.; Tay, F.R. Solvent and Water Retention in Dental Adhesive Blends after Evaporation. Biomaterials 2005, 26, 6863–6872. [CrossRef] [PubMed]
12. Al-Salamony, H.; Naguibb, E.A.; Hamzac, H.S.; Younisd, S.H. The Effect of Warm Air Solvent Evaporation on Microtensile Bond Strength of Two Different Self-Etch Adhesives to Dentin (In Vitro Study). SYLWAN 2020, 164, 479–497.
13. Ferreira, J.C.; Pires, P.T.; Azevedo, A.F.; Oliveira, S.A.; Melo, P.R.; Silva, M.J. Influence of Solvents and Composition of Etchand-Rinse and Self-Etch Adhesive Systems on the Nanoleakage within the Hybrid Layer. J. Contemp. Dent. Pract. 2013, 14, 691. [CrossRef] [PubMed]
14. Chimeli, T.B.C.; D'Alpino, P.H.P.; Pereira, P.N.; Hilgert, L.A.; Di Hipolito, V.; Garcia, F.C.P. Effects of Solvent Evaporation on Water Sorption/Solubility and Nanoleakage of Adhesive Systems. J. Appl. Oral Sci. 2014, 22, 294–301. [CrossRef] [PubMed]
15. Hardan, L.; Bourgi, R.; Kharouf, N.; Mancino, D.; Zarow, M.; Jakubowicz, N.; Haikel, Y.; Cuevas-Suárez, C.E. Bond Strength of Universal Adhesives to Dentin: A Systematic Review and Meta-Analysis. Polymers 2021, 13, 814. [CrossRef] [PubMed]
16. Yesilyurt, C.; Bulucu, B. Bond Strength of Total-Etch and Self-Etch Dentin Adhesive Systems on Peripheral and Central Dentinal Tissue: A Microtensile Bond Strength Test. J. Contemp. Dent. Pract. 2006, 7, 26–36. [CrossRef] [PubMed]
17. Özer, F.; Ünlü, N.; Sengun, A. Influence of Dentinal Regions on Bond Strengths of Different Adhesive Systems. J. Oral Rehabil. 2003, 30, 659–663. [CrossRef] [PubMed]

18. Armstrong, S.; Geraldeli, S.; Maia, R.; Raposo, L.H.A.; Soares, C.J.; Yamagawa, J. Adhesion to Tooth Structure: A Critical Review of “Micro” Bond Strength Test Methods. Dent. Mater. 2010, 26, e50–e62. [CrossRef] [PubMed]
19. Sirisha, K.; Rambabu, T.; Ravishankar, Y.; Ravikumar, P. Validity of Bond Strength Tests: A Critical Review-Part II. J. Conserv. Dent. J.C.D. 2014, 17, 420. [CrossRef] [PubMed
20. Ermis, R.B.; Ugurlu, M.; Ahmed, M.H.; Van Meerbeek, B. Universal Adhesives Benefit from an Extra Hydrophobic Adhesive Layer When Light Cured Beforehand. J. Adhes. Dent. 2019, 21, 179–188.
21. Hardan, Louis, et al. "Effect of different application modalities on the bonding performance of adhesive systems to dentin: a systematic review and meta-analysis." *Cells* 12.1 (2023): 190.
22. ABDULAMIR, Shahed Wissam, et al. Fracture resistance of endodontically treated Maxillary Premolar Teeth restored with wallpapering technique: a comparative in Vitro Study. International Journal of Dentistry, 2023, 2023.
23. AL-HASAN, R. M.; AL-TAEE, L. A. Interfacial Bond Strength and Morphology of Sound and Caries-affected Dentin Surfaces Bonded to Two Resin-modified Glass Ionomer Cements. Operative Dentistry, 2022, 47.4: E188-E196.
24. Manso, A.P.; Marquezini Jr, L.; Silva, S.M.; Pashley, D.H.; Tay, F.R.; Carvalho, R.M. Stability of Wet versus Dry Bonding with Different Solvent-Based Adhesives. Dent. Mater. 2008, 24, 476–482. [CrossRef] [PubMed]
25. Serafim, M.F.D.; Leal, A.M.A.; Bauer, J.; Gomes, I.A.; Carneiro, K.G.K. Effect of an Hydrophobic Layer on a Universal Adhesive. RGO-Rev. Gaúcha Odontol. 2018, 66, 339–344. [CrossRef]
26. de Andrade Silva, S.M.; de Oliveira Carrilho, M.R.; Marquezini Junior, L.; Garcia, F.C.P.; Manso, A.P.; Alves, M.C.; de Carvalho, R.M. Effect of an Additional Hydrophilic versus Hydrophobic Coat on the Quality of Dentinal Sealing Provided by Two-Step Etchand-Rinse Adhesives. J. Appl. Oral Sci. 2009, 17, 184–189. [CrossRef]
27. Cadenaro, M.; Antoniolli, F.; Sauro, S.; Tay, F.R.; Di Lenarda, R.; Prati, C.; Biasotto, M.; Contardo, L.; Breschi, L. Degree of Conversion and Permeability of Dental Adhesives. Eur. J. Oral Sci. 2005, 113, 525–530. [CrossRef]

28. Ito, S.; Tay, F.R.; Hashimoto, M.; Yoshiyama, M.; Saito, T.; Brackett, W.W.; Waller, J.L.; Pashley, D.H. Effects of Multiple Coatings of Two All-in-One Adhesives on Dentin Bonding. J. Adhes. Dent. 2005, 7, 133–141. [PubMed]
29. Pashaev, D.; Demirci, M.; Tekçe, N.; Tuncer, S.; Baydemir, C. The Effect of Double-Coating and Times on the Immediate and 6-Month Dentin Bonding of Universal Adhesives. Biomed. Mater. Eng. 2017, 28, 169–185. [CrossRef]
30. Reis, A.; de Carvalho Cardoso, P.; Vieira, L.C.C.; Baratieri, L.N.; Grande, R.H.M.; Loguercio, A.D. Effect of Prolonged Application Times on the Durability of Resin–Dentin Bonds. Dent. Mater. 2008, 24, 639–644. [CrossRef] [PubMed]
31. Chowdhury, A.; Saikaew, P.; Alam, A.; Sun, J.; Carvalho, R.M.; Sano, H. Effects of Double Application of Contemporary Self-Etch Adhesives on Their Bonding Performance to Dentin with Clinically Relevant Smear Layers. J. Adhes. Dent. 2019, 21, 59–66.
32. Hashimoto, M.; De Munck, J.; Ito, S.; Sano, H.; Kaga, M.; Oguchi, H.; Van Meerbeek, B.; Pashley, D.H. In Vitro Effect of Nanoleakage Expression on Resin-Dentin Bond Strengths Analyzed by Microtensile Bond Test, SEM/EDX and T.E.M. Biomaterials 2004, 25, 5565–5574. [CrossRef
33. Pasquantonio, G.; Tay, F.R.; Mazzoni, A.; Suppa, P.; Ruggeri Jr, A.; Falconi, M.; Di Lenarda, R.; Breschi, L. Electric Device Improves Bonds of Simplified Etch-and-Rinse Adhesives. Dent. Mater. 2007, 23, 513–518. [CrossRef]
34. Visintini, E.; Mazzoni, A.; Vita, F.; Pasquantonio, G.; Cadenaro, M.; Di Lenarda, R.; Breschi, L. Effects of Thermocycling and Use of ElectroBond on Microtensile Strength and Nanoleakage Using Commercial One-step Self-etch Adhesives. Eur. J. Oral Sci. 2008, 116, 564–570. [CrossRef]
35. Chen, H.; Fu, D.; Yang, H.; Liu, Y.; Huang, Y.; Huang, C. Optimization of Direct Currents to Enhance Dentine Bonding of Simplified One-step Adhesive. Eur. J. Oral Sci. 2014, 122, 286–292. [CrossRef]
36. Pashley, D.H. Dentin Permeability, Dentin Sensitivity, and Treatment through Tubule Occlusion. J. Endod. 1986, 12, 465–474. [CrossRef
37. Puapichartdumrong, P.; Ikeda, H.; Suda, H. Facilitation of Iontophoretic Drug Delivery through Intact and Caries-affected Dentine. Int. Endod. J. 2003, 36, 674–681. [CrossRef]

38. Pashley, D.H.; Agee, K.A.; Carvalho, R.M.; Lee, K.-W.; Tay, F.R.; Callison, T.E. Effects of Water and Water-Free Polar Solvents on the Tensile Properties of Demineralized Dentin. Dent. Mater. 2003, 19, 347–352. [CrossRef]
39. Velasquez, L.M.; Sergent, R.S.; Burgess, J.O.; Mercante, D. Effect of Placement Agitation and Placement Time on the Shear Bond Strength of 3 Self-Etching Adhesives. Oper. Dent. 2006, 31, 426–430. [CrossRef]
40. Miyazaki, M.; Platt, J.; Onose, H.; Moore, B. Influence of Dentin Primer Application Methods on Dentin Bond Strength. Oper. Dent. 1996, 21, 167–172. [PubMed]
41. Velasquez, L.M.; Sergent, R.S.; Burgess, J.O.; Mercante, D. Effect of Placement Agitation and Placement Time on the Shear Bond Strength of 3 Self-Etching Adhesives. Oper. Dent. 2006, 31, 426–430. [CrossRef]
42. Guarda, MB; Di Nizo, P.T.; Abuna, G.F.; Catelan, A.; Sinhoreti, M.A.C.; Vitti, R.P. Effect of Electric Current-Assisted Application of Adhesives on Their Bond Strength and Quality. J. Adhes. Dent. 2020, 22, 393–398.
43. Awad, M.M., Alhalabi, F., Bamuqadm, M. *et al.* Adhesive sonic agitation improves bonding durability to class-II cavity preparation. *Odontology* **111**, 409–419 (2023). https://doi.org/10.1007/s10266-022-00751-3
44. Mena-Serrano, A.; Costa, T.; Patzlaff, R.T.; Loguercio, A.D.; Reis, A. Effect of Sonic Application Mode on the Resin-Dentin Bond Strength and Dentin Permeability of Self-Etching Systems. J. Adhes. Dent. 2014, 16, 435–440.
45. Bagis, B.; Turkarslan, S.; Tezvergil-Mutluay, A.; Uctasli, S.; Vallittu, P.K.; Lassila, L.V. Effect of Ultrasonic Agitation on Bond Strength of Self-Etching Adhesives to Dentin. J. Adhes. Dent. 2008, 10, 441–445. [PubMed]

Studying the Effect of Tea Tree Oil on the Surface Hardness, and Detail Reproduction of Type III Dental Stone

Yahya Khalid Yahya [1], Aseel Mohammed Al-Khafaji [1]

1Department of Prosthetic Dentistry, College of Dentistry, Baghdad University, Baghdad, Iraq.

The corresponding author (:email: aseel.khafaji@codental.uobaghdad.edu.iq **)**

Studying the Effect of Tea Tree Oil on the Surface Hardness, and Detail Reproduction of Type III Dental Stone

Yahya Khalid Yahya [1], Aseel Mohammed Al-Khafaji [1]

1Department of Prosthetic Dentistry, College of Dentistry, Baghdad University, Baghdad, Iraq.

The corresponding author(: email: aseel.khafaji@codental.uobaghdad.edu.iq **)**

Abstract

Gypsum materials have been utilized throughout various industries, such as dentistry, to perform several procedures. Restorative dentistry involves a substantial risk of spreading pathogenic germs from saliva to molds. Hence, it is necessary to disinfect these casts after every clinical and laboratory procedure. This study aims to assess the impact of tea tree oil (TTO) as a disinfecting solution on the characteristics of type III dental stones, such as surface hardness and detail reproduction, by immersion techniques. A total number of 60 stone specimens were created, with 30 samples designated for each test. Three groups were randomly chosen, each consisting of ten samples. The control group was immersed in distilled water for 10 minutes as the negative control. The test groups were exposed to 0.75% and 1.0% TTO. The study revealed that after disinfection with TTO, all of the specimens achieved the reproduction of detail test requirements, and there was no noticeable alteration in the surface hardness. Based on the results of all trials, it is evident that both 0.75% TTO and 1% TTO are suitable for disinfecting dental stone, making TTO a great choice for dentists and dental laboratory staff to sterilize casts.

Keywords: Tea Tree essential oil, Type III dental stone, Surface Hardness, Reproduction of Details, Disinfection

1. INTRODUCTION

Gypsum and its associated byproducts have a long history of usage in a wide range of industries. Casts and other dental laboratory procedures mostly include gypsum components. There is a very significant danger of cross-contamination with stone casts in dental work because of the numerous potential paths for infectious organisms to be transported from the patient's saliva to the impression and cast. So, following every clinical and laboratory operation, these molds should be disinfected [1]. The primary risk faced by a dental practitioner is the potential for contracting and transmitting serious transmissible diseases.

Equipment parts, tools, impressions, and castings have been identified as potential sources of microbial contamination due to their ability to facilitate the spread of infections through blood and saliva. Therefore, additional measures need to be implemented when designing, managing, and installing prostheses. (2). From a laboratory standpoint, cleaning the imprints before creating the stone cast can effectively remove visible contamination like blood and saliva containing residues found in the mouth, such as non-adherent microorganisms, cellular material, and food debris. (3). Dental impressions or gypsum models need to be disinfected before being used, according to the American Dental Association (ADA) and the Centers for Disease Control and Prevention (CDC)(3,4). Cast disinfection is considered essential to constructing disinfect models as well as establishing a cross-contamination control process due to the challenges and issues associated with impression disinfection. (5). It is important to keep the physical features of the mold or die, such as gypsum's ability to maintain its size, from being damaged by the disinfection solution while effectively eliminating microbes. (6). Michael et al.'s research found that the mechanical characteristics of stone specimens were considerably altered following 24 hours of immersion and spraying disinfection with 0.5% sodium hypochlorite (NaOCl) compared to the control group. (7,8). Another study found that the mechanical properties of type III and IV dental stones were significantly changed after being chemically disinfected with 1% Virkon, 0.525% sodium hypochlorite, and a different slurry solution. (3). The perfect disinfectant or sanitizer should be safe, non-corrosive, effective for different formulations, and reasonably priced. Essential oils are volatile and fragrant compounds produced naturally by plants through secondary metabolism. They possess various therapeutic properties and have been valued for their safety and effectiveness in promoting human health since ancient times. (9,10). Tea tree oil (TTO) is a naturally derived antibacterial with broad-spectrum properties that has been used for over 80 years in medicine to treat many different medical conditions. (11). Reports show M. alternifolia oil kills E. coli, Staphylococcus species, Lactobacillus, Actinomyces viscosus, S. epidermidis, B. subtilis, S. aureus, and S. typhimurium,(12–14). Moreover, it is biostatic against Pseudomonas aeruginosa, Serratia marcescens strains, and Halobacterium violaceum(15). Studies discuss the efficacy of TTO as a disinfectant against coronaviruses. (16). In dentistry, natural plant components are becoming more common in toothpaste and mouthwashes. (17). TTO reduces oral bacteria to prevent dental caries, periodontal disease, oral mucosal infections, and other oral ailments. (18) Research has found that using essential oils on dental implant surfaces prevents the formation of biofilms. It can expedite the healing process and improve the effectiveness of therapy and recovery following oral surgery. (19,20). On the other hand, there is not a great deal of study on the impact that TTO has on dental stone. Given these results, TTO is an excellent choice for the study that is currently going on. To the best of the authors' knowledge, there is no previous research that evaluates the influence of TTO disinfecting solution on certain characteristics of type III dental stones. Given this, the purpose of the current study was to analyse several physico-mechanical properties of type III dental stone that had been submerged in TTO as a disinfectant solution for 10 minutes. These properties included surface hardness and replication of details. Under the supposition that TTO, when used as a disinfectant, does

not affect the surface hardness and reproduction of type III dental stone features, the null hypothesis was rejected.

2. MATERIALS AND METHODS

Specimen preparation

The main components utilized in the study were Dental stone type III (Elite model, Zhermack S.p.A., Rovigo, Italy), Distilled water (Dis water, Iraq), and Tea tree oil (Now foods; Bloomingdale, IL 60108, USA). The mixing technique, testing circumstances, and equipment used were following Revised ANSI/ADA Standard No. 25-2015. An incubator from Memmert GmbH, Germany, was utilized to preserve the specimens at a temperature of 23 ±2ºC and a relative humidity of 50(±10%) to avoid contamination or alterations in the stone's physical properties before testing. They allocated a minimum of 15 hours for suitable exposure to the conditions above. All equipment utilized for mixing and testing was sterile, devoid of moisture, and free from contaminants, including dental stone remnants. The dental stone was kept in a safe, moisture-proof pouch, firmly sealed to avoid contamination or alterations to its physical properties. Before use, the dental stone powder was effectively blended by swirling it thoroughly with a dry spatula inside the bag. Water was measured with a graduated cylinder accurate to 0.5 mL, while dental stone powder was measured with an electronic balance accurate to 0.01 g. According to the manufacturer's guidelines, dental stones are often mixed manually for 1 minute at a water-to-powder ratio of 30 mL per 100 g to achieve a consistent and practical mixture. The dental stone mixture was prepared according to Revised ANSI/ADA Standard No. 25-2015 and then poured into a rubber ring of 20 mm in height and 30 mm in diameter to create the stone specimens. The dental stone combination was consistently vibrated using a vibrator at 4000 revolutions per minute (rpm). To minimize air bubbles and decrease porosity during the pouring process. Glass slabs were positioned on the top and bottom edges of the rubber ring to create examples with surfaces that looked uniform, sleek, and parallel. After 30 minutes of mixing, all stone samples were removed from the rubber ring and left for a whole day at an average temperature of 23± 2°C and a relative

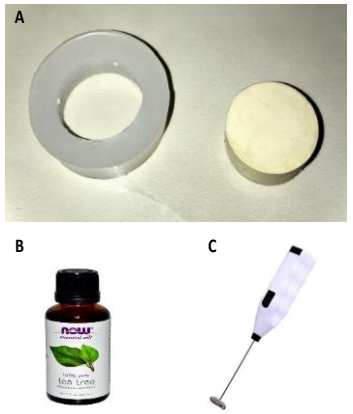

Fig. 1. (A) Rubber ring and type III stone sample (B) Tea tree essential oil and (C) Electric hand mixer.

humidity of 50 ±10%, as depicted in Figure 1A.

TTO disinfectant solution preparation

The concentration, handling, and storage of the testing solutions were conducted according to the manufacturer's requirements. The TTO disinfecting solution was utilized for the initial time in conjunction with a dental stone. The experimental concentrations (0.75% and 1%) and immersion duration (10 min) in this study were chosen based on previous research that utilized Tea Tree Oil (TTO) as a disinfectant with various dental materials like acrylic, soft liner, and dental impression materials.(21–26) The TTO displayed in Figure 1B was diluted for use in the test according to the following equation(27) :

$$C_1V_1=C_2V_2 \quad (1)$$

Where C_1=100% TTO concentration, V_1=volume of TTO removed, C_2=required TTO concentration, and V_2=volume of the final solution. Mixing was carried out for one minute using an electric hand mixer, as shown in Figure 1C—preparation of the disinfecting chemical solutions. TTO was diluted by organic solvent Polysorbate 80 (Tween 80 Sigma, USA) and by (1%volume) to improve TTO solubility and ease of solution mixing(27–29) .To make a 0.75% TTO disinfection solution, combine 1.5 ml of TTO and 2 ml of Tween 80 with 200 ml of distilled water. A 1.0% TTO disinfection solution was made by combining 2 ml of TTO and 2 ml of Tween 80, then adding it to 200 ml of distilled water.

Specimen groups and immersion in disinfectant solutions

A total number of 60 specimens of type III dental stone were divided into two groups: 30 for surface hardness testing and 30 for detail reproduction testing. These samples were then randomly assigned to three groups, each containing 10 samples.

Group A used distilled water immersion for 10 minutes as a negative control, without any disinfection treatment.

Group B: Stone samples were submerged in a 0.75% solution of TTO for 10 minutes.

Group C: Stone samples were submerged in a 1% solution of TTO for 10 minutes.

Disinfection of stone specimens by immersion method

The stone samples were placed in a container of an appropriate size and completely submerged in the disinfection solutions that had been prepared for ten minutes at room temperature before use. Following the removal of the samples from the solution, they were washed with distilled water and then allowed to dry themselves naturally for one hour at a temperature of 23±2 °C and a relative humidity of 50±10 %. After that, they were stored in an incubator with a desiccator until the time arrived for the tests to be performed. A tweezer was used to move the stone samples into and out of the cleaning solutions when they were being cleaned.

Testing procedure

A. Surface hardness test

The Shore (Durometer) hardness assessment employed in this investigation corresponds with all applicable international standards and remains simple. Each durometer type has been designed to a specific scale (A, B, C, or D) and can yield a number between 0 and 100. A value of 0 is acquired if the indenter entirely penetrates the sample; on the contrary, a reading of 100 is obtained. The Shore D hardness tester (Time Group Inc., China) was used to test each specimen. According to the manufacturer, the device applied a constant force of 50 N on the sample's surface with a pointed indenter. After the pointed indenter had penetrated the specimen's outermost layer, the hardness test results appeared on the device's screen after roughly 5 seconds. The findings are shown as the average of five measurements on each specimen: one in the center, two to the right, and two to the left of the center (30,31).

B. Reproduction of details test

Using specially manufactured test equipment (a test block, a ring mold, and a slit mold), this test was carried out following the Revised ANSI/ADA Standard No. 25-2015. Using AutoCAD software, the design of the test apparatus was duplicated as a print file that could be printed by a 3D printer (Max UV385, Asiga), with an accuracy of 10 µm, photo polymerized resin for dental models (MAZIC D) was used as the 3D printing material. The following characteristics apply to the equipment are illustrated in (Figures 2A and 2B).

A-The test block's upper surface includes five grooves at an angle of 90°±5°, with widths of X= 50±8 µm, Y=20±4 µm, and Z=75±8 µm. The distance between each groove is 2.5 mm. In addition, there are two additional grooves, each with a width of (75±8 µm) and the same V-shaped angle as the previous grooves shown in (Figure 2C).

B-A ring mold with an interior diameter of 30 mm and a height of 6 mm is used to pour silicone impression or duplicating material onto test blocks with grooved surfaces.

C-A slit mold with internal diameters of 20 mm and 30 mm was also used.

A non-reacting mold release agent (separating agent) was applied to the ring mold before placing it on the text block. Silicone duplicating material was combined according to the manufacturer's recommendations at a 1:1 ratio until slightly overfilled. A glass plate was placed on the mold, and a load of 1500 g was applied for 5±1 sec before being withdrawn to allow the material to be set. The ring mold was gently removed after 30±1 min to prevent distortion. A non-reacting mold-releasing agent was applied to the slit mold, which was then covered with silicone duplicating material and placed over the ring mold. The dental stone was prepared as previously aforementioned, poured into the slit mold, and gently vibrated for 30 seconds to prevent air bubble entrapment. Once the mold was filled, it was placed in ambient air with a relative humidity of 50±10% and a temperature of 23±2°C. The dental stone

samples were then separated and appeared as shown in Figure 2D after 45±1 min. Under an optical microscope (Dino-lite) positioned at a fixed distance and ×4 magnification, the disintegration of duplicated 25-mm-long and 50 μm-wide lines was investigated to determine the effect of solutions on the samples. For type III dental stone, the relevant groove for the reproduction of details test evaluation is the 50 μm-wide "a" groove. Specimen examination under an optical microscope reveals whether a complete or incomplete groove reproduction has occurred to determine whether the specimen met this test requirement. The assessments were performed, and the examiners were not informed of the type of specimens being evaluated. Each specimen was evaluated using the I–IV scoring method(32). The following criteria were set up to evaluate the reproduction capabilities of stone specimens, and the 0.05 mm line received the following scores:

Score I: Distinct and continuous line throughout the whole ring.

Score II: The line was unbroken and clear for more than half the width of the ring.

Score III: The line's continuity and clarity were less than half the ring's width

Score IV: The line was not extending the whole width of the ring.

Statistical analysis

The average roughness, hardness, and dimensional stability test results from the control and test groups were compared using one-way ANOVA. To look into the normality of the distribution of values, the Shapiro-Wilk test was performed on all test results. The statistical parameter of interest is the test statistic (W), calculated by comparing the observed data distribution to the expected distribution of a normal distribution with the same mean and variance. The test statistic (W) measures the degree of similarity between the observed distribution and the expected normal distribution by calculating a p-value, which measures the evidence against the null hypothesis that the data come from a normal distribution. If the p-value is less than 0.05, the null hypothesis is rejected, and it is concluded that the data do not come from a normal distribution. Levene's test assessed the equality of variances for a variable calculated for the groups. A post hoc test (Fisher’s LSD) was conducted to confirm the differences between the test groups. If the p-value from the ANOVA is less than 0.05, the null hypothesis can be rejected, and it can be said that at least one of the group means differs from the others. A post-hoc test determines precisely which groups differ from one another.

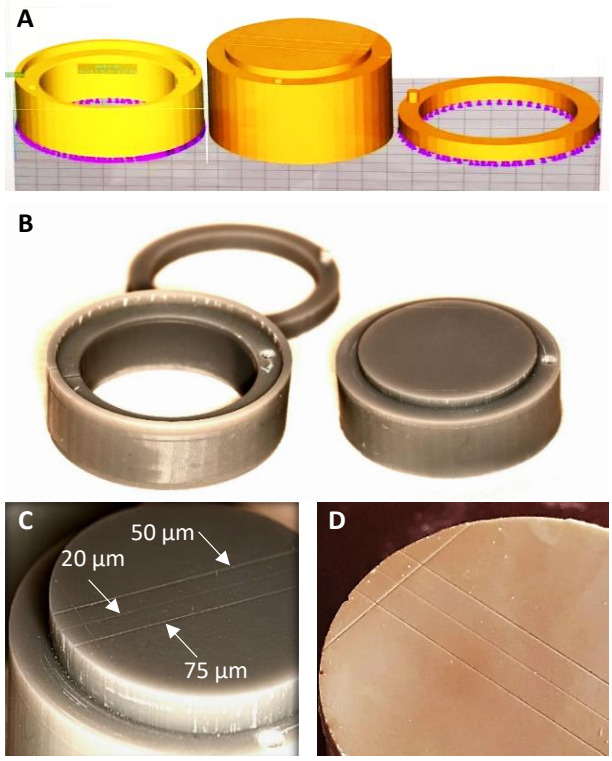

Fig. 2 (A) CAD model at the start of the printing process, (B) Printed test equipment utilized in the reproduction of details test, (C) Test Block utilized in the reproduction of details test with three parallel lines, (D) Stone sample utilized in the reproduction of details test.

3. RESULTS AND DISCUSSION

The results of the experiments show that all values were normally distributed (Table 1). For every stone sample, two evaluations were made: one before the disinfection process began (24 hours after mixing and pouring the stone) and one after one hour after the disinfection process. The difference between the two measurements was considered for evaluation. Figure 3 presents the effect of using a TTO disinfectant solution on surface hardness.

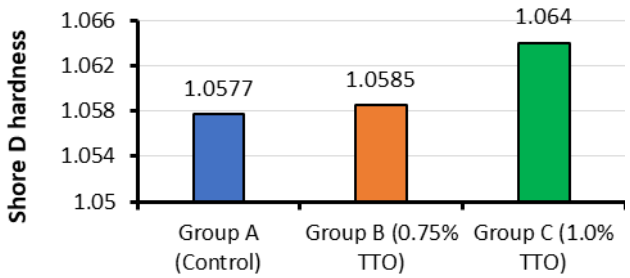

Fig.3 Results for surface hardness of type III dental stone.

Table 1. Normality of the distribution of values using the Shapiro-Wilk test on all test results

Tests	Group A		Group B		Group C	
	P-Value	Passed	P-Value	Passed	P-Value	Passed
Surface hardness	73 (NS)	es	0.141 (NS)	es	0.198 (NS)	es

Table 2. Statistics of surface hardness test for type III dental stone utilizing one-way ANOVA

The resulting alteration in surface hardness was determined as an alteration in the Shore D hardness value after 24 hours. The test groups' mean values are shown in Figure 3. The highest value was for Group C, then Group B, and the least was for Group A (control). One-way ANOVA revealed that the difference among the groups was insignificant (P=0.578) as shown in(table 2).

Test	Groups	N	Mean	± SD	F-Value	P-Value	Levene's test	df	p-value
Surface hardness	**Group A**	10	1.0577	0.0195	0.559	**0.578**	5.482	2	0.01 (S.)
	Group B	10	1.0585	0.0081					
	Group C	10	1.064	0.0134					

Regarding the reproduction of the details, the test outcomes showed that all specimens from the test groups (0.75% and 1.0% TTO solutions) and the control group (0.0% TTO) had successfully reproduced (Scale I for all samples) a complete 50 m-wide "a" groove. Hence, it met the requirement of ADA specifications, as shown in (Figure 4).

Despite digital technology for virtual cast construction, dental stones continue to be widely utilized in dentistry for many different uses within private practices and laboratories for cast construction, in addition to mounting casts in articulators. Its popularity may be linked to its low prices, usability, and capacity for generating accurate outcomes(33). Disinfection of the cast is essential in preventing cross-contamination because microorganisms have been detected in the cast poured against contaminated impressions. Many studies have attempted to disinfect gypsum casts by immersing or spraying the casts with disinfectant solutions(34,35).

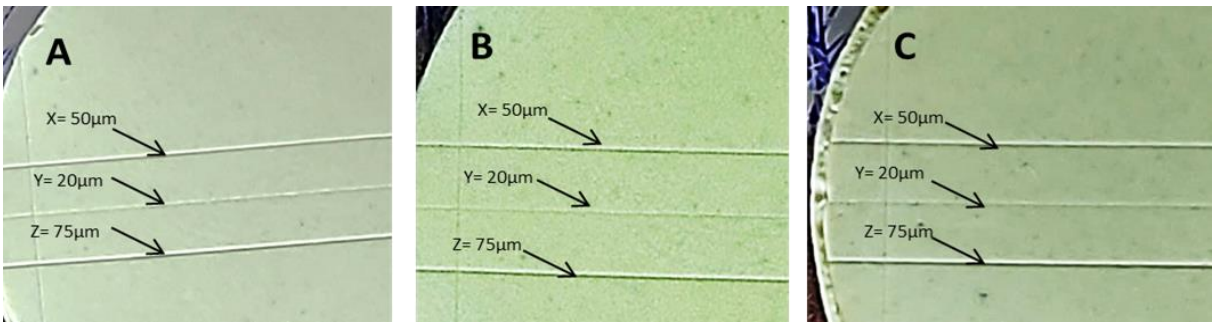

Fig.4 A sample of reproduction of details test specimens: (A) 0% TTO (B) 0.75% TTO (C) 1.0% TTO. For all groups, the results showed Score I.

Oral impressions frequently contain blood and salivary microorganisms, which can easily contaminate stone casts and survive up to seven days in set gypsum(36). An ideal disinfectant and sanitizer must also be noncorrosive, nontoxic to surface contact, effective in various forms, and inexpensive(37). Direct disinfection of stone casts by immersion, spraying, or mixing the disinfectant with water appears to be a safer and more efficient alternative(38) Natural herbal remedies from aromatic and therapeutic plants, such as essential oils, are frequently used as antibacterial, antifungal, antioxidant, and anti-inflammatory agents. These extracts have significant advantages over synthetic products because they do not develop antibacterial resistance or lead to toxicity(39,40).

Surface hardness testing is essential to dental stone evaluation. According to the majority, harder stones will provide better wear resistance and less chance of destruction during a pattern or casting manufacturing and finishing. Dental stone, which must be sufficiently strong to resist the stresses of the construction process, has been utilized mainly to create indirect dental prostheses (41) III Dental stone samples were disinfected with TTO, and their surface hardness was evaluated 24 hours later to ensure a complete setting. It was not significantly different from the control group. The natural product affects the properties of dental stone, such as surface hardness, color, or texture, depending on the concentration, duration, and application method. Insignificant differences in the result may be due to the surface hardness of the dental stone being determined by its crystalline structure and the strength of the bonds between its atoms. TTO cannot alter these fundamental properties in this short immersion period (10 min) used in this study. As TTO disinfectant solution is being used with dental stones for the first time, the findings of this study cannot be directly compared to those of earlier studies but are generally consistent with previous research that found some disinfectant solutions did not alter surface hardness value(42). The surface hardness of stone casts immersed in slurry and 1% peroxy genic acid solutions were not significantly different (43). While Ibrahim and Al-Harbi F. (2015) found no appreciable difference in the surface hardness of dental stone following disinfection using acid glutaraldehyde and iodophor in their studies(44) Another study by Moslehifard et al. (2013) evaluated the effect of disinfectant solutions on the surface hardness of dental stone casts and found that there was no significant difference in surface hardness between the control group and the groups treated with 0.5% sodium hypochlorite, 2% chlorhexidine gluconate, or 2% glutaraldehyde(45). Different disinfection solution types, immersion times, and measurement methods may alter the findings.

Regarding the quality of the reproduction of details, the findings showed that the disinfection of type III dental stone specimens with 0.75 % and 1.0% TTO by immersion method did not affect the quality of the reproduction of details when compared to the control group, meaning that all of the specimens from both the control group and the experimental groups had successfully reproduced the test's required 50 µm-wide "a" groove. This result aligns with other studies where no noticeable difference between the experimental and control groups regarding detail reproduction was found (46). Additionally, Abdullah, in 2006, claimed that with repeated immersion in a slurry containing 0.525% NaOCl and drying of a stone cast, surface characteristics for type III stones were slightly damaged by disinfectant solution. However, the difference was insignificant, so it could be used in the lab without negatively affecting the quality of the surface details(32). Also, Al-khafaji et al. concluded that stone specimens immersed in or sprayed with NaOCl and SOLO disinfection solutions did not lose any surface details(47). The study by Zaid and Abass in 2022 found that immersion in 0.1% hypochlorous acid disinfectant for 10 minutes did not result in a significant difference in surface hardness or detail reproduction of type III dental stone compared to the control group(31). The careful mixing of dental stone in small increments and vibration of the rubber ring mold to minimize air bubbles may have helped reproduce the 0.05 mm-wide groove with little distortion. Reducing air bubble entrapment in the dental stone mixture may have improved grooved surface reproduction, exceedingly narrow grooves with little distortion. The results may not apply to clinical settings because the study was in vitro. The study did not explain tea tree oil's long-term effects or how different disinfection techniques affected dental stone.The use of tea tree oil as a disinfectant for dental stone may increase the surface roughness of the dental stone, which can negatively affect the fit of dental restorations and prostheses and lead to increased plaque accumulation and bacterial colonization. Further research is needed to investigate the long-term effects of tea tree oil on the properties of dental stone and to optimize the disinfection protocols using tea tree oil to minimize any adverse effects on the properties of dental stone. The applicability of TTO can be compared with other popular disinfectant materials. Clinically using natural plant extracts, such as TTO, as a disinfectant is becoming increasingly popular due to its effectiveness, simplicity, safety, biodegradability, absence of harmful chemicals, and cost-effectiveness. TTO's unique properties make it an efficient disinfectant, especially when used at the proper concentrations. Findings have shown that immersing type III dental stone in a diluted essential oil disinfectant is a practical way to disinfect without affecting the model's accuracy, surface roughness, and hardness. However, further research is necessary to optimize the disinfection method of stone models using this oil solution.

4. CONCLUSIONS

Within the limitations of this study, the following conclusions can be drawn. It is possible to immerse Type III dental stones in a TTO disinfectant solution to disinfect them without affecting their accuracy. The surface hardness of type III dental stones was similar to that of the control group after 10 minutes in TTO solutions.

Data Availability

The data supporting this study's findings are available from the corresponding author upon reasonable request.

Conflicts of interest

The authors declare no conflicts of interest.

References

1. Meghashri, K., Kumar, P., Prasad, D. K., & Hegde, R. (2014). Evaluation and comparison of high-level microwave oven disinfection with chemical disinfection of dental gypsum casts. *Journal of International Oral Health: JIOH*, *6*(3), 56.

2. Carr, A. B., & Brown, D. T. (2010). *McCracken's removable partial prosthodontics-e-book*. Elsevier Health Sciences.

3. Mawlood, Z. S., & Naji, G. A.-H. (2020). Bergamot Essential Oil Effect against Candida Albicans Activity on Heat Cure Acrylic Denture Base. *Indian Journal of Forensic Medicine & Toxicology*, *14*(2).

4. Molinari, J. A. (2003). Infection control: its evolution to the current standard precautions. *The Journal of the American Dental Association*, *134*(5), 569–574.

5. Chidambaranathan, A. S., & Balasubramanium, M. (2019). Comprehensive review and comparison of the disinfection techniques currently available in the literature. *Journal of Prosthodontics*, *28*(2), e849–e856.

6. Goel, K., Gupta, R., Solanki, J., & Nayak, M. (2014). A comparative study between microwave irradiation and sodium hypochlorite chemical disinfection: a prosthodontic view. *Journal of Clinical and Diagnostic Research: JCDR*, *8*(4), ZC42.

7. Jwad Michael, B. D. S. (2010). Compressive strength and surface roughness of die stone cast after repeated disinfection with sodium hypochlorite solution. *Surfaces*, *7*, 8.

8. Block, M. S., & Rowan, B. G. (2020). Hypochlorous acid: a review. *Journal of Oral and Maxillofacial Surgery*, *78*(9), 1461–1466.

9. Mawlood, Z. S., & Naji, G. A. (2021). Influence of Addition of Bergamot Essential Oil on Physico-Mechanical Behavior of Heat Cure Acrylic Denture Base. *Int Med J*, *28*, 21–25.

10. Kairey, L., Agnew, T., Bowles, E. J., Barkla, B. J., Wardle, J., & Lauche, R. (2023). Efficacy and safety of Melaleuca alternifolia (tea tree) oil for human health—A systematic review of randomized controlled trials. *Frontiers in Pharmacology*, *14*, 1116077.

11. Guenther, E. (2014). *The essential oils-Vol 1: History-origin in plants-production-analysis*. Read Books Ltd.

12. Shapiro, S., Meier, A., & Guggenheim, B. (1994). The antimicrobial activity of essential oils and essential oil components towards oral bacteria. *Oral Microbiology and Immunology*, *9*(4), 202–208.

13. Christoph, F., Stahl-Biskup, E., & Kaulfers, P.-M. (2001). Death kinetics of Staphylococcus aureus exposed to commercial tea tree oils sl. *Journal of Essential Oil Research*, *13*(2), 98–102.

14. Schnitzler, P., Schön, K., & Reichling, J. (2001). Antiviral activity of Australian tea tree oil and eucalyptus oil against herpes simplex virus in cell culture. *Die Pharmazie*, *56*(4), 343–347.

15. Li, Y., Ye, Z., Wang, W., Yang, C., Liu, J., Zhou, L., Shen, Y., Wang, Z., Chen, J., & Wu, S. (2018). Composition analysis of essential oil from Melaleuca bracteata leaves using ultrasound-assisted extraction and its antioxidative and antimicrobial activities. *BioResources*, *13*(4), 8488–8504.

16. Romeo, A., Iacovelli, F., Scagnolari, C., Scordio, M., Frasca, F., Condò, R., Ammendola, S., Gaziano, R., Anselmi, M., & Divizia, M. (2022). Potential use of tea tree oil as a disinfectant agent against coronaviruses: A combined experimental and simulation study. *Molecules*, *27*(12), 3786.

17. Azaripour, A., Mahmoodi, B., Habibi, E., Willershausen, I., Schmidtmann, I., & Willershausen, B. (2017). Effectiveness of a miswak extract-containing toothpaste on gingival inflammation: a randomized clinical trial. *International Journal of Dental Hygiene*, *15*(3), 195–202.

18. Dalwai, S., Rodrigues, S. J., Baliga, S., Shenoy, V. K., Shetty, T. B., Pai, U. Y., & Saldanha, S. (2016). Comparative evaluation of antifungal action of tea tree oil, chlorhexidine gluconate, and fluconazole on heat polymerized acrylic denture base resin–an in vitro study. *Gerodontology*, *33*(3), 402–409.

19. Al-Radha, A. S. D., Younes, C., Diab, B. S., & Jenkinson, H. F. (2013). Essential oils and zirconia dental implant materials. *International Journal of Oral & Maxillofacial Implants*, *28*(6).

20. Dawkins, E., Michimi, A., Ellis-Griffith, G., Peterson, T., Carter, D., & English, G. (2013). Dental caries among children visiting a mobile dental clinic in South Central Kentucky: a pooled cross-sectional study. *BMC Oral Health*, *13*, 1–9.

21. Noori, Z. S., Al-Khafaji, A. M., & Dabaghi, F. (2023). Effect of tea tree oil on candida adherence and surface roughness of heat cure acrylic resin. *Journal of Baghdad College of Dentistry*, *35*(4), 46–54.

22. Guiotti, A. M., Cunha, B. G., Paulini, M. B., Goiato, M. C., Dos Santos, D. M., Duque, C., Caiaffa, K. S., Brandini, D. A., de Oliveira, D. T. N., & Brizzotti, N. S. (2016). Antimicrobial activity of conventional and plant-extract disinfectant solutions on microbial biofilms on a maxillofacial polymer surface. *The Journal of Prosthetic Dentistry*, *116*(1), 136–143.

23. Macêdo, L. O., da Nóbrega Alves, D., Carreiro, A. da F. P., de Castro, R. D., & Batista, A. U. D. (2022). Effects of long-term cinnamaldehyde immersion on the surface roughness and color of heat-polymerized denture base resin. *The Journal of Prosthetic Dentistry*, *128*(3), 521-e1.

24. Kumar, P. (2021). Evaluation of Cymbopogon Citratus as Disinfectant and its Effect on the Dimensional Stability of the Resultant Gypsum Casts: An in Vitro Study. *UNIVERSITY JOURNAL OF DENTAL SCIENCES*, *7*(3).

25. Krishnaveni, G., Sampath, A., Krishna, G. P., Krishna, K. R., Sushma, D. S., & Hita, B. (2021). Assessment of disinfectants on adherence of Candida albicans to soft denture liner. *Annals of the Romanian Society for Cell Biology*, 8750–8758.

26. Krishnan Rajkumar, M. D. S. (2022). Effect Of Vaccinium Macrocarpon On Candida Albicans Adhesion To Denture Base Resin. *Journal of Pharmaceutical Negative Results*, 989–997.

27. Sader, H. S., Rhomberg, P. R., Flamm, R. K., & Jones, R. N. (2012). Use of a surfactant (polysorbate 80) to improve MIC susceptibility testing results for polymyxin B and colistin. *Diagnostic Microbiology and Infectious Disease*, *74*(4), 412–414.

28. Xu, Y., Wei, J., Wei, Y., Han, P., Dai, K., Zou, X., Jiang, S., Xu, F., Wang, H., & Sun, J. (2021). Tea tree oil controls brown rot in peaches by damaging the cell membrane of Monilinia fructicola. *Postharvest Biology and Technology*, *175*, 111474.

29. Dahham, M. T., & Dheeb, B. I. (2019). Synergistic effect of tea tree oil on fungi causing vaginal thrush in pregnant women. *Journal of Biotechnology Research Center*, *13*(2), 35–44.

30. Czajkowska, M., Walejewska, E., Zadrożny, Ł., Wieczorek, M., Święszkowski, W., Wagner, L., Mijiritsky, E., & Markowski, J. (2020). Comparison of dental stone models and their 3D printed acrylic replicas for accuracy and mechanical properties. *Materials*, *13*(18), 4066.

31. Jasim, Z. M., Abass, S. M., Jasim, Z. M. A., & Abass, S. M. (2022). The Effect of Hypochlorous Acid Disinfectant on the Reproduction of Details and Surface Hardness of Type III Dental Stone. *Cureus*, *14*(11).

32. Abdullah, M. A. (2006). Surface detail, compressive strength, and dimensional accuracy of gypsum casts after repeated immersion in hypochlorite solution. *The Journal of Prosthetic Dentistry*, *95*(6), 462–468.

33. Azer, S. S., Kerby, R. E., & Knobloch, L. A. (2008). Effect of mixing methods on the physical properties of dental stones. *Journal of Dentistry*, *36*(9), 736–744.

34. de Magalhães Silveira, C. F., Cunha, R. S., Fontana, C. E., de Martin, A. S., de Almeida Gomes, B. P. F., Motta, R. H. L., & da Silveira Bueno, C. E. (2011). Assessment of the antibacterial activity of calcium hydroxide combined with chlorhexidine paste and other intracanal medications against bacterial pathogens. *European Journal of Dentistry*, *5*(01), 1–7.

35. Al-Shammari, S. S., & Abdul-Ameer, F. M. (2023). The influence of lemongrass essential oil addition on some of the properties of the heat-cured acrylic resin material. *Bionatura*, *8*(2), 646–652. https://doi.org/10.21931/RB/CSS/2023.08.02.75

36. Kumar, P. (2021). Evaluation of Cymbopogon Citratus as Disinfectant and its Effect on the Dimensional Stability of the Resultant Gypsum Casts: An in Vitro Study. *UNIVERSITY JOURNAL OF DENTAL SCIENCES*, *7*(3).

37. Block, M. S., & Rowan, B. G. (2020). Hypochlorous acid: a review. *Journal of Oral and Maxillofacial Surgery*, *78*(9), 1461–1466.

38. Hafezeqoran, A., Rahbar, M., Koodaryan, R., & Molaei, T. (2021). Comparing the Dimensional Accuracy of Casts Obtained from Two Types of Silicone Impression Materials in Different Impression Techniques and Frequent Times of Cast Preparation. *International Journal of Dentistry*, *2021*, 1–8.

39. Salehi, B., Mishra, A. P., Shukla, I., Sharifi-Rad, M., Contreras, M. del M., Segura-Carretero, A., Fathi, H., Nasrabadi, N. N., Kobarfard, F., & Sharifi-Rad, J. (2018). Thymol, thyme, and other plant sources: Health and potential uses. *Phytotherapy Research*, *32*(9), 1688–1706.

40. Ghate, M., Devi, P., Parikh, J., & K Vyas, V. (2013). Synthesis and QSAR Modeling of Novel Benzimidazolo Thiazolidinones, Thiazinones, and 5-arylidene-2-imino Thiazolidinones as Antibacterial Agents. *Medicinal Chemistry*, *9*(3), 474–485.

41. Singh, P., Aggarwal, S., Kapoor, A. M. S., Kaur, R., & Kaur, A. (2015). A prospective study assessing clinicians' attitudes and knowledge on radiation exposure to patients during radiological investigations. *Journal of Natural Science, Biology, and Medicine*, *6*(2), 398.

42. Talluri, S., & AD MK, R. S. (2022). To evaluate the dimensional accuracy and hardness of gypsum cast on repeated immersion in sodium hypochlorite and peroxygenic acid: an in-vitro study. *Int J App Dent Sci*, *8*, 598–604.

43. Maiya, A., Shetty, Y. R., Rai, K., Padmanabhan, V., & Hegde, A. M. (2015). Use of different oral hygiene strategies in children with cerebral palsy: A comparative study. *Journal of International Society of Preventive & Community Dentistry*, *5*(5), 389.

44. El Mekawy, N., Algraisi, M. I., & El Shaheed, N. H. (2018). In vitro Comparison of denture cleansers effect on locator attachment retentive male inserts (scanning electron microscope study). *Oral Health Dent. Manag*, *17*, 1–8.

45. Moslehifard, E., Nasirpouri, F., & Gasemzadeh, S. (2013). Effect of disinfectants on the hardness of dental stones. *Journal of Iranian Dental Association*, *25*(3), 183–189.

46. Kumar, R. N., Reddy, S. M., Karthigeyan, S., Punithavathy, R., Karthik, K. S., & Manikandan, R. (2012). The effect of repeated immersion of gypsum cast in sodium hypochlorite and glutaraldehyde on its physical properties: An in vitro study. *Journal of Pharmacy & Bioallied Sciences*, *4*(Suppl 2), S353.

47. Al-khafaji, A. M., Abass, S. M., & Khalaf, B. S. (2013). The effect of SOLO and sodium hypochlorite disinfectant on some properties of different types of dental stone. *Journal of Baghdad College of Dentistry*, *25*(2), 8–17.

Analytical Solution of the Broer-Kaup Equations by the Differential Transform Method

Asal B. Saleh[1, a)] and, Abdulghafor M. Al-Rozbayani[2 b)]

[1, 2] *Department of Mathematics*
University of Mosul,
Mosul – Iraq
[a)] *asal.23csp19@student.uomosul.edu.iq*
[b)] *abdulghafor_rozbayani@uomosul.edu.iq*

Analytical Solution of the Broer-Kaup Equations by the Differential Transform Method

Asal B. Saleh[1, a)] and, Abdulghafor M. Al-Rozbayani[2 b)]

[1, 2] *Department of Mathematics*
University of Mosul,
Mosul – Iraq
[a)]*asal.23csp19@student.uomosul.edu.iq*
[b)] *abdulghafor_rozbayani@uomosul.edu.iq*

ABSTRACT.

The Broer-Kaup system is one of the basic systems in studying and understanding mathematical and physical applications, as it contributes to understanding and studying difficult physical phenomena such as wave correlations, as this system consists of a set of non-linear partial differential equations that define variables across space and time.By using and integrating the differential transformation method (DTM) with the ADM analysis method, we provide a complete methodology for solving the Broer-Kaup equation in this study.The DTM differential transformation method has been widely used to solve many differential equations in many different mathematical and physical fields and applications. We have overcome the difficulties resulting from the nonlinear part of the Purer-Cup equation by integrating the DTM differential transformation method with the ADM analysis method, which improves efficiency and accuracy. Arithmetic. We have found the good performance and effective flexibility of our proposed method by implementing numerical and theoretical tests. The study and analysis of the Brewer Coup system is an interesting topic for researchers in different fields, especially in mathematical, engineering and physics applications. Absorbing and understanding this system makes it easy and possible to develop new applications and more complex understanding of difficult physical phenomena that are involved in different fields.

Keywords :Partial Differential equation, Broer-Kaup Equations, Differential transformation method, Adomain Decomposition Method

1. INTRODUCTION

Partial differential equations(PDE), are one of the important branches of mathematics that fall within the applied sciences and that play a pivotal role in the mechanism of perceiving and understanding natural phenomena and studying them in various applications and scientific and engineering fields. The partial differential equation can be considered as a relationship between the dependent variable (the function) And independent variables (partial derivatives), and they can also be used in physical and mathematical computational systems by describing the application at a specific time and place, such as heat transfer, wave motion, fluid flow, and other natural physical phenomena [1-3]

One of the important mathematical systems concerned with understanding and interpreting non-linear mathematical phenomena in applied mathematics and physics is known as the Broer-Kaup equation system This system includes a community of nonlinear partial differential equations and also contains a set of rather difficult and complex vocabulary. This system is also of great importance and effectiveness in understanding and interpreting wave interactions and other difficult and complex basic physical phenomena. The most important features that distinguish the Broer-Kaup system of equations are its comprehensive comprehension and ability to analyze and interpret solution solutions, which provides a good approach to comprehending and understanding complex physical phenomena. And its applications are diverse in a wide range of fields, for example, fluid motion, engineering, plasma physics, and its applications in multidisciplinary fields. It is clear that understanding and studying the Broer-Kaup system of equations is a thought-provoking challenge. Researchers because it requires a deep understanding of nonlinear interactions and their various applications.[4][7-5]

The differential transformation method is considered within of the approximate(numerical) methods that require numerical calculations, and it is an important tool to solve ordinary differential equations(ODE). The differential transformation method(DTM) uses polynomial mathematical functions to find the best solution near to the precise solution. The differential transformation method differs from the rest of the other methods that require complex operations in calculating the derivatives in each step, as in the Taylor expansion series. Also, the differential transformation method(DTM) does not require creating these calculations, which are considered somewhat complicated, as the differential transformation method(DTM) is an Recursiveness method, and thus we obtain The Tyler series has a high degree of structure, which is important in solving complex mathematical problems[8-14]

The Adomian analysis method is considered one of the methods that is characterized by a scientific-mathematical method that divides mathematical solutions into multiple and small partial sub-solutions, where it deals with each solution separately until the problem is solved, and by finding solutions from the sub-solutions iteratively, which makes the mathematical solutions improve, and after hybridization With the differential transformation method, the Adomian analysis method becomes more useful in dealing with complex problems represented by the presence of the nonlinear part in the differential equations, as the differential transformation method facilitates finding solutions to the differential equations by converting them into mathematical equations, where the DTM method has been integrated. And ADM, which in turn has become a powerful and effective fundamental image for solving complex mathematical problems that exist in many different engineering and mathematical sciences. [15-19]

2. Differential Transformation Method (DTM)

One of the important mathematical procedures in solving differential equations, which is involved in many diverse scientific and engineering fields, is the differential transformation method (DTM). Its effective potential and ability to solve differential equations has its beginnings with applied mathematics, by avoiding some of the problems and difficulties experienced by classical methods, like the differential transformation method. (DT M) understands important basics for any approach and able to solve ordinary differential equations in this introductory period [20, 21]

The differential transformation method is based on a set of mathematical functions that are used in transformations, usually called differential mathematical transformations, which in turn convert differential equations into algebraic mathematical equations. The purpose of the transformation is to facilitate the differential equation, facilitate dealing with it, and find its solutions in an easier way, as these transformations accomplish finding mathematical limits between the function. The original and its derivatives, as the essential point in this topic is to employ an appropriate auxiliary parameter to represent the unknown function in the form of a series expansion, then use differential mathematical transformations to find multiple algebraic equations. It is also possible to employ a series of series expansion operations that are acquired by solving this system to reshape the solution to fundamental differential equation. [22-24]

DTM is characterized by its ability to interact with non-homogeneous differential-equations like non-linear equations. This type of equation is widespread in the real world, as this type is difficult to solve using analytical numerical methods. The DTM method transforms the differential equation into a system Mathematical algebraic equations. This method can be modeled on scientific fields such as engineering, mechanics, physics, and many other diverse fields. [25]

Comparing the characteristics with other solution methods and methods, the differential transformation method has many positives and advantages because it does not require specifying the field. DTM is a typical method for difficult and complex engineering applications or non-linear boundaries, unlike finite difference methods or finite elements as well, as the possibility of the DTM method To provide solutions close to the exact solution, which allows comparison between computational efficiency and the correctness of the solution. [26]

To sum up, the possibility of solving with the differential transformation method(DTM) is a successful flexible method for solve differential equations available in many scientific and engineering contexts, which allows of its applications through the possibility to converting differential equation into algebraic mathematical equations, which in turn allows for more effective and systematic methods and methods for solving them, especially solving systems. Controlled by dynamic differential equations, the DTM method is a very suitable tool that can deal with nonlinear terms and non-homogeneous differential equations.

Combining the Adomian analysis method (ADM) with the differential transformation method(DTM) is an effective way for find the solution to partial differential equations(PDES) with good efficiency, as the solution domain is divided into smaller subdomains and each domain is treated separately. The differential problem solution is obtained by iteratively optimizing solutions in different subdomains, each of which is solved analytically using the DTM method. DTM works to transform partial differential equations into algebraic mathematical equations, which allows accurate solutions within each subfield, as these two methods work on effective and successful processors to obtain faster convergence to the solution. [25]. We take into account that a mapping consists of two variables $w(x,t)$ assuming that it is possible to represent it.

We take into account that a function consists of two independent variables $w(x,t)$ and assume that it can be represented As the combine of two functions of one variable, i.e. $w(x,t) = f(x)g(t)$. Based on the properties of one-dimensional differential transform ,function $w(x,t)$ can be written as :

$$w(x,t) = \sum_{i=0}^{\infty} \sum_{j=0}^{\infty} W(i,j)\, x^i t^j \quad (1)$$

Where $W(i,j)$ is named the spectrum of $w(x,y)$. Now we give the basic,The definitions and properties of 2-dimensional . If $w(x,t)$ and continuously differentiable With respect to time t in the domain of interest, then:

$$w(k,h) = \frac{1}{k!\,h!}\left[\frac{\partial^{k+h}}{\partial x^k \partial t^h} w(x,t)\right]_{x_0=0,t_0=0} \quad (2)$$

Where the spectrum function $W(k,h)$ is the transformation function, which is also called the T function. Let $w(x,y)$ be the original function while the capital letter $W(k,h)$ denotes the transformed function. Now we define the differential inverse transform of $W(k,h)$ as following:

$$w(x,t) = \sum_{k=0}^{\infty} \sum_{h=0}^{\infty} W(k,h)(x-x_0)^k (t-t_0)^h \quad (3)$$

Using equation (3) in equation (4), we have

$$w(k,h) = \frac{1}{k!\,h!}\left[\frac{\partial^{k+h}}{\partial x^k \partial t^h} w(x,t)\right]_{x_0=0,t_0=0} \quad x^k t^h$$

$$w(k,h) = \sum_{k=0}^{\infty} \sum_{h=0}^{\infty} W(k,h) x^k t^h \quad (4)$$

Now from the definitions and equation (3) *and* (4) above, we can get some basic mathematical operations that are performed by the two-dimensional differential transformation in schedule 1. [23]

Table 1.Show some transforms for multi types of functions

Original function	**Transformed function**
$w(x,t) = u(x,t) \pm v(x,t)$	$W(k,h) = U(k,h) \pm V(k,h)$
$w(x,t) = cu(x,t)$	$W(k,h) = cU(k,h)$
uu_x	$W(k,h) = \sum_{r=0}^{k} \sum_{s=0}^{h} U(r,h-s)(k-r+1)\,U(k-r+1,s)$
$w(x,t) = \frac{\partial}{\partial x} u(x,t)$	$W(k,h) = (k+1)U(k+1,h)$
$w(x,t) = \frac{\partial}{\partial x} v(x,t)$	$W(k,h) = (k+1)V(k+1,h)$
$w(x,t) = \frac{\partial}{\partial t} u(x,t)$	$W(k,h) = (h+1)U(k,h+1)$
$w(x,t) = \frac{\partial}{\partial t} v(x,t)$	$W(k,h) = (h+1)V(k,h+1)$
$(uv)_x$	$W(k,h) = \sum_{r=0}^{k} \sum_{s=0}^{h} (r+1)U(r+1,h-s)V(k-r,s) + \sum_{r=0}^{k} \sum_{s=0}^{h} (r+1)V(r+1,h-s)U(k$
u_{xxx}	$(k+1)(k+2)(k+3)U(k+3,h)$

3. Application method

(Broer-Kaup system) Consider the following, [27]

$$u_t + uu_x + v_x = 0 \quad (5)$$

$$v_t + u_x + (uv)_x + u_{xxx} = 0 \quad (6)$$

Having exact solution defined by :

$$u(x,t) = 1 - 2\tanh\,(t-x)$$

$$v(x,t) = 1 - 2\tanh^2(t-x)$$

with the initial conditions:

$$u(x,0) = 1 + 2\tanh(x) \quad (7)$$

$$v(x,0) = 1 - 2\tanh^2(x) \quad (8)$$

Taking the differential transform (DTM) of system (5-6) and using the relevant operations in table(1) we get:

$$(h+1)\mathrm{U}(k,h+1) + \sum_{r=0}^{k}\sum_{s=0}^{h}\mathrm{U}(r,h-s)(k-r+1)\mathrm{U}(k-r+1,s) + (k+1)V(k+1,h) = 0 \quad (9)$$

$$(h+1)V(k,h+1) + (k+1)\mathrm{U}(k+1,h) + \sum_{r=0}^{k}\sum_{s=0}^{h}(r+1)\mathrm{U}(r+1,h-s)V(k-r,s) + \sum_{r=0}^{k}\sum_{s=0}^{h}(r+1)V(r+1,h-s)\mathrm{U}(k-r,s) + (k+1)(k+2)(k+3)\mathrm{U}(k+3,h) = 0 \quad (10)$$

From the initial conditions, we use differential transformation (DTM) to convert the initial conditions for u and v as :

$$u(x,0) = 1 + 2\tanh(x) \quad \text{to } U(k,0) \quad ,k = 0,1,2,3\ldots \quad (11)$$

$$v(x,0) = 1 - 2\tanh^2(x) \quad \text{to } V(k,0) \quad ,k = 0,1,2,3\ldots \quad (12)$$

Such that

$$\mathrm{U}(k,0) = \frac{1}{k!}\left[\frac{d^k u(x,0)}{dx^k}\right]_{x=0} \quad k = 0,1,2,3\ldots\ldots \quad (13)$$

$$V(k,0) = \frac{1}{k!}\left[\frac{d^k v(x,0)}{dx^k}\right]_{x=0} \quad k = 0,1,2,3\ldots\ldots \quad (14)$$

From equation (13) we get $\mathrm{U}(k,0)$:

$\mathrm{U}(0,0) = 1$	$\mathrm{U}(1,0) = 2$	$\mathrm{U}(2,0) = 0$	$\mathrm{U}(3,0) = -0.6666666667$
$\mathrm{U}(4,0) = 0$	$\mathrm{U}(5,0) = 0.2666666667$	$\mathrm{U}(6,0) = 0$	

And From equation (14) we get $V(k,0)$:

$V(0,0) = 1$	$V(1,0) = 0$	$V(2,0) = -2$	$V(3,0) = 0$
$V(4,0) = 1.333333333$	$V(5,0) = 0$	$V(6,0) = -0.7555555556$	

Equation (9) becomes as follow:

$$U(k,h+1) = \frac{1}{(h+1)} * \left[-\sum_{r=0}^{k}\sum_{s=0}^{h}\mathrm{U}(r,h-s)(k-r+1)\mathrm{U}(k-r+1,s) - (k+1)\ V(k+1,h)\right]$$

And equation (10) becomes as follow:

$$V(k,h+1) = \frac{1}{(h+1)}\left[-(k+1)\mathrm{U}(k+1,h) - \sum_{r=0}^{k}\sum_{s=0}^{h}(r+1)\mathrm{U}(r+1,h-s)\ V(k-r,s) - \sum_{r=0}^{k}\sum_{s=0}^{h}(r+1)\ V(r+1,h-s)\mathrm{U}(k-r,s) - (k+1)(k+2)(k+3)\mathrm{U}(k+3,h)\right]$$

We obtain $\mathrm{U}(k,h)$ *for* $k = 0,1,2,3\ldots\ldots\ldots$ *and* $h = 0,1,2,3\ldots\ldots\ldots$

$\mathrm{U}(k,h)$	$h=0$	$h=1$	$h=2$	$h=3$	$h=4$	$h=5$
$k=0$	1	-2	0	0.6666666683	$-2.500000000 * 10^{-9}$	0.2666666510

$k=1$	2	0	-2	0	1.333333330	$2.360000000 * 10^{-7}$
$k=2$	0	2	0	-2.666666661	$-1.825000000 * 10^{-7}$	2.266667744
$k=3$	-0.6666666667	0	2.666666666	$1.333333333 * 10^{-8}$	-3.777777915	$6.600000000 * 10^{-7}$
$k=4$	0	-1.333333333	0	3.777777787	$-7.500000000 * 10^{-8}$	5.511111676
$k=5$	0.2666666667	0	-2.266666667	$1.333333333 * 10^{-8}$	5.511110932	$8.040000000 * 10^{-6}$

And we obtain $V(k,h)$ *for* $k = 0,1,2,3 \ldots \ldots \ldots$ *and* $h = 0,1,2,3 \ldots \ldots \ldots$

$V(k,h)$	$h=0$	$h=1$	$h=2$	$h=3$	$h=4$	$h=5$
$k=0$	**1**	0	-2	0	1.333333309	$1.920000000 * 10^{-}$
$k=1$	0	4	$-5.000000000 * 10^{-9}$	-5.333333327	$-7.000000000 * 10^{-8}$	4.533334044
$k=2$	-2	0	8	0	-11.33333372	$3.780000000 * 10^{-}$
$k=3$	0	-5.333333333	$-5.000000000 * 10^{-9}$	15.11111133	$-1.275000000 * 10^{-6}$	-22.04439052
$k=4$	1.333333333	0	-11.33333334	$1.000000000 * 10^{-7}$	27.55555508	$6.600000000 * 10^{-}$
$k=5$	0	4.5333333333	$-5.000000000 * 10^{-8}$	-22.04444440	$7.750000000 * 10^{-7}$	49.13779022

$$u(x,t) = \sum_{k=0}^{5}\sum_{h=0}^{5} \mathrm{U}(k,h)x^k t^h = 1 + 8.040000000 * 10^{-6}\ x^5t^5 - 2.500000000 * 10^{-9}t^4 - 7.500000000 * 10^{-8}x^4t^4 + 1.333333333 * 10^{-8}x^5t^3 - \frac{4}{3}x^4t + 6.600000000 * 10^{-7}x^3t^5 + 1.333333333 * 10^{-8}x^3t^3 - 1.825000000 * 10^{-7}x^2t^4 + 2.360000000 * 10^{-7}xt^5 - 2t + 2x + 0.6666666683t^3 - 0.2666666510t^5 - 0.6666666667x^3 + 0.2666666667x^5 - 2xt^2 + 1.333333330xt^4 + 2x^2t - 2.666666661x^2t^3 + 2.266667744x^2t^5 + 2.666666666x^3t^2 - 3.77777791x^3t^4 + 3.777777787x^4t^3 - 5.511111676x^4t^5 - 2.266666667x^5t^2 + 5.511110932x^5t^4$$

$$v(x,t) = \sum_{k=0}^{5}\sum_{h=0}^{5} V(k,h)x^k t^h = 1 + 4 * x * t - 5.333333327 * x * t^3 + 4.533334044 * x * t^5 + 8 * x^2 * t^2 - 11.33333372 * x^2 * t^4 + 15.11111133 * x^3 * t^3 - 22.04439052 * x^3 * t^5 - 11.33333334 * x^4 * t^2 + 27.55555508 * x^4 * t^4 - 22.04444440 * x^5 * t^3 + 49.13779022 * x^5 * t^5 + 1.333333333 * x^4 - 2 * t^2 + 1.333333309 * t^4 - 2 * x^2 + 1.920000000 * 10^{-7} * t^5 + 7.750000000 * 10^{-7} * x^5 * t^4 + 68/15 * x^5 * t + 6.600000000 * 10^{-6} * x^4 * t^5 - 5.000000000 * 10^{-8} * x^5 * t^2 + 1.000000000 * 10^{-7} * x^4 * t^3 - 1.275000000 * 10^{-6} * x^3 * t^4 + 3.780000000 * 10^{-6} * x^2 * t^5 - 16/3 * x^3 * t - 8.000000000 * 10^{-9} * x^3 * t^2 - 7.000000000 * 10^{-8} * x * t^4 - 5.000000000 * 10^{-9} * x * t^2$$

After expanding the series with additional terms and by substituting the values of x and t by fixing one of them and moving the other to some values chosen in the domain of the problem, we find the results that we will mention in the table:

Error results for the *u* series

x	DTM(x)	EXACT(x)	Error
-0.5	-0.2725260419	-0.270297905	2.23 e-3

-0.4	−0.1439555833	−0.143339932	6.16e-4
-0.3	−0.00118012504	−0.001040422	1.40e-4
-0.2	0.1561601252	0.1562019894	4.19e-5
-0.1	0.3272262085	0.3272489114	2.27e-5
0	0.5101562500	0.5101626752	6.4252e-6
0.1	0.7022412918	0.7022299328	1.14e-5
0.2	0.9001011253	0.9000832501	1.79e-5
0.3	1.099860126	1.099916750	5.66e-5
0.4	1.297323084	1.297770067	4.47e-4
0.5	1.488151042	1.489837325	1.69e-3
Mse			7.65e-7

x	DTM(x)	EXACT(x)	Error
-0.5	−0.5270833411	−0.523188312	3.90e-3
-0.4	−0.4350640024	−0.432595740	2.47e-3
-0.3	−0.3303280006	−0.328073541	2.25e-3
-0.2	−0.21087866672	−0.208735554	2.14e-3
-0.1	−0.07575933320	−0.074099134	1.66e-3
0	0.07500000054	0.0757656854	7.66e-4
0.1	0.2404360017	0.2401020754	3.34e-4
0.2	0.4187053366	0.4173747750	1.33e-3
0.3	0.6071380056	0.6052493596	1.89e-3
0.4	0.8022906767	0.8006640108	1.63e-3
0.5	1.000000019	1.0	1.90e-8
Mse			3.85e-6

Error results for the v series

x	DTM(x)	EXACT(x)	Error
-0.5	0.1930750809	0.1931716166	9.65e-5
-0.4	0.3464734527	0.3463868998	8.66e-5
-0.3	0.4990028510	0.4989590364	4.38e-5
-0.2	0.6440731721	0.6440024586	7.07e-5
-0.1	0.7738398951	0.7737029864	1.37e-4
0	0.880208333	0.8800296976	1.79e-4
0.1	0.9558378828	0.9556664935	1.71e-4
0.2	0.9951462726	0.9950083215	1.38e-4
0.3	0.9953138164	0.9950083215	3.05e-4
0.4	0.9572876593	0.9556664935	1.62e-3
0.5	0.8867860320	0.8800296976	6.76e-3
Mse			4.41e-6

x	DTM(x)	EXACT(x)	Error
-0.5	−0.1667362974	−0.160051317	6.68e-3
-0.4	−0.03116240238	−0.026165278	5.00e-3
-0.3	0.1159398975	0.1181103354	2.17e-3
-0.2	0.2717539474	0.2694791800	2.27e-3
-0.1	0.4302284243	0.4231555252	7.07e-3
0	0.583333338	0.5728954658	1.04e-2

0.1	0.7223160309	0.7112775720	1.10e-2
0.2	0.8389571808	0.8302739236	8.68e-3
0.3	0.9268267971	0.9220859660	4.74e-3
0.4	0.9825402288	0.9801325817	2.41e-3
0.5	1.007014154	1.0	7.01e-3
Mse			4.67e-5

4. CONCLUSION

From more complex systems than ever before and improving our understanding of fundamental physical processes as we continue to investigate and enhance this integrated approach, the (ADM) field analysis method and the (DTM) differential transformation method together provide a powerful method for solving the Broer-Kaup equations. Our research has proven the effectiveness of this integrated method in solving complex differential equations that control thermodynamics and fluid dynamics efficiently and accurately. The nonlinearities and bounds in the equations of the Broer-Kaup equations have proven to be formidable obstacles, but we have overcome them by combining the two approaches, and the results are robust and reliable. (DTM) is a powerful and flexible tool for academics in many different fields, including applied mathematics and engineering techniques.

REFERENCES

[1] G. Evans, J. Blackledge, and P. Yardley, *Analytic methods for partial differential equations*: Springer Science & Business Media, 2012.

[2] M. Schechter, *Modern methods in partial differential equations*: Courier Corporation, 2014.

[3] E. Zauderer, *Partial differential equations of applied mathematics*: John Wiley & Sons, 2011.

[4] K.-J. Wang and K.-L. Wang, "Variational principles for fractal Whitham–Broer–Kaup equations in shallow water," *Fractals,* vol. 29, p. 2150028, 2021.

[5] K. Nonlaopon, M. Naeem, A. M. Zidan, R. Shah, A. Alsanad, and A. Gumaei, "Numerical investigation of the time-fractional Whitham–Broer–Kaup equation involving without singular kernel operators," *Complexity,* vol. 2021, pp. 1-21, 2021.

[6] A. Ali, K. Shah, and R. A. Khan, "Numerical treatment for traveling wave solutions of fractional Whitham-Broer-Kaup equations," *Alexandria Engineering Journal,* vol. 57, pp. 1991-1998, 2018.

[7] A. P. Shakir, T. A. Sulaiman, H. F. Ismael, N. A. Shah, and S. M. Eldin, "Multiple fusion solutions and other waves behavior to the Broer-Kaup-Kupershmidt system," *Alexandria Engineering Journal,* vol. 74, pp. 559-567, 2023.

[8] M. Hatami, D. D. Ganji, and M. Sheikholeslami, *Differential transformation method for mechanical engineering problems*: Academic Press, 2016.

[9] O. O. Agboola, A. A. Opanuga, and J. A. Gbadeyan, "Solution of third order ordinary differential equations using differential transform method," *Global Journal of Pure and Applied Mathematics,* vol. 11, pp. 2511-2517, 2015.

[10] A. A. Opanuga, H. I. Okagbue, S. O. Edeki, and O. O. Agboola, "Differential transform technique for higher order boundary value problems," *Modern Applied Science,* vol. 9, p. 224, 2015.

[11] J. Munganga, J. Mwambakana, R. Maritz, T. Batubenge, and G. Moremedi, "Introduction of the differential transform method to solve differential equations at undergraduate level," *International Journal of Mathematical Education in Science and Technology,* vol. 45, pp. 781-794, 2014.

[12] A. Gökdoğan, M. Merdan, and A. Yildirim, "The modified algorithm for the differential transform method to solution of Genesio systems," *Communications in Nonlinear Science and Numerical Simulation,* vol. 17, pp. 45-51, 2012.

[13] H. A. Peker, O. Karaoğlu, and G. Oturanç, "The differential transformation method and Pade approximant for a form of Blasius equation," *Mathematical and Computational Applications,* vol. 16, pp. 507-513, 2011.

[14] Y. Keskin and G. Oturanc, "Reduced differential transform method for generalized KdV equations," *Mathematical and Computational applications,* vol. 15, pp. 382-393, 2010.

[15] M. Turkyilmazoglu, "Determination of the correct range of physical parameters in the approximate analytical solutions of nonlinear equations using the Adomian decomposition method," *Mediterranean Journal of Mathematics,* vol. 13, pp. 4019-4037, 2016.

[16] Y. Q. Hasan and Z. A. A. AL-Rabahi, "APPROXIMATE SOLUTIONS TO BOUNDARY VALUE PROBLEMS OF HIGHER-ORDER BY THE MODIFIED ADOMAIN DECOMPOSITION METHOD," *EPH-International journal of Mathematics and statistics,* vol. 2, pp. 20-31, 2016.

[17] A.-M. Wazwaz, *Partial differential equations and solitary waves theory*: Springer Science & Business Media, 2010.

[18] C. H. Che Hussin and A. Kiliçman, "On the solutions of nonlinear higher-order boundary value problems by using differential transformation method and Adomian decomposition method," *Mathematical problems in engineering,* vol. 2011, 2011.

[19] O. González-Gaxiola and R. Bernal-Jaquez, "Applying Adomian decomposition method to solve Burgess equation with a non-linear source," *International Journal of Applied and Computational Mathematics,* vol. 3, pp. 213-224, 2017.

[20] İ. DEMİR, M. F. KARAHAN, and N. AKTÜRK, "Application of differential transformation method for nonlinear cutting tool vibration," *Gazi University Journal of Science Part A: Engineering and Innovation,* vol. 8, pp. 109-122, 2021.

[21] M. Omoloye, M. Yusuff, and O. Emiola, "Application of differential transformation method for solving dynamical transmission of lassa fever model," *International Journal of Physical and Mathematical Sciences,* vol. 14, pp. 151-154, 2020.

[22] M. Mohanty and S. R. Jena, "Differential transformation method (DTM) for approximate solution of ordinary differential equation (ODE)," *Advances in Modelling and Analysis B,* vol. 61, pp. 135-138, 2018.

[23] B. Soltanalizadeh and S. Branch, "Application of differential transformation method for solving a fourth-order parabolic partial differential equations," *International journal of pure and applied mathematics,* vol. 78, pp. 299-308, 2012.

[24] A. R. Kanth and K. Aruna, "Differential transform method for solving linear and non-linear systems of partial differential equations," *Physics Letters A,* vol. 372, pp. 6896-6898, 2008.

[25] C. Bervillier, "Status of the differential transformation method," *Applied Mathematics and Computation,* vol. 218, pp. 10158-10170, 2012.

[26] A. Khatib, "Differential Transform Method for Differential Equations," 2016.

[27] Y. Jiang, D.-Q. Xian, and Z.-D. Dai, "New exact solutions of the (2+ 1)-dimensional Broer-Kaup equation by the consistent Riccati expansion method," *Thermal Science,* vol. 21, pp. 1783-1788, 2017.

الحل العددي لمعادلة الحركة باستخدام مفهوم دالة الجريان

أمير زبير كريت[1] , احمد محمد جمعة[2]

[1,2]قسم الرياضيات,كلية علوم الحاسوب و الرياضيات , جامعة الموصل , الموصل , العراق

[1]Ameer.23csp83@student.uomosul.edu.iq

[2]Ahmed.M.j.jassim@uomosul.edu.iq

الحل العددي لمعادلة الحركة باستخدام مفهوم دالة الجريان

أمير زبير كريت[1] , احمد محمد جمعة[2]

[1,2]قسم الرياضيات,كلية علوم الحاسوب و الرياضيات , جامعة الموصل , الموصل , العراق

[1]Ameer.23csp83@student.uomosul.edu.iq

[2]Ahmed.M.j.jassim@uomosul.edu.iq

الخلاصة

تم في هذا البحث حل معادلة الحركة و التي قد نشأت من نموذج لجريان مائع محصور بين جدارين معزولين مع وجود تباين في درجات الحرارة لكليهما على طول المحور الذي يمر في منتصف القناة و بشكل دالة للمتغير العمودي بالإضافة الى وجود مجال مغناطيسي عمودي على المحور الافقي للقناة باعتبار ان المائع يتدفق بالاتجاه الموجب للمحور الافقي حيث ان في مثل هذه المسائل تتشكل مجموعة من المعادلات التي تتحكم في مثل هكذا نموذج و هي نوع من المعادلات التفاضلية الجزئية المتداخلة و التي تحتوي على متغيرات معتمدة متعددة و بعد حل معادلة الطاقة و هي احدى المعادلات المهمة التي تتحكم في مثل النموذج أعلاه و حساب قيمتها التقريبية باعتبارها معلومة و التي تؤثر على حركة جريان المائع و تعويضها في معادلة الحركة حيث تتشكل معادلة جديدة هي ايضاً معادلة تفاضلية جزئية خاضعة لشروط المسألة باستخدام طريقة الاتجاهات المتعاقبة الضمنية(ADI) وهي احدى طرق الفروقات المنتهية و التي استخدم فيها مفهوم دالة الجريان لغرض تحويل معادلة الحركة بدلالة متغيرين إلى معادلة بدلالة متغير واحد ولكن من الرتبة الرابعة و لأجل تطبيق طريقة ADI المصممة لمعالجة المعادلات ذات الرتبة الثانية تم استخدام مفهوم الدردورية ξ(Vorticity) وبذلك تم تخفيض رتبة المعادلة من الرتبة الرابعة الى الرتبة الثانية ، وأصبحت معادلة الحركة بدلالة مفهوم الدردورية و هي الصيغة التي يمكن استخدام فيها الطريقة المذكورة اعلاه حيث انها معادلة تفاضلية جزئية من صيغة القطع المكافئ و تم الحصول على النتائج باستخدام قيم مختلفة لبعض البارامترات مثل عدد هارتمان ، عدد برانتدل و عدد رالي .و أظهرت النتائج أن هناك تأثير واضح على حركة الماء داخل القناة.

Abstract

In this research, the equation of motion was solved, which appeared from a model of the flow of a fluid confined between two insulated walls, with a temperature variation for both of them along the axis that passes through the middle of the channel and as a function of the vertical variable, in addition to the presence of a magnetic field perpendicular to the horizontal axis of the channel, considering the fluid flows in the positive direction of the horizontal axis. In such problems, a set of equations is formed that controls such a model. It is a type of nested partial differential equation that contains multiple dependent variables. After solving the energy equation, it is one of the important

equations that control In a model like the one above, its approximate value is calculated as a piece of information that affects the fluid flow movement, and its compensation is in the equation of motion, where a new equation is formed, which is also a partial differential equation subject to the conditions of the problem, using the successive implicit directions (ADI) method, which is one of the finite difference methods that was used. It contains the concept of the flow function for the purpose of converting the equation of motion in terms of two variables into an equation in terms of one variable, but of the fourth order. In order to apply the ADI method designed to treat second-order equations, the concept of vorticity (ξ) was used, and thus the rank of the equation was reduced from the fourth order to the second order. The equation of motion in terms of the concept of circularity became the form in which the above-mentioned method can be used, as it is a partial differential equation of the parabolic form. The results were obtained using different values for some parameters, such as the Hartmann number, the Prandtl number, and the Raleigh number. The results showed that there was a clear effect on the movement of water within the channel.

1. المقدمة

تعتبر الطرق العددية من اهم الطرق الرياضية في حل المسائل التطبيقية الناتجة من مسائل انتقال الحرارة داخل القنوات و الاوعية و في هذا البحث تم الحصول على معادلات تفاضلية جزئية مع الشروط الحدودية و التي تمثل معادلة من نوع القطع المكافئ حيث تم اختيار طريقة ADI التقريبية لحلها بعد استخدام مفهوم دالة الجريان حيث تتحول المعادلة الى معادلة من الرتبة الرابعة و تم بعد ذلك استخدام دالة الدردورية (Vorticity) حيث تخفض رتبة المعادلة الى الرتبة الثانية و بالتالي يمكن حلها بالطريقة المذكورة أعلاه و هي طريقة تعتبر من الطرق التقريبية الجيدة و قد استخدمها كثير من الباحثين لإيجاد الحلول التقريبية لكثير من المسائل التطبيقية .

قدم Verma وBansal دراسة حول تدفق مائع لزج غير قابل للانضغاط بين لوحين متوازيين، أحدهما في حركة منتظمة والآخر في حالة سكون مع شفط منتظم في اللوحة الثابتة [1]. وناقش Bhuyan وHazarika تأثير المجال المغناطيسي على تدفق الدم النابض في قناة مسامية [2]. درس Taheri تأثير المجال المغناطيسي على تدفق الموائع وبين تأثير رقم هارتمان ورينولدز على طول التطور المغناطيسي وقوة لورنتز[3] .واستخدم Rasmussen واخرون طريقة عددية 3D–ADI–DG لحل مشكلة نقل الحرارة ثلاثية الأبعاد[4] . قام Mehta واخرون بدراسة تدفق الموائع التذبذبية وانتقال الحرارة عبر وسط مسامي بين الصفائح المتوازية في وجود مجال مغناطيسي مائل وتدفق حراري إشعاعي ومصدر للحرارة وتم حل معادلة الحركة التي تحكم تدفق الموائع باستخدام طريقة عددية وتمت ملاحظة تأثير البارامترات الفيزيائية المختلفة على حركة المائع[5] . قدم Almishlih الحل العددي بطريقة ADI لمعادلات الحركة والحرارة لمسألة تدفق الموائع في القناة الأفقي تحت تأثير المجال الإشعاعي وبين تأثير الباراميترات مثل عدد برانتدل، عدد شميدت وعدد غراتشوف [6]. ايضاً استخدم كل من Amen و Jassim طريقة العددية ADI لحل مسألة كهرومغناطيسية في الاحداثيات القطبية [7]. وعالج Ala'a واخرون المعادلات التفاضلية الناتجة من

نموذج الرياضي لانتقال الحرارة بالحمل الحراري والاشعاع الحراري لمائع ينساب في قناة افقية وتحت تأثير مجال مغناطيسي عمودي على مستوى القناة باستخدام الطريقة العددية [8] . و في الدراسة الحالية تم حل معادلة الحركة باستخدام دالة الجريان و التي تؤدي الى تقليل عدد المتغيرات المعتمدة لمعادلة الحركة الا انها ترفع درجتها الى الرتبة الرابعة،وباستخدام مفهوم الدردورية يتم تخفيض رتبتها الى الرتبة الثانية و بالتالي يمكن حلها باستخدام الطريقة العددية ADI . وبعد الحصول على النتائج ظهر بأن هنالك تأثير لبعض المتغيرات المعروفة مثل عدد برانتدل و عدد هادتمان على اتجاه منحنيات الحركة داخل القناة .

2. التمثيل الهندسي للمسألة

يتكون النموذج من مقطع عرضي من قناة افقية وقد تم تسليط مجال كهرومغناطيسي ثابت B_0 عمودي على مستوي القناة مع وجود مائع موصل للكهربائية داخل القناة. فيتحول المائع الى مائع ممغنط، حيث نفرض إن درجة الحرارة عند الجدارين الافقيين تكون مختلفة، حيث T_0 تمثل درجة الحرارة عند الجدار الافقي السفلي و T_1 تمثل درجة الحرارة عند الجدار الافقي العلوي و تكون $T_1 > T_0$ ، ونفترض ان مجالاً مغناطيسياً عمودياً ثابتاً مسلط باتجاه المحور y حيث يتكون مائع ممغنط يجري باتجاه محور x وكذلك يتكون مجال كهرومغناطيسي مضاد باتجاه محور z حيث يكون مقداره صغيرة جدا يمكن اهماله . كما مبين في الشكل التالي:

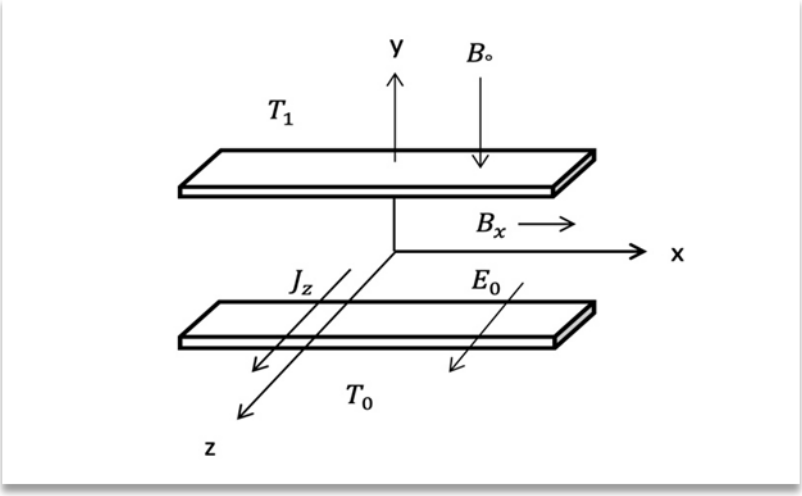

2.1 فرضيات على المسالة:

بعد تحديد النموذج الرياضي قيد الدراسة، نضع بعض الشروط الرئيسية التي تصف المسألة وصفاً دقيقاً والشروط هي:

١- المائع الموجود داخل القناة غير قابل للانضغاط. ٢- خواص المائع تبقى ثابتة (بالنسبة للنموذج قيد الدراسة). ٣- لا يوجد مصدر حراري داخل القناة. ٤- لا يوجد مصدر للإشعاع.

2.2 المعادلات التي تحكم المسألة:

المعادلات المطلوبة لوصف النموذج قيد الدراسة كالاتي :

2.2.1 معادلة الاستمرارية

$$\frac{\partial u^*}{\partial x^*}+\frac{\partial v^*}{\partial y^*}=0 \qquad (2.2.1)$$

حيث u^* و v^* هي مركبات السرعة باتجاه x^* و y^* على التوالي .

2.2.2 معادلة الكهرومغناطيسية

$$J_z=-\frac{1}{\mu_0}\frac{\partial B_x}{\partial y^*}=\sigma(E_0+u^*B_0-v^*B_x)\,. \qquad (2.2.2)$$

حيث أن : J_z هي كثافة الكهربائية باتجاه z ، μ_0 اللزوجة الديناميكية لمائع ، B_x المجال المغناطيسي المولد باتجاه x ، B_0 مجال مغناطيسي مسلط على القناة باتجاه محور y ، σ اللزوجة الكينماتية E_0 مجال كهربائي باتجاه z

2.2.3 معادلة الحركة

$$\rho\left[\frac{\partial \vec{V}}{\partial t^*}+(\vec{V}.\nabla)\vec{V}\right]-\vec{J}\times\vec{B}+\nabla P-\mu\nabla^2\vec{V}=0 \qquad (2.2.3)$$

معادلة الحركة باتجاه محور x:

$$\frac{\partial u^*}{\partial t^*}+u^*\frac{\partial u^*}{\partial x^*}+v^*\frac{\partial u^*}{\partial y^*} =-\frac{\partial p}{\rho\partial x^*}-\frac{\sigma E_0B_0}{\rho}-\frac{\sigma {B_0}^2u^*}{\rho}+\frac{\sigma B_0B_xv^*}{\rho}+\frac{\mu}{\rho}\nabla^2u^* \qquad (2.2.4)$$

معادلة الحركة باتجاه محور y :

$$\frac{\partial v^*}{\partial t^*}+u^*\frac{\partial v^*}{\partial x^*}+v^*\frac{\partial v^*}{\partial y^*} =-\frac{\partial p}{\rho y^*}+\frac{\sigma E_0B_x}{\rho}+\frac{\sigma B_0B_xu^*}{\rho}-\frac{\sigma {B_x}^2v^*}{\rho}+\frac{\mu}{\rho}\nabla^2v^* -g\beta(T-T_0) \qquad (2.2.5)$$

حيث ان : t هي الوقت ، p هي الضغط ، ρ هي الكثافة ، g التعجيل الأرضي ، T درجة الحرارة المطلقة ، T_0 درجة الحرارة الابتدائية و β معامل التمدد الحراري .

ولتوحيد المعادلتين (2.2.4) و (2.2.5) نتبع ما يلي:

نشتق المعادلة (2.2.4) بالنسبة الى y و المعادلة (2.2.5) بالنسبة الى x و بعد تبسيط المعادلتين نحصل على المعادلة التالية :

$$\frac{\partial}{\partial t^*}\left(\frac{\partial v^*}{\partial x^*}-\frac{\partial u^*}{\partial y^*}\right)+\left[\frac{\partial}{\partial x^*}\left(u^*\frac{\partial v^*}{\partial x^*}+v^*\frac{\partial v^*}{\partial y^*}\right)-\frac{\partial}{\partial y^*}\left(u^*\frac{\partial u^*}{\partial x^*}+v^*\frac{\partial u^*}{\partial y^*}\right)\right]$$
$$=\frac{\mu}{\rho}\nabla^2\left(\frac{\partial v^*}{\partial x^*}-\frac{\partial u^*}{\partial y^*}\right)-g\beta\left(\frac{\partial T}{\partial x^*}\right)+\frac{\sigma B_0 B_x}{\rho}\left[\frac{\partial u^*}{\partial x^*}-\frac{\partial v^*}{\partial y^*}\right]-\frac{\sigma {B_x}^2}{\rho}\frac{\partial v^*}{\partial x^*}$$
$$+\frac{\sigma {B_0}^2}{\rho}\frac{\partial u^*}{\partial y^*} \qquad (2.2.6)$$

و التي تمثل معادلة الحركة التي تتحكم بالمسألة.

2.2 الشروط الحدودية للمسألة:

الشروط التي تتحكم في المسألة هي ان السرعة عند جميع الحدود في حالة السكون أي ان:

$$u^*=v^*=w^*=0$$

3. الصيغة اللابعدية

بعد إيجاد المعادلات الأساسية التي تتحكم في المسألة نجد ان هناك صعوبة في حل هذه المعادلات بصيغتها الحالية و لغرض حل المعادلات التي تتحكم في المسالة و لتبسيط صيغة المعادلات و وضعها في الحالة اللابعدية ندخل التعاريف اللابعدية التالي[9] ،[10]، [11] .

$$u=\frac{u^*}{U}\ ,\ v=\frac{v^*}{U}\ ,\ x=\frac{x^*}{L}\ ,\ y=\frac{y^*}{L}\ ,\ U=\frac{a}{L}\sqrt{RaPr}=\sqrt{g\beta\Delta TE\ L}\ ,$$
$$t=\frac{Ut^*}{L}\quad ,\quad B_x=B_0\mu_0\sigma ULb\quad ,\quad \theta=\frac{T-T_0}{\Delta T}\quad ,\quad Ra=\frac{pg\beta\Delta TL^3}{\mu a}\quad ,$$
$$Pr=\frac{U}{a}=\frac{C_p\mu}{k}\ ,\quad Ha=B_0L\sqrt{\frac{\sigma}{\mu}}$$

حيث ان Pr ، Ha ، Ra يشير الى عدد برانتدل ، عدد هارتمان و عدد رالي على التوالي .

وبتعويض الصيغ اللابعدية ستتحول المعادلات الأساسية الى الصيغة اللابعدية وكما يأتي:

3-1 معادلة الاستمرارية اللابعدية

$$\frac{\partial u}{\partial x}+\frac{\partial v}{\partial y}=0 \qquad (3.1)$$

3-2 معادلة الحركة اللابعدية

$$\frac{\partial}{\partial t}\left(\frac{\partial v}{\partial x}-\frac{\partial u}{\partial y}\right)+\left[\frac{\partial}{\partial x}\left(u\frac{\partial v}{\partial x}+v\frac{\partial v}{\partial y}\right)-\frac{\partial}{\partial y}\left(u\frac{\partial u}{\partial x}+v\frac{\partial u}{\partial y}\right)\right]$$
$$=\sqrt{\frac{Pr}{Ra}}\nabla^2\left(\frac{\partial v}{\partial x}-\frac{\partial u}{\partial y}\right)-\frac{\partial \theta}{\partial x}+IHa^2\sqrt{\frac{Pr}{Ra}}\left[\frac{\partial u}{\partial x}-\frac{\partial v}{\partial y}\right]-\boldsymbol{I^2}Ha^2\sqrt{\frac{Pr}{Ra}}\frac{\partial v}{\partial x}$$
$$+Ha^2\sqrt{\frac{Pr}{Ra}}\frac{\partial u}{\partial y} \qquad (3.2)$$

بحيث $I=\frac{B_0}{B_x}$.

4. حل معادلة الحركة Solve the Motion Equation

سنقوم باستخدام صيغة دالة الجريان ψ (Stream Function) ، و هذا معروف و متبع لغرض تحويل معادلة الحركة بدلالة متغيرين إلى معادلة الحركة بدلالة متغير واحد، و ذلك بتبسيط معادلة الحركة دون التأثير على عموميتها ، و وضعها ضمن اطار الحل بطريقة الاتجاهات المتعاقبة الضمنية (ADI) وذلك باستخدام التعريف التالي[12]،[13] :

$$v=-\frac{\partial \psi}{\partial x} \quad , \quad u=\frac{\partial \psi}{\partial y}$$

بالتعويض في معادلة (3.2) وبعد التبسيط نحصل على:

$$\frac{\partial}{\partial t}\left[-\frac{\partial^2\psi}{\partial x^2}-\frac{\partial^2\psi}{\partial y^2}\right]+\frac{\partial}{\partial x}\left[-\frac{\partial^3\psi}{\partial y\partial x^2}+\frac{\partial^3\psi}{\partial y\partial x^2}\right]-\frac{\partial}{\partial y}\left[\frac{\partial^3\psi}{\partial x\partial y^2}-\frac{\partial^3\psi}{\partial x\partial y^2}\right]$$
$$=\sqrt{\frac{Pr}{Ra}}\nabla^2\left(-\frac{\partial^2\psi}{\partial x^2}-\frac{\partial^2\psi}{\partial y^2}\right)-\frac{\partial \theta}{\partial x}+IHa^2\sqrt{\frac{Pr}{Ra}}\left[\frac{\partial^2\psi}{\partial x\partial y}+\frac{\partial^2\psi}{\partial x\partial y}\right]$$
$$+\boldsymbol{I^2}Ha^2\sqrt{\frac{Pr}{Ra}}\frac{\partial^2\psi}{\partial x^2}+Ha^2\sqrt{\frac{Pr}{Ra}}\frac{\partial^2\psi}{\partial y^2} \qquad (4.1)$$

ومنها نحصل على:

$$-\frac{\partial}{\partial t}\nabla^2\psi=-\sqrt{\frac{Pr}{Ra}}\nabla^4\psi-\frac{\partial \theta}{\partial x}+2IHa^2\sqrt{\frac{Pr}{Ra}}\frac{\partial^2\psi}{\partial x\partial y}+\boldsymbol{I^2}Ha^2\sqrt{\frac{Pr}{Ra}}\frac{\partial^2\psi}{\partial x^2}$$
$$+Ha^2\sqrt{\frac{Pr}{Ra}}\frac{\partial^2\psi}{\partial y^2} \qquad (4.2)$$

ولأجل ان يكون الحل ممكناً سنفرض بأن المجال المحتث المتولد B_x يساوي B_0 وهذا يعني أن $I=1$

إذا معادلة (4.2) تصبح بالشكل الاتي:

$$-\frac{\partial}{\partial t}\nabla^2\psi = -\sqrt{\frac{Pr}{Ra}}\nabla^4\psi - \frac{\partial\theta}{\partial x} + 2Ha^2\sqrt{\frac{Pr}{Ra}}\frac{\partial^2\psi}{\partial x\partial y} + Ha^2\sqrt{\frac{Pr}{Ra}}\frac{\partial^2\psi}{\partial x^2} + Ha^2\sqrt{\frac{Pr}{Ra}}\frac{\partial^2\psi}{\partial y^2} \quad (4.3)$$

وبعد تبسيط معادلة (4.3) نحصل على:

$$-\frac{\partial}{\partial t}\nabla^2\psi = -\sqrt{\frac{Pr}{Ra}}\nabla^4\psi - \frac{\partial\theta}{\partial x} + Ha^2\sqrt{\frac{Pr}{Ra}}\left[\frac{\partial^2\psi}{\partial x\partial y} + \frac{\partial^2\psi}{\partial x^2}\right] + Ha^2\sqrt{\frac{Pr}{Ra}}\left[\frac{\partial^2\psi}{\partial x\partial y} + \frac{\partial^2\psi}{\partial y^2}\right] \quad (4.4)$$

ومنها نحصل على:

$$-\frac{\partial}{\partial t}\nabla^2\psi = -\sqrt{\frac{Pr}{Ra}}\nabla^4\psi - \frac{\partial\theta}{\partial x} + Ha^2\sqrt{\frac{Pr}{Ra}}\left[\frac{\partial\psi}{\partial y} + \frac{\partial\psi}{\partial x}\right]\left[\frac{\partial}{\partial x} + \frac{\partial}{\partial y}\right] \quad (4.5)$$

و هذا يعني :

$$-\frac{\partial}{\partial t}\nabla^2\psi = -\sqrt{\frac{Pr}{Ra}}\nabla^4\psi - \frac{\partial\theta}{\partial x} + Ha^2\sqrt{\frac{Pr}{Ra}}\nabla^2\psi \quad (4.6)$$

ولتطبيق طريقة ADI المصممة لمعالجة المعادلات ذات الرتبة الثانية سنقوم باستخدام مفهوم الدردورية (Vorticity)، وذلك بتخفيض رتبة المعادلة (4.6) وجعلها من الرتبة الثانية وذلك باستخدام التعريف التالي[12].:

$$\xi = -\nabla^2\psi$$

وبالتعويض في المعادلة (4.6) نحصل على:

$$\frac{\partial\xi}{\partial t} = \sqrt{\frac{Pr}{Ra}}\nabla^2\xi - \frac{\partial\theta}{\partial x} - Ha^2\sqrt{\frac{Pr}{Ra}}\xi \quad (4.7)$$

ولحل المعادلة (4.7) باستخدام طريقة الاتجاهات المتعاقبة الضمنية (ADI) سنقوم بشطرها الى معادلتين الأولى باتجاه المحور x والثانية باتجاه المحور y كما يأتي:

اولاً: باتجاه محور x :

باستخدام صيغ الفروقات المركزية لدينا[14]،[15] :

$$\frac{\partial \xi}{\partial t} = \frac{\xi^*_{i,j} - \xi_{i,j,n}}{\frac{\Delta t}{2}} \quad , \quad \frac{\partial^2 \xi}{\partial x^2} = \frac{\xi^*_{i+1,j} - 2\xi^*_{i,j} + \xi^*_{i-1,j}}{(\Delta x)^2} \quad ,$$

$$\frac{\partial^2 \xi}{\partial y^2} = \frac{\xi_{i,j+1,n} - 2\xi_{i,j,n} + \xi_{i,j-1,n}}{(\Delta y)^2} \quad , \quad \frac{\partial \theta}{\partial x} = \frac{\theta_{i+1,j,n+1} - \theta_{i-1,j,n+1}}{2(\Delta x)} \quad , \quad \xi = \xi_{i,j,n}$$

نعوض الصيغ أعلاه في معادلة (4.7) ينتج:

$$\frac{\xi^*_{i,j} - \xi_{i,j,n}}{\frac{\Delta t}{2}} = \sqrt{\frac{Pr}{Ra}}\left[\frac{\xi^*_{i+1,j} - 2\xi^*_{i,j} + \xi^*_{i-1,j}}{(\Delta x)^2} + \frac{\xi_{i,j+1,n} - 2\xi_{i,j,n} + \xi_{i,j-1,n}}{(\Delta y)^2}\right]$$

$$- \left[\frac{\theta_{i+1,j,n+1} - \theta_{i-1,j,n+1}}{2(\Delta x)}\right] - Ha^2 \sqrt{\frac{Pr}{Ra}}\, \xi_{i,j,n} \qquad (4.8)$$

نضرب معادلة (4.8) في $\left(\frac{\Delta t}{2}\right)$ ينتج:

$$\xi^*_{i,j} - \xi_{i,j,n} = \frac{\Delta t}{2}\sqrt{\frac{Pr}{Ra}}\left[\frac{\xi^*_{i+1,j} - 2\xi^*_{i,j} + \xi^*_{i-1,j}}{(\Delta x)^2} + \frac{\xi_{i,j+1,n} - 2\xi_{i,j,n} + \xi_{i,j-1,n}}{(\Delta y)^2}\right]$$

$$- \frac{\Delta t}{2}\left[\frac{\theta_{i+1,j,n+1} - \theta_{i-1,j,n+1}}{2(\Delta x)}\right] - \frac{\Delta t}{2}\, Ha^2 \sqrt{\frac{Pr}{Ra}}\, \xi_{i,j,n} \qquad (4.9)$$

ليكن $\beta = \sqrt{\frac{Pr}{Ra}}$, $\Delta t = L$, $\Delta x = \Delta y = h$ نعوضها في المعادلة (4.2.2) ينتج :

$$\xi^*_{i,j} - \xi_{i,j,n} = \frac{L\beta}{2h^2}\left[\xi^*_{i+1,j} - 2\xi^*_{i,j} + \xi^*_{i-1,j} + \xi_{i,j+1,n} - 2\xi_{i,j,n} + \xi_{i,j-1,n}\right]$$

$$- \frac{L}{4h}\left[\theta_{i+1,j,n+1} - \theta_{i-1,j,n+1}\right] - \frac{L\beta}{2}\, Ha^2\, \xi_{i,j,n} \qquad (4.10)$$

وليكن $\gamma = \frac{L}{h^2}$ نعوض في المعادلة (4.2.3) نحصل على:

$$\xi^*_{i,j} - \xi_{i,j,n} = \frac{\gamma\beta}{2}\left[\xi^*_{i+1,j} - 2\xi^*_{i,j} + \xi^*_{i-1,j} + \xi_{i,j+1,n} - 2\xi_{i,j,n} + \xi_{i,j-1,n}\right]$$

$$- \frac{\gamma h}{4}\left[\theta_{i+1,j,n+1} - \theta_{i-1,j,n+1}\right] - \frac{\gamma\beta h^2}{2}\, Ha^2\, \xi_{i,j,n} \qquad (4.11)$$

وسيتم الحصول على:

$$\xi^*_{i,j} - \frac{\gamma\beta}{2}\left[\xi^*_{i+1,j} - 2\xi^*_{i,j} + \xi^*_{i-1,j}\right] = \xi_{i,j,n} + \frac{\gamma\beta}{2}\left[\xi_{i,j+1,n} - 2\xi_{i,j,n} + \xi_{i,j-1,n}\right] - \frac{\gamma\beta h^2}{2} Ha^2\, \xi_{i,j,n} - \frac{\gamma h}{4}\left[\theta_{i+1,j,n+1} - \theta_{i-1,j,n+1}\right] \quad (4.12)$$

ومنها:

$$\xi^*_{i,j} - \frac{\gamma\beta}{2}\xi^*_{i+1,j} + \gamma\beta\xi^*_{i,j} - \frac{\gamma\beta}{2}\xi^*_{i-1,j} = \xi_{i,j,n} + \frac{\gamma\beta}{2}\xi_{i,j+1,n} - \gamma\beta\xi_{i,j,n} + \frac{\gamma\beta}{2}\xi_{i,j-1,n} - \frac{\gamma\beta h^2}{2} Ha^2\, \xi_{i,j,n} - \frac{\gamma h}{4}\left[\theta_{i+1,j,n+1} - \theta_{i-1,j,n+1}\right] \quad (4.13)$$

ومنها نحصل على:

$$-\frac{\gamma\beta}{2}\xi^*_{i-1,j} + [1+\gamma\beta]\,\xi^*_{i,j} - \frac{\gamma\beta}{2}\xi^*_{i+1,j} = \frac{\gamma\beta}{2}\xi_{i,j-1,n} + \left[1 - \gamma\beta - \frac{\gamma\beta h^2}{2} Ha^2\right]\xi_{i,j,n} + \frac{\gamma\beta}{2}\xi_{i,j+1,n} - \frac{\gamma h}{4}\left[\theta_{i+1,j,n+1} - \theta_{i-1,j,n+1}\right] \quad (4.14)$$

نقسم المعادلة (4.14) على $\left[\frac{\gamma\beta}{2}\right]$ ينتج:

$$-\xi^*_{i-1,j} + \frac{2[1+\gamma\beta]}{\gamma\beta}\,\xi^*_{i,j} - \xi^*_{i+1,j} = \xi_{i,j-1,n} + \left[\frac{2(1-\gamma\beta)}{\gamma\beta} - h^2\, Ha^2\right]\xi_{i,j,n} + \xi_{i,j+1,n} - \frac{h}{2\beta}\left[\theta_{i+1,j,n+1} - \theta_{i-1,j,n+1}\right] \quad (4.15)$$

نفرض إن:

$$g_1 = \frac{[1+\gamma\beta]}{\gamma\beta}\ ,\ g_2 = \frac{2[1-\gamma\beta]}{\gamma\beta} - h^2\, Ha^2\ ,\ g_3 = \frac{h}{2\beta}\ ,\ g_4 = \theta_{i+1,j,n+1} - \theta_{i-1,j,n+1}$$

نعوض الفرضيات في المعادلة (4.15) نحصل على:

$$-\xi^*_{i-1,j} + 2g_1\,\xi^*_{i,j} - \xi^*_{i+1,j} = \xi_{i,j-1,n} + g_2\xi_{i,j,n} + \xi_{i,j+1,n} - g_3 g_4 \quad (4.16)$$

وعليه يكون:

$$A(i) = -1 \quad , \quad B(i) = 2g_1 \quad , \quad C(i) = -1 \quad ,$$

$$D(i) = \xi_{i,j-1,n} + g_2\xi_{i,j,n} + \xi_{i,j+1,n} - g_3g_4 \quad , \quad i = 1,2,\dots.N$$

و بذلك يتكون لدينا نظام ثلاثي الأقطار (Tri-Diagonal System)، و سيتم إيجاد الحل بطريقة الحذف لكاوس [16]، و حل هذا النظام يمثل حل المعادلة الحركة (3.2) عند الزمن $\frac{t+1}{2}$.

ثانياً: باتجاه محورy:

باستخدام صيغ الفروقات المركزية لدينا[14]،[15] :

$$\frac{\partial\xi}{\partial t} = \frac{\xi_{i,j,n+1} - \xi^*_{i,j}}{\frac{\Delta t}{2}} \quad , \quad \frac{\partial^2\xi}{\partial x^2} = \frac{\xi^*_{i+1,j} - 2\xi^*_{i,j} + \xi^*_{i-1,j}}{(\Delta x)^2} \quad , \quad \xi = \xi_{i,j,n+1}$$

$$\frac{\partial^2\xi}{\partial y^2} = \frac{\xi_{i,j+1,n+1} - 2\xi_{i,j,n+1} + \xi_{i,j-1,n+1}}{(\Delta y)^2} \quad , \quad \frac{\partial\theta}{\partial x} = \frac{\theta_{i+1,j,n+1} - \theta_{i-1,j,n+1}}{2(\Delta x)}$$

نعوض الصيغ أعلاه في معادلة (4.7) ينتج:

$$\frac{\xi_{i,j,n+1} - \xi^*_{i,j}}{\frac{\Delta t}{2}} = \sqrt{\frac{Pr}{Ra}}\left[\frac{\xi^*_{i+1,j} - 2\xi^*_{i,j} + \xi^*_{i-1,j}}{(\Delta x)^2} + \frac{\xi_{i,j+1,n+1} - 2\xi_{i,j,n+1} + \xi_{i,j-1,n+1}}{(\Delta y)^2}\right]$$

$$- \left[\frac{\theta_{i+1,j,n+1} - \theta_{i-1,j,n+1}}{2(\Delta x)}\right] - Ha^2\sqrt{\frac{Pr}{Ra}}\,\xi_{i,j,n+1} \qquad (4.17)$$

نضرب معادلة (4.17) في $\left(\frac{\Delta t}{2}\right)$ ينتج:

$$\xi_{i,j,n+1} - \xi^*_{i,j}$$

$$= \frac{\Delta t}{2}\sqrt{\frac{Pr}{Ra}}\left[\frac{\xi^*_{i+1,j} - 2\xi^*_{i,j} + \xi^*_{i-1,j}}{(\Delta x)^2} + \frac{\xi_{i,j+1,n+1} - 2\xi_{i,j,n+1} + \xi_{i,j-1,n+1}}{(\Delta y)^2}\right]$$

$$- \frac{\Delta t}{2}\left[\frac{\theta_{i+1,j,n+1} - \theta_{i-1,j,n+1}}{2(\Delta x)}\right] - \frac{\Delta t}{2}\,Ha^2\sqrt{\frac{Pr}{Ra}}\,\xi_{i,j,n+1} \qquad (4.18)$$

ليكن $\beta = \sqrt{\frac{Pr}{Ra}}$, $\Delta t = L$, $\Delta x = \Delta y = h$ نعوضها في المعادلة (4.18) ينتج :

$$\xi_{i,j,n+1} - \xi^*_{i,j} = \frac{L\beta}{2h^2}\left[\xi^*_{i+1,j} - 2\xi^*_{i,j} + \xi^*_{i-1,j} + \xi_{i,j+1,n+1} - 2\xi_{i,j,n+1} + \xi_{i,j-1,n+1}\right] - \frac{L}{4h}\left[\theta_{i+1,j,n+1} - \theta_{i-1,j,n+1}\right] - \frac{L\beta}{2} Ha^2\, \xi_{i,j,n+1} \qquad (4.19)$$

وليكن $\gamma = \frac{L}{h^2}$ نعوض في المعادلة (4.19) نحصل على:

$$\xi_{i,j,n+1} - \xi^*_{i,j} = \frac{\gamma\beta}{2}\left[\xi^*_{i+1,j} - 2\xi^*_{i,j} + \xi^*_{i-1,j} + \xi_{i,j+1,n+1} - 2\xi_{i,j,n+1} + \xi_{i,j-1,n+1}\right] - \frac{\gamma h}{4}\left[\theta_{i+1,j,n+1} - \theta_{i-1,j,n+1}\right] - \frac{\gamma\beta h^2}{2} Ha^2\, \xi_{i,j,n+1} \qquad (4.20)$$

ومنها نحصل على:

$$\xi_{i,j,n+1} - \frac{\gamma\beta}{2}\left[\xi_{i,j+1,n+1} - 2\xi_{i,j,n+1} + \xi_{i,j-1,n+1}\right] + \frac{\gamma\beta h^2}{2} Ha^2\, \xi_{i,j,n+1} = \xi^*_{i,j} + \frac{\gamma\beta}{2}\left[\xi^*_{i+1,j} - 2\xi^*_{i,j} + \xi^*_{i-1,j}\right] - \frac{\gamma h}{4}\left[\theta_{i+1,j,n+1} - \theta_{i-1,j,n+1}\right] \qquad (4.21)$$

وسيتم الحصول على:

$$\xi_{i,j,n+1} - \frac{\gamma\beta}{2}\xi_{i,j+1,n+1} + \gamma\beta\xi_{i,j,n+1} - \frac{\gamma\beta}{2}\xi_{i,j-1,n+1} + \frac{\gamma\beta h^2}{2} Ha^2\, \xi_{i,j,n+1} = \xi^*_{i,j} + \frac{\gamma\beta}{2}\xi^*_{i+1,j} - \gamma\beta\xi^*_{i,j} + \frac{\gamma\beta}{2}\xi^*_{i-1,j} - \frac{\gamma h}{4}\left[\theta_{i+1,j,n+1} - \theta_{i-1,j,n+1}\right] \qquad (4.22)$$

ومنها نحصل على:

$$-\frac{\gamma\beta}{2}\xi_{i,j-1,n+1} + \left[1 + \gamma\beta + \frac{\gamma\beta h^2}{2} Ha^2\right]\xi_{i,j,n+1} - \frac{\gamma\beta}{2}\xi_{i,j+1,n+1} = \frac{\gamma\beta}{2}\xi^*_{i-1,j} + [1 - \gamma\beta]\xi^*_{i,j} + \frac{\gamma\beta}{2}\xi^*_{i+1,j} - \frac{\gamma h}{4}\left[\theta_{i+1,j,n+1} - \theta_{i-1,j,n+1}\right] \qquad (4.23)$$

نقسم المعادلة (4.23) على $\left[\frac{\gamma\beta}{2}\right]$ ينتج:

$$-\xi_{i,j-1,n+1}+\left[\frac{2(1+\gamma\beta)}{\gamma\beta}+h^2\,Ha^2\right]\xi_{i,j,n+1}-\xi_{i,j+1,n+1}$$

$$=\xi^*_{i-1,j}+\left[\frac{2(1-\gamma\beta)}{\gamma\beta}\right]\xi^*_{i,j}+\xi^*_{i+1,j}-\frac{h}{2\beta}\left[\theta_{i+1,j,n+1}-\theta_{i-1,j,n+1}\right] \qquad (4.24)$$

نفرض إن:

$$g_3=\frac{h}{2\beta}\ ,\ g_4=\theta_{i+1,j,n+1}-\theta_{i-1,j,n+1}\ ,\ g_5=\frac{2[1+\gamma\beta]}{\gamma\beta}+h^2\,Ha^2\ ,\ g_6=\frac{(1-\gamma\beta)}{\gamma\beta}$$

نعوض الفرضيات في المعادلة (4.24) نحصل على:

$$-\xi_{i,j-1,n+1}+g_5\,\xi_{i,j,n+1}-\xi_{i,j+1,n+1}=\xi^*_{i-1,j}+g_6\,\xi^*_{i,j}+\xi^*_{i+1,j}-g_3g_4 \qquad (4.25)$$

وعليه يكون:

$$AA(i)=-1\quad,\quad BB(i)=g_5\quad,\quad C(i)=-1\quad,$$

$$D(i)=\xi^*_{i-1,j}+2g_6\,\xi^*_{i,j}+\xi^*_{i+1,j}-g_3g_4 \qquad i=1,2,\ldots.N$$

و بذلك يتكون لدينا نظام ثلاثي الأقطار (Tri-Diagonal System)، و سيتم إيجاد الحل بطريقة الحذف لكاوس [16]، و حل هذا النظام يمثل حل المعادلة الحركة (3.2) عند الزمن $t+1$.

5. النتائج و الاشكال:

بعد حل معادلة الحركة التي تم الحصول عليها من النموذج الرياضي والتي تم تطويرها حسب ظروف المسألة مع الشروط الحدودية و باستخدام مفهوم دالة الجريان حيث تحولت الى معادلة من الرتبة الرابعة و لاجل استخدام طريقة الاتجاهات المتعاقبة الضمنية ADI تم تخفيض رتبة المعادلة الى الرتبة الثانية وذلك باستخدام مفهوم الدردورية لغرض استخدام الطريقة المذكورة أعلاه ، و بعد تطوير الخوارزمية المناسبة لها باستخدام برنامج فورتران ، تم الحصول على النتائج و التي تمثل حركة المائع و تاثير البراميترات مثل عدد هارتمان ، عدد رالي و عدد براندتل على الحركة داخل القناة و كما موضح في الاشكال . ويلاحظ ان تاثير عدد رالي على حركة المائع طفيف جداً، كما مبين في الاشكال

(١–أ) و(١–ب)، ومن الاشكال (٢–أ)، (٢–ب) ، (٣–أ) و(٣–ب) يلاحظ ان عدد براندتل و عدد هارتمان لهما تاثير واضح على حركة المائع داخل القناة

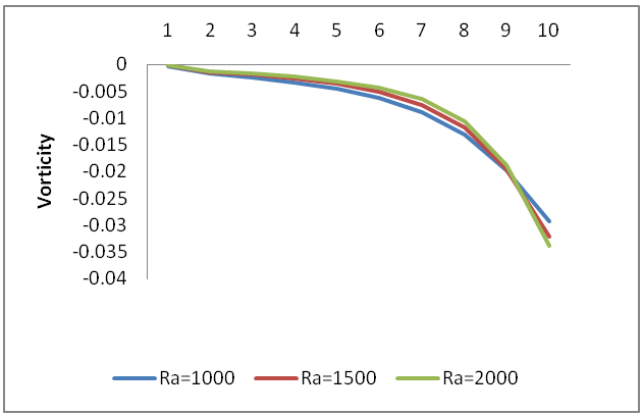

الشكل (١–أ)

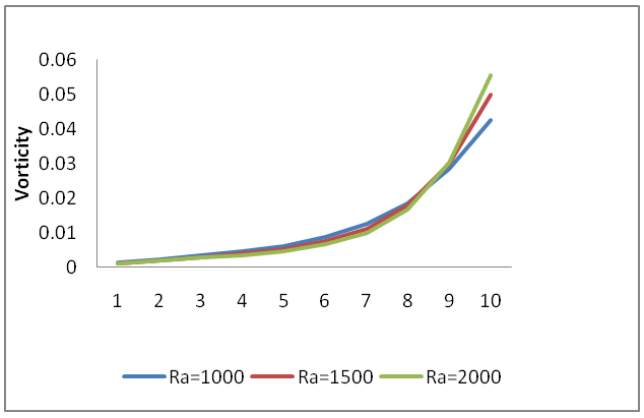

الشكل (١–ب)

الاشكال (١–أ) و(١–ب) يمثل تأثير عدد رالي على حركة المائع داخل قناة في منطقة البداية والنهاية على التوالي.

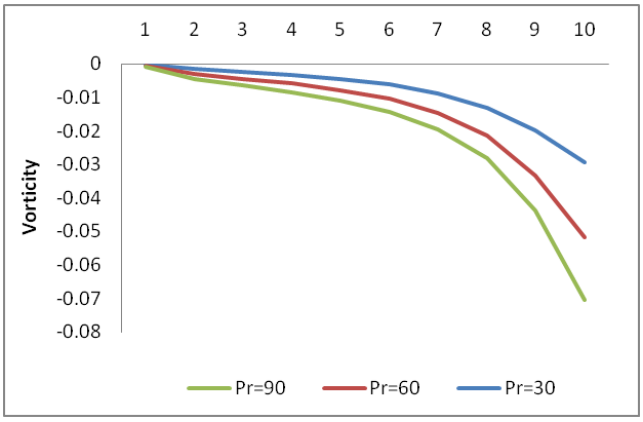

الشكل (٢–أ)

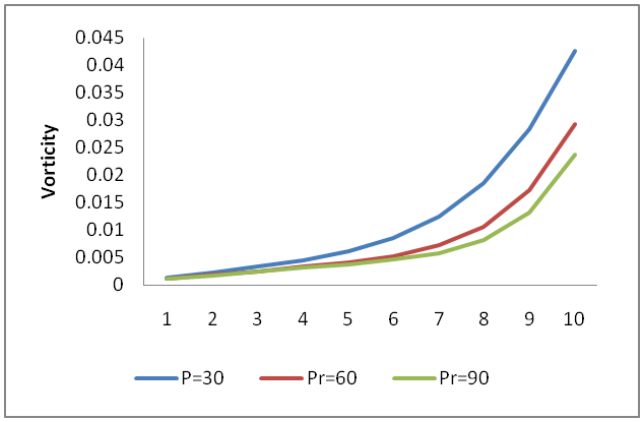

الشكل (٢–ب)

الاشكال (٢–أ) و (٢–ب) يمثل تأثير عدد برانتدل على حركة المائع داخل قناة في منطقة البداية والنهاية على التوالي.

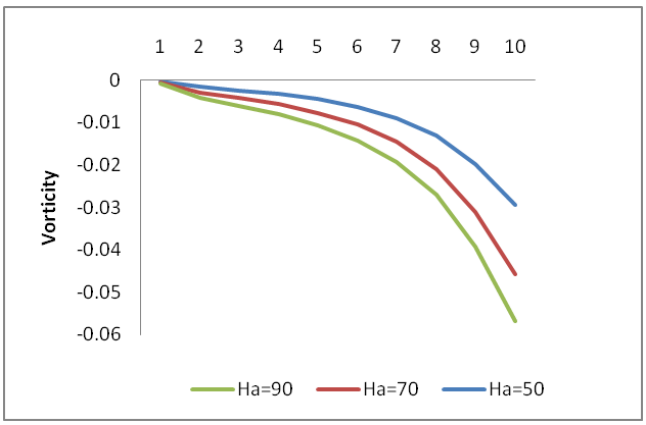

الشكل (٣–أ)

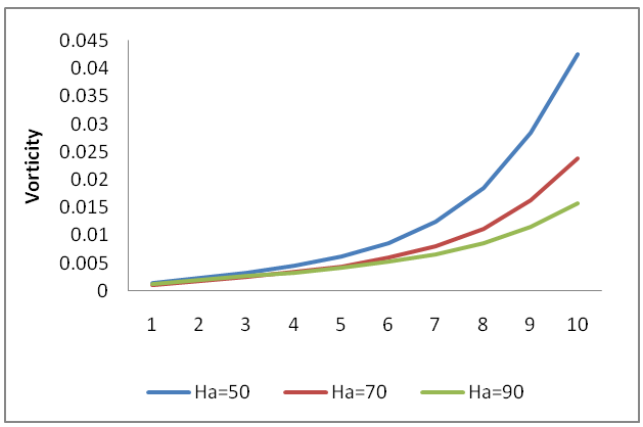

الشكل (٣–ب)

الاشكال (٣–أ) و (٣–ب) يمثل تأثير عدد هارتمان على حركة المائع داخل قناة في منطقة البداية والنهاية على التوالي.

6. الاستنتاجات

من خلال هذه الدراسة توصلنا إلى انه وباستخدام بعض المفاهيم الرياضية المتعلقة بخواص الموائع مثل دالة الجريان والتي بواسطتها تم تخفيض عدد المتغيرات للمسألة وجعلها بدلالة متغير واحد فقط وبعد ذلك استخدم مبدأ آخر وهو الدردورية (Vorticity) وهي من خواص المائع ايضاً لأجل تخفيض رتبة المعادلة التي تم الحصول عليها باستخدام مفهوم دالة الجريان وهذا الأسلوب يختلف عن البحوث السابقة التي تم فيها حل مسائل مشابهة و بأساليب رياضية مختلفة و تبين من النتائج أن تأثير عدد رالي على حركة الماء داخل القناة قليل جداً حيث تراوحت قيم رالي بين ١٠٠٠ الى ٢٠٠٠ وكما موضح في الاشكال (١–أ) و (١–ب). وتأثير عدد برانتدل و عدد هارتمان اوضح على حركة الماء داخل القناة حيث تراوحت قيم براندتل بين ٣٠ الى ٩٠ و تراوحت قيم هارتمان بين ٥٠ الى ٩٠ و كما موضح في الاشكال (٢–أ)، (٢–ب) ، (٣–أ) و(٣–ب) على التوالي. وتبين أيضا من الاشكال بأن الدالة الدردورية تتأثر داخل القناة عندما يتغير عدد برانتدل او عدد هارتمان.

المصادر:

[1] P. D. Verma and J. L. Bansal, “Flow of a viscous incompressible fluid between two parallel plates, one in uniform motion and the other at rest with uniform suction at the stationary plate,” in *Proceedings of the Indian Academy of Sciences-Section A*, Springer, 1966, pp. 385–396.

[2] B. C. Bhuyan and G. C. Hazarika, “Effect of magnetic field on pulsatile flow of blood in a porous channel,” *Bio-Sci Res. Bull*, vol. 17, no. 2, pp. 105–112, 2001.

[3] M. H. Taheri, “The influence of magnetic field on the fluid flow in the entrance region of channels: analytical/numerical solution,” *SN Appl Sci*, vol. 1, no. 10, p. 1233, 2019.

[4] F. S. Rasmussen, C. G. Klingaa, M. R. Sonne, and J. H. Hattel, “Numerical Modelling of Heat Transfer using the 3D-ADI-DG Method-with Application for Pultrusion.: Technical report,” 2019.

[5] T. Mehta, R. Mehta, and A. Mehta, “Oscillatory fluid flow and heat transfer through porous medium between parallel plates with inclined magnetic field, radiative heat flux and heat source,” *International Journal of Applied Mechanics and Engineering*, vol. 25, no. 2, pp. 88–102, 2020.

[6] Z. A. Almishlih, “Numerical solution of fluid flow in horizontal tube under effects of radiation field,” *Open Access Library Journal*, vol. 7, no. 5, pp. 1–12, 2020.

[7] A. M. J.Jassim and A. S.J. Amen, “Numerical Solution of Electromagnetic Problem MHD in a Polar Coordinates,” *AL-Rafidain Journal of Computer Sciences and Mathematics*, vol. 15, no. 1, pp. 23–34, 2021.

[8] A. H. Ala’a, O. T. Al-Bairaqdar, and A. T. Hammodat, “Numerical solution of energy equation in porous channels under effects of radiation field,” *Iraqi Journal of Science*, pp. 3620–3633, 2021.

[9] H. E. Marcroft and M. V Karwe, “FLOW FIELD IN A HOT AIR JET IMPINGEMENT OVEN-PART I: A SINGLE IMPINGING JET,” *J Food Process Preserv*, vol. 23, no. 3, pp. 217–233, 1999.

[10] Y. Yang, *Natural convective flow and heat transfer in vertical and inclined glazing cavities*. University of Massachusetts at Amherst, 2003.

[11] M. K. Goyal, *Fluid Mechanics and Hydraulic Machines*. PHI Learning Pvt. Ltd., 2015.

[12] A. A. Hammodat and H. D. Saleem, "Numerical solution of electromagnetic problem in horizontal porous medium."

[13] H. B. Wilson, L. H. Turcotte, and David. Halpern, *Advanced mathematics and mechanics applications using MATLAB*. Chapman & Hall/CRC, 2003.

[14] A. ~R. Mitchell and D. ~F. Griffiths, *The finite difference method in partial differential equations*. 1980.

[15] D. J. Duffy, "Finite Difference Methods in Financial Engineering : A Partial Differential Equation Approach."

[16] B. Carnahan, H. A. Luther, and J. O. Wilkes, *Applied numerical methods*, Wiley New York., vol. 2. 1969.

The effect of bio-prepared zinc nanoparticles from the fungus *Verticillium lecanii* on combating third-instar larvae of the date moth *Ephestia cautella*

[1] Doaa Abdulmajeed Mohamed

eduhm230154@uosamarra.edu.iq

[1,2] Department of Biology, College of Education - University of Samarra

[2]Hisham naji hameed

Hisham.n370@uosamarra.edu.iq

The effect of bio-prepared zinc nanoparticles from the fungus *Verticillium lecanii* on combating third-instar larvae of the date moth *Ephestia cautella*

[1] Doaa Abdulmajeed Mohamed

eduhm230154@uosamarra.edu.iq

[1,2] Department of Biology, College of Education - University of Samarra

[2]Hisham naji hameed

Hisham.n370@uosamarra.edu.iq

Abstract:

The study was conducted in the Department of Biology - College of Education - University of Samarra, which aims to combat the third instar larvae of the date moth *Ephestia cautella* using bio-prepared zinc nanoparticles from the fungus *Verticillium lecanii* and comparing it with the biomass of the fungus *Verticillium lecanii* and finding out which is most effective in eliminating the third instar of the date moth *Ephestia. cautella* and biomass concentrations were used (1, 1.5, 2) g / L.

Only distilled water was used in the control plants, with a time period of (24, 48, 72) hours for each concentration, Three concentrations of zinc nanoparticles were used: (0.250, 0.125, 0.62) ml / liter , and only distilled water was used in the control laboratories, with a period of time of (24, 48, 72) hours for each concentration, and for each concentration, three replicates were used for each concentration, and 10 larvae of the date moth *Ephestia cautella* were placed in each replicate for each replicate of the

experiment, and the results of each were given: Biomass had high killing results at a concentration of 2 ml/L after 72 hours, and nano zinc at a concentration of 0.250 ml/L after 72 hours.

Introduction:

The date moth is an insect with complete metamorphosis and has four stages: the egg, the larva, the pupa, and the adult. The female date moth lays her eggs in groups or individually on the outer surface of the date [1].

Although the female insect lives for approximately 14 days, The eggs laid by one female are approximately 135 eggs, and approximately 90% of the eggs are laid in the first four days. The eggs are characterized by containing prominent lines on the surface of the egg, both longitudinally and transversely, arranged in 24 irregular rows, with the length of one egg ranging from (0.33 - 0.38 mm).

Their width ranges between (0.22 - 0.32 mm), and the eggs are white when first laid by the adult insect, then they turn orange before the hatching process, with clear longitudinal and transverse elevations on the outer surface [2],The hatching process may take from 3-4 days after the female lays her eggs, the date moth, *Ephestia cautella*, is a polyphagous insect that infects different types of stored foodstuffs, most notably dates, whether they are on palm trees or fallen on the ground or in stores, as well as feeding on many stored foodstuffs such as dried figs, raisins, tarshana, and grains. And their products, legumes, nuts, oilseeds, cocoa and other food families[3].

Nanocomposites are materials to which nanoparticles are added during the manufacture of these materials. As a result, the nanomaterials show an improvement in their properties. Nanotechnology is considered a broad field of scientific research and opens up a wide field in various fields.

It is considered the main advantage of modern insecticides, as it has a useful pesticide effect to eliminate insects. It is not harmful to the main environmental components, and the word nano (Nanos) is originally a Greek word that means dwarf and is used to describe materials with small sizes from (1−100 nanometers). Nanobjects are bio-manufactured using microorganisms such as fungi, bacteria, viruses, and nano-extracts.

One of the advantages of this method is that it is cheap and does not require Energy, fast and at the same time environmentally friendly [4].

Fungi that infect insects and products derived from fungi have been used in biological control of targeted insects, The *Verticillum lecanii* fungus is one of the most common fungi on target insect families and is used to eliminate insects that cause economic damage [5].

Aim of the Study:

1- Evaluation of the effectiveness of biomass prepared from the fungus *Verticillum lecanii* on third-instar larvae of the date moth *Cautella Ephestia.*

2- The effectiveness of a nano-prepared biological preparation from the *Verticillum lecanii* fungus on eliminating the larvae of the date moth *Ephestia cautella*.

key words: *Verticillium lecanii,, Ephestia cautella* , PDA, ZnoNPs, nano

Materials and Methods:

Medium Solid Potato Dextrose Agar (PDA):

Prepare the medium according to the manufacturer's instructions, HIMEDIA, by dissolving 39 grams of potato medium in a liter of distilled water, placing it in a 1000 ml

glass baker, shaking well, closing the nozzle with a cotton plug, then sterilizing with an autoclave at a temperature of 121°C and a pressure of 15 pounds/inch for 15 minutes, then Leave the medium to cool and before it hardens, pour it into sterilized dishes.

Liquid potato dextrose medium (PDB) Potato Dextrose Broth:

Prepare the medium according to the manufacturer's instructions by dissolving 24 grams of powdered medium in 1 liter of distilled water. Distribute the medium into conical flasks with a capacity of 250 ml and plug their nozzles with cotton plugs. Then sterilize with an autoclave at a temperature of 121 °C and a pressure of 15 pounds/in2 for 15 minutes, Prepare this medium to obtain the biomass of the *Verticillium lecanii* fungus.

Activation of the fungus *V. lecanii*

Activating the fungal isolate by replanting it on new PDA media 7-9 days before starting to produce biomass in order to use it in preparing biomass.

Preparation of *V. lecanii* biomass

To obtain biomass, the fungal isolate was grown in a sterile Petri dish containing sterile Potato Dextrose Agar medium, and incubated at a temperature of 2 ± 26 °C and a relative humidity of 5 ± 85% for 7 days.

After that, four discs were taken from the colonies growing on the medium. The solid food PDA, with a diameter of 5 mm, was multiplied on the sterile liquid medium placed in a 1000 ml glass container with the addition of 125 mg of tetracycline to ensure that bacteria did not grow, while continuing to move the glass containers incubated at a temperature of 2 ± 26 °C for 21 days with daily manual shaking. Biomass after 21 days of incubation by using a glass funnel and filter paper.

After that, the biomass was washed with distilled water three times, followed by washing it with deionized water twice to get rid of all residual nutrient medium. Weighed 10 grams of fungal biomass using a sensitive balance and transferred to 1000 ml glass containers containing 250 ml deionized water were also incubated under the same conditions above with daily shaking using a shaker for 120 hours.

After the expiration of the period, the fungal biomass was filtered using filters to obtain the fungal biomass filtrate. The filtrate was collected and incubated at a temperature of 26 ± 2 °C and a relative humidity of 5 ± 75% until use [6].

The biomass is then dried to obtain a powder for experiments on the third instar larvae of the date moth.

For fungal biomass, concentrations of (1, 1.5, and 2) grams were used, with three replicates for each concentration. The control factor in the experiment was used only distilled water for 24, 48, and 72 hours. The concentrations gave high rates of death.

Bio-prepared nanocomposite from *Verticillium lecanii*

The nanocomposite zinc oxide (ZnoNPs) that was used in the study was obtained from the Ministry of Science and Technology in Baghdad Governorate / Iraq. The compound was in the form of a white-yellowish powder, with a particle size of less than 5 micrometers with a purity of 99% , The Ministry prepared the compound in A plastic box containing 7 grams. It was received in the form of a nanopowder with a particle size of less than 100 nanometers.

Preparation of nanocomposites (ZnoNPs):

Silver nanoparticles were manufactured by crushing the mushroom extract using an ultrasound device for five minutes, after which the previously prepared zinc oxide

solution was placed on a hot plate with a magnetic stirrer for 30 minutes, after which the mushroom extract was added to the oxide solution.

Zinc in drops, then placed in an ultrasound machine for 30 minutes, then mixed with a magnetic mixer without heat for 30 minutes [7].

An amount of nano-zinc oxide was weighed 0.5 grams of powder and a drop of concentrated nitric acid was placed on it and mixed with the powder, noting the rise of vapors from the powder after mixing it with nitric acid.

Then the homogeneous material was placed in a glass beaker containing 1000 ml of distilled water with continuous stirring for 10 minutes. To ensure that the nanocomposite dissolves with water, and thus we have the main stock concentration.

After that, we conduct several dilutions to reach the concentrations required in the experiment, which are a concentration of 0.250, 0.125, 0.062) and for a period of time of (24, 48, 72, 96), with three replicates for each concentration and a coefficient was used. The control in this experiment was only distilled water.

Statistical Analysis:

The results analyzed statistically by applying the statistical program (MINITAB VER.17) according to the Anova analysis test (Anova). The mathematical averages were compared according to the Duncuns Multiple Range test and at a possibility of $0.05 \geq p$ [8].

Results :

The results of the table (1) and the effect of the interaction of the different concentrations (0.062, 0.125, 0.250 mg/L) of the zinc oxide nano composite, as well as the time period for the death of the third instar of the date moth, showed that there were significant differences in the killing rates due to the interaction between the

concentrations and the duration of exposure, as the highest percentage of killing was for the third instar larvae. The third was 96.7% at a concentration of 2500 after 96 hours of treatment, while the lowest killing percentage was 23.3% at a concentration of 0.062 after 24 hours of treatment, while averages of the killing percentage as a result of the concentrations showed that the highest killing percentage was at a concentration of 0.250 reaching 72.5%, while The lowest average kill rate at a concentration of 0.062 was 59.2%.

As for the average kill rate based on the duration of killing, the highest kill rate after 96 hours was 70.0%, and the lowest kill rate after 24 hours was 24.2%.

From the results it was shown that the percentage Larval killing increased with increasing concentration and duration of treatment. The results of the study were consistent with the findings of [9].

As they indicated that the zinc oxide nanocomposite had an effective effect in combating the red flour beetle T. castaneum compared to the pesticide malathion, as the results showed that there was a significant effect of the nanocomposite.

Zinc oxide affects the percentage of killing, productivity and weight loss of whole grains. These percentages increase with increasing concentration and duration of exposure, as these particles cause deformities and dehydration of the insect and provide protection for the grain by reducing the rate of the first generation of the insect T. castaneum and then reducing the percentage of weight loss in the grain. It was also similar The results of this study are based on the findings of [10].

Who indicated the effect of nano composites, including zinc oxide, in protecting grains from infection with the Khabra insect for a period of up to 40 days, where the

percentage of weight loss was 0.67, 0.73, and 3.44%, while the percentage of weight loss was 3.44%.

The loss in the control treatment is 11.74%. Zinc oxide nanoparticles have been used to develop pesticides due to their antimicrobial, physical and some other properties [11]; [12].

Table (1) shows the effect of nano-zinc oxide (ZNPs) on the mortality rates of third-instar larvae of the date moth.

Concentration Average	Time				Concentration ml /l
	96 Hours	72 Hours	48 Hours	24 Hours	
7.25 A	9.67 a	8.67 b	6.33 d	4.33 f	0.250
6.25 B	9.33 ab	7.33 c	5.33 e	3.00 g	0.125
5.92 B	9.00 b	7.33 c	5.00 e	2.33 h	0.062
0.0 C	0 i	0 i	0 i	0 i	Control
	7.00 a	5.83 b	4.17 c	2.42 d	Time average

Small letters that are similar horizontally mean that there are no significant differences between them.

The results of the table (2) and the effect of the interaction of different concentrations (2, 1.5, 1) g/Lon biomass as well as the time period for the death of the third instar of the date moth showed that there were significant differences in the killing rates due to the interaction between the concentrations and the duration of exposure, as the highest percentage of killing for the third instar larvae was 93.3 % at concentration 2 after 72 hours of treatment, while the lowest killing rate was 23.3% at concentration 1 after 24

hours of treatment, while averages of the killing rate as a result of the concentrations showed that the highest killing rate was at concentration 2, reaching 72%, The lowest average kill rate at concentration 1 was 23.3%.

As for the average kill rate based on the duration of killing, the highest kill rate after 72 hours was 50.0%, and the lowest kill rate after 24 hours was 28.3%.

From the results it was shown that the percentage of Killing third instar larvae of date moth increased with increasing concentration and duration of treatment. The results of this study agreed with [13].

Through the use of suspensions of three types of chrysogenum fungi. *penicillium*, *V.lecanii, Aspergillus.niger*) in its effect on the larval stages of *C.quinquefasciatus* mosquitoes, as the insect-pathogenic fungus *V.lecanii* outperformed the rest of the fungi in influencing mosquito larvae with percentages of death reaching 20, 16.66, 13.33, and 10% after 48 hours of treatment and rose to 63.33), 60, 56.66 and 53.33 after 96 hours of treatment.

The high rate of death rates in the first larval ages with the last instar and adults is attributed to the incompleteness of the defense cells in the first larval ages, in addition to the lack of thickness of the cuticle layer, or it may be explained by changes in the biological and chemical composition of the insect's body wall, such as the presence of toxic compounds, which may To prevent the germination of fungal spores [14].

The results of other studies that are consistent with this study showed what was mentioned by [15].

that they were more sensitive to infection by *E. cautella*. The results showed that individuals of the first larval stages of the date moth were exposed to biological factors (bacteria and fungi) from later ages. The ability of the fungus to adhere to the body The

insect, its structure, the germination tube and adhesion organ, and the amount of enzymes secreted by the fungus, such as chitinase, lipase, and protease enzymes, played a major role in destroying the insect's body.

The current study showed that increasing the concentration and duration of treatment of biologically prepared biomass from mushrooms has a significant impact on eliminating third-instar larvae of the date moth.

Table (2) shows the effect of biosynthetic mass from the fungus *V. lecanii*. On third instar larvae of the date moth *E. cautella*

Concentration Average	**Time**			**Concentration ml /l**
	72 Hours	**48 Hours**	**24 Hours**	
3.33 C	**4.00 e**	**3.67 e**	**2.33 f**	**1**
5.56 B	**6.67 bc**	**6.33 c**	**3.67 e**	**1.5**
7.22 A	**9.33 a**	**7.00 b**	**5.33 d**	**2**
0.0 D	**0 g**	**0 g**	**0 g**	**Control**
	5.00 a	**4.25 b**	**2.83 c**	**Time average**

Small letters that are similar horizontally mean that there are no significant differences between them.

Conclusion:

1-The fungus *V. lecanii* showed high efficiency in the biosynthesis of zinc oxide nanoparticles.

2- Biologically prepared nanoparticles have a promising future in controlling insect pests.

3. Treatment with zinc nanoparticles led to the killing of third-instar larvae of the date moth three days after treatment, with a direct relationship between concentrations and killing rates.

References:

1- Arthington, A. H., Pearson, R. G., Connolly, N. M., James, C. S., Kennard, M. J., Loong, D., ... & Pusey, B. J. (2007). Biological Indicators of Ecosystem Health in Wet Tropics Streams. *Catchment to Reef Research Program, CRC for Rainforest Ecology and Management and CRC for the Great Barrier Reef.(James Cook University, Townsville.)*.

2- Abdul Hussein, Ali. 1979. Palm trees and dates and their pests in Iraq. faculty of Agriculture . University of Basra. 190 pages.

3- Aldawood,A.S.(2013) Effect of covering dates fruit bunches on Ephestia cautella Walker (Lepidoptera: pyralidae)infestation: population dynamics studies in the field. Int. J. Agric. Appl. Sci. Vol. 5, No.1,:98-100.

4- Ribeiro , L. P.; Blume, E.; Bogorni , P. C. ; Dequech , S. T.B.; Brand , S. C. and Junges,E.(2012) Compatibility of *Beauveria bassiana* commercial isolate with botanical insecticides utilized in organic crops in southern Brazil. December 2012Biological Agriculture and Horticulture. 28(4):223-240.

5- **Kamalakannan** S. K. Vnaik kGChauhanA. **(2021)** .Sources of fungal bio-generated nano particies for potential control of mosquito –born diseases review.

6- **Al-Shammari,** Hazem Eidan (2015) The effect of the predator Dicrodiplosis manihoti Harris (Diptera: Cecidomyiidae) and silver nanoparticles prepared by biological methods on some biological aspects of the citrus mealybug Planococcus (Risso) Hemiptera: Pseudococcidae. Doctoral thesis. College of Agriculture, University of Baghdad.

7- **Al-Naimi,** MT. Hamdan, N.T. Abdel-Rahim, E., and Al-Janabi, .(2019).ZZ. Biodegradation of malathion pesticides by silver bioparticles from Bacillus licheniformis extracts. Research in Crops, 20. spl), (79-84.

8 -**Al-Rawi**, Khashi Mahmoud and Abdul Aziz Muhammad Khalaf Allah (1980). Design and analysis of agricultural experiments, Dar Al-Kutub Printing and Publishing Foundation, Ministry of Higher Education and Scientific Research, University of Mosul.

9 - Abd-El-Salam, S. A., Hamzah, A. M., & El-Taweelah, N. M. (2015). Aluminum and zinc oxides nanoparticles as a new method in controlling the red flour beetle, Tribolium castaneum (Herbest) compared to Malathion insecticide. *International Journal of Scientific Research in Agricultural Sciences*, *2*(Proceedings), 001-006.

10 - **Radhiu**, Ghadeer Abdul Jabbar. 2020. Evaluation of the efficiency of some commercial nanocomposites and alcoholic extracts of some plants in controlling the insect Trogodema granarium Evest 1898 (coleopteran): Dermestidae under laboratory conditions. Master's thesis. College of Agriculture, University of Kufa, Republic of Iraq. Issue (2) 1.

11 – **Akbar**, S., Tauseef, I., Subhan, F., Sultana, N., Khan, I., Ahmed, U., & Haleem, K. S. (2020). An overview of the plant-mediated synthesis of zinc oxide nanoparticles and their antimicrobial potential. *Inorganic and Nano-Metal Chemistry*, *50*(4), 257-271.

12 - **Akintelu**, S. A., & Folorunso, A. S. (2020). A review on green synthesis of zinc oxide nanoparticles using plant extracts and its biomedical applications. *BioNanoScience*, *10*(4), 848-863.

13- **Al-Fatlawi**, Ali Abdel Hamid Abdel Amir. (2021). Evaluating the effectiveness of biosynthetic silver nanoparticles using filtrate and suspensions of some fungal species in resisting mosquitoes. Master's thesis, College of Science, Al-Qadisiyah University. p. 134

14 - **Raduw, G. G., & Mohammed, A. A.** (2020). Insecticidal efficacy of three nanoparticles for the control of Khapra beetle (Trogoderma granarium) on different grains. *Journal of Agricultural and Urban Entomology*, *36* (1), 90-100.

15 - **Abdel Aoun**, Lara Sharif 2021. Evaluating the efficiency of some local isolates of the fungus Beauveria bassiana, the bio-commercial preparation Naturalis-L, the pathogenic bacteria Bacillus thuringiensis, and nanocomposites SNPs, ANPs, and ZNPs in controlling the date (fig) moth Ephestia cautella in laboratory conditions. Master's thesis - College of Agriculture - University of Karbala. 176 pages.

تأثير جزيئات الزنك النانوية المحضرة حيويا من الفطر *Verticillium lecanii* في مكافحة يرقات العمر الثالث لفراشة التمر *Ephestia cautella*

1,2

[1,2]كلية التربية , قسم علوم الحياة – جامعة سامراء

دعاء عبدالمجيد محمد [1]

eduhm230154@uosamarra.edu.iq

هشام ناجي حميد [2]

Hisham.n370@uosamarra.edu.iq

المستخلص:

أجريت الدراسة في قسم علوم الحياة – كلية التربية – جامعة سامراء، وتهدف إلى مكافحة يرقات العمر الثالث لعثة التمر *Ephestia cautella* باستخدام جزيئات الزنك النانوية المحضرة حيوياً من فطر Verticillium lecanii ومقارنتها مع الكتلة الحيوية للفطر *Verticillium lecanii* ومعرفة أيهما أكثر فعالية في القضاء على العمر الثالث لعثة التمر *Ephestia*. واستخدمت تراكيز من النانو والكتلة الحيوية (1، 1.5، 2) غرام/لتر.

تم استخدام الماء المقطر فقط في محطات المراقبة وبمدة زمنية (24، 48، 72) ساعة لكل تركيز، وتم استخدام ثلاث تراكيز من جزيئات الزنك النانوية: (0.250، 0.125، 0.62) مل/لتر، والماء المقطر فقط. تم استخدام مختبرات المقارنة بفترة زمنية (24، 48، 72) ساعة لكل تركيز، ولكل تركيز تم استخدام ثلاث مكررات لكل تركيز، وتم وضع 10 يرقات من فراشة التمر *Ephestia cautella* في مكررات للمقارنة.

تم إعطاء نتائج كل مكرر لكل مكرر للتجربة: أظهرت الكتلة الحيوية نتائج قتل عالية عند تركيز 2 مل/لتر بعد 72 ساعة، ونانو زنك بتركيز 0.250 مل/لتر بعد 72 ساعة.

الكلمات المفتاحيه: *Verticillium lecanii*, *Ephestia cautella* , PDA, ZnoNPs, nano

The Effectiv of the Testing Chemical Pesticide Nishan 20sc and the Biopesticide Spinosad on the Larvae and Pupae of the *Culex Theileri Theobald* Mosquitoes of the Genus *Culex* (Diptera: Culicidea) in Samarra

[1,2,3]Department of Biology, College of Education – University of Samarra-Iraq

Mustafa Abdul khaliq Hamad[1]

eduhm230006@uosamarra.edu.iq

Husham Naji Hameed[2]

Hisham.n370@uosamarra.edu.iq

Harith Ahmed Mustafa[3]

harith.a.m@uosamarra.edu.iq

The Effectiv of the Testing Chemical Pesticide Nishan 20sc and the Biopesticide Spinosad on the Larvae and Pupae of the *Culex Theileri Theobald* Mosquitoes of the Genus *Culex* (Diptera: Culicidea) in Samarra

[1,2,3]Department of Biology, College of Education – University of Samarra–Iraq

Mustafa Abdul khaliq Hamad[1]

eduhm230006@uosamarra.edu.iq

Husham Naji Hameed[2]

Hisham.n370@uosamarra.edu.iq

Harith Ahmed Mustafa[3]

harith.a.m@uosamarra.edu.iq

Abstract:

The study was conducted in the Department of Life Sciences – College of Education – University of Samarra, which aims to combat mosquito larvae and pupae using the chemical pesticide 20 Sc Nishan and knowing the percentage of its effect on the larvae and pupae of the *Culex thieleri* mosquito along with the use of the biological pesticide known as Spinosad and knowing which of the two is more effective in eliminating mosquito larvae and pupae in particular. *Culex* genus, and three concentrations of the chemical pesticide were used (0.25, 0.5, 1) ml/L.

The effect of different concentrations of Nishan 20 Sc pesticide on the death of *Culex* mosquito larvae indicated that there were significant differences in the killing rates due to the interaction between the concentrations and the duration of exposure, as the highest killing rate was 100 mosquito larvae. *Culex* % at a concentration of 1.0 ml pesticide/liter after 72 hours of treatment, while the lowest killing rate was 30.0% at a concentration of 0.25 ml pesticide/liter after24hours of treatment. Only distilled water was used in the control plants and for a period of 72 hours,24 and 48 hours for each concentration. Three concentrations of the biocide known as Spinosad, 12% (0.50, 0.25, 0.125) ml/L, were used for each Spinnosad pesticide to kill *Culex* mosquito larvae. There were significant differences in the killing rates due to the interaction between the concentrations and the duration. Exposure: The highest killing rate of *Culex* mosquito larvae was 100% at a concentration of 500 ml pesticide/liter after 72 hours of treatment, while the lowest killing rate was 23.3% at a concentration of 0.125 ml pesticide/liter after 24 hours of treatment. It was used in control laboratories.

Only distilled water, with a time period of 72, 48, and 24 hours for each concentration. For each concentration, three replicates were used for both larvae and pupae, and 10 larvae were placed in each replicate, Also, 10 pupae were placed in each replicate for each replicate of the experiment. The results of both pesticides gave high killing results when The concentration was 1 ml/liter after 72 hours for the chemical pesticide 20 Sc Nishan, while the biopesticide Spinosad was more effective at a concentration of 0.5 ml/liter after 72 hours.

The results of the study confirmed that there is a direct relationship between increasing the concentration, the time period of exposure, and the percentage kill rates, and that mosquito larvae were more sensitive than pupae in being affected by all the treatments under study.

keywords: *Culex*, , Spinosad, IPM, Nishan, DDT

Introduction:

Mosquitoes are medically important insects as they transmit many dangerous and deadly pathogens to humans and animals. Mosquitoes remain one of the most important major threats to public health and economic growth in many parts of the world Mosquitoes are Diptera insects that act as biological and mechanical vectors for many diseases.

Parasites and mosquitoes can transmit endemic and even epidemic diseases and other diseases[1].

Mosquitoes are small insects belonging to the Diptera order of the Culicidea family, Mosquitoes can be identified by their small size, which is approximately 3-9 mm. They have one pair of wings covered by scales, long legs, and parts The mouth of female mosquitoes contains a long proboscis and its mouthparts are piercing and absorbent to feed on blood to mature the eggs, while male mosquitoes have mouthparts that are only absorbent to feed on plant juices [2].

The mosquito control program relies heavily and extensively on chemical pesticides, as is known in the field. Integrated pest control (IPM) has many benefits, including that mosquitoes are unable to develop resistance to them, unlike chemical pesticides, and it also contributes to combating all immature stages of mosquitoes [3].

Control using chemical pesticides has a rapid and significant effect on insects, but they cause great damage to humans, animals, plants, soil, and the environment. Chemical pesticides affect targeted and non-targeted insects, and their cost is high, in addition to their persistence in animal and plant tissues, which leads to the emergence of resistance in vectors [4]. The insecticide (Diphenyl-Dichloro-Trichloroethane) DDT

was among the first pesticides used to control arthropods that transmit diseases. It was originally sprayed to combat malaria and typhus during World War II , With the end of the war, DDT became used to control mosquitoes that transmit malaria after it was proven Its effectiveness in Europe. Through the application of DDT, malaria infection rates decreased significantly throughout the world. In 1947, the first resistance to DDT appeared in Anopheles taeniorhynchus mosquitoes. *Culex* mosquitoes in Baghdad became resistant and tolerant to high concentrations of DDT, despite widespread resistance, For both organophosphorus pesticides and brothroids, large numbers of their pesticides are still used to control mosquitoes, largely because there are very few effective alternatives [5].

They are among the most important types of insect control because they quickly kill insects, are easy to use, and give quick results, Chemical pesticides have been used to completely eliminate insects of all kinds. The disadvantages of this control include the occurrence of environmental disturbances, as well as the deposition of chemical components in food chains, the emergence of insects that have resistance to the pesticide, and the indistinguishability of toxic and dangerous chemical pesticides between beneficial insects, as well as against predators and natural enemies of the targeted insect, as well as those with it. A toxic effect on humans, animals, plants, soil and air, which leads to an imbalance in environmental systems and the economic and expensive cost of the pesticide.

Nishan 20sc is a non-systemic pesticide used to combat all motile and immobile insect stages. The pesticide category works to eliminate a wide spectrum of insects, especially some Diptera families. Its toxicity is by contact. The molecular formula of the pesticide Nishan is C12H4CL2F6N4, Nishan 20 Sc can be sprayed comprehensively and has the ability to be mixed with other pesticides except alkaline ones.

Biopesticide: Spinosad is one of the pesticides that has been recently used in pest control and is a natural metabolic product produced by Actinomycetes bacteria, For the spinosa species, Saccharopolyspor Spinosad is a mixture of two types of metabolites, Spinosy A and Spinosyn B, which are deadly infectious toxins when taken orally, as it has a direct effect on the nervous system of the insect, as it works in binding to the Nicotinic Acetyl cline receptor of the insect and thus causes involuntary movement of the body's muscles that It results in tremors and paralysis of the insect's body, all chemical pesticides, regardless of their method of action, will lead to the emergence of resistance in the target species, and thus the necessity of finding new pesticides to replace them, In addition to that, the unintended harm to non-target species that results from the application of pesticides determines their benefit [6].

Aim of the Study:

Testing the effectiveness of the chemical pesticide Nishan 20sc , the biocide Spinosad on the larvae and pupae of *Culex theileri theobald* mosquitoes.

Materials and Methods:

Areas of Salah al-Din Governorate/ Samarra were chosen to collect the larvae and pupae of the *Culex* ***theiler*** *theobald* mosquito, especially the areas where there are many ponds and swamps in which mosquitoes breed.

The larvae and pupae were collected during the months of November and December and in separate areas of Samarra, which is the Qasr al-Ashiq area, the southeastern coast of the city. Al-Qalaa, Al-Abbasiya area, Al-Qatul area pool.

The biopesticide Spinosad was obtained from in Baghdad on the recommendation, The chemical pesticide Nishan 20sc was obtained from a pesticide seller in the city of Samarra.

Laboratory breeding of mosquitoes *Culex theiler theobald* :

A new strain was used in the study in Samarra, which was recorded for the first time in the city of Samarra by the researcher *Culex theileri theobald*, belonging to the genus *Culex* , It was obtained in different areas of the Samarra district, which are the Qasr al-Ashiq area, the southeastern coast of the city of the Citadel, the Abbasiya area, and the pool of the Qatul area, in which it is found. Ponds, swamps, and stagnant water, where Culex mosquitoes abound due to the presence of organic materials, vegetation, wild animals, and birds. Larvae and pupae of *Culex* mosquitoes were collected during the months of November and December, and samples of larvae and pupae of *Culex theileri theobald* mosquitoes were classified at the University of Baghdad Research Center and Natural History Museum in their book No. 3/ 7/1287 on 12/12/2023 and the diagnosis was made by.

A medium-handled scoop was used for the purpose of collecting mosquito larvae and pupae, then they were placed in plastic containers prepared for this purpose with a capacity of 2 liters and containing a liter of water similar to water in the wild environment and free of chlorine. It was transferred to the incubator under laboratory conditions at a temperature of 2 ± 26 °C and a relative humidity of 5. ± 65% and a lighting period of 10-14 hours.

The experiments were conducted in sterile plastic petri dishes, and tap water was placed in it exposed to the sun for three days to get rid of the chlorine present in the water.

The experiments were conducted with three replicates for each concentration, in addition to using a control factor for each of the three concentrations and using 10 larvae as well as 10 pupa, the concentrations of the biocide were (0.125, 0.250, 0.5) Spinosad ml/L, the concentrations of the Nishan pesticide were (0. 25, 0.5, 1) ml/L for each replicate. The test was done after 24, 48, and 72 hours for the chemical pesticide and the biocide known as Spinosad. When the dead larvae and pupae were counted, a medium-sized scoop was used to collect mosquito larvae and pupae, then they were placed in plastic containers prepared for this purpose, with a capacity of 2 liters and containing a liter of water similar to water in the wild environment and free of chlorine. They were transferred to the incubator under laboratory conditions at 100 °C. The temperature was 26±2°C, the relative humidity was 65±5%, and the lighting period was 10-12 hours. After that, they were placed in the rearing cage, whose dimensions were length 85 cm x width 50 cm x height 85 cm, which was designed by the researcher. The larvae were fed by adding ground and prepared mouse diet. Of wheat, yellow corn, and protein (soybeans) in a ratio of 1:1:1, 2 grams per tank [7].

Biscuits were also used to feed the larvae, and the water was replaced every 7 days to avoid rotting. Females need proteins and blood for the purpose of fertilization and egg production, so they must be fed. On a blood meal by placing the feathered pigeons from the chest and back areas in the breeding cage for the purpose of absorbing the blood. After that, plastic boxes were placed inside the breeding cage containing water to lay the eggs. The eggs are then transferred to pots with dimensions of 25 x 25 cm to raise the larvae.

Figure(1) Mosom breeding cage is designed by the researcher

Prepare concentrations of Nishan 20 Sc pesticide to eliminate *Culex theileri theobald* larvae and pupae

Different concentrations of Nishan pesticide were prepared, namely, (1,0.50,0.25) ml/liter, according to the recommendations of the pesticide manufacturer, and 1000 ml of distilled water was added to each concentration. As for the control, only distilled water was used without adding the pesticide, and three concentrations were used for each concentration.

Replicates of mosquito larvae were obtained after 24, 48 and 72 hours. The results were recorded and it was found that the highest percentage of killing larvae was after 72 hours at a concentration of 1 ml/l. The same previous steps were performed on the Virgin Mary. Trade name: Nishan 20 sc. Store at room temperature.

Active ingredient: Aziloctin

Dosage recommended by the manufacturer: 1 ml/l

Producing company: HOUSE AGRICULTVRE

Production date: 03/2022

Effective date: 03/2025

Figure (2) Explains the chemical pesticide Nishan 20 SC

Preparing spinosad pesticide concentrations to eliminate *Culex theileri theobald* larvae and pupae

Different concentrations of spinosad pesticide were prepared, namely (0.125, 0.250, 0.5) ml/liter, and 1000 ml of distilled water was added to each concentration. As for the control, only distilled water was used without adding the pesticide for a period of (24, 48, 72) hours.

Trade name: Mozkill

Active ingredient: spinosad 12%

Dosage recommended by the manufacturer: 1 ml/L

the Producing company:

Production date: 2023/6

Effective date: 6/2025

For each concentration, three replicates of mosquito larvae were used after 24, 48 and 72 hours. The results were recorded and it was found that the highest percentage of killing larvae was after 72 hours at a concentration of 0.5 ml/l The same previous steps were performed on the pupal stage.

Statistical Analysis:

The results analyzed statistically by applying the statistical program (MINITAB VER.17) according to the Anova analysis test (Anova), the mathematical averages were

compared according to the Duncuns Multiple Range test and at a possibility of $0.05 \geq$ p [8].

Results:

Three Chemical pesticide concentrations were used in this experiment Nishan 20 SC $(0.250, 0.500, 1.0)$ milligrams / L by each concentration of three repeat, for a period of $(24, 48, 72)$ hours, the control coefficient of the experiment was used in the distilled water to know the killing rate And put in each bis 10 larva of larvae and pupal of 10 mosquitoes. And one put one tired of each concentration in all the repeated, knowing that the concentration recommended by the company was 1 ml of the pesticide, but it was very toxic, as the larvae were eliminated by 100% in less than 24 hours that led to the use of the above -mentioned concentrations.

The results of **Table** (1) showed the effect of the different concentrations of Nishan 20 SC in the destruction of larvae with mosquito Concentration of 1.0 ml pesticide / L after 72 hours of transaction, while it was the lowest killing rate of 30.0 % at the concentration of 0. 25 ml / L after 24 hours of treatment, while the average killing rate showed the effect of the concentrations that the highest killing rate was when concentrated 1.0 ml / L. It was killed after 24 hours 34.2 %.

The results of the current studies have interviewed with what it reached [9], as she showed through her study that there are moral differences in the virgin killing rates for home flies 24 and 48 hours after her treatment of Mid Al -Mallathion .

The results of the current study match with what was reached [10] in his study in which the diclorfos was used in the anti -household adults, as the pesticide was given the highest killing rate of 46.77 - 50.55% .

The results of the current study agreed with the results of the study [11]. conducted in Sudan to know the sensitivity of the phlebotomus papatasi insect that was collected from three regions of Sudan for many pesticides such as (Permethrin, DDT, Malathion and Proboxur Provoxur. Which showed the inability of the insect to resist the toxic influence of the triumphic pesticide in two regions, and this insect showed its resistance to the pesticide in the last or third region .

The results of the current study agreed with the findings of the [12] when using the diclorovus pesticide in the fight against the mosquitoes that the highest killing of the pesticide in the larvae life is 100 % in the PPM100 concentration and the lowest killing rate of 66. 16 % in the PPM10 concentration.

Table (1) The effect of Nishan's pesticide on larvae *culex* mosquito

Concentration ml / L	24 Hours	48 Hours	72 Hours	Concentration Average
0.25	3.00 g	5.33 e	7.67 c	5.33 C
0.50	4.33 f	6.33 d	8.67 b	6.44 B
1.0	6.33 d	8.67 b	10.00 a	8.33 A
Control	0 h	0 h	0 h	0.00 D
Time average	3.42 c	5.08 b	6.58 a	

*Similar lowercase letters horizontally mean there is no statistical difference between them.

*Capital letters that are vertically similar mean there is no statistical difference between them.

When increased the recesses used and this is due to the NISHAN 20 SC, the toxic effect increases with increased concentrations and exposure duration, and that this toxic effect inhibits the cholel cholin ethrase in the nervous system of the insect and thus leads to an increase in the secretion of the Astyle Colin that has a role in transferring the instrument ,the nervous so that this substance accumulates at the end of the nerves, and paralysis of the insect occurs and then its death.

The results of the Table (2) showed the effect of the different concentrations of Nishan 20 SC in the death of pupal in mosquito Concentration of 1.0 ml pesticide / L after 72 hours of treatment, while the lowest killing rate was 13.3 % at the concentration of 0. 25 ml / L after 24 hours of treatment, while the average killing rate showed the effect of the concentrations that the highest killing rate was when concentrated 1.0 ml / L. It was killed 24 hours later 22.5.%.

The results of the current studies were interviewed with the findings of [9], as she showed, through her study, that there are moral differences in the pupal killing rates for home flies 24 and 48 hours of treatment with Mid Al -Mallathion.

The results of the current study match with what was reached [10]. in his study in which the diclorfos was used in the anti -household anti On the watermelon fly B. Diversa, where it was noticed that the killing rate increases by increasing the period of exposure to the toxic substance and the killing rate reached 50 % when the period increases to 24 hours.

Table (2) The effect of Nishan's pesticide on pupal *culex* mosquito

Concentration ml / L	Hours 24	Hours 48	Hours 72	Concentration Average
0.25	1.33 h	3.33 f	6.00 d	3.56 C
0.50	2.33 g	5.00 e	7.33 c	4.89 B
1.00	5.33 de	8.33 b	10.00 a	7.89 A
Control	0	0	0	0.00
Time average	2.25 c	4.17 b	5.83 a	

*Similar lowercase letters horizontally mean there is no statistical difference between them.

*Capital letters that are vertically similar mean there is no statistical difference between them.

When increased the recesses used and this is due to the NISHAN 20 SC, the toxic effect increases with increased concentrations and exposure duration, and that this toxic effect inhibits the cholel cholin ethrase in the nervous system of the insect and thus leads to an increase in the secretion of the Astyle colin that has a role in transferring the instrument The nervous so that this substance accumulates at the end of the nerves, and paralysis of the insect occurs and then its death.

Discussions:

1- When the concentrations used increase, this is due to the toxic effect that Nishan 20 Sc pesticide has, which increases with increasing concentrations and duration of exposure. This toxic effect inhibits the enzyme acetyl cholin esterase in the nervous system of the insect and thus leads to an increase in the secretion of acetylcholine, which has a role in transmitting instructions. Nerve, such that this substance accumulates at the end of the nerves, causing paralysis and then death of the insect.

2- This pesticide works to affect mosquitoes as a result of the binding of the compounds of this pesticide, Spinosyn A and Spinosyn D, to the nerve receptors of the nervous system, thus inhibiting the enzyme Acetylcholin esterase, which decomposes the substance acetylcholin that transmits nerve impulses, thus preventing its connection with nerve connections, leading to the occurrence of involuntary movements that result in body tremors and paralysis. And then death,

References:

1-WHO, 2019. World Health Organization, " farme work for the implementation of the global vector control response in the WHO African region ", 2019.

2 - Areej Emhamed Shenebish, **Enas** Saleh Al-Mayhoub, & **Walid** Khalifa Al-Saadawi. **(2021). A** taxonomic study of some types of mosquitoes found inside homes in the Sabratha region, northwestern Libya. Scientific Journal of Applied Sciences of Sabratha University, 112-1223.

3 - Becker, N., D. Petric, C. Boase, J. Lane, M. Zgomba, C. Dahl, and AKaiser (2010)Mosquitoes and Their Control. Springer, Berlin, Germany.

4 - **Rajesh, K., Dhanasekaran, D., & Tyagi, B. K.** (2015). Mosquito survey and larvicidal activity of actinobacterial isolates against Culex larvae (Diptera: Culicidae). *Journal of the Saudi Society of Agricultural Sciences*, *14* (2), 116-122.

5 - Jones, P. A. (2012). Functions of DNA methylation: islands, start sites, gene bodies and beyond. Nature reviews genetics, 13(7), 484-492.

6 - Copping, L. G., & Menn, J. J. (2000). Biopesticides: a review of their action, applications and efficacy. Pest Management S*cience: Formerly Pesticide Science,* 56(8), 651-676.

7 - Soni, N .E.; and **Prakson,** S. B. **(2012).** Larvicidal effect of *Verticillium lecanii* metabolites on *Culex quinquefasciatus* and *Aedes aegypti* larvae Asian pacific Journal of Tropical Disease , 2(3)220-224.

8- **Reddy**, S. J. (2015). Silver Nanoparticles - Synthesis, Applications an Toxic Effects on Humans: A Review. *International Journal of Bioassays* 4(11) Pp 4563-4573

9- Narrator, Khashia Mahmoud and Abdel Aziz Muhammad Khalaf Allah **(1980).** Design and analysis of agricultural experiments, Dar Al-Kutub Foundation for Printing and Publishing, Ministry of Higher Education and Scientific Research, University of Mosul.

10- Jalil, Sarah Qais Alwan (2021). The effect of colossal plant extract and some biological and chemical pesticides in combating the house fly (Musca domestica L. (Diptera:Muscidae), Master's thesis, College of Science - Tikrit University

11- Al-Mashhadani Omar Hatem Muhammad**, (2011),** an environmental and biological study of the cotton white fly on the saplings of vegetable crops in Nineveh Governorate, Master's thesis, College of Agriculture and Forestry, University of Mosul, 105 pages.

12 - **Hassan**, M.M. ;Widaa, S.O. ;Osman, O.M. ;Numiary, M.S.M. ;Ibrahim, M.A.; and Abushama, H.M.(**2012**).Insecticide resistance in the sand fly , *phlebotomus papatasi* from Khartoum state , Sudan . J. par. Vec. Vol.5(46).10 pages

13 - **Al-Douri,** Istabraq Mahmoud Mahdi **(2014).** Study of the effect of some plant extracts and the Beauveria bassiana fungus on the life expectancy of Culex pipiens pipiens L. mosquitoes (Diptera: Culicidae). Master's thesis, College of Science, Tikrit University, Iraq.

اختبار فعالية المبيد الكيميائي Nishan 20sc والمبيد الحيوي Spinosad على يرقات وعذارى بعوض *Culex theileri theobald* التابعة لجنس ***Culex*** (Diptera: Culicidea) في سامراء

[1,2,3]كلية التربية , قسم علوم الحياة – جامعة سامراء

مصطفى عبدالخالق حمد[*,1]

eduhm230006@uosamarra.edu.iq

هشام ناجي حميد[2]

Hisham.n370@uosamarra.edu.iq

حارث احمد مصطفى[3]

harith.a.m@uosamarra.edu.iq

المستخلص:

أجريت الدراسة في قسم علوم الحياة – كلية التربية – جامعة سامراء التي تهدف الى مكافحة يرقات وعذارى البعوض بأستعمال المبيد الكيميائي Nishan 20 Sc ومعرفة نسبة تأثيره على يرقات وعذارى بعوض *Culex thieleri* مع استعمال المبيد الحيوي المعرف باسم Spinosad ومعرفة الاكفأ بينهما في القضاء على

يرقات وعذارى البعوض وخاصة جنس *Culex* وتم استعمال ثلاث تراكيز للمبيد الكيميائي (0.25, 0.5 ,1) مل / لتر, تأثير التراكيز المختلفة من مبيد Nishan 20 Sc في هلاك يرقات *بعوض Culex* الى وجود فروق معنوية في نسب القتل للتداخل بين التراكيز ومدة التعريض اذ كانت اعلى نسبة قتل يرقات بعوضة *Culex* 100 % عند تركيز 1.0 مل مبيد/ لتر بعد مرور 72 ساعة من المعاملة , بينما كانت اقل نسبة قتل 30.0 % عند تركيز 0. 25 مل مبيد / لتر بعد مرور 24 ساعة من المعاملة, استعمل في معامل السيطرة فقط الماء المقطر وبفترة زمنية (24, 48 ,72) ساعة لكل تركي, تم استعمال ثلاث تراكيز للمبيد الحيوي المعرف ب Spinosad 12% (0.25,0.5 , 0.125) مل / لتر, ولكل مبيد Spinnosad في هلاك يرقات بعوض *Culex* الى وجود فروق معنوية في نسب القتل للتداخل بين التراكيز ومدة التعريض اذ كانت اعلى نسبة قتل يرقات بعوضة *Culex* 100 % عند تركيز 500 مل مبيد/ لتر بعد مرور 72 ساعة من المعاملة , بينما كانت اقل نسبة قتل 23.3% عند تركيز 0.125 مل مبيد / لتر بعد مرور 24 ساعة من المعاملة ,استعمل في معامل السيطرة فقط الماء المقطر وبفترة زمنية (24, 48 , 72) ساعة لكل تركيز تم استعمال ثلاث مكررات لكلا من اليرقة والعذراء ووضع في كل مكرر 10 يرقات وكذلك وضع في كل مكرر 10 عذارى لكل مكرر من التجربة واعطت نتائج كلا المبيدان نتائج قتل عالية عند تركيز 1 مل / لتر بعد مرور 72 ساعة بالنسبة للمبيد الكيميائي Nishan 20 Sc اما المبيد الحيوي Spinosad كان اكثر فعالية عند تركيز 0.5 مل / لتر بعد مرور 72 ساعة.

اكدت نتائج الدراسة ان هناك علاقة طردية بين زيادة التركيز والفترة الزمنية للتعريض ونسب القتل المئوية وكانت ليرقات للبعوض اكثر حساسية من العذارى في تأثرها بجميع المعاملات قيد الدراسة .

الكلمات المفتاحيه:

DDT, Nishan, IPM , Spinosad , *Culex*

Revolutionizing Image Classification with MopileNetV3, PCA, and Bayesian-Optimized Algorithms

[1]Alula Jamal Mawlood ,[2]Muhaned Mahdi Thiab2

[1 2]College of computer science and mathematics, Tikrit University, Tikrit, Iraq

[1] alulajamal1997@gmail.com, [2] muhanedthiab @tu.edu.iq

Revolutionizing Image Classification with MopileNetV3, PCA, and Bayesian-Optimized Algorithms

[1]Alula Jamal Mawlood ,[2]Muhaned Mahdi Thiab2

[12]College of computer science and mathematics, Tikrit University, Tikrit, Iraq

[1] alulajamal1997@gmail.com, [2] muhanedthiab @tu.edu.iq

Abstract.

The field of image classification has made great strides with Machine Learning (ML) and Deep Learning (DL), but still encounters difficulties in attaining high efficiency and accuracy. MobileNetV3 architecture, which is famous for its performance and dept, holds a chance for betterment when utilized together with advanced algorithms. Though MobileNetV3 has been successful, there exists an opportunity to use techniques of dimensionality reduction as well as optimization to improve its performance. To this point, studies have mainly concentrated on using MobileNetV3 for image classification. However, these methods mentioned above have not been thoroughly examined in combination. This research seeks to create a new image classification model through integrating MobileNetV3 with Principal Component Analysis (PCA) and Bayesian-optimized algorithms. The aims are diminishing computational complexity, enhancing classification accuracy and optimizing model parameters. The study concentrates on image classification tasks with publicly accessible datasets. It investigates the integration regarding DL together with statistic as well as optimization methods to handle the existing limitations. The research uses a two-step method. First, it employs MobileNetV3 for extracting features and after that reduces its dimensions using PCA. Secondly, the research applies Bayesian Optimization (BO) for fine-tuning model parameters. The suggested approaches are assessed with the use of standard metrics and in comparison, with baseline models.

The integration regarding MobileNetV3 with BO and PCA showed an important advance in classification accuracy. The model which has been optimized through Bayesian method performed better than the baseline MobileNetV3; it achieved a classification accuracy of 96.17%, whereas the model without any optimization reached only 66.57% accuracy rate. Moreover, for the optimized model but not using (BO), we got recall 66.59%, precision 66.39%, and F1 score 65.60%. For the same one, but now with (BO), we saw results like this: precision at 98.88%, recall 98.48%, and F1score is 98.67% - both these measures improved significantly. The computational cost was brought down by using dimensionality reduction with PCA. The research brings an important contribution to image classification area because it suggests a robust model that merges DL with advanced statistical as well as optimization methods. The outcomes emphasize how much promise this combined technique holds for improving tasks related to classifying images.

.

Keywords: Deep Learning, Machine learning, Principal Component Analysis (PCA), MobileNetV3, eXtreme Gradient Boosting (XGBOOST).

1. Introduction

The teeth and mouth are an integral part of the body, supporting and enabling essential human functions, and the mouth is a fundamental feature of personal identity. Oral health is subjective and dynamic, enabling eating, speaking, smiling, and socializing, without discomfort, pain, or embarrassment. Good oral health reflects an individual's ability to adapt to physiological changes throughout life and to maintain their own teeth and mouth through independent self-care **[1]**. Oral diseases and disorders, although largely preventable, are ubiquitous and affect the vast majority of the world's population with varying degrees of severity. The available mechanisms of oral disease prevention are effective at the individual level and have also had success at the population level. However, although the severity of oral diseases has been reduced, they are still highly prevalent and there is scope for development of new approaches to prevention that are less reliant on behavioral change at the individual level **[2]**. Oral disease is a pathological phenomenon that occurs in the oral cavity under the conditions of damage by external physical and chemical factors, invasion by pathogens, and systemic diseases, characterized by high incidence **[3]**.

Artificial intelligence (AI) is being utilized to produce intelligent robots which could do various tasks that would normally require human brains. Artificial intelligence is vital to the development of new technologies. AI is a general phrase for all the various technologies required to give machines intelligence comparable to that of humans. Machine learning (ML) is an algorithm-based self-learning system that falls under the umbrella of artificial intelligence (AI). A subset of ML called Deep Learning (DL) is typically applied to large databases **[4]**. account everything mentioned above, dental diseases place a financial strain on society because they affect treatment costs directly, indirectly, and intangibly through lost productivity, speaking, eating, and smiling difficulties, as well as behaviors which could interfere with family and social activities **[5]**.

Previous studies have addressed identify teeth in dental periapical films **[6]**, teeth recognition model **[7]**, dental restorations in the panoramic radiographs **[8]**, automatic periodontal disease detection in the orthodontic patients **[9]**, staging periodontitis on the dental panoramic radiographs **[10]**, recognize inflamed disease sites in intraoral photos **[11]**, identify white spot lesions in dental photos **[12]**, the dental periapical radiographs **[13]**, to categorize teeth as caries- or non-caries, dental visual images and deep neural network (CNN) have been utilized **[14]**, identification and categorization of the common dental problems in panoramic X-ray images **[15] [16]**, six dental diseases are recognizing tooth periapical disease, wear, periodontitis, tooth decay, missing teeth, and impacted teeth **[17]**, Investigated using DL object detection models in place of X-rays for detecting dental cavities **[18]**, DL-based oral disease diagnosis. Using InceptionResNet-V2 **[19]**, classifying teeth with periodontal diseases using frontal optical color images **[20]**, and training a CNN-based model for automatic classification of oral lesion images **[21]**.The deep feed forward ANN, which is widely utilized for visual image processing, is adapted into CNN. The network can encrypt image properties thanks to its convolution layer and pooling layer**[22]** With the use of the ML method known as transfer learning (TL), a pre-trained model that is built on a large data-set is utilized as a starting point for tackling a

new assignment. Instead of starting from scratch and training a new model on a limited dataset, TL entails optimizing a pre-trained model through utilizing previously learnt features and tailoring them to the current task. In DL, where training large models on vast data-sets could be expensive and time-consuming, TL is especially useful**[23]**. Convolutional neural network architectures have been proposed recently to tackle many convolutional different problems and improve their performance in terms of speed and size. Efficient neural networks implementing the depth wise convolution structure such as Mobile Nets **[24]** The architecture of MobileNetV3 is composed of a series of bottleneck blocks. Some of the bottleneck blocks include residual structure **[25]**. Is a recently released machine learning algorithm that has shown exceptional capability for modeling complex systems and is the most superior machine learning algorithm in terms of prediction accuracy and interpretability and classification versatility. XGBoost is an enhanced distributed scaling enhancement library that is built to be extremely powerful, adaptable, and portable. It uses augmented scaling to incorporate machine learning algorithms. It is a parallel tree boost that addresses a variety of data science problems quickly and accurately .The gradient boosting algorithm known as XGBOOST (Extreme Gradient Boosting) was enhanced in terms of flexibility, scalability, and efficiency**[26]**. In our research, we will propose a new model using two methods: the first method is to reduce dimensionality with PCA method depending on transfer learning (MopileNetV3), after that we enhance best decision through applying ensemble decision making (XGBOOST) when creating the model. Secondly, we can apply the BO on ensemble methods. This approach helps us optimize and select the best decision to create our optimize model.

Moreover, we use transfer learning to extract features by MopileNetV3 then dimensionality reduce by PCA technique. According to these methods we will classify diseases of the mouth and oral, including: Canker sores (CaS), Gangivostomatitis (Gum), Oral lichen planus (OLP), Cold sores (CoS), Mouth cancer (MC), Oral thrush (OT) and Oral cancer (OC). In addition, we will enhance and improve the Accuracy and Consistency, Frequency of Diagnosis, Patient Comfort, Scalability and Data Handling.

.

2. Methods

The research methodology can be defined as a systematic approach utilized for the purpose of conducting research as well as gathering relevant data for answering research questions or investigating a specific problem. It outlines the procedures, methods, along with the tools that researchers apply for analyzing, designing, executing, and planning their studies. A well-defined research methodology is important to ensure the reliability, validity, and credibility regarding the research findings **[27]**.The method includes four steps; the first step is related work this include: the Oral and Mouth Disease Diagnosis (OMDD) taxonomy to Study the limitation in these researches and explain the gap of the MODD study as definition in the introduction. The second one is Dataset collection that includes: find the dataset from google dataset engine, dataset description that include 7 disease based on 5128 images, and selecting environment using Anaconda. Third step is Preparation dataset include: data augmentation, label encoding, feature extraction, and

dimensionality reduction. Fourth step is evaluation of optimum model, it include: initiation parameters of XGBOOST according to using Ensemble learning (Boosting), proposed model (with and without Bayesian optimization (BO)) figure (1), and in finally evaluation the model by the confusion matrix.

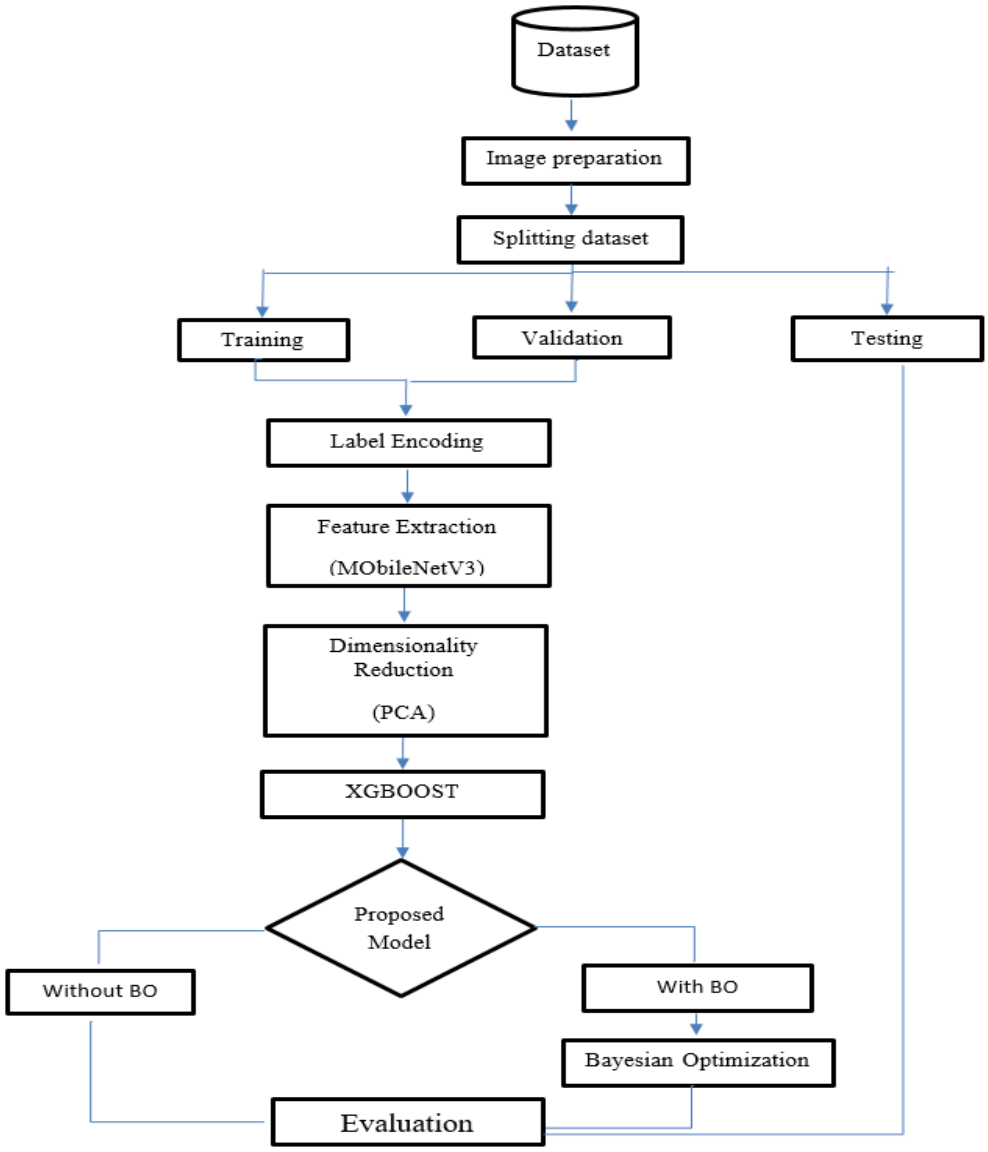

Figure 1: Research methodology step

2.1. Dataset Description

The "Mouth and Oral Disease (MOD) dataset," which is publicly available, was made available by "dental clinics in Okara, Punjab, Pakistan, and other locations (dental websites, etc.)" Table 1: MODD dataset description lists the 5128 samples which comprise the raw Mouth and Oral Disease Diagnosis

(MODD) data-set. The total number of labels and samples for each category is also included in the table. The class labels in this collection reflect seven illnesses of the mouth and oral cavity: canker sores, cold sores, Gangivostomatitis, mouth cancer, oral thrush, oral cancer, and oral lichen planus. No one had disclosed their gender, height, or age during, prior to, or following the photo shoot. The MODD dataset was labeled with the assistance of skilled pretensioners. Figure (2) is show one of image to each class in dataset.

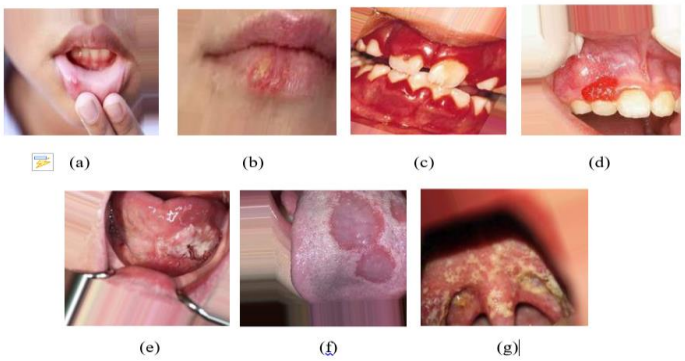

Figure 2:(a) CaS, (b) CoS, (c) Gum, (d) MC, (e) OC, (f) OLP and (g) OT MODD data-set classes

Table 1: MODD dataset description

Class labels	**Images**
Canker Sores (CaS)	729
Gangivostomatitis (Gum)	749
Cold Sores (CoS)	733
Oral Cancer (OC)	740
Mouth Cancer (MC)	720
Oral Thrush (OT)	723
Oral lichen planus (OLP)	734
Total Samples (TS)	5128

In this paper, the data set divided into three sections: training, testing and validation, each stage of which is divided into seven sections for seven diseases of the mouth and gums, which are of the multi-class type. It is a balanced data set, each of which has dimensions of 224*224 pixels. Table 2: MODD dataset (Training, Testing, and Validation) provides a description of aforementioned dataset

Table 2: MODD dataset (Training, Testing, and Validation)

Dataset	No. of samples	**No. of MODD image**

		Training	Testing	Validation
MODD dataset	5128	3091	1017	1020

2.2. Exploratory Data Analysis and Visualize

To identify the relevant information, we will create some statistics and visualize this data. The data sets were subjected to a range of exploratory data analysis techniques, and the resulting data sets were displayed to offer an effective understanding of MODD. Visualization facilitates comprehension of MODD instances. From the representation EDA, it has been shown that the dataset is divided into three parts: (60%) for training with 441 image in CaS, 445 image in CoS, 455 image in Gum, 432 image in MC, 452 image in OC, 434 in OLP and 432 image in OT and (20%) for the both testing and validation with 144 image in each of CaS, CoS, MC, and OC, 147 image in Gum, 150 image in OLP for each testing and validation and 144 image in OT for testing, 147 image in OT for validation

In this result, the number of images for each disease from each stage and the class distribution chart appear as shown in figure (3). However, due to space constraints, displaying them is not possible at this time.

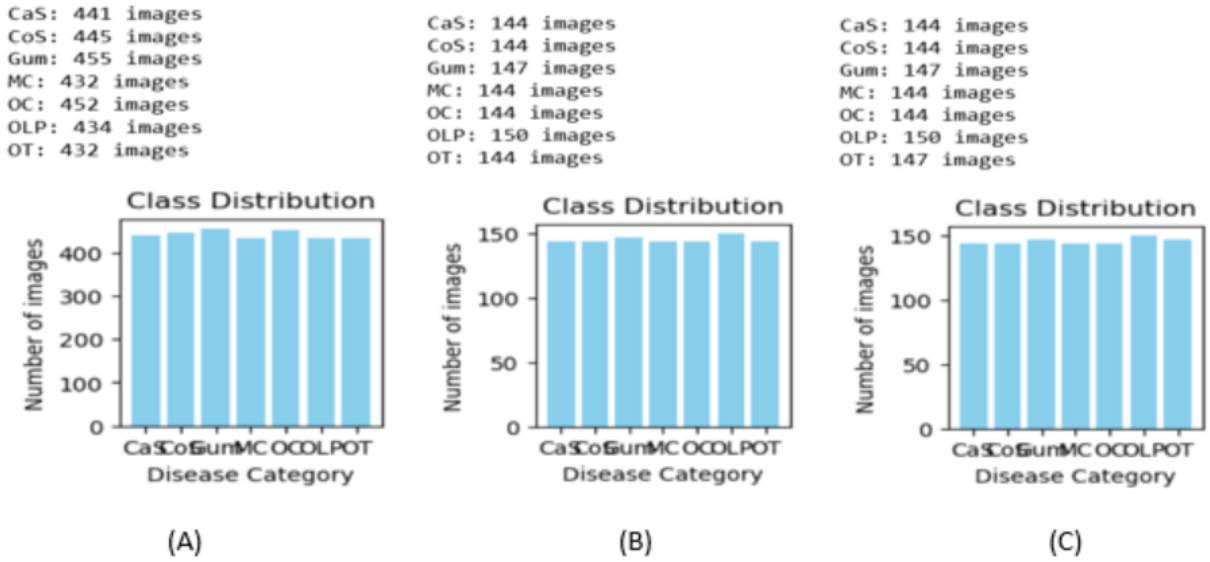

Figure 3: The result of EDA for (A) training, (B) testing, and(C) validation

2.3. Statistics for Testing, Training, and Validation Dataset

These statistics help in understanding the distribution of brightness levels, which is important for preprocessing and normalization tasks. The histogram also makes clear how often different values occur, giving a better idea about the distribution of data sets. Figure (4) and Figure (5) are showing what we got from Statistics for (A) Training (B) Testing and (C) Validation Datasets.

A

```
Statistics for Training Data:
Mean Brightness: 133.5062915838094
Median Brightness: 131.6057676977041
Mode Brightness: 137.87350526147958
```

B

```
Statistics for Testing Data:
Mean Brightness: 133.73237043365467
Median Brightness: 131.32495615433675
Mode Brightness: 79.52861926020408
```

C

```
Statistics for Validation Data:
Mean Brightness: 133.27110676301768
Median Brightness: 136.48084741709184
Mode Brightness: 126.61152742346938
```

Figure 4: (A) Statistics for Training Data, (B) Statistics for Testing Data (C) Statistics for Validation Data

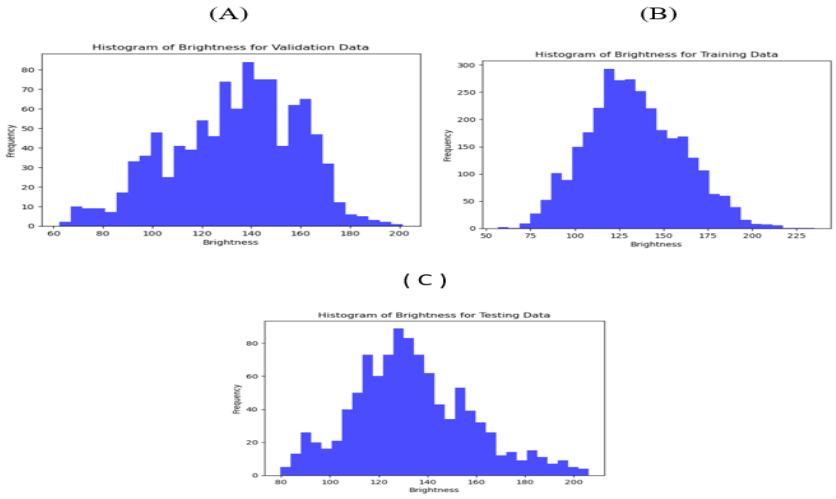

Figure 5: Result for Histogram of Brightness for (A) training, (b) testing, and (C) validation Data

2.4 Training, Testing, and Validation Features Sample (CaS)

These features are crucial for maximizing the model's performance and adjusting its parameters within the validation set. They also form a basis to gauge how well it does initially during training and tweak any adjustable settings accordingly. Hence, the feature samples from "Training Features Sample", "Testing Features Sample" and "Validation Features Sample" clarify diverse characteristics used in every dataset – this helps understand data attributes across model's stages of training, testing as well validating. The disease CaS was taken for example as can be seen in table 3**:** the Result of Training, Testing, and Validation Features Sample for the disease CaS.

Table 3: The Result of Training, Testing, and Validation Features Sample for the disease CaS

Feature sample	No.	Brightness	Contrast	Saturation	Sharpness	Hue	Category
Training	0	192.167809	33.964650	122.397082	-0.168058	6.136001	CaS
	1	121.260902	33.042695	116.819356	-0.035316	6.845006	CaS
	2	137.877372	36.617221	110.052475	-0.157545	6.220484	CaS
	3	126.517419	31.907667	120.652244	-0.004524	5.919523	CaS
	4	133.027942	36.865754	104.708546	-0.238909	7.319595	CaS

Testing	0	206.221281	44.130182	47.989417	0.013403	88.878129	CaS
	1	200.767478	43.060150	53.977519	0.031140	80.088050	CaS
	2	194.795061	44.738309	59.355210	-0.066755	87.174964	CaS
	3	191.951889	45.691815	61.525949	-0.041912	86.807478	CaS
	4	194.320580	44.574301	63.170898	-0.005680	78.091279	CaS
Validation	0	137.017000	38.721601	144.196688	0.046576	14.822445	CaS
	1	135.622070	27.245461	148.394651	0.042869	15.743343	CaS
	2	132.882912	27.141358	150.421895	-0.068170	14.209283	CaS
	3	133.162887	23.684673	149.537229	-0.036900	14.352021	CaS
	4	131.256059	47.155815	145.045540	0.093650	15.545759	CaS

3.Result and Discussion

After completing the preparation and processing of the images, as well as dividing the dataset, it is now ready for using. Model training was conducted prior to feature extraction due to the nature of the model's properties, with the trainer handling this task. A detailed discussion of the results from each step of preparing the model will follow:

3.1 Label Encoding

In ML, label encoding is a technique used to transform categorical data into numerical data. Since many ML algorithms could just process numerical input, this transformation is crucial. Each separate category in a feature is given a unique integer via the label encoding procedure.

3.2 Dimensionality Reduce Using PCA

Any high-dimensional data analysis could use the preprocessing procedure known as DR before the data is modeled and shown. DR could be performed in two ways. Essential features are chosen from the input data set using feature selection techniques in the first approach. Feature extractions, the second technique, generate new features from the already features in the input dataset. Combining or separating the feature extraction and selection processes enhances the DL model's computed accuracy and precision **[28]**. Principal Component Analysis (PCA) can be defined as a method utilized for dimensionality reduction while preserving as much variance as possible in the dataset.

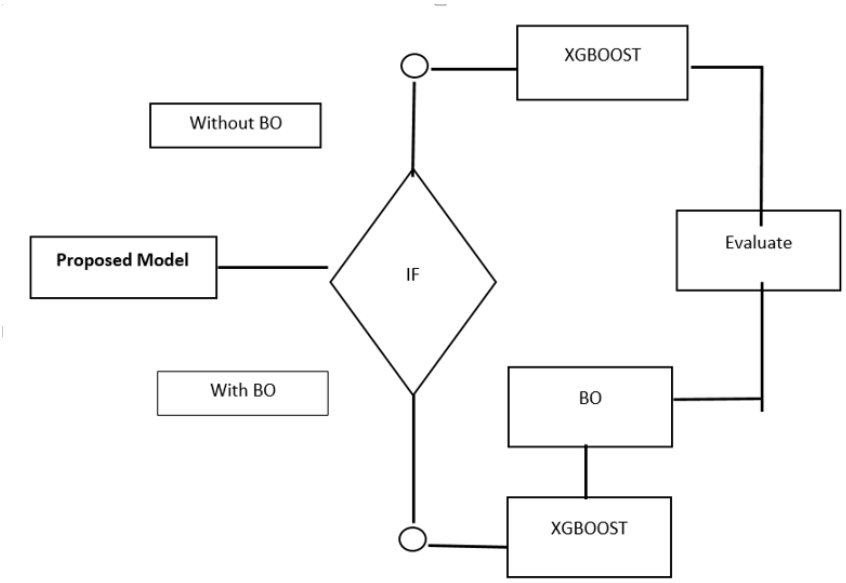

Figure 6: Flowchart of Proposed Model

3.3 MobileNetV3 and XGBOOST without Bayesian Optimization (BO)

Because of its sample efficiency, BO is a widely used paradigm for improving the hyperparameters of ML models [28]. After the features have been extracted, the dimensions have been reduced, and each stage has been reviewed, the space function will be loaded to prepare the model that was trained for the following operations**.** Figure (6) Flowchart of Proposed Model.

Table 3: Confusion Matrix of MobileNetV3 and XGBOOST

		Predicted							
		CaS	CoS	Gum	MC	OC	OLP	OT	Total
Actual	CaS	108	16	1	0	1	10	8	144
	CoS	4	140	0	0	0	0	0	144
	Gum	1	1	136	9	0	0	0	147
	MC	13	0	38	68	8	15	2	144
	OC	11	10	1	6	88	6	22	144
	OLP	5	2	4	10	9	74	46	150
	OT	21	22	2	5	3	28	63	144
Total		163	191	182	98	109	133	141	1017

To calculate the four criteria mathematically:

a) Accuracy:

Accuracy is determined by dividing the total number of predictions by the sum of correct predictions (diagonal elements).

$$accuracy = \frac{\text{sum of diagonal elements (correct predictions)}}{\text{Total number of predictions}}$$

Accuracy=108+140+136+68+88+74+63\108+16+1+1+10+8+4+140+1+1+136+9+13
+38+68+8+15+2+11+10+1+6+88+6+22+5+2+4+10+9+74+46+21+22+2+5+3+28+63

=677\1017≈ 0.6657.

b) Precision:

Precision measures the accuracy of positive predictions for a specific class. Mathematically, for each class i, precision is calculated as:

$$precision_i = \frac{\text{True Positive}_i}{\text{True Positive}_i + \text{false Positive}_i}$$

Precision for each class:

Class1: True Positive1=108, False Positive1=16+1+0+1+10+8=36

$$\frac{108}{108+36} \equiv 0.750$$

Class 2: True Positive2=140, False Positive2=4+1+0+10+2+22=39

$$\frac{140}{140+39} \equiv 0.782$$

Class 3: True Positive3=136, False Positive3=1+0+38+1+4+2=46

$$\frac{136}{136+46} \equiv 0.748$$

Class 4: True Positive4=68, False Positive4=13+38+8+15+5+3=82

$$\frac{68}{68+82} \equiv 0.453$$

Class 5: True Positive5=88, False Positive5=11+10+1+6+6+22=56

$$\frac{88}{88+56} \equiv 0.611$$

Class 6: True Positive6=74, False Positive6=5+2+4+10+9+46=76

$$\frac{74}{74+76} \equiv 0.493$$

Class 7: True Positive7=63, False Positive7=21+22+2+5+3+28=81

$$\frac{63}{63+81} \equiv 0.438$$

$$precision = \frac{\Sigma precision_i}{n} = 0.6639$$

Recall:

Recall for each class i
is determined by dividing the total number of actual instances of that class by the ratio of true positive predictions for that class.

$$Recall_i = \frac{\text{True Positive}_i}{\text{True Positive}_i + false\ Negative_i}$$

Recall for each class:

Class1: False Negative1=4+1+13+11+5+21=55$\rightarrow \frac{108}{108+55} \equiv 0.663$

Class 2: False Negative2= 16+1+0+10=27$\rightarrow \frac{140}{140+27} \equiv 0.839$

Class 3: False Negative3= 1+9=10$\rightarrow \frac{136}{136+10} \equiv 0.932$

Class 4: False Negative4= 13+38+8+15+5=79$\rightarrow \frac{68}{68+79} \equiv 0.462$

Class 5: False Negative5= 11+10+1+6+6=34$\rightarrow \frac{88}{88+34} \equiv 0.721$

Class 6: False Negative6= 5+2+4+10+9+46=76$\rightarrow \frac{74}{74+76} \equiv 0.493$

Class 7: False Negative7= 21+22+2+5+3+28=81$\rightarrow \frac{63}{63+81} \equiv 0.438$

$$Recall = \frac{\Sigma Recall_i}{n} = 0.6659$$

c) F1 Score:

F1 Score for each class i is the harmonic mean of precision and recall for that class.

$$F1\ Score_i = 2 \times \frac{precision_i \times Recall_i}{precision_i + Recall_i}$$

F1 Score for each class:

Class1: $F1$=2× 0.750×0.663\0.750+0.663≈0.704

Class2: $F1$=2× 0.782×0.839\ 0.782+0.839≈0.810

Class3: $F1$=2× 0.748×0.932\ 0.748+0.932≈0.831

Class4: $F1$=2× 0.453×0.462\ 0.453+0.462≈0.457

Class5: $F1$=2× 0.611×0.721\ 0.611+0.721=0.661

Class6: $F1$=2× 0.493×0.493\ 0.493+0.493≈0.493

Class7: $F1=2\times 0.438\times 0.438 \backslash 0.438+0.438=0.438$

$$F1\ score = \frac{\sum F1\ score_i}{n} = 0.656$$

3.4 MobileNetV3 and XGBOOST with Bayesian Optimization (BO)

Table 4: Confusion Matrix of MobileNetV3 and XGBOOST with BO

		Predicted							
		CaS	CoS	Gum	MC	OC	OLP	OT	Total
Actual	CaS	137	0	0	0	1	4	2	144
	CoS	0	144	0	0	0	0	0	144
	Gum	0	0	147	0	0	0	0	147
	MC	0	0	0	139	3	2	0	144
	OC	2	0	1	1	136	1	3	144
	OLP	5	0	1	5	1	137	1	150
	OT	4	0	0	1	1	0	138	144
Total		148	144	149	146	142	144	144	1017

True Positive (TP): Sum of values on the main diagonal (correctly predicted instances).

TP = 137 + 144 + 147 + 139 + 136 + 137 + 138 = 978

False Positives (FP): Sum of values in each column on the diagonal excluding true positives.

- Column sums: 2,0,1,0,1,0,1
- FP for each column (excluding diagonal value):

$$FP = (2 + 5 + 4) = 11$$

False Negatives (FN): Sum of values in each row on the diagonal excluding true positives.

- Row sums: 1,0,0,2,0,3,0
- FN for each row (excluding diagonal value):

$$FN = (1 + 0 + 0 + 5 + 1 + 5 + 1) = 13$$

TN=n-TP-FP-FN →TN=1017-978-11-13=15

a. Accuracy:

$$accuracy = \frac{TP + TN}{\text{Total number of Population}}$$

$$= \frac{978+15}{1017} \approx 0.9617$$

b. Precision:

$$Precision = \frac{TP}{TP + FP}$$
$$= \frac{978}{978+11} \approx 0.9888$$

c. Recall:

$$Recall = \frac{TP}{TP + FN}$$
$$= \frac{978}{978+13} \approx 0.9848$$

d. F1 score:

$$F1\ score = 2 \times \frac{Precision \times Recall}{Precision + Recall}$$
$$= 2 \times \frac{0.9888 \times 0.9848}{0.9888 + 0.9848} \approx 0.9867$$

3.5 Comparison between MobileVetV3 without Optimization and with Optimization

The comparison is quite clear from the results and accuracy rates that have been proven, when the MobileNetV3 model was used and we using feature engineering to prepared the data architecture according to our objectives. We proposed a novel model by using advance methodology from a prepared dataset, scaling (ranged from 0 to 1), rotation (40^0), zooming (0.20), horizontal flipping (true), shear (20^0), label encoding, extracted features using MobileNetV3 then dimensionality reduce using PCA, proposed model using XGBOOST without BO where the result approximate 66.57% as a first method. While the proposed model using XGBOOST with BO the results was 96.17% as a second method table (5) and table (6). Moreover, comparison was made between trained models with receiver operating characteristic curve which shows the difference between the two models. Look at figure (7), which represents the curve of the first method, and the figure (8), which represents the curve of the second method.

Table 5: The accuracy of two method

dataset	**Accuracy of XGBOOST With BO**	**Accuracy of XGBOOST Without BO**
MODD dataset	96.17%	66.57%

Table 6: Recall, Precision and F1 score for two methods

Precision, Recall, and F1 score for two methods			
Model	Precision	Recall	F1 score
XGBOOST with BO	98.88%	98.48%	98.67&

XGBOOST without BO	66.39%	66.59%	65.60%

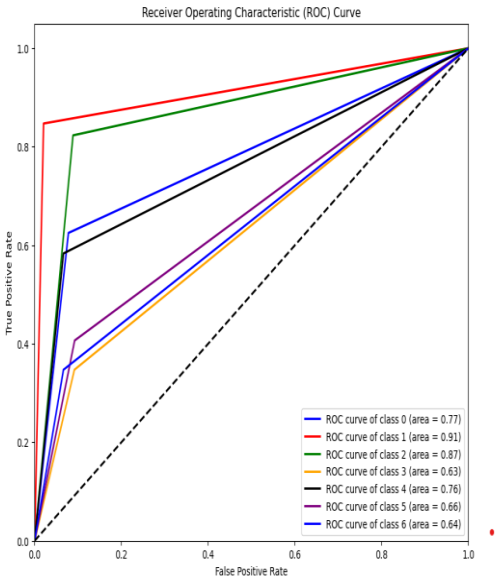

Figure 7: ROC Curve of first approach

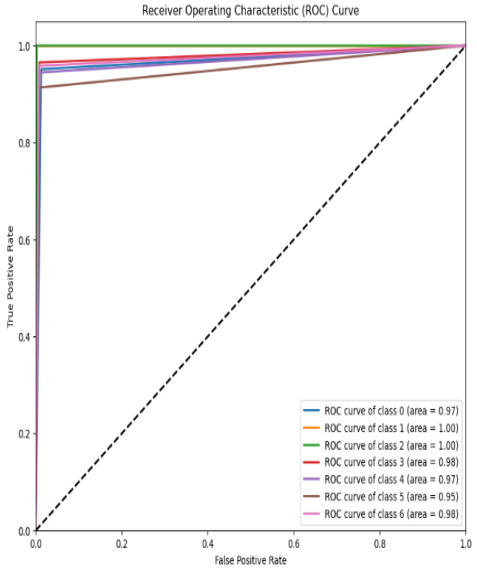

Figure 8: ROC Curve of second approach

4.Conclusion and Future Work

Diagnosing oral diseases was tackled using deep learning methods, comparing CNNs with XGBOOST, both with and without Bayesian optimization. Our study, conducted on the MODD dataset, revealed significant performance differences among the methods tested. Combining MobileNetV3 feature extraction with XGBOOST yielded 66.57% accuracy, while adding Bayesian optimization a
chieved nearly perfect precision at 96.17%. These results underscore the importance of hyper parameter tuning for model performance.

Implications extend to medical image analysis, suggesting that well-configured deep learning models could enhance oral disease diagnoses, potentially improving clinical decisions and patient outcomes. However, limitations include reliance on a single dataset and specific model designs, affecting generalizability and scalability. Future research should explore larger datasets, diverse model architectures, and incorporation of additional data modalities for comprehensive understanding and improved adaptability. Overall, our study lays the groundwork for leveraging advanced ML techniques in healthcare diagnostics and decision support systems

References

1. Peres MA, Macpherson LMD, Weyant RJ, Daly B, Venturelli R, Mathur MR, et al. Oral diseases: a global public health challenge. The Lancet. 2019;394(10194):249-260.
2. Whelton H. Nutrition and Health | Nutritional and Oral Health-Promoting Properties of Dairy Products: Caries Prevention and Oral Health. In: Fuquay JW, editor. Encyclopedia of Dairy Sciences (Second Edition). San Diego: Academic Press; 2011. p. 1034-1040.
3. Wang M, Gao M, Yi Z. Biological effects of IL-33/ST2 axis on oral diseases: autoimmune diseases and periodontal diseases. International Immunopharmacology. 2023;122:110524.
4. Sharma S, Gupta S, editors. Recognition of Various Scripts Using Machine Learning and Deep Learning techniques-A Review. 2021 6th International Conference on Signal Processing, Computing and Control (ISPCC); 2021 7-9 Oct. 2021.
5. Lee JH, Kim DH, Jeong SN, Choi SH. Diagnosis and prediction of periodontally compromised teeth using a deep learning-based convolutional neural network algorithm. J Periodontal Implant Sci. 2018;48(2):114-123.
6. Chen H, Zhang K, Lyu P, Li H, Zhang L, Wu J, et al. A deep learning approach to automatic teeth detection and numbering based on object detection in dental periapical films. Sci Rep. 2019;9(1):3840.
7. Mahdi FP, Motoki K, Kobashi S. Optimization technique combined with deep learning method for teeth recognition in dental panoramic radiographs. Sci Rep. 2020;10(1):19261.
8. Abdalla-Aslan R, Yeshua T, Kabla D, Leichter I, Nadler C. An artificial intelligence system using machine-learning for automatic detection and classification of dental restorations in panoramic radiography. Oral Surgery, Oral Medicine, Oral Pathology and Oral Radiology. 2020;130(5):593-602.
9. Alalharith DM, Alharthi HM, Alghamdi WM, Alsenbel YM, Aslam N, Khan IU, et al. A Deep Learning-Based Approach for the Detection of Early Signs of Gingivitis in Orthodontic Patients Using Faster Region-Based Convolutional Neural Networks. Int J Environ Res Public Health. 2020;17(22).
10. Liu L, Xu J, Huan Y, Zou Z, Yeh SC, Zheng LR. A Smart Dental Health-IoT Platform Based on Intelligent Hardware, Deep Learning, and Mobile Terminal. IEEE J Biomed Health Inform. 2020;24(3):898-906.
11. Li GH, Hsung TC, Ling WK, Lam WY-H, Pelekos G, McGrath C, editors. Automatic Site-Specific Multiple Level Gum Disease Detection Based on Deep Neural Network. 2021 15th International Symposium on Medical Information and Communication Technology (ISMICT); 2021 14-16 April 2021.
12. Askar H, Krois J, Rohrer C, Mertens S, Elhennawy K, Ottolenghi L, et al. Detecting white spot lesions on dental photography using deep learning: A pilot study. J Dent. 2021;107:103615.

13. Chen H, Li H, Zhao Y, Zhao J, Wang Y. Dental disease detection on periapical radiographs based on deep convolutional neural networks. Int J Comput Assist Radiol Surg. 2021;16(4):649-661.
14. Sonavane A, Yadav R, Khamparia A. Dental cavity Classification of using Convolutional Neural Network. IOP Conference Series: Materials Science and Engineering. 2021;1022(1):012116.
15. Almalki YE, Din AI, Ramzan M, Irfan M, Aamir KM, Almalki A, et al. Deep Learning Models for Classification of Dental Diseases Using Orthopantomography X-ray OPG Images. Sensors [Internet]. 2022; 22(19).
16. Lee S K, D, Jeong, HG. Detecting dental diseases with AI dental image analysis. Research Outreach. Health & Medicine. 2022.
17. Jaiswal P, Katkar V, Bhirud S. Multi Oral Disease Classification from Panoramic Radiograph using Transfer Learning and XGBoost. International Journal of Advanced Computer Science and Applications. 2022;13.
18. Juyal A, Tiwari H, Singh U, Kumar N, Kumar S. Dental Caries Detection Using Faster R-CNN and YOLO V3. ITM Web of Conferences. 2023;53:02005.
19. Rashid J, Qaisar BS, Faheem M, Akram A, Amin Ru, Hamid M. Mouth and oral disease classification using InceptionResNetV2 method. Multimedia Tools and Applications. 2024;83(11):33903-33921.
20. Park S, Erkinov H, Hasan MA, Nam S-H, Kim Y-R, Shin J, et al. Periodontal Disease Classification with Color Teeth Images Using Convolutional Neural Networks. Electronics [Internet]. 2023; 12(7).
21. Gomes RFT, Schmith J, Figueiredo RM, Freitas SA, Machado GN, Romanini J, et al. Use of Artificial Intelligence in the Classification of Elementary Oral Lesions from Clinical Images. Int J Environ Res Public Health. 2023;20(5).
22. Hasan M, Barman S, Islam S, Reza AW. Skin Cancer Detection Using Convolutional Neural Network2019. 254-258 p.
23. Zhang Y, Dai W, Pan S. Transfer learning. Cambridge: Cambridge Press; 2020.
24. Abd Elaziz M, Dahou A, Alsaleh NA, Elsheikh AH, Saba AI, Ahmadein M. Boosting COVID-19 Image Classification Using MobileNetV3 and Aquila Optimizer Algorithm. Entropy [Internet]. 2021; 23(11).
25. Zhao L, Wang L. A new lightweight network based on MobileNetV3. KSII Transactions on Internet and Information Systems (TIIS). 2022;16(1):1-15.
26. Arif Ali Z, H. Abduljabbar Z, A. Taher H, Bibo Sallow A, Almufti SM. Exploring the Power of eXtreme Gradient Boosting Algorithm in Machine Learning: a Review. Academic Journal of Nawroz University. 2023;12(2):320-334.
27. Khan J, Raman A, Sambamoorthy N, Prashanth K. Research Methodology (Methods, Approaches And Techniques)2023.
28. Velliangiri S, Alagumuthukrishnan S, Thankumar joseph SI. A Review of Dimensionality Reduction Techniques for Efficient Computation. Procedia Computer Science. 2019;165:104-111.

حقق مجال تصنيف الصور خطوات كبيرة من خلال التعلم الآلي (ML) والتعلم العميق (DL)، ولكنه لا يزال يواجه صعوبات في تحقيق الكفاءة والدقة العالية. تتمتع بنية MobileNetV3، المشهورة بأدائها وعمقها، بفرصة للتحسين عند استخدامها مع الخوارزميات المتقدمة. على الرغم من نجاح MobileNetV3، إلا أن هناك فرصة لاستخدام تقنيات تقليل الأبعاد بالإضافة إلى التحسين لتحسين أدائها. إلى هذه النقطة، ركزت الدراسات بشكل أساسي على استخدام MobileNetV3 لتصنيف الصور. ومع ذلك، لم يتم فحص هذه الأساليب المذكورة أعلاه بدقة في تركيبة. يسعى هذا البحث إلى إنشاء نموذج جديد لتصنيف الصور من خلال دمج MobileNetV3 مع تحليل المكونات الرئيسية (PCA) وخوارزميات بايزي المحسنة. وتتمثل الأهداف في تقليل التعقيد الحسابي، وتعزيز دقة التصنيف، وتحسين معلمات النموذج. تركز الدراسة على مهام تصنيف الصور باستخدام مجموعات البيانات المتاحة للجمهور. إنه يبحث في التكامل فيما يتعلق بالتعلم مع DL مع الأساليب الإحصائية وكذلك طرق التحسين للتعامل مع القيود الحالية. يستخدم البحث طريقة من خطوتين. أولاً، يستخدم MobileNetV3 لاستخراج الميزات وبعد ذلك يقلل أبعاده باستخدام PCA. ثانيًا، يطبق البحث التحسين الافتراضي (BO) لضبط معلمات النموذج. يتم تقييم الأساليب المقترحة باستخدام المقاييس القياسية وبالمقارنة مع النماذج الأساسية.

أظهر التكامل فيما يتعلق بـ MobileNetV3 مع BO وPCA تقدمًا مهمًا في دقة التصنيف. النموذج الذي تم تحسينه من خلال الطريقة الافتراضية كان أداؤه أفضل من النموذج الأساسي MobileNetV3؛ فقد حقق دقة تصنيف بلغت 96.17%، في حين وصل النموذج دون أي تحسين إلى معدل دقة 66.57% فقط. علاوة على ذلك، بالنسبة للنموذج الأمثل ولكن بدون استخدام (BO)، حصلنا على نسبة استدعاء 66.59%، ودقة 66.39%، ودرجة F1 65.60%. لنفس الإجراء، ولكن الآن مع (BO)، رأينا نتائج مثل هذه: الدقة بنسبة 98.88%، والتذكر 98.48%، و98.67% F1score - تحسن كلا هذين المقياسين بشكل ملحوظ. تم تخفيض التكلفة الحسابية باستخدام تقليل الأبعاد باستخدام PCA. يقدم البحث مساهمة مهمة في مجال تصنيف الصور لأنه يقترح نموذجًا قويًا يدمج DL مع الأساليب الإحصائية وكذلك أساليب التحسين المتقدمة. تؤكد النتائج على مدى الوعد الذي تحمله هذه التقنية المدمجة لتحسين المهام المتعلقة بتصنيف الصور.